toxins

Research on Pathogenic Fungi and Mycotoxins in China (Volume II)

Edited by

Shihua Wang, Yang Liu and Qi Zhang

Printed Edition of the Special Issue Published in *Toxins*

www.mdpi.com/journal/toxins

MDPI

Research on Pathogenic Fungi and Mycotoxins in China (Volume II)

Research on Pathogenic Fungi and Mycotoxins in China (Volume II)

Editors

Shihua Wang
Yang Liu
Qi Zhang

MDPI • Basel • Beijing • Wuhan • Barcelona • Belgrade • Manchester • Tokyo • Cluj • Tianjin

Editors

Shihua Wang
Fujian Agriculture and Forestry University
China

Yang Liu
Foshan University/South China Food Safety Research Center
China

Qi Zhang
Chinese Academy of Agricultural Sciences
China

Editorial Office
MDPI
St. Alban-Anlage 66
4052 Basel, Switzerland

This is a reprint of articles from the Special Issue published online in the open access journal *Toxins* (ISSN 2072-6651) (available at: https://www.mdpi.com/journal/toxins/special_issues/Fungi_Mycotoxins_China_v2).

For citation purposes, cite each article independently as indicated on the article page online and as indicated below:

LastName, A.A.; LastName, B.B.; LastName, C.C. Article Title. *Journal Name* **Year**, *Volume Number*, Page Range.

ISBN 978-3-0365-7384-7 (Hbk)
ISBN 978-3-0365-7385-4 (PDF)

Cover image courtesy of Shihua Wang

Contents

Seyni Ndiaye, Minhui Zhang, Mouhamed Fall, Nicolas M. Ayessou, Qi Zhang and Peiwu Li
Current Review of Mycotoxin Biodegradation and Bioadsorption: Microorganisms, Mechanisms, and Main Important Applications
Reprinted from: *Toxins* **2022**, *14*, 729, doi:10.3390/toxins14110729 . . . . . **1**

Ke Li, Dongmei Liu, Xin Pan, Shuwei Yan, Jiaqing Song, Dongwei Liu, et al.
Deoxynivalenol Biosynthesis in *Fusarium pseudograminearum* Significantly Repressed by a Megabirnavirus
Reprinted from: *Toxins* **2022**, *14*, 503, doi:10.3390/toxins14070503 . . . . . **23**

Hoyda Elsir Mokhtar, Aidi Xu, Yang Xu, Mohamed Hassan Fadlalla and Shihua Wang
Preparation of Monoclonal Antibody against Deoxynivalenol and Development of Immunoassays
Reprinted from: *Toxins* **2022**, *14*, 533, doi:10.3390/toxins14080533 . . . . . **39**

Shan Wei, Chaojiang Hu, Ping Nie, Huanchen Zhai, Shuaibing Zhang, Na Li, et al.
Insights into the Underlying Mechanism of Ochratoxin A Production in *Aspergillus niger* CBS 513.88 Using Different Carbon Sources
Reprinted from: *Toxins* **2022**, *14*, 551, doi:10.3390/toxins14080551 . . . . . **55**

Ling Qin, Lan Yang, Jiaru Zhao, Wanlin Zeng, Minxuan Su, Shihua Wang and Jun Yuan
GTPase Rac Regulates Conidiation, AFB1 Production and Stress Response in Pathogenic Fungus *Aspergillus flavus*
Reprinted from: *Toxins* **2022**, *14*, 581, doi:10.3390/toxins14090581 . . . . . **71**

Sen Wang, Ranxun Lin, Elisabeth Tumukunde, Wanlin Zeng, Qian Bao, Shihua Wang and Yu Wang
Glutamine Synthetase Contributes to the Regulation of Growth, Conidiation, Sclerotia Development, and Resistance to Oxidative Stress in the Fungus *Aspergillus flavus*
Reprinted from: *Toxins* **2022**, *14*, 822, doi:10.3390/toxins14120822 . . . . . **85**

Qiaomei Qin, Yingying Fan, Qinlan Jia, Shuaishuai Duan, Fengjuan Liu, Binxin Jia, et al.
The Potential of *Alternaria* Toxins Production by *A. alternata* in Processing Tomatoes
Reprinted from: *Toxins* **2022**, *14*, 827, doi:10.3390/toxins14120827 . . . . . **101**

Xiuna Wang, Wenjie Zha, Bin Yao, Lan Yang and Shihua Wang
Genetic Interaction of Global Regulators AflatfA and AflatfB Mediating Development, Stress Response and Aflatoxins B1 Production in *Aspergillus flavus*
Reprinted from: *Toxins* **2022**, *14*, 857, doi:10.3390/toxins14120857 . . . . . **113**

Jing Wang, Liuke Liang, Shan Wei, Shuaibing Zhang, Yuansen Hu and Yangyong Lv
Histone 2-Hydroxyisobutyryltransferase Encoded by *Afngg1* Is Involved in Pathogenicity and Aflatoxin Biosynthesis in *Aspergillus flavus*
Reprinted from: *Toxins* **2023**, *15*, 7, doi:10.3390/toxins15010007 . . . . . **135**

Dandan Yang, Hailian Wei, Xianglong Yang, Ling Cheng, Qi Zhang, Peiwu Li and Jin Mao
Efficient Inhibition of *Aspergillus flavus* to Reduce Aflatoxin Contamination on Peanuts over Ag-Loaded Titanium Dioxide
Reprinted from: *Toxins* **2023**, *15*, 216, doi:10.3390/toxins15030216 . . . . . **151**

toxins

MDPI

Review

Current Review of Mycotoxin Biodegradation and Bioadsorption: Microorganisms, Mechanisms, and Main Important Applications

Seyni Ndiaye [1,2,3,4,5], Minhui Zhang [1,2,3,4], Mouhamed Fall [6], Nicolas M. Ayessou [5], Qi Zhang [1,2,3,4,7,*] and Peiwu Li [1,2,3,4,7]

[1] Key Laboratory of Biology and Genetic Improvement of Oil Crops, Ministry of Agriculture and Rural Affairs, Wuhan 430062, China
[2] Oil Crops Research Institute, Chinese Academy of Agricultural Sciences, Wuhan 430062, China
[3] Key Laboratory of Detection for Mycotoxins, Ministry of Agriculture and Rural Affairs, Wuhan 430062, China
[4] Laboratory of Risk Assessment for Oilseeds Products (Wuhan), Ministry of Agriculture and Rural Affairs, Wuhan 430062, China
[5] Laboratoire D'Analyses et D'Essai, Ecole Supérieure Polytechnique, Université Cheikh Anta Diop, Fann-Dakar 5085, Senegal
[6] Key Laboratory of Agro-Products Processing, Institute of Agro-Products Processing Science and Technology, Chinese Academy of Agricultural Sciences, Ministry of Agriculture, Beijing 100193, China
[7] Hubei Hongshan Laboratory, Wuhan 430070, China
* Correspondence: zhangqi01@caas.cn; Tel.: +86-27-86711839; Fax: +86-27-86812862

Abstract: Mycotoxins are secondary metabolites produced by fungi. Food/feed contamination by mycotoxins is a great threat to food safety. The contamination can occur along the food chain and can cause many diseases in humans and animals, and it also can cause economic losses. Many detoxification methods, including physical, chemical, and biological techniques, have been established to eliminate mycotoxins in food/feed. The biological method, with mycotoxin detoxification by microorganisms, is reliable, efficient, less costly, and easy to use compared with physical and chemical ones. However, it is important to discover the metabolite's toxicity resulting from mycotoxin biodegradation. These compounds can be less or more toxic than the parent. On the other hand, mechanisms involved in a mycotoxin's biological control remain still unclear. Mostly, there is little information about the method used by microorganisms to control mycotoxins. Therefore, this article presents an overview of the most toxic mycotoxins and the different microorganisms that have a mycotoxin detoxification ability. At the same time, different screening methods for degradation compound elucidation are given. In addition, the review summarizes mechanisms of mycotoxin biodegradation and gives some applications.

Keywords: mycotoxins; aflatoxins; contamination; microorganisms; biodegradation; enzymes

Key Contribution: This review highlights the current research in mycotoxin biodegradation and bioadsorption. As such, an emphasis is placed on microorganism species; mechanisms; resulting compounds after biodegradation; and main important applications.

Citation: Ndiaye, S.; Zhang, M.; Fall, M.; Ayessou, N.M.; Zhang, Q.; Li, P. Current Review of Mycotoxin Biodegradation and Bioadsorption: Microorganisms, Mechanisms, and Main Important Applications. *Toxins* **2022**, *14*, 729. https://doi.org/10.3390/toxins14110729

Received: 24 August 2022
Accepted: 28 September 2022
Published: 25 October 2022

Publisher's Note: MDPI stays neutral with regard to jurisdictional claims in published maps and institutional affiliations.

1. Introduction

Mycotoxins are secondary metabolites with low molecular weight produced by filamentous fungal species [1–3]. Their chemical structures are very different [4], and they cause various degrees of toxicity in humans and animals. Mycotoxins are often genotypically specific but can be produced by one or more fungal species; one species can produce more than one kind of mycotoxin. In the environment, there are more than 200 kinds of mycotoxins [5]. Some of them can exhibit carcinogenic, teratogenic, mutagenic, and neurotoxic properties, and others can show antitumor capacity and cytotoxic and antimicrobial properties [4,6].

Mycotoxin contamination can occur throughout the whole food process, from pre-harvest to food storage [5,7–9]. It is estimated that 25% of the world's agricultural products may be contaminated by mycotoxins each year [10], which leads to economic losses and causes a variety of toxic effects in humans and animals. According to the RASFF (Rapid Alert System for Food and Feed), for the 10-year period from 2010–2019, almost 98.9% of U.S. food notifications on mycotoxins were due to aflatoxin contamination in almonds, peanuts, and pistachio nuts [11]. A multi-mycotoxin analysis of sorghum and finger millet in 2014 showed that these two types of cereals were contaminated with major mycotoxins, with a prevalence of 6 to 52% for finger millet and less than 15% for sorghum [12]. A similar study about the occurrence of mycotoxins in peanuts and peanut products showed that the level of aflatoxins was higher than the maximum limit in 90% of the samples [13]. A study by Monyo et al. on the occurrence of aflatoxin contamination in groundnut demonstrated that the amount of aflatoxin was higher than the maximal limit in 11 to 28% of the samples and below the limit in 2 to 10% of the samples [14]. A study on the occurrence of ochratoxin A (OTA) in food products available in Silesia markets showed that around 22% of the samples were contaminated [15]. Up to 30 or 31% of total wheat-based product samples collected from some districts of Punjab were found to be contaminated with aflatoxins and zearalenone (ZEN) [16]. A three-year survey about Fusarium mycotoxin contamination in wheat samples showed the presence of deoxynivalenol (DON) and nivalenol (NIV) in about 540 and 337 μg/kg, respectively [17]. To deal with this worldwide problem, many detoxification methods have been found against mycotoxins: physical methods, chemical methods, and biological methods [18,19].

Physical control refers to all methods that use the physical properties of a detoxication agent. This can include adsorption, extrusion, cooking, ozonation, the mechanical separation of the clean product from contaminated one, heating at high temperatures, use of radiation and light, grinding, and washing [20,21]. At present, the utilization of mycotoxin-binding adsorbents is the most frequently applied method to protect animals from contaminated feed [22]. Agro-product processing can also reduce mycotoxin contamination. Fermentation has been useful for some Fusarium mycotoxins [23]. It is considered an excellent technique for mycotoxin control in African countries [24].

Chemical control refers to methods that require the use of chemical compounds. This includes techniques such as ammonization [25], the influence of acids and bases, and the influence of oxidizing agents or various inorganic and organic chemicals [20]. However, these methods have some limitations because of the possible deterioration of animal health caused by excessive residual chemical substances in the feed and even some environmentally negative impacts [22].

Nowadays, the biological control of mycotoxins has gained great interest because most chemical and physical detoxification pathways have limitations such as high cost, residual compounds in food and feed, and loss of nutrients. Biological methods include the action of yeasts, bacteria, and enzymes against mycotoxins [26,27]. This detoxification pathway offers an excellent alternative to eliminate toxins and safeguards the nutritional value of food and feed. Nonetheless, biodegradation can result in more toxic compounds. Therefore, there is a need to study the toxicity of the resulting compounds [28].

This paper first describes the most common mycotoxins, then it provides a summary of different mycotoxin detoxification methods by microorganisms and detoxification mechanisms already found. Finally, some important microorganism applications are provided.

2. Major Mycotoxin Overview

Along the food chain, aflatoxins, ochratoxin A, zearalenone, deoxynivalenol, nivalenol, fumonisin B1 and B2, and patulin are the most common mycotoxins that can contaminate food and feed [29].

Aflatoxins are secondary fungi metabolites mostly produced by *Aspergillus flavus*, *Aspergillus parasiticus*, *Aspergillus nominus*, and *Aspergillus niger* [5,30,31]. Approximately 18 aflatoxins have been identified [32], but the most common are aflatoxin B1 (AFB1),

aflatoxin B2 (AFB2), aflatoxin G1 (AFG1), aflatoxin G2 (AFG2), aflatoxin M1 (AFM1), and aflatoxin M2 (AFM2). Due to their capacity to bind with the DNA of cells, aflatoxins affect protein synthesis [33]. Group B has blue fluorescence and group G has green fluorescence under ultraviolet light [33]. Aflatoxin contamination occurs mainly in hot and humid regions [34]. AFB1 is the most toxic and is cancerogenic, teratogenic, and mutagenic [35]. It is included in category 1A of active carcinogenic compounds (IARC, 1993). The liver is its number one target [36]. On the other hand, AFM1 is a metabolite of AFB1 mainly present in dairy products [37] and is included in group 2B by International Agency for Research on Cancer (IARC) (1993) with a maximum of 0.5 µg/kg in milk [38]. Aflatoxin B1 is bio-transformed into AFB1-8,9-epoxide via cytochrome p450 enzymes, which can induce DNA damage [39].

Patulin (PAT) is a mycotoxin produced mostly by penicillium [40], Byssochlamys, and Aspergillus species [41]. Patulin contamination can cause a lot of damage to animals, such as cancer, by affecting different organs, including the kidney, liver, and intestine [42]. It can contaminate foodstuffs such as fruits and vegetables, especially apples and apple by-products [43–45].

Ochratoxin A (OTA) is the most common toxin in grapes and grape-derived products [46], but it can also contaminate food such as coffee, spices, beer [47], and some meat products [48]. OTA is mainly produced by *Aspergillus ochraceus* and *Penicillium verrucosum* [49]. *Aspergillus carbonarius*, and *Aspergillus niger* can also produce OTA, especially in grapes and wines [50]. OTA is very stable at high temperatures [51]. It has neurotoxicological effects [52,53] nephrotoxic effects and can affect mammary functions [54]. OTA production in grapes and grape-derived products is a severe problem in the wine production field, especially in European countries where the climate conditions favor the growth of ochratoxigenic Aspergillus species. Thus, since March 2002, maximum OTA levels in cereals and dried vine fruits are regulated by the EU [55,56].

Fumonisin B1 (FB1) is the most abundant and toxic of the more than 15 types of fumonisins that have been identified [57]. FB1 can cause many diverse toxic effects in animals, including neurotoxicity, hepatotoxicity, and nephrotoxicity [58]. FB1 is a mycotoxin produced by *Fusarium* species such as *Fusarium verticilloides* and *Fusarium proliferatum* [59]. It is found in various crops, but mostly in corn and corn-based food or feed products. It is classified by the IARC 2002 as a carcinogen to humans (group 2B) [60].

Trichothecene mycotoxins are a group of sesquiterpenoid metabolites produced by Fusarium species. They usually contaminate cereals and threaten human and animal health [61]. Around 200 tetracyclic sesquiterpenoids have been identified as part of the trichothecene group [62]. Deoxynivalenol (DON) and nivalenol (NIV), and T-2 Toxin (T-2) are the more significant trichothecenes [63]. Type-B trichothecenes include deoxynivalenol (DON), nivalenol (NIV), and their acetylated derivatives, whereas Type-A includes T-2 and HT-2 toxins [10]. They are distinguished by the presence or absence of a carbonyl group in the C8 position.

Deoxynivalenol (DON) has been found to contaminate cereal crops such as barley [64], wheat [65], and maize, as well as their by-products [66]. It is mainly produced by *Fusarium* species [67]. DON may cause toxic and immune-toxic effects in animal species [6]. It is a potent inhibitor of protein synthesis. Fusarium mycotoxins such as DON and ZEN have been shown to affect liver morphology [68] and to have an immunosuppressive effect [69].

Zearalenone is a β-resorcylic acid lactone [70] that is produced by several species of Fusarium, including *Fusarium graminearum*, *Fusarium culmorum*, *Fusarium cerealis*, *Fusarium equiseti*, and *Fusarium semitectum* [71]. This mycotoxin infects cereals such as maize and wheat and can cause many hazards to humans and animals, such as cytogenetic toxicity, decrease fertility, embryotoxicity, and immunotoxicity [72–74]. ZEN has the ability to bind to the estrogen receptors of a cell, making it hazardous to humans and animals [75]. ZEN is mostly bio-transforming in α-ZEN and β-ZEN [76].

Due to their toxicity and effects on human health, many countries and international organizations, such as the World Health Organization (WHO), the Food and Agriculture

Organization (FAO), and the European Union (EU) through the European Food Safety Authority (EFSA) [77], have set up strict controls of maximum residue levels in foodstuffs. Figure 1 provides some examples of mycotoxin structures.

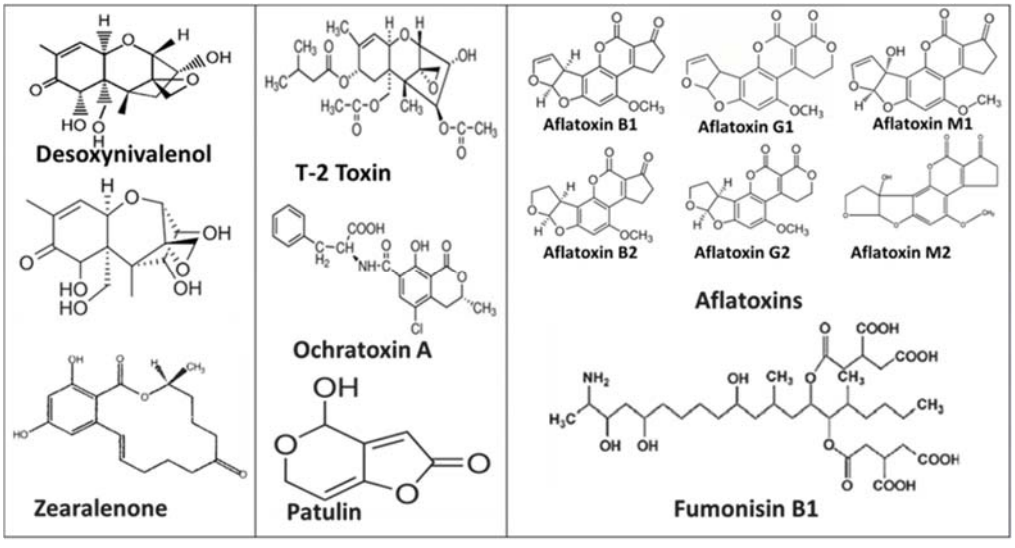

Figure 1. Most common mycotoxin structures.

Table 1 provides an overview of the characteristics of some mycotoxins, including their effects and corresponding recommendations from the World Health Organization [38].

Table 1. Some mycotoxin characterizations.

Toxins	Effects	Fungi Producer	WHO Recommendation	References
Aflatoxin B1	Cancerogenic, teratogenic, mutagenic	*Aspergillus flavus*, *Aspergillus parasiticus*, *Aspergillus nominus*, and *Aspergillus niger*	15 µg/kg in peanuts	[5,30,31,39,78–80]
Patulin	Genotoxicity, mutagenicity, gastrointestinal disorders, edema	*Penicillium*, *Byssochlamys*, and *Aspergillus* species	50 µg/kg in apple juice	[27,81–85]
OTA	Nephrotoxic and neurotoxic effects, affects mammary functions	*Aspergillus ochraceus*, *Penicillium verrucosum*, *Aspergillus carbonarius*, and *Aspergillus niger*	5 µg/kg in wheat and barley	[50,52,54,86,87]
DON	Intestinal damage, emetic effects, immune-toxic	*Fusarium graminearum* and *Fusarium culmorum*	2000 µg/kg in wheat, barley, and maize	[88–90]
ZEN	Cytogenetic toxicity, decreases fertility, embryotoxicity, immunotoxicity, estrogenic, anti-androgenic activities	*Fusarium graminearum*, *Fusarium culmorum*, *Fusarium cerealis*, *Fusarium equiseti*, and *Fusarium semitectum*	TDI[1] 0.25 µg/kg by EFSA[2]	[70–74,91–93]
Fumonisin B1	Neurotoxicity, Hepatotoxicity, nephrotoxicity	*Fusarium verticilloides* and *Fusarium proliferatum*	Total of FB_1 + FB_2: 2000 µg/kg in maize flour and maize meal	[59,94–96]

[1]TDI: Tolerable daily intake; [2]EFSA: European Food Safety Authority.

3. Microorganism Degradation

3.1. Toxin Detoxification by Bacteria

Many species of bacteria have the ability to degrade mycotoxins, including lactic acid bacteria [97] and other species [98]. *Tetragenococcus halophilus* [99], *Rhodococcus erythropolis*, and *Mycobacterium fluoranthenivorans* [100] were proven to degrade AFB1; *Pediococcus parvulus* [101] and *Lactobacillus acidophilus* [102,103] are effective for OTA, AFB1, and AFM1 biocontrol; *Bifidobacterium animalis* [104] is useful for patulin control; *Pseudomonas otitidis* [105] and *Bacillus velezensis* Strain ANSB01E [106] are able to detoxify ZEN. The degradation process depends on many factors, such as the incubation time, the medium, the microorganism species, the concentration of the bacteria cells, and the pH.

The degradation time changes according to the bacteria strain; the microbiota from the thermophilic compost of agricultural waste have degraded AFB1 in 5 days, with a degradation yield of more than 95% after cultivation in a PCS medium at 55 °C [107], and *Rhodococcus pyridinivorans* K408 took 12 days to detoxify AFB1 in bioethanol [26]; the *Lacticaseibacillus rhamnosus* (previously *Lactobacillus rhamnosus)* strains LBGG and LC705, however, removed AFB1 very rapidly [108].

The detoxification rate can depend on the medium; *Bacillus subtilis* UTBSP1 is able to detoxify AFB1 in a higher yield in pistachio nuts than in a medium culture [109], and *Pseudomonas fluorescens* strain 3JW1 can degrade AFB1 in potato dextrose broth and peanut medium by 97.8% and 99.4%, respectively [18].

Many bacteria have been reported to be able to degrade more than one mycotoxin [110]. AFB1 and ZEN have been degraded simultaneously by a microbial consortium, TADC7 [111]; *Rhodococcus pyridinivorans* strains (K408 and AK37) are able to degrade AFB1, T-2, and ZEN simultaneously [22], but also, some *lactic acid bacteria* strains can degrade multi-mycotoxins [112,113]. On the other hand, *Pseudomonas fluorescens* strain 3JW1 is able not only to degrade AFB1 but also to inhibit the AFB1 production of *Aspergillus flavus*. It reduces the amount of AFB1 produced by Aspergillus by 97.8%, 99.4%, and 55.8%, respectively, in the medium culture, peanut medium, and peanut kernels [18].

pH also plays an important role in mycotoxin biodegradation. An *Alcaligenes faecalis* strain called ANSA176 is able to detoxify OTA at a rate of 97.43% per 1 mg/mL OTA into OTα within 12 h at 37 °C. The optimal pH is between 6.0–9.0. The bacterial species subjected to the tested pH, ranging from 2.5 to 5.0, were unable to grow [114].

Therefore, mycotoxin biodegradation is an effective method, but it depends on multiple factors. Strict studies are needed for each biocontrol strain to determine the optimal conditions for its use. Table 2 provides an overview of AFB1 detoxification by bacteria with regard to the medium culture used and the main effect on the mycotoxin.

Table 3 provides a global vision of mycotoxin detoxification by bacteria. The main effects on each mycotoxin are provided, as well as the medium culture used.

3.2. Mycotoxin Detoxification by Yeast

Yeasts are able to detoxify mycotoxins in different ways: biodegradation, bioadsorption, or the inhibition of mycotoxin production [126].

The biodegradation method can happen with an enzyme isolated from the yeast or the use of the yeast itself. Hong Cao et al. [127] demonstrated the aflatoxin B1 degradation activity of an oxidase enzyme from the fungus *Armillariella tabescens*. The degradation ability of aflatoxin oxidase has been shown by high-performance thin-layer chromatography (HPTLC). The main mechanism was thought to be the cleavage of the bis-furan ring of the aflatoxin molecule. *Meyerozyma guilliermondii* has been shown to be able to control patulin in pear. The patulin degradation ability of *Meyerozyma guilliermondii* in pear wounds increases with a higher concentration of yeast cells. The optimal temperatures are 20 °C and 4 °C in wounds, as well as in whole fruits [128].

Table 2. Aflatoxin B1 detoxification by bacteria.

Bacteria	Medium Culture	Main Effects	References
Bacillus subtilis UTBSP1	(1) Nutrient broth culture (2) Pistachio nut	Detoxification of AFB1 by 85.66% and 95%, respectively, in the nutrient broth culture and the pistachio nuts in optima conditions of 35–40 °C during 24 h.	[109]
Mycobacterium fluoranthenivorans sp.	Medium culture with AFB1	The AFB1 concentration was reduced by 70% to 80% within 36 h.	[115]
Myroides odoratimimus strain 3J2MO	Medium culture with AFB1	Degradation of 93.82% of the AFB1 after incubation for 48 h at 37 °C.	[116]
Pseudomonas fluorescens strain 3JW1	(1) Medium culture with AFB1 (2) Peanut medium (3) Peanut kernels	Degradation of AFB1 by 88.3% in 96 h.	[18]
Rhodococcus pyridinivorans K408	Bioethanol produced by *Aspergillus flavus*-contaminated corn	Degradation rate was more than 63% in the solid phase and 75% in the liquid phase after 12 experiment days.	[26]
Staphylococcus warneri, *Sporosarcina* sp., *Lysinibacillus fusiformis*	Medium culture with AFB1 standard	Both cultures and lysates degraded AFB1, and the addition of a protease inhibitor enhanced the degradation rate of the lysate.	[117]
Enterococcus faecium M74 and EF031 strains	Medium culture with FB1 solution	AFB1 removal by 19.3 to 30.5% for M74 strain and 23.4 to 37.5% for EF031 strain.	[110]
Pontibacter specie	Medium culture with aflatoxin B1 standard	Lysates and cultures both degraded AFB1.	[118]
Microbial consortium, *TADC7*	Medium culture with aflatoxin B1 standard	Degradation of more than 95% of the amount of AFB1 after five days cultivation in PCS medium at 55 °C.	[107]
Lacticaseibacillus rhamnosus (previously *Lactobacillus rhamnosus)* strains LBGG and LC705	Medium culture with aflatoxin B1 standard	A rapid removal of 80% of AFB1 by both two strains.	[108]
Lacticaseibacillus rhamnosus (previously *Lactobacillus rhamnosus*) *TISTR 541*	Bread produced by contaminated wheat flour	Decrease in AFB1 levels during mixing and fermentation process.	[119]
Rhodococcus erythropolis	Medium culture with aflatoxin B1 standard	A significant reduction in the amount of AFB1 when treated with the *Rhodococcus erythropolis* extracellular extracts.	[120]
Lactobacillus acidophilus and prebiotics	Whole cow's milk	Reduction in AFB1 of 13.53 to 35.53%.	[103]
Lactobacillus acidophilus and Lacticaseibacillus (previously *Lactobacillus rhamnosus*)	Yogurt samples	Binding of AFB1 by 64.56 to 96.58% during 21 days of storage.	[121]

On the other hand, yeast biocontrol can involve bioadsorption mechanisms. Some *Saccharomyces* strains are able to remove OTA contamination via adsorption; the mechanism of removal can be enhanced from 45% to 90% by heat treatment of the microorganism and with a lower pH in the medium [129]. In another case, during OTA reduction caused by *Saccharomyces cerevisiae*, the addition of sugar at a temperature of 30 °C enhanced the OTA reduction rate in a semi-synthetic medium [130]. The binding capacity of AFB1, ZEN, OTA, and DON with respect to the *Saccharomyces cerevisiae* contained in beer fermentation residue was studied by Campagnollo et al. [131]. The results showed that beer fermentation residue has a higher binding capacity for ZEN at levels of 75.1% and 77.5% at pH 3.0 and 6.5, respectively. The volatiles of non-fermenting yeasts have shown significant binding activity against mycotoxins. The highest mycotoxin binding activities of these strains were noted against ochratoxin A (92%), AFB2 (66%), AFG2 (59%), and AFB1 (31%) [132]. One issue concerning mycotoxin biocontrol by yeast is that it can sometimes be a reversible mechanism, as has been noted with *S. cerevisiae* CECT 1891 and *L. acidophilus* 24, which were able to remove FB1 from a liquid medium. The removal was a fast and reversible process [133]. Yeasts' complicated interactions with mycotoxins indicate that cell wall structural integrity, physical structure and morphology, and chemical components all play

important roles in the adsorption process. On this basis, future approaches may rely on combinations of different microorganisms to provide complementary advantages in mycotoxin adsorption by yeast [134].

Table 3. Other mycotoxins detoxification by bacteria.

Bacteria	Toxins	Medium Culture	Main Effects	References
Enterococcus faecium M74 and EF031 strains	Patulin	Medium culture enriched with patulin solution	Patulin removal of 15.8 to 41.6% for M74 strain and 19.5 to 45.3% for EF031 strain.	[110]
Bacillus pumilus ES-21	Zearalenone	Medium culture with ZEN standard	The degradation rate was more than 95.7%.	[91]
Bacillus amyloliquefaciens ZDS-1	Zearalenone	(1) Medium culture with ZEN standard (2) Contaminated wheat samples	ZEN degradation with a concentration ranging from 1 mg/L to 100 mg/L for specific optimal conditions, which are temperature 30 °C, pH from 6.0 to 7.0, and a microorganism concentration of 5.1×10^8 CFU/mL.	[122]
Rhodococcus pyridinivorans strains (K408 and AK37)	AFB1, T2 toxin, ZEA	Medium culture with mycotoxin standard solutions	Degradation of the 03 mycotoxins and increase in the ZON degradation capacity from 60% to 95% in the multi-mycotoxin degradation system	[22]
Microbial consortium TADC7	AFB1, ZEN	Medium culture with mycotoxin standard solutions	Degradation of AFB1 by 98.9% and ZEN by 88.5% after 168 h.	[111]
Pseudomonas otitidis TH-N1	Zearalenone	Medium culture with a ZEN standard	Degradation of ZEN under optimal conditions: Temperature 37 °C, pH 4 to pH 5, and bacterial concentration of 10^9 CFU/mL.	[105]
Bacterial consortium PGC-3	DON, NIV	Medium culture with mycotoxin standard solution	Biotransformation of DON into de-epoxy-DON and NIV into de-epoxy-NIV with optimal conditions of pH 5–10 and temperatures of 20–37 °C in aerobic conditions.	[123]
Lactic acid bacteria	DON, T-2, HT-2, ZEN	Malting wheat	Reduction in the amount of DON, T-2, HT-2, and ZEN of, respectively, 23%, 34%, 58%, and 73% in malting wheat samples.	[112]
Lactic acid bacteria	FB1, ZEN	Maize meal	Reduction in ZEN of 68.3% and FB1 of 75% after 4 incubation days.	[124]
Limosilactobacillus reuteri (previously *Lactobacillus reuteri*)	ZEN	Nutrient broth and maize kernels	Hydrolysis of 5.0 mg/L ZEN for 8 h in nutrient broth and hydrolysis of 2.5 mg/kg ZEN for 4 h in ZEN-contaminated maize kernels.	[125]
Bacillus velezensis Strain ANSB01E	ZEN	Liquid medium and moldy corn	ZEN degradation of 95% in the liquid medium and of 25% in the moldy corn after 48 h.	[106]

Finally, mycotoxin biocontrol by yeast can concern the inhibition of mycotoxin production. Ponsone et al. studied the activity of some yeast strains isolated from Argentinean vineyards against the growth of the ochratoxigenic *Aspergillus* strain Nigri and also evaluated their effects on OTA. This study demonstrated the natural occurrence of biocontrol agents in the environment to reduce fungi and mycotoxin problems. The results showed that these yeast strains have the ability, under different water activity (aw) and temperature conditions, to control *Aspergillus carbonarius* and *A. niger* aggregate growth and OTA accumulation with a reduction of at least 50% [135]. The same results were obtained when non-fermenting and low-fermenting yeasts were used by Fiori et al. to reduce OTA contamination in grape juice [136]. Nonetheless, some yeast strains are just able to inhibit growth parameters but not mycotoxin production.

Table 4 provides a summary of mycotoxin detoxification by yeast. Emphasis is given to related medium culture and its main effects on mycotoxins.

Table 4. Toxin detoxification by yeasts.

Yeasts	Toxins	Medium Culture	Main Effects	References
Saccharomyces cerevisiae	Beauvericin (BEA)	(1) Standard of BEA (2) Corn flour	In total, 89.1 to 99.3% degradation rate in the standard solution against 73.5 to 91% in the cornflour.	[137]
Rhodosporidium paludigenum	Patulin	Patulin standard	Removal of the total amount of patulin after two days at 28 °C.	[138]
Armillariella tabescens	Aflatoxin B1	Aflatoxin B1 standard	Cleavage of the bis-furan ring.	[127]
Candida versatilis CGMCC 3790	Aflatoxin B1	A mixture of steamed soybean and baked wheat flour	Degradation dependent on initial AFB1 concentration.	[139]
Rhizopus stolonifer	OTA	Wheat contaminated by OTA	Degradation of 96.5% of OTA.	[140]
Candida intermedia, Lachancea thermotolerans, Candida friedrichii	OTA	Grape juice	Reductions in OTA by *Candida intermedia, Lachancea thermotolerans, Candida friedrichii* of 73%, 75%, and 70%, respectively.	[136]
Candida tropicalis, Torulaspora delbriickii, Zygosaccharomyces rouxii, and *Saccharomyces* strains	ZEN	Growth media	Biodegradation of ZEN into α- zearalenol and β-zearalenol.	[141]
Saccharomyces cerevisiae W13	OTA	Semi-synthetic medium	Removal of an amount of OTA from 6 to 57.21% with the highest level obtained at 30 °C with 250 g/L of sugar.	[130]

3.3. Toxin Detoxification by Enzymes

Some enzymes isolated from microorganisms or mushrooms are able to degrade one or multiple mycotoxins. This is the case for the Ery4 laccase from *Pleurotus eryngii*, which can degrade AFB1, FB1, OTA, ZEN, and T-2 at the same time [142]. Other enzymes can detoxify only one mycotoxin; this is the case for *Armillariella tabescens*, which has been demonstrated to have an AFB1 degradation ability [127]. The degradation mechanism depends on the enzyme type and the type of mycotoxins. Enzymes can transform the parent into a new compound [91,127,143] or digest it completely [122]. Zeinvand-Lorestani et al. studied the action of a laccase enzyme against AFB1. Under optimal conditions, 67% of the total amount of AFB1 was degraded by the laccase after two days. The degraded product's prooxidative properties and mutagenicity were lower than the AFB1 one [144]. *Bacillus amyloliquefaciens* ASAG1 can detoxify OTA by 98.5% after 24 h of incubation and 100% after 72 h. On the other hand, the carboxypeptidase cloned from the bacterium is also able to degrade OTA at a level of 41% and 72%, respectively, when cultivated with the supernatant and the purified protein of the carboxypeptidase [145]. Another study showed the effect of carboxypeptidases against OTA. Commercial protease A, commercial pancreatin, and an enzyme extract isolated from *Aspergillus niger* MUM have been proven to degrade OTA to Otα, respectively, by 87.3%, 43.4%, and 99.8% under the optimal conditions of pH 7.5 and temperature 37 °C after 25 h [146]. Porcine pancreatic lipase degraded PAT in pear juice [147].

Table 5 provides an overview of mycotoxin degradation by enzymes with emphasis given to the medium culture and its main effects.

Table 5. Toxin detoxification by enzymes.

Toxins	Medium	Enzymes	Main Effects	References
Patulin	Apple juice	Orotate phosphoribosyltransferase	The degradation rate can reach over 80%.	[148]
Aflatoxin B1	Medium culture with aflatoxin B1 standard	Aflatoxin-oxidase (AFO)	Cleavage of the bis-furan ring.	[127]
Aflatoxin B1	Citrate buffer solution containing 20% DMSO	Laccase	Under optimal conditions, which are a temperature of 35 °C, a pH of 4.5, and a laccase activity of 30 U/mL, 67% of the AFB1 total amount was degraded after two days.	[144]
OTA	LB medium	Carboxypeptidase from *Bacillus amyloliquefaciens* ASAG1	Decrease of 41% and 72%, respectively, when cultivated with the supernatant and the purified protein of carboxypeptidase.	[145]
OTA	Buffer systems with enzymes	Commercial protease A, commercial pancreatin, and an enzyme extract isolated from *Aspergillus niger* MUM	At pH 7.5 and 37 °C, protease A and pancreatin reduce the OTA level, respectively, by 87.3%, 43.4%, and 99.8% after 25 h.	[146]
AFB1	Reaction mixture	Manganese protease MnP	In total, 86% of AFB1 levels decrease after 48 h and 5 nkat of MnP.	[143]
Patulin	Pear juice	Porcine pancreatic lipase (PPL)	Patulin degradation with 0.02 g/mL PPL and 0.375 mg/L of PAT at 40 °C within 24 h.	[147]
Aflatoxin B1, Fumonisin B1, Ochratoxin A, Zearalenone, T-2	Medium culture with a standard solution of mycotoxins	Ery4 laccase from *Saccharomyces cerevisiae*	AFB1, FB1, OTA, ZEN, and T-2 toxin degradations of 73%, 74%, 27%, 100%, and 40%, respectively.	[142]
Aflatoxin B1	Medium culture with aflatoxin B1 standard	Laccase from white rot fungi	In total, 40.45% degradation of AFB1 by *Peniophora* sp. SCC0152; 35.90% degradation of AFB1 by *Pleurotus ostreatus* St2; 3; 87.34% degradation of AFB1 by pure laccase from *Trametes versicolor*.	[149]

4. Detoxification Mechanism

4.1. Biodegradation Mechanism

The toxin biodegradation mechanism depends on the microorganism and toxin nature. In their study of AFB1 biodegradation, J. Li et al. demonstrated that aflatoxin B1 degradation by *Tetragenococcus halophilus* is first caused by adsorption and then by the enzymatical pathway. The amount of AFB1 binding caused by adsorption was smaller than the one degraded by the enzymatical pathway. Two mechanisms have been offered as possible pathways for enzymatical action, and six degradation products have been identified: $C_{14}H_{10}O_4$, $C_{18}H_{16}O_8$, $C_{14}H_{12}O_3$, $C_{16}H_{20}O_4$, $C_{14}H_{16}O_2$, and $C_{14}H_{20}O_2$. The first pathway involves the lactone ring, and the second one involves the double bond of the furan ring. Both mechanisms result in the same compound: $C_{14}H_{20}O_2$ [99]. The same results were obtained with another salt-tolerant *Candida versatilis*, CGMCC 3790 [139]. In that case, four resulting compounds were identified by LC/TOF-MS: $C_{14}H_{10}O_4$, $C_{14}H_{12}O_3$, $C_{13}H_{12}O_2$, and $C_{11}H_{10}O_4$. Elsewhere, Hong Cao et al. suggested that the aflatoxin oxidase (AFO) extracted from *Armillariella tabescens* detoxifies the AFB1 by cleaving the bis-furan ring [127]. Adebo et al. found that the pathway of AFB1 degradation by the culture and lysate of a *Pontibacter* species is enzymatical and suggested that when the AFB1 is hydrolyzed, it has probably been transformed into new compounds, which were not identified in that paper [118]. AFB1 has been partially bio-transformed into aflatoxin D1 (AFD1) by deleting a mutant of the bacC gene in *Baccilus subtilis* UTB1. The mechanism was a reduction in the double bond of the lactone ring in the coumarin moiety, followed by the hydrolysis of the

ester bond and, finally, the des-carboxylation of the yield to aflatoxin D1 (AFD1); all the processes were catalyzed by the BacC [150]. AFD1, AFD2, and AFD3 have been shown to be degradation compounds of AFB1 detoxification by *Pseudomonas putida*. The mechanism might be lactone [151]. *Phanerochaetesordida YK-624* is able to transform AFB1 into AFB1-8,9-epoxide by, firstly, the oxidation of the manganese protease; thereafter, hydrolysis obtains the final product, AFB1-8,9-dihydrodiol [143]

A yeast enzyme, orotate phosphoribosyltransferase, from *Rhodotorula mucilaginosa* was tested against patulin in apple juice samples and under optimum degradation conditions, which are 0.15 g/L of orotate phosphoribosyltransferase for every 1 mg/L patulin at 25 °C for 18 h; the degradation rate of patulin reached over 80% [148]. During a study of patulin degradation by the yeast *Rhodosporidium paludigenum*, the authors of [138] made the statement that the enzyme(s) responsible for patulin degradation synthesis was enhanced by the presence of patulin. In fact, an assay with protein extracted from cells contaminated by patulin was more active than those with proteins from cells grown without patulin. This difference was attributed to the synthesis of the enzyme. Patulin degradation screening of *Saccharomyces cerevisiae*, tested by M. Li et al., showed that the mechanism was enzymatical and that the PAT-metabolizing enzyme production by the yeast cells is not induced by PAT preincubation [27]. These results were not in accordance with those of Ianiri et al., who concluded in their study that the patulin degradation mechanism by the yeast *Sporobolomyces* sp. IAM 13481 can be induced via pretreatment with the mycotoxin; the pre-incubation with patulin can induce the earlier activation of the gene-encoding proteins of the antioxidant system and the proteins involved in the patulin efflux and patulin degradation [152].

Young et al., in their study, showed that microbial isolate microbiota and pure cultures from chicken intestines have the ability to degrade twelve trichothecenes. The degradation compound identification by MS has suggested that the mechanism includes de-epoxidation and or a diacylation, with the route depending on the presence and position of acyl functionalities [153]. In addition, Gao et al. isolated a bacterium, *Eggerthella* sp. DII-9, which has the ability to degrade some types of trichothecenes, including DON, HT-2, T-2 triol, and T-2 tetraol, into other compounds. T-2 triol was degraded into de-epoxy T-2triol (88.0%), de-epoxy HT-2 (8.6%), and de-epoxy T-2tetraol (2.3%). T-2 tetraol was converted into de-epoxy T-2 tetraol (85.9%), and about 2.3% de-epoxy T-2 triol. HT-2 was transformed into de-epoxy HT-2 (81.4%) and 4.7% de-epoxy T-2 triol. To identify the molecular mechanism, the complete genome of DII-9 was sequenced, but the location of the responsible genes was not found. After the enzymatical study, de-epoxidation was found to be a complex phenomenon [62].

The zearalenone degradation of Bacillus pumilus ES-21 was studied by G. Wang et al. The degradation rate was more than 95.7%, and the degradation compound was identified as 1-(3,5-dihydroxyphenyl)-60-hydroxy-l0-undecen-l00-one. Nonetheless, the compound was not very stable and degraded very rapidly. The mechanism was found to be enzymatical and was thought to be due to esterase activity [91]. on the other hand, during the process of ZEN degradation by Bacillus amyloliquefaciens [122], no resulting compounds were detected. It was concluded that during the biodegradation of Zen by the bacteria's extracellular enzyme, no ZEN derivatives were produced; in fact, a study of ZEN derivative biodegradation by Bacillus amyloliquefaciens, including α-zearalenol, β-zearalenol, α-zearalanol, and β-Zearalanol, resulted in no metabolites. Koch et al. (2014) studied the ZEN detoxification ability of nine different fungal strains of the genera Rhizopus and Aspergillus, which are known to produce and transform steroids. The results showed that all the strains were able to detoxify ZEN. Biodegradation and adsorption happen simultaneously. Five resulting compounds were identified: ZEN-14-sulfate, ZEN-O-14, ZEN- O-16-glucoside, α-zearalenol, and α- zearalenol-sulfate. The nine biocontrol agents were divided into three groups: (1) *Rhizhopus oryzae* DSM 907 and *Rhizhopus stolonifera* DSM 855, which can catalyze ZEN glycosylation; (2) *Rhizhopus oryzae* DSM 906 and *Rhizhopus oligosporus* DSM 1964 and *Aspergillus oryzae* DSM 1864 and *Aspergillus oryzae* NBRC

100959, which are involved in the formation of sulfated ZEN metabolites; (3) Rhizopus DSM 908, DSM 1834, and Rhizopus oligosporus LMH 1133 T, which have shown the ability to produce the metabolite of both patterns [154]. The bacterial gut flora of pigs are able to transform ZEN into α-zearalenol and an unidentified compound via hydrolysis and DON into de-epoxy-DON via a de-epoxydation reaction [155].

OTA biodegradation by *Pediococcus parvulus* UTAD depended on the inoculum size and the incubation temperature coupled with a latency phase before biodegradation initiation. This later effect is due to the biodegradation enzyme synthesis of the bacteria [101]. OTA has been biodegraded into Otα by OTA amide group hydrolysis. On the other hand, OTA reduction by *Debaryomyces hansenii* involves neither absorption nor detoxification. It is a repression of the expression of the non-ribosomal peptide synthetase (otanpsPN) gene linked to the OTA biosynthetic pathway, which was observed in [48].

Generally, mechanisms of mycotoxin degradation by microorganisms include different types of enzymes (protease, esterase, intracellular enzymes, etc.). The degradation process can include one or two types of reactions. The mechanisms elucidated by now include oxidation, hydrolysis, the cleavage of the lactone ring, des-carboxylation, de-epoxidation, glycosylation, and sulfate-conjugation reactions. Figure 2 provides a general scheme of different enzymes that participate in mycotoxin degradation caused by microorganisms and the involved reactions.

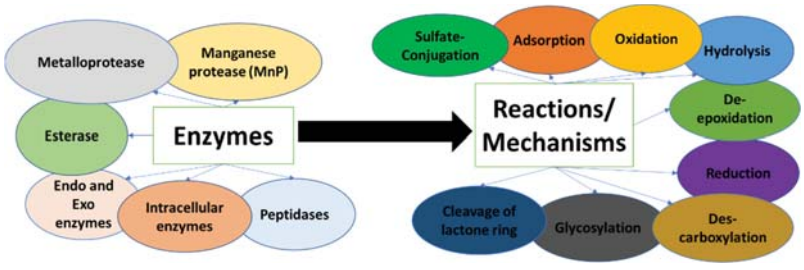

Figure 2. Mycotoxin biodegradation: Enzymes and reactions/mechanisms.

Many studies have focused on the mycotoxin detoxification abilities of microorganisms, but a better understanding of responsible enzymes and the mechanisms involved is still needed. In some specific cases, no resulting metabolites were detected after mycotoxin biodegradation caused by microorganisms, but mostly, one or multiple compounds are usually detected. Table 6 provides an overview of mycotoxin degradation caused by microorganisms with a focus on the involved enzymes, degradation reactions, and resulting metabolites.

4.2. Decontamination by Removal Mechanism

The use of microorganisms as agents for toxin sequestration in order to remove them from food and feed is an approach that has shown many good results.

Taheur et al. showed that strains isolated from a kefir culture are efficient in binding mycotoxins. The binding ability was dependent on the strain and the mycotoxin type [158]. From the same perspective, *Saccharomyces cerevisiae CECT 1891* and *Lactobacillus acidophilus 24* FB1 were shown to have a binding ability by Pizzolitto et al. The binding process needed a little time (1 min), and the mechanism involved was demonstrated to be a toxin molecule via the physical adsorption of the microorganism's cell wall components. Cell viability was not necessary for FB1 binding, but the microorganism's cell wall structural integrity was required, and the process did not involve FB1 chemical modification [133]. From the same perspective, two strains of *Enterococcus faecium*, which are present in dairy products, particularly in cheese, are efficient in AFB1 and PAT removal [110]. The same results were obtained by Elsanhoty et al. when they studied the AFM1 removal ability of some strains of *Lactobacillus* in milk samples [159].

Table 6. Toxin degradation by microorganism mechanisms summary.

Microorganisms	Genes or Enzymes	Toxins	Degradation Reactions	Obtained Metabolites	References
Tetragenococcus halophilus	Enzyme ND *	Aflatoxin B1	Adsorption + enzymatical action	$C_{14}H_{10}O_4$, $C_{18}H_{16}O_8$, $C_{14}H_{12}O_3$, $C_{16}H_{20}O_4$, $C_{14}H_{16}O_2$, $C_{14}H_{20}O_2$	[99]
Candida versatilis CGMCC 3790	Enzyme ND	Aflatoxin B1	Adsorption + enzymatical action	$C_{14}H_{10}O_4$, $C_{14}H_{12}O_3$, $C_{13}H_{12}O_2$, $C_{11}H_{10}O_4$.	[139]
Phanerochaetesordida YK-624	Manganese protease MnP	Aflatoxin B1	Oxidation + hydrolysis	AFB1-8,9-dihydrodiol	[143]
Rhodosporidium paludigenum	Enzyme ND	Patulin	ND	Desoxypatulinic acid	[138]
Bacillus pumilus ES-21	Esterase	Zearalenone (ZEN)	Cleavage of the lactone ring, followed by des-carboxylation. The enzymatic process follows first-order kinetics with $t_{1/2}$ of 6.52 h.	1-(3,5-dihydroxyphenyl)-60-hydroxy-l0-undecen-l00-one	[91]
Eggerthella sp.	Enzyme ND	DON, HT-2, T-2 triol and T-2 tetraol	De-epoxidation	De-epoxy- DON, de-epoxy T-2triol, de-epoxy HT-2, de-epoxy T-2 tetraol for the 04 parents in different ratios	[62]
Saccharomyces cerevisiae	Endo and Exo enzymes synthesized by the yeast during the fermentation	Patulin	The mechanism was enzymatical and the production of the relevant PAT-metabolizing enzymes synthesized by the yeast cells is not induced by PAT preincubation	E-ascladiol	[27]
Sporobolomyces sp. IAM 13481	ND	Patulin	The mechanism was induced by pretreatment with patulin.	DPA and (Z)-ascladiol	[152]
Pediococcus parvulus UTAD	Peptidases	OTA	Hydrolysis of the OTA amide group.	Otα	[101]
Rhizopus and *Aspergillus* species		ZEN	Glycosylation, sulfate-conjugation	ZEN-14-sulfate, ZEN-O-14, ZEN- O-16-glucoside, α-zearalenol, α-zearalenol-sulfate	[154]
Phaffia rhodozyma	Metalloprotease	OTA	ND	Otα	[156]
Gut Microflora of Pigs	ND	DON	De-epoxidation	De-epoxy-DON	[155]
Gut Microflora of Pigs	ND	ZEN	Hydrolyze	α-zearalenol	[155]
Bacillus subtilis UTB1	Gene bacC,	AFB1	Reduction in the double bond Hydrolysis of the ester bond Des-carboxylation	AFD1	[150]
Pseudomonas putida	ND	AFB1	Opening of the lactone ring	AFD1, AFD2, AFD3	[151]
Pichia caribbica	Intracellular enzymes	Patulin	Unidentified	Ascladiol and unknown compound	[157]

* ND: not determined.

OTA removal by *Saccharomyces* strains was demonstrated by Bejaoui et al. to be an adsorption mechanism. This mechanism was dependent on the OTA molecule's ionic properties, the yeast membrane state, and the biomass concentration [129].

Lactococcus lactis and *Bifidobacterium* sp. Isolated from milk are able to neutralize ZEN contents via absorption. The *Lactococcus lactis* absorption is not homogeneous, and the

process happens in two different steps. The first one includes a ZEN absorption of 88%, and the second one consists of ZEN diffusion into bacterial cells. This was contrary to that of *Bifidobacterium* sp., where the adsorption mechanism only had a single homogeneous step. The deprotonated carboxyl groups of the bacterial proteins and peptidoglycan play a significant role in the absorption process [71].

AFB1 binding via the *Saccharomyces cerevisiae* mannoprotein is possible because of AFB1 absorption onto mannose sites, where the new structure is maintained. Indeed, the new structure nature does not match that of a natural AFB1 molecule, so AFB1 can be removed from the media [160].

4.3. Degradation Compound Toxicity

Knowing the degraded compound's toxicity is very important because it can be more or less toxic than the parent. Therefore, many cytotoxicity studies have been conducted.

Adebo et al. studied the toxicity of the compounds resulting from AFB1 degradation caused by *Staphylococcus warneri*, *Sporosarcina* sp., and *Lysinibacillus fusiformis*. The experiment was conducted by monitoring the mortality of lymphocyte cells (from human blood) after the cells were exposed to degraded compounds. A lower mortality rate was recorded compared with aflatoxin B1. The authors concluded that there was lower toxicity [117]. On the other hand, *Escherichia coli* DH5a, *Arabidopsis thaliana*, and human hepatocyte LO2 were used by [138] to determine the degradation toxicity of the compound identified as desoxypatulinic acid (DPA) due to patulin detoxification caused by *Rhodosporidium paludigenum*. The lower toxicity of DPA compared with PAT was demonstrated.

Elsewhere, no toxicity reduction has been found after ZEN and FB1 biocontrol using lactic acid bacteria. One toxicity study was conducted using human esophageal carcinoma cell lines [124]. Some ZEN degradation products are known to be more toxic than ZEN. In the case of α-ZOL, it shows higher estrogenicity than ZEN [71]. The compounds derived from ZEN biocontrol toxicity can be ranked as follows: α-zearalenol > α-zearalanol > zearalenone > β-zearalenol [161].

Figure 3 provides some mycotoxin degradation pathways.

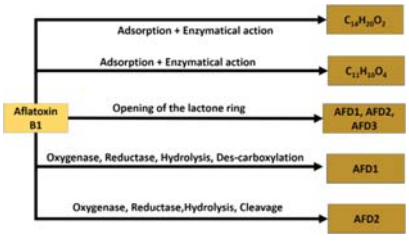

(**a**) Aflatoxin B1 degradation pathways.

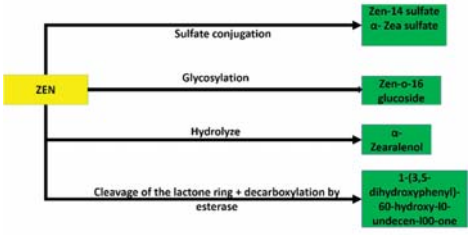

(**b**) Zearalenone degradation pathways.

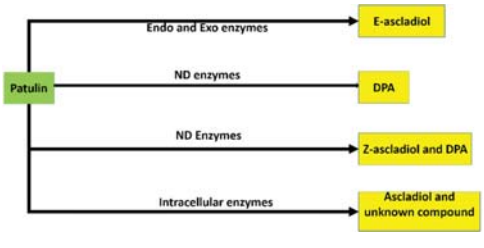

(**c**) Patulin degradation pathways.

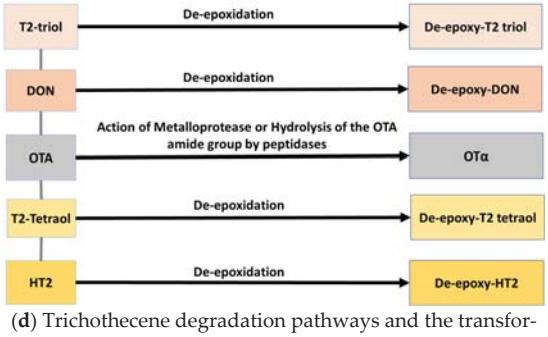

(**d**) Trichothecene degradation pathways and the transformation of OTA into OTα.

Figure 3. Some mycotoxin degradation pathways.

5. Functional Enzymes Extraction from Bacteria

Nowadays, enzymes, as shown in Section 3.3, play a key role in mycotoxin biodegradation. Therefore, it is important to have a general method of enzyme extraction from microorganisms.

The process of enzyme extraction from microorganisms can be divided into three parts: extraction, purification, and characterization.

The extraction step's main idea is to extract the enzyme outside the host. Some procedures are performed by harvesting the mycelia pellet via centrifugation and then washing it with phosphate buffer, followed by a second centrifugation to remove cell debris [127]. More recently, the homogenization of cells with protein extraction buffer followed by ultrasonication and centrifugation has been performed [148].

The purification step's aim is, after the extraction step, to obtain an enzyme that is as pure as possible. Ammonium sulfate is the most used compound to precipitate enzymes [162]. This step is generally followed by centrifugation. In some cases, the precipitation step can be performed by using both organic solvents, such as methanol, ethanol, or acetone, and ammonium sulfate separately [163]. After enzyme activity determination, some purification techniques are used. Chromatography purification can be performed by using hydrophobic interaction chromatography (HIC) followed by immobilized metal ion affinity chromatography (IMAC) [127] or ion-exchange chromatography on a DEAE-Sepharose GE column, followed by dialysis and lyophilization [163]; dialysis can also be performed with a DEAE-Sepharose column [164]. Further purification can be performed using a Superdex 75 column followed by dialysis and lyophilization [163].

The last step is purified enzyme characterization. This step permits us to find the characteristics of the enzyme. It can be feasible to use SDS polyacrylamide gel electrophoresis (SDS-PAGE) to determine the molecular weight [127,163], HPTLC analysis to determine the enzymatic activity, and ESI-MS/MS to identify the enzyme [127]. Finally, the determination of the optimum pH, the optimum temperature, the ion metal effect on the enzyme activity [163], and the protein concentration (which can be determined using the method of Bradford) can be performed. Then, the enzyme can be stored at −85 °C until used.

Figure 4 provides a brief scheme of all the steps of enzyme extraction from microorganisms.

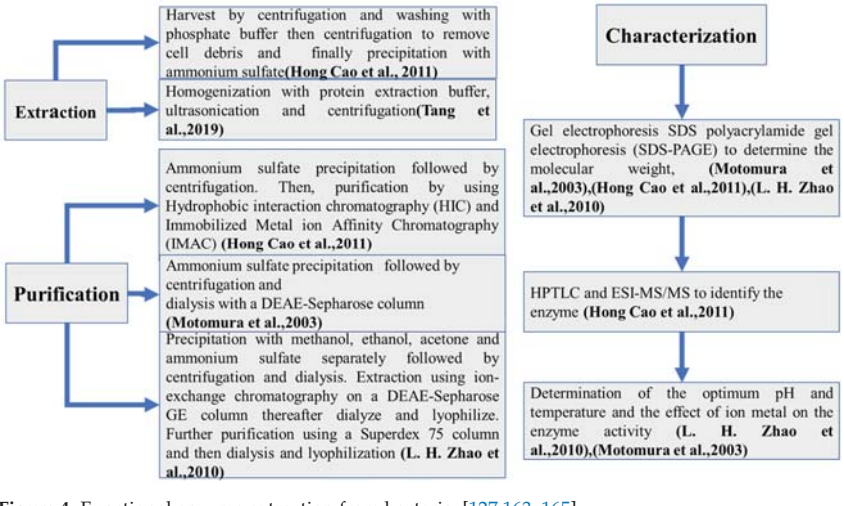

Figure 4. Functional enzyme extraction from bacteria. [127,163–165].

6. Application and Perspectives

Microorganisms that can detoxify hazardous mycotoxins into low-toxicity compounds are of great importance. Being able to utilize them in the field and industries would be of

great interest to food/feed safety. Therefore, it is advantageous to use microorganisms for mycotoxin detoxification on a large scale. Nevertheless, any applications to be set up must take into account both biocontrol agents and the life cycle of mycotoxigenic species, as well as the environmental conditions and plant agronomy [166]. Microorganisms that show activity against mycotoxins provide important properties because of the future possibility of exchanging the chemical and physical methods of preservation with a biological method based on those microorganisms and enzymes. Metabolism products of biocontrol agents are propitious for the bioconservation of food due to their ability to reduce the proliferation of mycotoxigenic fungi and mycotoxin production [167].

Microorganisms are used in many different ways. They are already used as probiotics to enhance the health of the host upon adequate administration. *Lactobacillus* species are most often used as probiotics [168], mainly via encapsulation [169], [170]. Encapsulation is one of the most effective methods of saving the viability and stability of microorganisms [113,171]. Therefore, it is a good alternative for microorganism applications in food and feed. Recently, the yeast *Sporidiobolus pararoseus*, which has a mycotoxin binding ability, was successfully produced with this approach on an industrial production scale with possible applications in feed additives [172].

Microorganisms can also be used as biopesticides [173]. The use of biofungicides is an approach that involves the application of different microorganisms that can suppress toxic fungi [174]. Recently, novel biofungicide formulations based on *Bacillus subtilis* 5, *Bacillus cereus* 3S5, and *Pseudomonas fluorecens* 10S2 were produced [175]. The same formulation has been created using other microorganisms [176–178].

Finally, the mycotoxin degradation enzyme can be especially valuable in the feed, food, and fermentation industry [109,120]. The α-amylase enzymes from some bacterial or fungal strains are widely used [179]. A carboxypeptidase that can degrade OTA has been cloned and used to detoxify the OTA mycotoxin [145].

7. Conclusions

This paper reviews mycotoxin degradation caused by microorganisms. Mycotoxins are secondary compounds produced by fungi with various chemical structures. Some of them are very hazardous for humans and animals, and strict regulations have been made for their content in food and feed. Physical, chemical, and biological methods can be used to control mycotoxin food/feed contamination. Biological control, which includes bacteria, yeast, and enzymatic activities against mycotoxins, is considered a very friendly control method compared with physical and chemical methods. However, more studies are needed to elucidate mycotoxin detoxification mechanisms. Unfortunately, most investigations do not address the real process involved with this biodegradation. In some cases, the degradation compound structures are elucidated, which helps to provide the hypothetically involved mechanisms. The detoxification of mycotoxins using bacterial strains augurs a new path for food/feed safety. From this perspective, more emphasis can be given to the toxicity of the resulting degradation compounds and the involved mechanisms of elucidation.

Author Contributions: S.N. wrote the article, conceptualized the idea, and designed the outline; Q.Z. conceptualized the idea, designed the outline, and revised and validated the manuscript; M.Z. helped to develop the figures; N.M.A. and M.F. revised the manuscript; P.L. supervised the work. All authors have read and agreed to the published version of the manuscript.

Funding: This research was funded by the Key Project of the National Natural Science Foundation of China (3203008), and the Major Project of the Hubei Hongshan Laboratory (2021hszd015).

Institutional Review Board Statement: Not applicable.

Informed Consent Statement: Not applicable.

Data Availability Statement: Not applicable.

Conflicts of Interest: The authors declare no conflict of interest.

References

1. Sanzani, S.M.; Reverberi, M.; Geisen, R. Mycotoxins in harvested fruits and vegetables: Insights in producing fungi, biological role, conducive conditions, and tools to manage postharvest contamination. *Postharvest Biol. Technol.* **2016**, *122*, 95–105. [CrossRef]
2. Luo, Y.; Liu, X.; Li, J. Updating techniques on controlling mycotoxins—A review. *Food Control* **2018**, *89*, 123–132. [CrossRef]
3. Ünüsan, N. Systematic review of mycotoxins in food and feeds in Turkey. *Food Control* **2019**, *97*, 1–14. [CrossRef]
4. Hoyos Ossa, D.E.; Hincapié, D.A.; Peñuela, G.A. Determination of aflatoxin M1 in ice cream samples using immunoaffinity columns and ultra-high performance liquid chromatography coupled to tandem mass spectrometry. *Food Control* **2015**, *56*, 34–40. [CrossRef]
5. Majer-Baranyi, K.; Zalán, Z.; Mörtl, M.; Juracsek, J.; Szendrő, I.; Székács, A.; Adányi, N. Optical waveguide lightmode spectroscopy technique-based immunosensor development for aflatoxin B1 determination in spice paprika samples. *Food Chem.* **2016**, *211*, 972–977. [CrossRef]
6. Gerez, J.R.; Pinton, P.; Callu, P.; Oswald, I.P.; Bracarense, A.P.F.L. Deoxynivalenol alone or in combination with nivalenol and zearalenone induce systemic histological changes in pigs. *Exp. Toxicol. Pathol.* **2015**, *67*, 89–98. [CrossRef]
7. Verheecke, C.; Liboz, T.; Mathieu, F. Microbial degradation of aflatoxin B1: Current status and future advances. *Int. J. Food Microbiol.* **2016**, *237*, 1–9. [CrossRef]
8. Zhang, Z.; Hu, X.; Zhang, Q.; Li, P. Determination for multiple mycotoxins in agricultural products using HPLC-MS/MS via a multiple antibody immunoaffinity column. *J. Chromatogr. B Anal. Technol. Biomed. Life Sci.* **2016**, *1021*, 145–152. [CrossRef]
9. Mwakinyali, S.E.; Ding, X.; Ming, Z.; Tong, W.; Zhang, Q.; Li, P. Recent development of aflatoxin contamination biocontrol in agricultural products. *Biol. Control* **2019**, *128*, 31–39. [CrossRef]
10. Ibáñez-Vea, M.; Lizarraga, E.; González-peñas, E.; López, A.; Cerain, D. Co-occurrence of type-A and type-B trichothecenes in barley from a northern region of Spain. *Food Control* **2012**, *25*, 81–88. [CrossRef]
11. Alshannaq, A.; Yu, J. Analysis of E.U. Rapid Alert System (RASFF) Notifications for Aflatoxins in Exported U.S. Food and Feed Products for 2010–2019. *Toxins* **2021**, *13*, 90. [CrossRef]
12. Chala, A.; Taye, W.; Ayalew, A.; Krska, R.; Sulyok, M.; Logrieco, A. Multimycotoxin analysis of sorghum (*Sorghum bicolor* L. Moench) and finger millet (*Eleusine coracana* L. Garten) from Ethiopia. *Food Control* **2014**, *45*, 29–35. [CrossRef]
13. Ezekiel, C.N.; Sulyok, M.; Warth, B.; Odebode, A.C.; Krska, R. Natural occurrence of mycotoxins in peanut cake from Nigeria. *Food Control* **2012**, *27*, 338–342. [CrossRef]
14. Monyo, E.; Njoroge, S.; Coe, R.; Osiru, M.; Madinda, F.; Waliyar, F.; Thakur, R.; Chilunjika, T.; Anitha, S. Occurrence and distribution of aflatoxin contamination in groundnuts (*Arachis hypogaea* L.) and population density of *Aflatoxigenic Aspergilli* in Malawi. *Crop Prot.* **2012**, *42*, 149–155. [CrossRef]
15. Hajok, I.; Kowalska, A.; Piekut, A.; Ćwieląg-Drabek, M. A risk assessment of dietary exposure to ochratoxin A for the Polish population. *Food Chem.* **2019**, *284*, 264–269. [CrossRef]
16. Zafar, S.; Ra, M.; Jinap, S.; Rashid, U. Detection of a fl atoxins and zearalenone contamination in wheat derived products. *Food Control* **2014**, *35*, 223–226.
17. Del, E.M.; Garda-buffon, J.; Badiale-furlong, E. Deoxynivalenol and nivalenol in commercial wheat grain related to Fusarium head blight epidemics in southern Brazil. *Food Chem.* **2012**, *132*, 1087–1091.
18. Yang, X.; Zhang, Q.; Chen, Z.Y.; Liu, H.; Li, P. Investigation of Pseudomonas fluorescens strain 3JW1 on preventing and reducing aflatoxin contaminations in peanuts. *PLoS ONE* **2017**, *12*, e0178810. [CrossRef]
19. Vila-Donat, P.; Marín, S.; Sanchis, V.; Ramos, A.J. A review of the mycotoxin adsorbing agents, with an emphasis on their multi-binding capacity, for animal feed decontamination. *Food Chem. Toxicol.* **2018**, *114*, 246–259. [CrossRef]
20. Agriopoulou, S.; Koliadima, A.; Karaiskakis, G.; Kapolos, J. Kinetic study of aflatoxins' degradation in the presence of ozone. *Food Control* **2016**, *61*, 221–226. [CrossRef]
21. Marković, M.; Daković, A.; Rottinghaus, G.E.; Kragović, M.; Petković, A.; Krajišnik, D.; Milić, J.; Mercurio, M.; de Gennaro, B. Adsorption of the mycotoxin zearalenone by clinoptilolite and phillipsite zeolites treated with cetylpyridinium surfactant. *Colloids Surf. B Biointerfaces* **2017**, *151*, 324–332. [CrossRef] [PubMed]
22. Cserháti, M.; Kriszt, B.; Krifaton, C.; Szoboszlay, S.; Háhn, J.; Tóth, S.; Nagy, I.; Kukolya, J. Mycotoxin-degradation profile of *Rhodococcus* strains. *Int. J. Food Microbiol.* **2013**, *166*, 176–185. [CrossRef] [PubMed]
23. Chilaka, C.A.; De Boevre, M.; Atanda, O.O.; De Saeger, S. Fate of *Fusarium* mycotoxins during processing of Nigerian traditional infant foods (ogi and soybean powder). *Food Res. Int.* **2019**, *116*, 408–418. [CrossRef] [PubMed]
24. Adebiyi, J.A.; Kayitesi, E.; Adebo, O.A.; Changwa, R.; Njobeh, P.B. Food fermentation and mycotoxin detoxification: An African perspective. *Food Control* **2019**, *106*, 106731. [CrossRef]
25. Peng, W.-X.; Marchal, J.L.M.; van der Poel, A.F.B. Strategies to prevent and reduce mycotoxins for compound feed manufacturing. *Anim. Feed Sci. Technol.* **2018**, *237*, 129–153. [CrossRef]
26. Prettl, Z.; Dési, E.; Lepossa, A.; Kriszt, B.; Kukolya, J.; Nagy, E. Biological degradation of aflatoxin B1by a *Rhodococcus pyridinivorans* strain in by-product of bioethanol. *Anim. Feed Sci. Technol.* **2017**, *224*, 104–114. [CrossRef]
27. Li, M.; Chen, W.; Zhang, Z.; Zhang, Z.; Peng, B. Fermentative degradation of Patulin by *Saccharomyces cerevisiae* in aqueous solution. *LWT—Food Sci. Technol.* **2018**, *97*, 427–433. [CrossRef]
28. Harkai, P.; Szabó, I.; Cserháti, M.; Krifaton, C.; Risa, A.; Radó, J.; Balázs, A.; Berta, K.; Kriszt, B. Biodegradation of aflatoxin-B1 and zearalenone by *Streptomyces* sp. collection. *Int. Biodeterior. Biodegrad.* **2016**, *108*, 48–56. [CrossRef]

29. Siri-Anusornsak, W.; Kolawole, O.; Mahakarnchanakul, W.; Greer, B.; Petchkongkaew, A.; Meneely, J.; Elliott, C.; Vangnai, K. The Occurrence and Co-Occurrence of Regulated, Emerging, and Masked Mycotoxins in Rice Bran and Maize from Southeast Asia. *Toxins* **2022**, *14*, 567. [CrossRef]
30. Xie, J.; Sun, Y.; Zheng, Y.; Wang, C.; Sun, S.; Li, J.; Ding, S.; Xia, X.; Jiang, H. Preparation and application of immunoaffinity column coupled with dcELISA detection for aflatoxins in eight grain foods. *Food Control* **2017**, *73*, 445–451. [CrossRef]
31. Zhao, F.; Tian, Y.; Shen, Q.; Liu, R.; Shi, R.; Wang, H.; Yang, Z. A novel nanobody and mimotope based immunoassay for rapid analysis of aflatoxin B1. *Talanta* **2019**, *195*, 55–61. [CrossRef]
32. Wang, X.; Niessner, R.; Tang, D.; Knopp, D. Nanoparticle-based immunosensors and immunoassays for aflatoxins. *Anal. Chim. Acta* **2016**, *912*, 10–23. [CrossRef]
33. Edite Bezerra da Rocha, M.; Freire, F.C.O.; Erlan Feitosa Maia, F.; Izabel Florindo Guedes, M.; Rondina, D. Mycotoxins and their effects on human and animal health. *Food Control* **2014**, *36*, 159–165. [CrossRef]
34. Xie, J.; Peng, T.; He, J.L.; Shao, Y. Preparation and characterization of an immunoaffinity column for the selective extraction of aflatoxin B_1 in 13 kinds of foodstuffs. *J. Chromatogr. B Anal. Technol. Biomed. Life Sci.* **2015**, *998–999*, 50–56. [CrossRef]
35. Peng, Z.; Chen, L.; Zhu, Y.; Huang, Y.; Hu, X.; Wu, Q.; Nüssler, A.K.; Liu, L.; Yang, W. Current major degradation methods for aflatoxins: A review. *Trends Food Sci. Technol.* **2018**, *80*, 155–166. [CrossRef]
36. Ji, C.; Fan, Y.; Zhao, L. Review on biological degradation of mycotoxins. *Anim. Nutr.* **2016**, *2*, 127–133. [CrossRef]
37. Mirzaei, A.; Hajimohammadi, A.; Badiei, K.; Pourjafar, M.; Naserian, A.A.; Razavi, S.A. Effect of dietary supplementation of bentonite and yeast cell wall on serum endotoxin, inflammatory parameters, serum and milk aflatoxin in high-producing dairy cows during the transition period. *Comp. Clin. Path.* **2020**, *29*, 433–440. [CrossRef]
38. WHO/FAO. *General Standard for Contaminants and Toxins in Food and Feed (Codex Stan 193-1995)*; World Health Organization: Geneva, Switzerland, 2015; Volume 51, pp. 39–54.
39. Engin, A.B.; Engin, A. DNA damage checkpoint response to aflatoxin B1. *Environ. Toxicol. Pharmacol.* **2019**, *65*, 90–96. [CrossRef]
40. Rodríguez-Bencomo, J.J.; Sanchis, V.; Viñas, I.; Martín-Belloso, O.; Soliva-Fortuny, R. Formation of patulin-glutathione conjugates induced by pulsed light: A tentative strategy for patulin degradation in apple juices. *Food Chem.* **2020**, *315*, 126283. [CrossRef]
41. Li, B.; Chen, Y.; Zong, Y.; Shang, Y. Dissection of patulin biosynthesis, spatial control and regulation mechanism in *Penicillium expansum*. *Environ. Microbiol.* **2019**, *21*, 1124–1139. [CrossRef]
42. Liu, M.; Wang, J.; Yang, Q.; Hu, N. Patulin removal from apple juice using a novel cysteine-functionalized metal-organic framework adsorbent. *Food Chem. Toxicol.* **2019**, *270*, 1–9. [CrossRef]
43. Kapetanakou, A.E.; Nestora, S.; Evageliou, V.; Skandamis, P.N. Sodium alginate–cinnamon essential oil coated apples and pears: Variability of *Aspergillus carbonarius* growth and ochratoxin A production. *Food Res. Int.* **2019**, *119*, 876–885. [CrossRef]
44. Sohrabi, H.; Arbabzadeh, O.; Khaaki, P.; Khataee, A.; Majidi, M.R.; Orooji, Y. Patulin and Trichothecene: Characteristics, occurrence, toxic effects and detection capabilities via clinical, analytical and nanostructured electrochemical sensing/biosensing assays in foodstuffs. *Crit. Rev. Food Sci. Nutr.* **2022**, *62*, 5540–5568. [CrossRef]
45. Guo, Y.; Zhou, Z.; Yuan, Y.; Yue, T. Survey of patulin in apple juice concentrates in Shaanxi (China) and its dietary intake. *Food Control* **2013**, *34*, 570–573. [CrossRef]
46. Pantelides, I.S.; Christou, O.; Tsolakidou, M.D.; Tsaltas, D.; Ioannou, N. Isolation, identification and in vitro screening of grapevine yeasts for the control of black aspergilli on grapes. *Biol. Control* **2015**, *88*, 46–53. [CrossRef]
47. Covarelli, L.; Beccari, G.; Marini, A.; Tosi, L. A review on the occurrence and control of ochratoxigenic fungal species and ochratoxin A in dehydrated grapes, non-forti fi ed dessert wines and dried vine fruit in the Mediterranean area. *Food Control* **2012**, *26*, 347–356. [CrossRef]
48. Peromingo, B.; Núñez, F.; Rodríguez, A.; Alía, A.; Andrade, M.J. Potential of yeasts isolated from dry-cured ham to control ochratoxin A production in meat models. *Int. J. Food Microbiol.* **2018**, *268*, 73–80. [CrossRef] [PubMed]
49. Abarca, M.L.; Bragulat, M.R.; Castellá, G.; Cabañes, F.J. Microbiology Impact of some environmental factors on growth and ochratoxin A production by *Aspergillus niger* and *Aspergillus welwitschiae*. *Int. J. Food Microbiol.* **2019**, *291*, 10–16. [CrossRef]
50. Ponsone, M.L.; Nally, M.C.; Chiotta, M.L.; Combina, M.; Köhl, J.; Chulze, S.N. Evaluation of the effectiveness of potential biocontrol yeasts against black sur rot and ochratoxin A occurring under greenhouse and field grape production conditions. *Biol. Control* **2016**, *103*, 78–85. [CrossRef]
51. Zhang, H.; Apaliya, M.T.; Mahunu, G.K.; Chen, L.; Li, W. Trends in Food Science & Technology Control of ochratoxin A-producing fungi in grape berry by microbial antagonists: A review. *Trends Food Sci. Technol.* **2016**, *51*, 88–97.
52. Park, S.; Lim, W.; You, S.; Song, G. Ochratoxin A exerts neurotoxicity in human astrocytes through mitochondria-dependent apoptosis and intracellular calcium overload. *Toxicol. Lett.* **2019**, *313*, 42–49. [CrossRef] [PubMed]
53. Khoi, C.; Chen, J.; Lin, T.; Chiang, C. Ochratoxin A-Induced Nephrotoxicity: Up-to-Date Evidence. *Int. J. Mol. Sci.* **2021**, *22*, 11237. [CrossRef] [PubMed]
54. Lee, J.; Lim, W.; Ryu, S.; Kim, J.; Song, G. Ochratoxin A mediates cytotoxicity through the MAPK signaling pathway and alters intracellular homeostasis in bovine mammary epithelial cells. *Environ. Pollut.* **2019**, *246*, 366–373. [CrossRef] [PubMed]
55. Vlachou, M.; Pexara, A.; Solomakos, N.; Govaris, A. Ochratoxin A in Slaughtered Pigs and Pork Products. *Toxins* **2022**, *14*, 67. [CrossRef] [PubMed]
56. Yang, C.; Abbas, F.; Rhouati, A.; Sun, Y.; Chu, X.; Cui, S.; Sun, B.; Xue, C. Design of a Quencher-Free Fluorescent Aptasensor for Ochratoxin A Detection in Red Wine Based on theGuanine-Quenching Ability. *Biosensors* **2022**, *12*, 297.

57. Chen, J.; Wen, J.; Tang, Y.; Shi, J.; Mu, G.; Yan, R.; Cai, J.; Long, M. Research progress on fumonisin b1 contamination and toxicity: A review. *Molecules* **2021**, *26*, 5238. [CrossRef]
58. Liu, X.; Fan, L.; Yin, S.; Chen, H.; Hu, H. Molecular mechanisms of fumonisin B1-induced toxicities and its applications in the mechanism-based interventions. *Toxicon* **2019**, *167*, 1–5. [CrossRef]
59. Arumugam, T.; Pillay, Y.; Ghazi, T.; Nagiah, S.; Abdul, N.S.; Chuturgoon, A.A. Fumonisin B1-induced oxidative stress triggers Nrf2-mediated antioxidant response in human hepatocellular carcinoma (HepG2) cells. *Mycotoxin Res.* **2019**, *35*, 99–109. [CrossRef]
60. Eskola, M.; Kos, G.; Elliott, C.T.; Hajšlová, J.; Mayar, S.; Krska, R. Worldwide contamination of food-crops with mycotoxins: Validity of the widely cited 'FAO estimate' of 25 %. *Crit. Rev. Food Sci. Nutr.* **2020**, *60*, 2773–2789. [CrossRef]
61. Schöneberg, T.; Jenny, E.; Wettstein, F.E.; Bucheli, T.D.; Mascher, F.; Bertossa, M.; Musa, T.; Seifert, K.; Gräfenhan, T.; Keller, B.; et al. Occurrence of Fusarium species and mycotoxins in Swiss oats—Impact of cropping factors. *Eur. J. Agron.* **2018**, *92*, 123–132. [CrossRef]
62. Gao, X.; Mu, P.; Wen, J.; Sun, Y.; Chen, Q.; Deng, Y. Detoxification of trichothecene mycotoxins by a novel bacterium, *Eggerthella* sp. DII-9. *Food Chem. Toxicol.* **2018**, *112*, 310–319. [CrossRef]
63. Zhang, J.; You, L.; Wu, W.; Wang, X.; Chrienova, Z.; Nepovimova, E.; Wu, Q.; Kuca, K. The neurotoxicity of trichothecenes T-2 toxin and deoxynivalenol (DON): Current status and future perspectives. *Food Chem. Toxicol.* **2020**, *145*, 111676. [CrossRef]
64. Piacentini, K.C.; Rocha, L.O.; Savi, G.D.; Carnielli-Queiroz, L.; Almeida, F.G.; Minella, E.; Corrêa, B. Occurrence of deoxynivalenol and zearalenone in brewing barley grains from Brazil. *Mycotoxin Res.* **2018**, *34*, 173–178. [CrossRef]
65. dos Santos, J.S.; Souza, T.M.; Ono, E.Y.S.; Hashimoto, E.H.; Bassoi, M.C.; de Miranda, M.Z.; Itano, E.N.; Kawamura, O. Natural occurrence of deoxynivalenol in wheat from Paraná State, Brazil and estimated daily intake by wheat products. *Food Chem.* **2013**, *138*, 90–95. [CrossRef]
66. Bracarense, A.-P.F.L.; Lucioli, J.; Grenier, B.; Pacheco, G.D.; Moll, W.-D.; Schatzmayr, G.; Oswald, I.P. Chronic ingestion of deoxynivalenol and fumonisin, alone or in interaction, induces morphological and immunological changes in the intestine of piglets. *Br. J. Nutr.* **2012**, *107*, 1776–1786. [CrossRef]
67. Bonnighausen, J.; Schauer, N.; Schafer, W.; Bormann, J. Metabolic profiling of wheat rachis node infection by *Fusarium graminearum*—Decoding deoxynivalenol-dependent susceptibility. *New Phytol.* **2019**, *221*, 459–469. [CrossRef]
68. Skiepko, N.; Przybylska-Gornowicz, B.; Gajecka, M.; Gajecki, M.; Lewczuk, B. Effects of Deoxynivalenol and Zearalenone on the Histology and Ultrastructure of Pig Liver. *Toxins* **2020**, *12*, 463. [CrossRef]
69. Ji, F.; He, D.; Olaniran, A.O.; Mokoena, M.P.; Xu, J.; Shi, J. Occurrence, toxicity, production and detection of *Fusarium mycotoxin*: A review. *Food Prod. Process. Nutr.* **2019**, *1*, 6. [CrossRef]
70. Frizzell, C.; Uhlig, S.; Miles, C.O.; Verhaegen, S.; Elliott, C.T.; Eriksen, G.S.; Sørlie, M.; Ropstad, E. Toxicology in Vitro Biotransformation of zearalenone and zearalenols to their major glucuronide metabolites reduces estrogenic activity. *Toxicol. In Vitro* **2015**, *29*, 575–581. [CrossRef]
71. Król, A.; Pomastowski, P.; Rafi, K.; Walczak, J. Microbiology neutralization of zearalenone using *Lactococcus lactis* and *Bifidobacterium* sp. *Anal. Bioanal. Chem.* **2018**, *410*, 943–952. [CrossRef]
72. Hueza, I.M.; Raspantini, P.C.F.; Raspantini, L.E.R.; Latorre, A.O.; Górniak, S.L. Zearalenone, an estrogenic mycotoxin, is an immunotoxic compound. *Toxins* **2014**, *6*, 1080–1095. [CrossRef] [PubMed]
73. Molina-Molina, J.-M.; Real, M.; Jimenez-Diaz, I.; Belhassen, H.; Hedhili, A.; Torné, P.; Fernández, M.F.; Olea, N. Assessment of estrogenic and anti-androgenic activities of the mycotoxin zearalenone and its metabolites using in vitro receptor-specific bioassays. *Food Chem. Toxicol.* **2014**, *74*, 233–239. [CrossRef] [PubMed]
74. Cao, H.; Zhi, Y.; Xu, H.; Fang, H.; Jia, X. Zearalenone causes embryotoxicity and induces oxidative stress and apoptosis in differentiated human embryonic stem cells. *Toxicol. In Vitro* **2019**, *54*, 243–250. [CrossRef]
75. Rogowska, A.; Pomastowski, P.; Sagandykova, G.; Buszewski, B. Zearalenone and its metabolites: Effect on human health, metabolism and neutralisation methods. *Toxicon* **2019**, *162*, 46–56. [CrossRef] [PubMed]
76. Keller, L.; Abrunhosa, L.; Keller, K.; Rosa, C.A.; Cavaglieri, L.; Venâncio, A. Zearalenone and Its Derivatives α-Zearalenol and β-Zearalenol Decontamination by *Saccharomyces cerevisiae* Strains Isolated from Bovine Forage. *Toxins* **2015**, *7*, 3297–3308. [CrossRef]
77. Schrenk, D.; Bodin, L.; Chipman, J.K.; Del Mazo, J.; GraslKraupp, B.; Hogstrand, C.; Hoogenboom, L.; Leblanc, J.-C.; Nebbia, C.S. Risk assessment of ochratoxin A in food. *EFSA J.* **2020**, *18*, 150.
78. Abbès, S.; Ben Salah-Abbès, J.; Jebali, R.; Younes, R.B.; Oueslati, R. Interaction of aflatoxin B1 and fumonisin B1 in mice causes immunotoxicity and oxidative stress: Possible protective role using lactic acid bacteria. *J. Immunotoxicol.* **2016**, *13*, 46–54. [CrossRef]
79. Hamid, A.S.; Tesfamariam, I.G. Aflatoxin B1-induced hepatocellular carcinoma in developing countries: Geographical distribution, mechanism of action and prevention (Review). *Oncol. Lett.* **2013**, *5*, 1087–1092. [CrossRef]
80. Xiulan, S.; Xiaolian, Z.; Jian, T.; Zhou, J.; Chu, F.S. Preparation of gold-labeled antibody probe and its use in immunochromatography assay for detection of aflatoxin B1. *Int. J. Food Microbiol.* **2005**, *99*, 185–194. [CrossRef]
81. Morales, H.; Sanchis, V.; Usall, J.; Ramos, A.J.; Marín, S. Effect of biocontrol agents *Candida sake* and *Pantoea agglomerans* on *Penicillium expansum* growth and patulin accumulation in apples. *Int. J. Food Microbiol.* **2008**, *122*, 61–67. [CrossRef]
82. Jayashree, G.V.; Krupashree, K.; Rachitha, P.; Khanum, F. Patulin Induced Oxidative Stress Mediated Apoptotic Damage in Mice, and its Modulation by Green Tea Leaves. *J. Clin. Exp. Hepatol.* **2017**, *7*, 127–134. [CrossRef]

83. Terezinha, F.; Melo, D.; Marques, I.; Greggio, S.; Dacosta, J.C.; Guecheva, T.N.; Saffi, J.; Rosa, R.M. DNA damage in organs of mice treated acutely with patulin, a known mycotoxin. *Food Chem. Toxicol.* **2012**, *50*, 3548–3555.
84. Saxena, N.; Ansari, K.M.; Kumar, R.; Chaudhari, B.P.; Dwivedi, P.D.; Das, M. Role of mitogen activated protein kinases in skin tumorigenicity of Patulin. *Toxicol. Appl. Pharmacol.* **2011**, *257*, 264–271. [CrossRef]
85. Drusch, S.; Kopka, S.; Kaeding, J. Stability of patulin in a juice-like aqueous model system in the presence of ascorbic acid. *Food Chem.* **2007**, *100*, 192–197. [CrossRef]
86. De Curtis, F.; de Felice, D.V.; Ianiri, G.; De Cicco, V.; Castoria, R. Environmental factors affect the activity of biocontrol agents against ochratoxigenic *Aspergillus carbonarius* on wine grape. *Int. J. Food Microbiol.* **2012**, *159*, 17–24. [CrossRef]
87. Paradells, S.; Rocamonde, B.; Llinares, C.; Garcia-verdugo, J.M.; Zipancic, I.; Miguel, J. Neurotoxic effects of ochratoxin A on the subventricular zone of adult mouse brain. *J. Apply Toxicol.* **2015**, 737–751. [CrossRef]
88. Wang, L.; Liao, Y.; Peng, Z.; Chen, L.; Zhang, W.; Nüssler, A.K.; Shi, S.; Liu, L.; Yang, W. Food raw materials and food production occurrences of deoxynivalenol in different regions. *Trends Food Sci. Technol.* **2019**, *83*, 41–52. [CrossRef]
89. Feizollahi, E.; Iqdiam, B.; Vasanthan, T.; Thilakarathna, M.S.; Roopesh, M.S. Effects of Atmospheric-Pressure Cold Plasma Treatment on Deoxynivalenol Degradation, Quality Parameters, and Germination of Barley Grains. *Appl. Sci.* **2020**, *10*, 3530. [CrossRef]
90. Chen, D.; Chen, P.; Cheng, Y.; Peng, P.; Liu, J.; Ma, Y.; Liu, Y.; Ruan, R. Deoxynivalenol Decontamination in Raw and Germinating Barley Treated by Plasma-Activated Water and Intense Pulsed Light. *Food Bioprocess Technol.* **2019**, *12*, 246–254. [CrossRef]
91. Wang, G.; Yu, M.; Dong, F.; Shi, J.; Xu, J. Esterase activity inspired selection and characterization of zearalenone degrading bacteria *Bacillus pumilus* ES-21. *Food Control* **2017**, *77*, 57–64. [CrossRef]
92. Abbasian, N.; Momtaz, S.; Baeeri, M.; Navaei-nigjeh, M. Molecular and biochemical evidence on the role of zearalenone in rat polycystic ovary. *Toxicon* **2018**, *154*, 7–14. [CrossRef] [PubMed]
93. Muthulakshmi, S.; Maharajan, K.; Habibi, H.R.; Kadirvelu, K.; Venkataramana, M. Zearalenone induced embryo and neurotoxicity in zebra fish model (*Danio rerio*): Role of oxidative stress revealed by a multi biomarker study. *Chemosphere* **2018**, *198*, 111–121. [CrossRef] [PubMed]
94. Antonissen, G.; Devreese, M.; De Baere, S.; Martel, A.; Van Immerseel, F.; Croubels, S. Impact of Fusarium mycotoxins on hepatic and intestinal mRNA expression of cytochrome P450 enzymes and drug transporters, and on the pharmacokinetics of oral enrofloxacin in broiler chickens. *Food Chem. Toxicol.* **2017**, *101*, 75–83. [CrossRef] [PubMed]
95. Chuturgoon, A.; Phulukdaree, A.; Moodley, D. Fumonisin B1 induces global DNA hypomethylation in HepG2 cells—An alternative mechanism of action. *Toxicology* **2014**, *315*, 65–69. [CrossRef] [PubMed]
96. Demirel, G.; Alpertunga, B.; Ozden, S. Role of fumonisin B1 on DNA methylation changes in rat kidney and liver cells. *Pharm. Biol.* **2015**, *53*, 1302–1310. [CrossRef]
97. Sadiq, F.A.; Yan, B.; Tian, F.; Zhao, J. Lactic Acid Bacteria as Antifungal and Anti-Mycotoxigenic Agents: A Comprehensive Review. *Compr. Rev. Food Sci. Food Saf.* **2019**, *18*, 1403–1436. [CrossRef]
98. Akbar, A.; Khan, G.I.; Shafee, M.; Samad, A.; Masood, H.; Khan, S.A. Biocontrol of Aflatoxin through Biodegradation by Using Environment Friendly Microbes. *Pol. J. Environ. Stud.* **2022**, *31*, 4985–4988. [CrossRef]
99. Li, J.; Huang, J.; Jin, Y.; Wu, C.; Shen, D.; Zhang, S.; Zhou, R. Aflatoxin B1 degradation by salt tolerant *Tetragenococcus halophilus* CGMCC 3792. *Food Chem. Toxicol.* **2018**, *121*, 430–436. [CrossRef]
100. Teniola, O.; Addo, P.; Brost, I.; Farber, P.; Jany, K.; Alberts, J.; Vanzyl, W.; Steyn, P.; Holzapfel, W. Degradation of aflatoxin B1 by cell-free extracts of *Rhodococcus erythropolis* and *Mycobacterium fluoranthenivorans* sp. nov. DSM44556. *Int. J. Food Microbiol.* **2005**, *105*, 111–117. [CrossRef]
101. Abrunhosa, L.; Inês, A.; Rodrigues, A.I.; Guimarães, A.; Pereira, V.L.; Parpot, P.; Mendes-Faia, A.; Venâncio, A. Biodegradation of ochratoxin A by *Pediococcus parvulus* isolated from Douro wines. *Int. J. Food Microbiol.* **2014**, *188*, 45–52. [CrossRef]
102. Fuchs, S.; Sontag, G.; Stidl, R.; Ehrlich, V.; Kundi, M.; Knasmüller, S. Detoxification of patulin and ochratoxin A, two abundant mycotoxins, by lactic acid bacteria. *Food Chem. Toxicol.* **2008**, *46*, 1398–1407. [CrossRef]
103. Wochner, K.F.; Moreira, M.C.C.; Kalschne, D.L.; Drunkler, D.A. Detoxification of Aflatoxin B1 and M1 by *Lactobacillus acidophilus* and prebiotics in whole cow's milk. *J. Food Saf.* **2019**, *39*, e12670. [CrossRef]
104. Marina, S.; Sajid, M.; Yahong, Y.; Tianli, Y. Mycotoxin patulin in food matrices: Occurrence and its biological degradation strategies. *Drug Metab. Rev.* **2019**, *51*, 105–120.
105. Tan, H.; Zhang, Z.; Hu, Y.; Wu, L.; Liao, F.; He, J.; Luo, B.; He, Y.; Zuo, Z.; Ren, Z.; et al. Isolation and characterization of Pseudomonas otitidis TH-N1 capable of degrading zearalenone. *Food Control* **2015**, *47*, 285–290. [CrossRef]
106. Guo, Y.; Zhou, J.; Tang, Y.; Ma, Q.; Zhang, J.; Ji, C.; Zhao, L. Characterization and Genome Analysis of a Zearalenone—Degrading *Bacillus velezensis* Strain ANSB01E. *Curr. Microbiol.* **2019**, *77*, 273–278. [CrossRef]
107. Wang, Y.; Zhao, C.; Zhang, D.; Zhao, M.; Zheng, D.; Lyu, Y.; Cheng, W.; Guo, P.; Cui, Z. Effective degradation of aflatoxin B1 using a novel thermophilic microbial consortium TADC7. *Bioresour. Technol.* **2017**, *224*, 166–173. [CrossRef]
108. El-Nezami, H.; Kankaanpaa, P.; Salminen, S.; Ahokas, J. Ability of dairy strains of lactic acid bacteria to bind a common food carcinogen, aflatoxin B1. *Food Chem. Toxicol.* **1998**, *36*, 321–326. [CrossRef]
109. Farzaneh, M.; Shi, Z.-Q.; Ghassempour, A.; Sedaghat, N.; Ahmadzadeh, M.; Mirabolfathy, M.; Javan-Nikkhah, M. Aflatoxin B1 degradation by *Bacillus subtilis* UTBSP1 isolated from pistachio nuts of Iran. *Food Control* **2012**, *23*, 100–106. [CrossRef]

110. Topcu, A.; Bulat, T.; Wishah, R.; BoyacI, I.H. Detoxification of aflatoxin B1 and patulin by *Enterococcus faecium* strains. *Int. J. Food Microbiol.* **2010**, *139*, 202–205. [CrossRef]
111. Wang, Y.; Zhao, C.; Zhang, D.; Zhao, M.; Zheng, D.; Peng, M.; Cheng, W.; Guo, P.; Cui, Z. Simultaneous degradation of aflatoxin B1 and zearalenone by a microbial consortium. *Toxicon* **2018**, *146*, 69–76. [CrossRef]
112. Juodeikiene, G.; Bartkiene, E.; Cernauskas, D.; Cizeikiene, D.; Zadeike, D.; Lele, V.; Bartkevics, V. Antifungal activity of lactic acid bacteria and their application for *Fusarium mycotoxin* reduction in malting wheat grains. *LWT—Food Sci. Technol.* **2018**, *89*, 307–314. [CrossRef]
113. Bartkiene, E.; Zavistanaviciute, P.; Lele, V.; Ruzauskas, M.; Bartkevics, V.; Bernatoniene, J.; Gallo, P.; Tenore, G.C.; Santini, A. Lactobacillus plantarum LUHS135 and paracasei LUHS244 as functional starter cultures for the food fermentation industry: Characterisation, mycotoxin-reducing properties, optimisation of biomass growth and sustainable encapsulation by using dairy by-produc. *LWT* **2018**, *93*, 649–658. [CrossRef]
114. Zheng, R.; Qing, H.; Ma, Q.; Huo, X.; Huang, S.; Zhao, L.; Zhang, J.; Ji, C. A Newly Isolated Alcaligenes faecalis ANSA176 with the Capability of Alleviating Immune Injury and Inflammation through Efficiently Degrading Ochratoxin A. *Toxins* **2022**, *14*, 569. [CrossRef] [PubMed]
115. Hormisch, D.; Brost, I.; Kohring, G.-W.; Giffhorn, F.; Kroppenstedt, R.; Stackebradt, E.; Färber, P.; Holzapfel, W. *Mycobacterium fluoranthenivorans* sp. nov., a Fluoranthene and Aflatoxin B1 Degrading Bacterium from Contaminated Soil of a Former Coal Gas Plant. *Syst. Appl. Microbiol.* **2004**, *27*, 653–660. [CrossRef] [PubMed]
116. Mwakinyali, S.E.; Ming, Z.; Xie, H.; Zhang, Q.; Li, P. Investigation and Characterization of *Myroides odoratimimus* Strain 3J2MO Aflatoxin B_1 Degradation. *J. Agric. Food Chem.* **2019**, *67*, 4595–4602. [CrossRef]
117. Adebo, O.A.; Njobeh, P.B.; Mavumengwana, V. Degradation and detoxification of AFB1 by *Staphylococcus warneri*, *Sporosarcina* sp. and *Lysinibacillus fusiformis*. *Food Control* **2016**, *68*, 92–96. [CrossRef]
118. Adebo, O.A.; Njobeh, P.B.; Sidu, S.; Adebiyi, J.A.; Mavumengwana, V. Aflatoxin B1 degradation by culture and lysate of a Pontibacter specie. *Food Control* **2017**, *80*, 99–103. [CrossRef]
119. Elsanhoty, R.M.; Ramadan, M.F.; El-Gohery, S.S.; Abol-Ela, M.F.; Azeke, M.A. Ability of selected microorganisms for removing aflatoxins invitro and fate of aflatoxins in contaminated wheat during baladi bread baking. *Food Control* **2013**, *33*, 287–292. [CrossRef]
120. Alberts, J.F.; Engelbrecht, Y.; Steyn, P.S.; Holzapfel, W.H.; van Zyl, W.H. Biological degradation of aflatoxin B1 by *Rhodococcus erythropolis* cultures. *Int. J. Food Microbiol.* **2006**, *109*, 121–126. [CrossRef]
121. Mosallaie, F.; Jooyandeh, H.; Hojjati, M.; Fazlara, A. Biological reduction of aflatoxin B1 in yogurt by probiotic strains of *Lactobacillus acidophilus* and *Lactobacillus rhamnosus*. *Food Sci. Biotechnol.* **2020**, *29*, 793–803. [CrossRef]
122. Xu, J.; Wang, H.; Zhu, Z.; Ji, F.; Yin, X.; Hong, Q.; Shi, J. Isolation and characterization of *Bacillus amyloliquefaciens* ZDS-1: Exploring the degradation of Zearalenone by *Bacillus* spp. *Food Control* **2016**, *68*, 244–250. [CrossRef]
123. He, W.-J.; Yuan, Q.-S.; Zhang, Y.-B.; Guo, M.-W.; Gong, A.-D.; Zhang, J.-B.; Wu, A.-B.; Huang, T.; Qu, B.; Li, H.-P.; et al. Aerobic De-Epoxydation of Trichothecene Mycotoxins by a Soil Bacterial Consortium Isolated Using In Situ. *Toxins* **2016**, *8*, 277. [CrossRef] [PubMed]
124. Mokoena, M.P.; Chelule, P.K. Reduction of Fumonisin B1 and Zearalenone by Lactic Acid Bacteria in Fermented Maize Meal. *J. Food Prot.* **2005**, *68*, 2095–2099. [CrossRef] [PubMed]
125. Liu, F.; Malaphan, W.; Xing, F.; Yu, B. Biodetoxification of fungal mycotoxins zearalenone by engineered probiotic bacterium *Lactobacillus reuteri* with surface-displayed lactonohydrolase. *Appl. Microbiol. Biotechnol.* **2019**, *103*, 8813–8824. [CrossRef] [PubMed]
126. Papp, L.A.; Horváth, E.; Peles, F.; Pócsi, I.; Miklós, I. Insight into Yeast—Mycotoxin Relations. *Agriculture* **2021**, *11*, 1291. [CrossRef]
127. Cao, H.; Liu, D.; Mo, X.; Xie, C.; Yao, D. A fungal enzyme with the ability of aflatoxin B1 conversion: Purification and ESI-MS/MS identification. *Microbiol. Res.* **2011**, *166*, 475–483. [CrossRef]
128. Yang, Q.; Ma, J.; Solairaj, D.; Fu, Y.; Zhang, H. Efficacy of Meyerozyma guilliermondii in controlling patulin production by Penicillium expansum in shuijing pears. *Biol. Control* **2022**, *168*, 104856. [CrossRef]
129. Bejaoui, H.; Mathieu, F.; Taillandier, P.; Lebrihi, A. Ochratoxin A removal in synthetic and natural grape juices by selected oenological *Saccharomyces* strains. *J. Appl. Microbiol.* **2004**, *97*, 1038–1044. [CrossRef]
130. Petruzzi, L.; Bevilacqua, A.; Baiano, A.; Beneduce, L.; Corbo, M.R.; Sinigaglia, M. Study of *Saccharomyces cerevisiae* W13 as a functional starter for the removal of ochratoxin A. *Food Control* **2014**, *35*, 373–377. [CrossRef]
131. Campagnollo, F.B.; Franco, L.T.; Rottinghaus, G.E.; Kobashigawa, E.; Ledoux, D.R.; Daković, A.; Oliveira, C.A. In vitro evaluation of the ability of beer fermentation residue containing *Saccharomyces cerevisiae* to bind mycotoxins. *Food Res. Int.* **2015**, *77*, 643–648. [CrossRef]
132. Ul Hassan, Z.; Al Thani, R.; Atia, F.A.; Alsafran, M.; Migheli, Q.; Jaoua, S. Application of yeasts and yeast derivatives for the biological control of toxigenic fungi and their toxic metabolites. *Environ. Technol. Innov.* **2021**, *22*, 101447. [CrossRef]
133. Pizzolitto, R.P.; Salvano, M.A.; Dalcero, A.M. Analysis of fumonisin B1 removal by microorganisms in co-occurrence with aflatoxin B1 and the nature of the binding process. *Int. J. Food Microbiol.* **2012**, *156*, 214–221. [CrossRef]
134. Luo, Y.; Liu, X.; Yuan, L.; Li, J. Complicated interactions between bio-adsorbents and mycotoxins during mycotoxin adsorption: Current research and future prospects. *Trends Food Sci. Technol.* **2020**, *96*, 127–134. [CrossRef]

135. Ponsone, M.L.; Chiotta, M.L.; Combina, M.; Dalcero, A.; Chulze, S. Biocontrol as a strategy to reduce the impact of ochratoxin A and Aspergillus section Nigri in grapes. *Int. J. Food Microbiol.* **2011**, *151*, 70–77. [CrossRef]
136. Fiori, S.; Paolo, P.; Hammami, W.; Razzu, S.; Jaoua, S.; Migheli, Q. International Journal of Food Microbiology Biocontrol activity of four non- and low-fermenting yeast strains against Aspergillus carbonarius and their ability to remove ochratoxin A from grape juice. *Int. J. Food Microbiol.* **2014**, *189*, 45–50. [CrossRef]
137. Meca, G.; Ritieni, A.; Zhou, T.; Li, X.Z.; Mañes, J. Degradation of the minor Fusarium mycotoxin beauvericin by intracellular enzymes of *Saccharomyces cerevisiae*. *Food Control* **2013**, *33*, 352–358. [CrossRef]
138. Zhu, R.; Feussner, K.; Wu, T.; Yan, F.; Karlovsky, P.; Zheng, X. Detoxification of mycotoxin patulin by the yeast *Rhodosporidium paludigenum*. *Food Chem.* **2015**, *179*, 1–5. [CrossRef]
139. Li, J.; Huang, J.; Jin, Y.; Wu, C.; Shen, D.; Zhang, S.; Zhou, R. Mechanism and kinetics of degrading aflatoxin B1 by salt tolerant Candida versatilis CGMCC 3790. *J. Hazard. Mater.* **2018**, *359*, 382–387. [CrossRef]
140. Varga, J.; Péteri, Z.; Tábori, K.; Téren, J.; Vágvölgyi, C. Degradation of ochratoxin A and other mycotoxins by *Rhizopus* isolates. *Int. J. Food Microbiol.* **2005**, *99*, 321–328. [CrossRef]
141. Bdswald, C.; Engelhardt, G.; Vogel, H.; Wallnofer, P.R. Metabolism of the Fusatium Mycotoxins Zearalenone and Deoxynivalenol by Yeast Strains of Technological Relevance. *Nat. Toxins* **1995**, *3*, 138–144. [CrossRef]
142. Loi, M.; Fanelli, F.; Cimmarusti, M.T.; Mirabelli, V.; Haidukowski, M.; Logrieco, A.F.; Caliandro, R.; Mule, G. In vitro single and combined mycotoxins degradation by Ery4 laccase from *Pleurotus eryngii* and redox mediators. *Food Control* **2018**, *90*, 401–406. [CrossRef]
143. Wang, J.; Ogata, M.; Hirai, H.; Kawagishi, H. Detoxification of aflatoxin B1 by manganese peroxidase from the white-rot fungus Phanerochaete sordida YK-624. *FEMS Microbiol. Lett.* **2011**, *314*, 164–169. [CrossRef] [PubMed]
144. Zeinvand-Lorestani, H.; Sabzevari, O.; Setayesh, N.; Amini, M.; Nili-Ahmadabadi, A.; Faramarzi, M.A. Comparative study of in vitro prooxidative properties and genotoxicity induced by aflatoxin B1 and its laccase-mediated detoxification products. *Chemosphere* **2015**, *135*, 1–6. [CrossRef] [PubMed]
145. Chang, X.; Wu, Z.; Wu, S.; Dai, Y.; Sun, C. Degradation of ochratoxin A by Bacillus amyloliquefaciens ASAG1. *Food Addit. Contam. Part A* **2015**, *32*, 564–571. [CrossRef]
146. Abrunhosa, L.; Santos, L.; Venâncio, A. Degradation of ochratoxin A by proteases and by a crude enzyme of Aspergillus niger. *Food Biotechnol.* **2006**, *20*, 231–242. [CrossRef]
147. Xiao, Y.; Liu, B.; Wang, Z.; Han, C.; Meng, X.; Zhang, F. Effective degradation of the mycotoxin patulin in pear juice by porcine pancreatic lipase. *Food Chem. Toxicol.* **2019**, *133*, 110769. [CrossRef]
148. Tang, H.; Li, X.; Zhang, F.; Meng, X.; Liu, B. Biodegradation of the mycotoxin patulin in apple juice by Orotate phosphoribosyltransferase from Rhodotorula mucilaginosa. *Food Control* **2019**, *100*, 158–164. [CrossRef]
149. Alberts, J.F.; Gelderblom, W.C.A.; Botha, A.; van Zyl, W.H. Degradation of aflatoxin B1 by fungal laccase enzymes. *Int. J. Food Microbiol.* **2009**, *135*, 47–52. [CrossRef]
150. Afsharmanesh, H.; Perez-Garcia, A.; Zeriouh, H.; Ahmadzadeh, M.; Romero, D. Aflatoxin degradation by *Bacillus subtilis* UTB1 is based on production of an oxidoreductase involved in bacilysin biosynthesis. *Food Control* **2018**, *94*, 48–55. [CrossRef]
151. Samuel, M.S.; Sivaramakrishna, A.; Mehta, A. Degradation and detoxification of aflatoxin B1 by *Pseudomonas putida*. *Int. Biodeterior. Biodegrad.* **2014**, *86*, 202–209. [CrossRef]
152. Ianiri, G.; Pinedo, C.; Fratianni, A.; Panfili, G.; Castoria, R. Patulin degradation by the biocontrol yeast *Sporobolomyces* sp. Is an inducible process. *Toxins* **2017**, *9*, 61. [CrossRef]
153. Young, J.C.; Zhou, T.; Yu, H.; Zhu, H.; Gong, J. Degradation of trichothecene mycotoxins by chicken intestinal microbes. *Food Chem. Toxicol.* **2007**, *45*, 136–143. [CrossRef]
154. Koch, M.; Maul, R.; Brodehl, A.; Anne, M. Biotransformation of the mycotoxin zearalenone by fungi of the genera Rhizopus and Aspergillus. *FEMS Microbiol. Lett.* **2014**, *359*, 124–130.
155. Kollarczik, B.; Gareis, M.; Hanelt, M. In Vitro Transformation of the Fusarium Mycotoxins Deoxynivalenol and ZearaLenone by the Normal Gut Microflora of Pigs. *Nat. Toxins* **1994**, *2*, 105–110. [CrossRef]
156. Péteri, Z.; Téren, J.; Vágvölgyi, C.; Varga, J. Ochratoxin degradation and adsorption caused by astaxanthin-producing yeasts. *Food Microbiol.* **2007**, *24*, 205–210. [CrossRef]
157. Zheng, X.; Li, Y.; Zhang, H.; Apaliya, M.T.; Zhang, X.; Zhao, L.; Jiang, Z.; Yang, Q.; Gu, X. Identification and toxicological analysis of products of patulin degradation by *Pichia caribbica*. *Biol. Control* **2018**, *123*, 127–136. [CrossRef]
158. Taheur, F.B.; Fedhila, K.; Chaieb, K.; Kouidhi, B.; Bakhrouf, A.; Abrunhosa, L. Adsorption of aflatoxin B1, zearalenone and ochratoxin A by microorganisms isolated from Kefir grains. *Int. J. Food Microbiol.* **2017**, *251*, 1–7. [CrossRef]
159. Elsanhoty, R.M.; Salam, S.A.; Ramadan, M.F.; Badr, F.H. Detoxification of aflatoxin M1 in yoghurt using probiotics and lactic acid bacteria. *Food Control* **2014**, *43*, 129–134. [CrossRef]
160. Abdolshahi, A.; Tabatabaie Yazdi, F.; Shabani, A.A.; Mortazavi, S.A.; Marvdashti, L.M. Aflatoxin binding efficiency of Saccharomyces cerevisiae mannoprotein in contaminated pistachio nuts. *Food Control* **2018**, *87*, 17–21. [CrossRef]
161. Alekinejad, H.M.; Franciscus, R.; Akker, M.A.A.S.; Remmels, J.F.I.N.K. Bioactivation of zearalenone by porcine hepatic biotransformation. *Vet. Res.* **2005**, *36*, 799–810. [CrossRef]

162. Liang, Y.-F.; Zhou, X.-W.; Wang, F.; Shen, Y.-D.; Xiao, Z.-L.; Zhang, S.-W.; Li, Y.-J.; Wang, H. Development of a Monoclonal Antibody-Based ELISA for the Detection of Alternaria Mycotoxin Tenuazonic Acid in Food Samples. *Food Anal. Methods* **2020**, *13*, 1594–1602. [CrossRef]
163. Zhao, L.; Guan, S.; Gao, X.; Ma, Q.; Lei, Y.; Bai, X.; Ji, C. Preparation, purification and characteristics of an aflatoxin degradation enzyme from Myxococcus fulvus ANSM068. *J. Appl. Microbiol.* **2010**, *110*, 147–155. [CrossRef] [PubMed]
164. Motomura, M.; Toyomasu, T.; Mizuno, K.; Shinozawa, T. Purification and characterization of an aflatoxin degradation enzyme from *Pleurotus ostreatus*. *Microbiol. Res.* **2003**, *158*, 237–242. [CrossRef] [PubMed]
165. Tang, H.; Peng, X.; Li, X.; Meng, X.; Liu, B. Biodegradation of mycotoxin patulin in apple juice by calcium carbonate immobilized porcine pancreatic lipase. *Food Control* **2018**, *88*, 69–74. [CrossRef]
166. Medina, A.; Mohale, S.; Samsudin, N.I.P.; Rodriguez-Sixtos, A.; Rodriguez, A.; Magan, N. Biocontrol of mycotoxins: Dynamics and mechanisms of action. *Curr. Opin. Food Sci.* **2017**, *17*, 41–48. [CrossRef]
167. Illueca, F.; Vila-Donat, P.; Calpe, J.; Luz, C.; Meca, G.; Quiles, J.M. Antifungal activity of biocontrol agents in vitro and potential application to reduce mycotoxins (Aflatoxin B1 and ochratoxin A). *Toxins* **2021**, *13*, 752. [CrossRef]
168. Zapasnik, A.; Sokołowska, B.; Bryła, M. Role of Lactic Acid Bacteria in Food Preservation and Safety. *Foods* **2022**, *11*, 1283. [CrossRef]
169. Yao, M.; Wu, J.; Li, B.; Xiao, H.; McClements, D.J.; Li, L. Microencapsulation of Lactobacillus salivarious Li01 for enhanced storage viability and targeted delivery to gut microbiota. *Food Hydrocoll.* **2017**, *72*, 228–236. [CrossRef]
170. Wang, M.; Yang, J.; Li, M.; Wang, Y.; Wu, H.; Xiong, L.; Sun, Q. Enhanced viability of layer-by-layer encapsulated *Lactobacillus pentosus* using chitosan and sodium phytate. *Food Chem.* **2019**, *285*, 260–265. [CrossRef]
171. Alehosseini, A.; Sarabi-jamab, M.; Ghorani, B.; Kadkhodaee, R. Electro-encapsulation of Lactobacillus casei in high-resistant capsules of whey protein containing transglutaminase enzyme. *LWT—Food Sci. Technol.* **2019**, *102*, 150–158. [CrossRef]
172. Tapingkae, W.; Srinual, O.; Lumsangkul, C.; Van Doan, H.; Chiang, H.-I.; Manowattana, A.; Boonchuay, P.; Chaiyaso, T. Industrial-Scale Production of Mycotoxin Binder from the Red Yeast Sporidiobolus pararoseus KM281507. *J. Fungi* **2022**, *8*, 353. [CrossRef]
173. Hynes, R.K.; Boyetchko, S.M. Research initiatives in the art and science of biopesticide formulations. *Soil Biol. Biochem.* **2006**, *38*, 845–849. [CrossRef]
174. Nešić, K.; Habschied, K.; Mastanjević, K. Possibilities for the Biological Control of Mycotoxins in Food and Feed. *Toxins* **2021**, *13*, 198. [CrossRef]
175. Chen, W.C.; Chiou, T.Y.; Delgado, A.L.; Liao, C.S. The control of rice blast disease by the novel biofungicide formulations. *Sustainability* **2019**, *11*, 3449. [CrossRef]
176. Zamoum, M.; Allali, K.; Benadjila, A.; Zitouni, A.; Goudjal, Y. Formulation of biofungicides based on *Streptomyces lincolnensis* strain SZ03 spores and efficacy against R. solani damping-off of tomato seedlings. *ResearchSquare* **2022**, 1–22. [CrossRef]
177. Mousumi Das, M.; Aguilar, C.N.; Haridas, M.; Sabu, A. Production of bio-fungicide, Trichoderma harzianum CH1 under solid-state fermentation using coffee husk. *Bioresour. Technol. Rep.* **2021**, *15*, 100708. [CrossRef]
178. Sudantha, I.M.; Suwardji, S. Trichoderma biofungicides formulations on shallot growth, yield and fusarium wilt disease resistance. *IOP Conf. Ser. Earth Environ. Sci.* **2021**, *824*, 12032. [CrossRef]
179. Souza, P.M.D.; Magalhães, P.D.O. Application of microbial α-amylase in industry—A review. *Braz. J. Microbiol.* **2010**, *41*, 850–861. [CrossRef]

toxins

MDPI

Article

Deoxynivalenol Biosynthesis in *Fusarium pseudograminearum* Significantly Repressed by a Megabirnavirus

Ke Li [1,†], Dongmei Liu [2,†], Xin Pan [1], Shuwei Yan [1], Jiaqing Song [1], Dongwei Liu [1], Zhifang Wang [1], Yuan Xie [1], Junli Dai [1], Jihong Liu [2], Honglian Li [1], Xiaoting Zhang [1,*] and Fei Gao [1,*]

[1] Department of Plant Protection, Henan Agricultural University, Zhengzhou 450002, China; mrleekk@126.com (K.L.); panxin241x@163.com (X.P.); yanshuwei0512@163.com (S.Y.); songjia-qing523@163.com (J.S.); ldw961225@163.com (D.L.); meretals@126.com (Z.W.); hnxieyuan@126.com (Y.X.); daijl666@126.com (J.D.); honglianli@sina.com (H.L.)

[2] Institute of Agricultural Quality Standards and Testing Technology, Henan Academy of Agricultural Sciences, Zhengzhou 450002, China; dongmeiliu80@163.com (D.L.); ljha3100@163.com (J.L.)

* Correspondence: zhangxiaoting@henau.edu.cn (X.Z.); gaofei@henan.edu.cn (F.G.)

† These authors contributed equally to this work.

Abstract: Deoxynivalenol (DON) is a mycotoxin widely detected in cereal products contaminated by *Fusarium*. Fusarium pseudograminearum megabirnavirus 1 (FpgMBV1) is a double-stranded RNA virus infecting *Fusarium pseudograminearum*. In this study, it was revealed that the amount of DON in *F. pseudograminearum* was significantly suppressed by FpgMBV1 through a high-performance liquid chromatography–tandem mass spectrometry (HPLC-MS/MS) assay. A total of 2564 differentially expressed genes were identified by comparative transcriptomic analysis between the FpgMBV1-containing *F. pseudograminearum* strain FC136-2A and the virus-free strain FC136-2A-V$^-$. Among them, 1585 genes were up-regulated and 979 genes were down-regulated. Particularly, the expression of 12 genes (*FpTRI1*, *FpTRI3*, *FpTRI4*, *FpTRI5*, *FpTRI6*, *FpTRI8*, *FpTRI10*, *FpTRI11*, *FpTRI12*, *FpTRI14*, *FpTRI15*, and *FpTRI101*) in the trichothecene biosynthetic (*TRI*) gene cluster was significantly down-regulated. Specific metabolic and transport processes and pathways including amino acid and lipid metabolism, ergosterol metabolic and biosynthetic processes, carbohydrate metabolism, and biosynthesis were regulated. These results suggest an unrevealing mechanism underlying the repression of DON and *TRI* gene expression by the mycovirus FpgMBV1, which would provide new methods in the detoxification of DON and reducing the yield loss in wheat.

Keywords: deoxynivalenol; *Fusarium pseudograminearum* megabirnavirus 1; mycoviruses; transcriptome

Key Contribution: The secondary metabolite and predominant mycotoxin deoxynivalenol (DON) of *Fusarium pseudograminearum* was significantly reduced by a megabirnavirus FpgMBV1. The expression of genes in the trichothecene biosynthetic (*TRI*) gene cluster was suppressed. These results provide an idea to detoxify of DON by directly using mycovirus FpgMBV1 or its regulation on related genes.

Citation: Li, K.; Liu, D.; Pan, X.; Yan, S.; Song, J.; Liu, D.; Wang, Z.; Xie, Y.; Dai, J.; Liu, J.; et al. Deoxynivalenol Biosynthesis in *Fusarium pseudograminearum* Significantly Repressed by a Megabirnavirus. *Toxins* **2022**, *14*, 503. https://doi.org/10.3390/toxins14070503

Received: 16 June 2022
Accepted: 15 July 2022
Published: 19 July 2022

1. Introduction

Fusarium is a genus of filamentous fungi ubiquitously existing in agricultural and natural ecosystems [1,2]. Some species in *Fusarium* cause diseases including wilts, blights, rots, and cankers on crops and some horticultural, ornamental, and forest plants [3,4]. Wheat crown rot (FCR), one of the most destructive wheat diseases worldwide, is caused by species in *Fusarium* [5]. The dominant causal agent of FCR is *F. pseudograminearum* [6–8]. The symptoms of FCR include dry seedlings at the seedling stage, browning and rot at the base of the stem at the adult stage, withered white ears at the filling stage, and shriveled grains at the harvest stage [9]. Besides the significant decrease in wheat yield, *F. pseudograminearum* produces a diverse array of toxic secondary metabolites including

mycotoxins [10,11]. Cereals contaminated with mycotoxins are unsuitable for food or feed [12,13]. The mycotoxins produced by *Fusarium* include trichothecenes, fumonisins, etc. The most common *Fusarium* mycotoxin is deoxynivalenol (DON), which causes the disease of emesis, oral lesions, dermatitis, and hemorrhaging in human and livestock [14,15]. The biosynthesis of DON starts from the cyclization of farnesyl pyrophosphate mediated by trichodiene synthases (encoded by *TRI5*) [16]. Then, multiple steps are followed by at least six additional enzymes encoded by *TRI4*, *TRI101*, *TRI11*, *TRI3*, *TRI1*, and *TRI8*. Moreover, two transcription factors, *TRI6* and *TRI10*; a transmembrane transporter, *TRI12;* and genes with unknown functions, *TRI9* and *TRI14,* may also be involved in DON biosynthesis and the virulence of *Fusarium* [17–21].

Mycoviruses are viruses hosted in fungi. They have been described in many fungal species. Some of the viruses are hypovirulence-related with an effect on reducing the virulence of the pathogenic fungi. Besides the hypovirulence effect, some mycoviruses have an influence on the cultivating features of host fungi including the morphology and development of the colonies and spores. For example, Cryphonectria hypovirus 1 (CHV1) decreased the pigmentation and spore production of *Cryphonectria parasitica* [22]. Sclerotinia sclerotiorum hypovirulence-associated DNA virus 1(SsHDV1) caused abnormal colony morphology and the reduction in colony growth and small sclerotia production to *Sclerotinia sclerotiorum* [23]. Rosellinia necatrix megabirnavirus 1 (RnMBV1) suppressed the growth and melanin biosynthesis in *Rosellinia* necatrix [24].

To date, 29 mycoviruses species have been reported in Fusarium spp. They belong to the families *Hypoviridae, Chrysoviridae, Totiviridae, Partitiviridae, Tymoviridae, Alternaviridae,* and *Megabirnaviridae* [25]. Among them, Fusarium graminearum virus 1 (FgV1) [26], Fusarium graminearum mycovirus-China 9 (FgV-ch9) [27], Fusarium graminearum hypovirus 2 (FgHV2) [28], and Fusarium pseudograminearum megabirnavirus 1 (FpgMBV1) were reported as hypovirulence-related viruses [29]. Hypovirulence-related viruses hosted in *F. graminearum*, specifically FgV1, FgV-ch9, and FgHV2, caused a significant reduction in the fungal vegetative growth [26–28]. FpgMBV1 hosted in *F. pseudograminearum* [29]. There were mild changes in the colony morphology and spore production, but significant reduction in the virulence of *F. pseudograminearum* to wheat caused by FpgMBV1 [30]. Moreover, there were two viruses in *F. graminearum*, FgV1 and Fusarium graminearum mycotymovirus 1 (FgMTV1/SX64), which were reported to have a reducing effect on the DON production. FgV1 had a hypovirulence effect on *F. graminearum*, while FgMTV1/SX64 had a mild effect on the virulence [26,31].

To reveal the mechanism underlying the regulation of mycoviruses on fungi, high-throughput mRNA sequencing (RNAseq) was applied. For instance, the differential expression of genes related to fungal metabolism, transcription, translation, and ribosomal RNA processing was shown to be related to FgV1 infection [32]. Host cell transport-related genes were down-regulated by Fusarium graminearum virus 3 (FgV3) [33]. Genes involved in RNA processing and ribosome transport assembly were down regulated during the infection of Fusarium graminearum virus 4 (FgV4) [33]. Genes related to glutamate metabolism, homoserine metabolism, cellular aldehyde metabolism, and lactate metabolism in *F. graminearum* were down-regulated by FgHV1 [34]. RNA silencing and virulence-related genes were considerably down-regulated in *S. sclerotiorum* strains infected by SsHADV-1 [35].

In this study, the DON production of the FpgMBV1-containing *F.* pseudograminearum strain was determined and compared with that of the virus-free strain by HPLC-MS/MS. The genome-wide transcriptional reprogramming in *F. pseudograminearum* under the infection of FpgMBV1 was outlined by RNA sequencing. Genes involved in the biosynthesis of DON and ergosterol and in RNA-silencing pathways were analyzed to unravel the interaction between FpgMBV1 and *F. pseudograminearum.* Data obtained in this study would provide a clue to the specific regulation mechanisms of mycovirus to DON biosynthesis and virulence of fungal pathogens including *Fusarium*.

2. Results

2.1. DON Synthesis Was Inhibited by Mycovirus FpgMBV1

To investigate the effect of FpgMBV1 on the content of DON in *F. pseudograminearum*, the isogenic strains FC136-2A and FC136-2A-V$^-$ were cultivated in wheat grains for 30 days at 25 °C. Then, 20mL acetonitrile/water/acetic acid (70:29:1, *v*/*v*/*v*) was used to extract DON from 5 g of these mixtures for each sample for HPLC-MS/MS analysis. Results showed that the content of DON in the FpgMBV1-containing *F. pseudograminearum* strain FC136-2A was 1.3 ± 0.1 μg/kg. The content of DON in the virus-free strain FC136-2A-V$^-$ was 10.6 ± 1.4 μg/kg. Compared to the virus-free strain FC136-2A-V$^-$, the content of DON in the FpgMBV1-containing strain FC136-2A was reduced by about 87% ($p < 0.05$) (Figure 1). No significant difference was found for the content of 15-ADON in the FpgMBV1-containing strain and the virus-free strain (Figure S2).

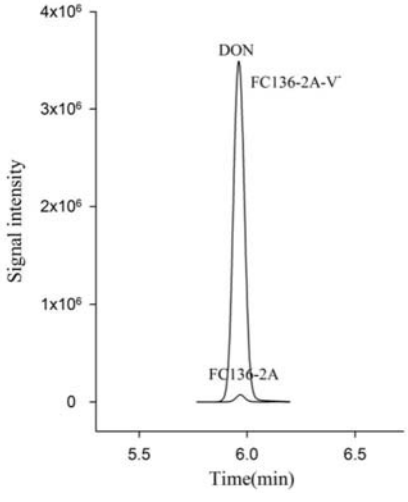

Figure 1. HPLC-MS/MS chromatograms showing DON production in wheat grain culture extracts of *F. pseudograminearum* strain FC136-2A harboring FpgMBV1 and the isogenic virus-free strain FC136-2A-V$^-$.

2.2. Overview of RNA-Seq Data for FC136-2A and FC136-2A-V$^-$

To reveal how the biosynthesis genes of DON were regulated by FpgMBV1, the FpgMBV1-containing *F. pseudograminearum* strain FC136-2A and the isogenic virus-free strain FC136-2A-V$^-$ were used in the transcriptome analysis with three biological replicates for each strain using the DNBSEQ platform (BGI, Shenzhen, China). Gene expression profiles of the strains FC136-2A and FC136-2A-V$^-$ were compared. An average of 7.24 Gb of data was yielded for each sample. The genome of *F. pseudograminearum CS3096* was used as the reference genome. An average of 94.57% and 94.27% of total reads (56–57 million) were aligned to the genome, respectively. A total of 11,500 genes were detected as expressed, of which 11417 were known and 83 were predicted as unknown genes (Table S1). The absolute fold change ≥ 2 and adjusted *p*-value ≤ 0.001 were used to define differently expressed genes (DEGs) (Figure 2A). Compared to the gene expression of the strain FC136-2A-V$^-$, a total of 2564 statistically significant DEGs were found in the strain FC136-2A. Among them, 1585 genes were up-regulated and 979 genes were down-regulated (Figure 2B).

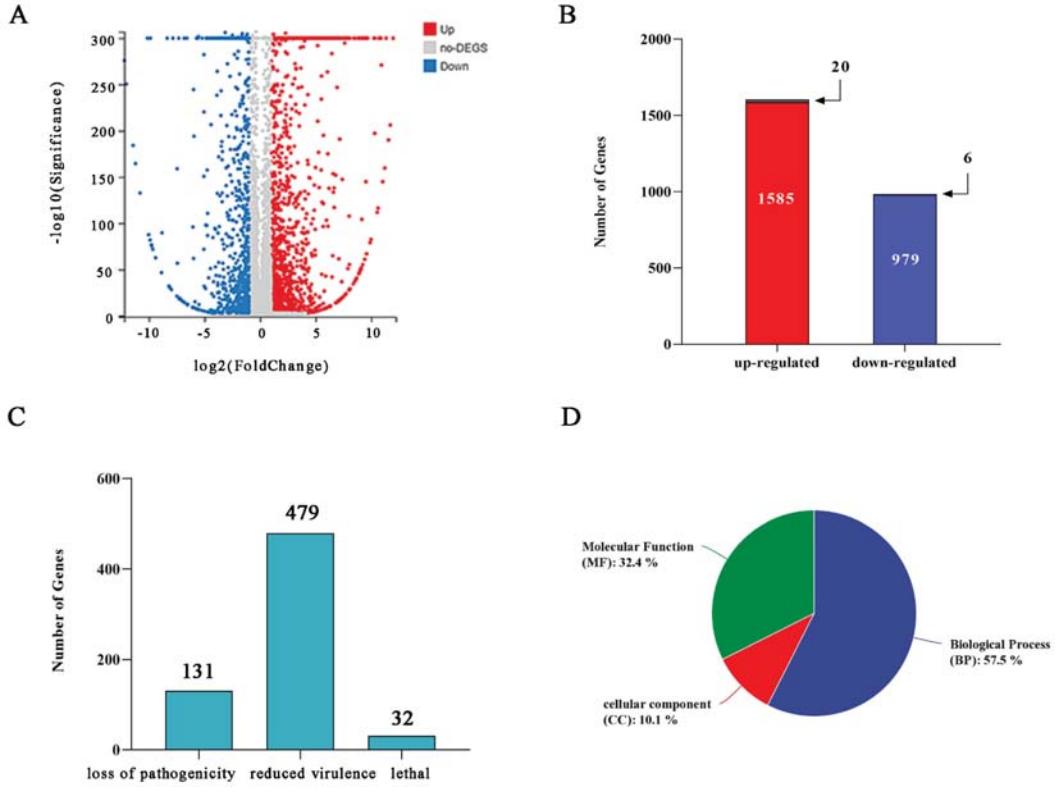

Figure 2. Effects of FpgMBV1 on the transcriptome profile of *F. pseudograminearum* as revealed by RNA-Seq. (**A**) The volcano plot showing gene signals detected in the strain FC136-2A comparing to FC136-2A-V^{-}. Up-regulated (red), no change (gray) and down-regulated (blue). (**B**) The histogram of the number of differentially expressed genes (DEGs), including numbers of up-regulated (red) and down-regulated (blue) genes. (**C**) The number of DEGs annotated in the PHI database. (**D**) The rate of numbers of DEGs annotated by Gene ontology terms in molecular function (MF) (green), cellular component (CC) (red) and biological process (BP) (blue).

The PHI database annotation was screened using the DIAMOND software. A total of 131 genes were associated with loss of pathogenicity, 479 genes with reduced virulence, and 32 genes with lethal consequences (Figure 2C). In this study, the DEGs with PHI identity > 80% were used for further screening and the heat map construction. There were 18 genes categorized as reduced virulence genes including 4 up-regulated genes and 14 down-regulated ones (Figure S1). There were four genes categorized as essential genes (Figure S1). All these essential genes were up-regulated. No genes associated with loss of pathogenicity were identified in this study. Moreover, 12 of these genes were associated with DON and ergosterol biosynthesis (Table 1).

Table 1. DON and ergosterol biosynthesis and metabolism-related genes according to the PHI database.

Gene Name	Gene ID	SwissProt_Description	log2(FC136_2A/FC136_2A_V$^-$)	Identity (%)	E-Value	PHI Accession
ERG3B	*FPSE_12291*	Probable Delta(7)-sterol 5(6)-desaturase	−1.656	92.3	7.3×10^{-179}	PHI:3036
ERG4	*FPSE_03901*	Delta(24(24(1)))-sterol reductase	−1.336	96.6	0	PHI:2728
ERG5A	*FPSE_09181*	Cytochrome P450 61	−1.584	99.3	0	PHI:3037
ERG5B	*FPSE_01847*	Sterol 22-desaturase	−7.320	94.3	1.6×10^{-292}	PHI:3038
TRI5	*FPSE_12160*	Trichodiene synthase	−3.030	100	1.1×10^{-228}	PHI:6846
TRI6	*FPSE_12161*	Trichothecene biosynthesis transcription regulator 6	−2.686	95.9	1.2×10^{-126}	PHI:1362
TRI12	*FPSE_12157*	Trichothecene efflux pump TRI12	−2.305	91.7	4.5×10^{-307}	PHI:2704
TRI10	*FPSE_12159*	Trichothecene biosynthesis transcription regulator 10	−2.702	93.3	1.5×10^{-232}	PHI:2328
TRI15	*FPSE_02457*	Cys(2)-His(2) zinc finger protein	−1.803	95.7	8.3×10^{-183}	PHI:1363
HMR1	*FPSE_03466*	Hydroxymethylglutaryl CoA reductase gene	−1.781	94.7	0	PHI:1006
VELB	*FPSE_11531*	Velvet complex subunit B	−1.760	83.3	1.1×10^{-159}	PHI:2427
GLX	*FPSE_04483*	WSC domain-containing protein ARB_07867	−1.238	87	0	PHI:5393

Gene ontology (GO) terms significantly enriched in the three major functional ontologies: 57.5% for biological process (BP), 10.1% for cellular component (CC) and 32.4% for molecular function (MF) (Figure 2D). For the 1585 up-regulated genes, the most enriched three for the BP were carbohydrate metabolic process, transmembrane transport, catechol-containing compound metabolic process, and oxidoreductase activity, catalytic activity, and cofactor binding for the MF (Figure 3A, Table S2). For the 979 down-regulated genes, the most enriched three of the BP were sterol metabolic and biosynthetic process, steroid metabolic and biosynthetic process, ergosterol metabolic and biosynthetic process; and oxidoreductase activity, iron ion binding, and cofactor binding for the MF (Figure 3B, Table S3). The most enrichedthree of the CC were integral component of membrane, an intrinsic component of membrane, membrane part, and membrane in all DEGs. There were 20 significantly enriched KEGG pathways for the up-regulated genes (Figure 3C, Table S4) and down-regulated genes, respectively (Figure 3D, Table S5). Sixteen pathways were related to metabolism.

2.3. The Metabolic Balance in F. pseudograminearum Was Disturbed by FpgMBV1

For the up-regulated DEGs, ten of the enriched KEGG pathways were related to metabolism, including tryptophan metabolism (ko00380), phenylalanine metabolism (ko00360), fatty acid metabolism (ko01212), biotin metabolism (ko00780), galactose metabolism (ko00052), arginine and proline metabolism (ko00330), starch and sucrose metabolism (ko00500), sphingolipid metabolism (ko00600), propanoate metabolism (ko00640), and linoleic acid metabolism (ko00591) (Figure 3C, Table S4). In addition, the meiosis–yeast pathway (ko04113) related to hyphal growth and development was also enriched.

Among the down-regulated genes, six pathways were related to metabolism (Figure 3D, Table S5). They were mainly classified into sulfur metabolism (ko00920), glycine, serine and threonine metabolism (ko00260), ether lipid metabolism (ko00565), fatty acid metabolism (ko01212), tyrosine metabolism (ko00350), and nitrogen metabolism (ko00910). Moreover, the biosynthesis of antibiotics, autophagy–yeast, steroid biosynthesis, and fatty acid degradation were also enriched.

The KEGG enrichment heat map shows that the fungal metabolic balance of amino acids and lipids was disturbed by FpgMBV1 (Figure 4). The transcription and translation of cell membrane-associated genes was also regulated by FpgMBV1.

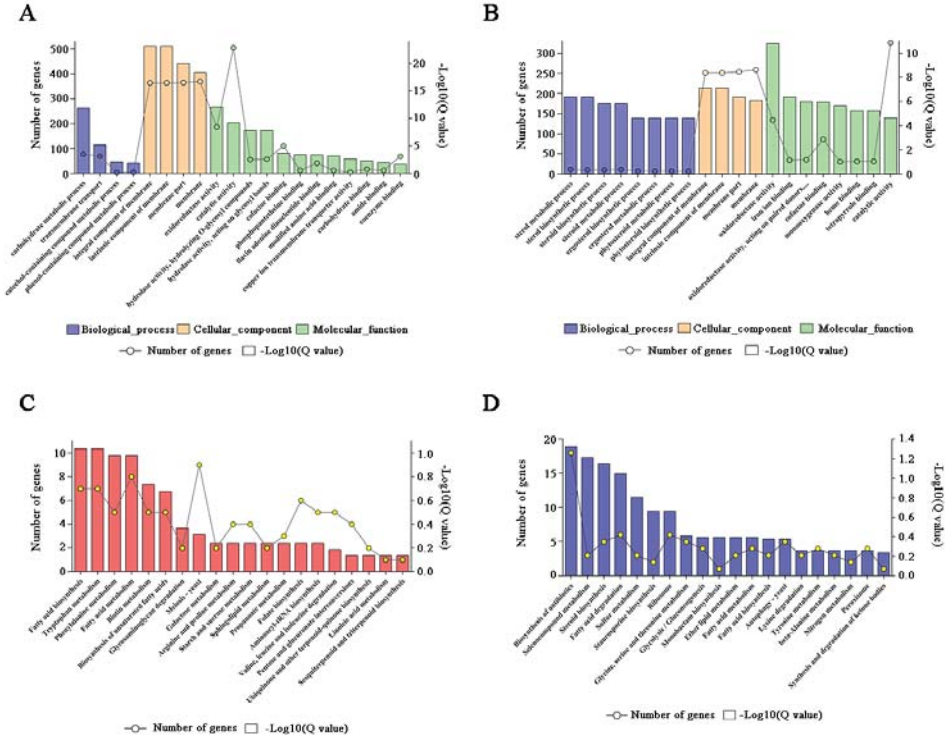

Figure 3. The Gene Ontology enrichment analysis of differently expressed genes, including up-regulated genes (**A**) and down-regulated genes (**B**) and the KEGG pathway enrichment analysis of the up-regulated genes (**C**) and down-regulated genes (**D**).

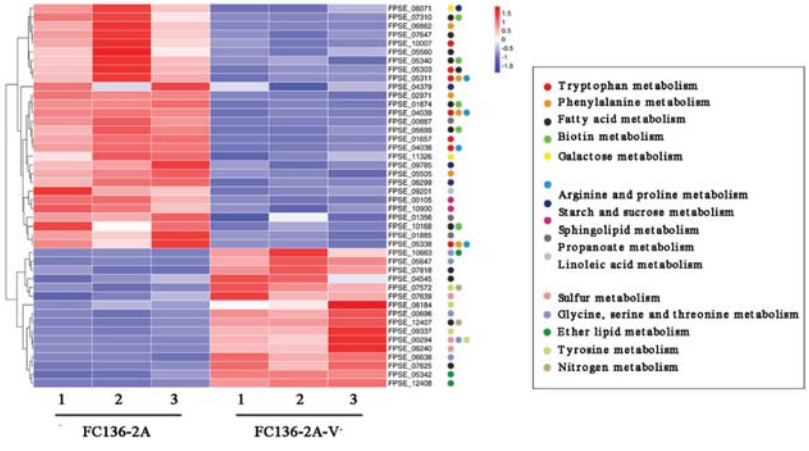

Figure 4. Heat map of metabolism-related genes differentially expressed in *F. pseudograminearum* strain FC136-2A compared to FC136-2A-V$^-$.

2.4. TRI Genes Regulating DON Biosynthesis Were Down-Regulated by FpgMBV1

The genes in the TRI gene cluster encoding key enzymes for DON biosynthesis were FgTRI1-FgTRI16 and FgTRI101 in F. graminearum [36]. Comparative transcriptomic results showed that 12 genes in the TRI gene cluster were down-regulated by FpgMBV1. They were *FpTRI1*, *FpTRI3*, *FpTRI4*, *FpTRI5*, *FpTRI6*, *FpTRI8*, *FpTRI10*, *FpTRI11*, *FpTRI12*, *FpTRI14*, *FpTRI15*, and *FpTRI101* (Figure 5). These *TRI* genes regulated by FpgMBV1 accounted for about two-thirds of the total gene number in the TRI gene cluster. Additionally, they were all significantly repressed.

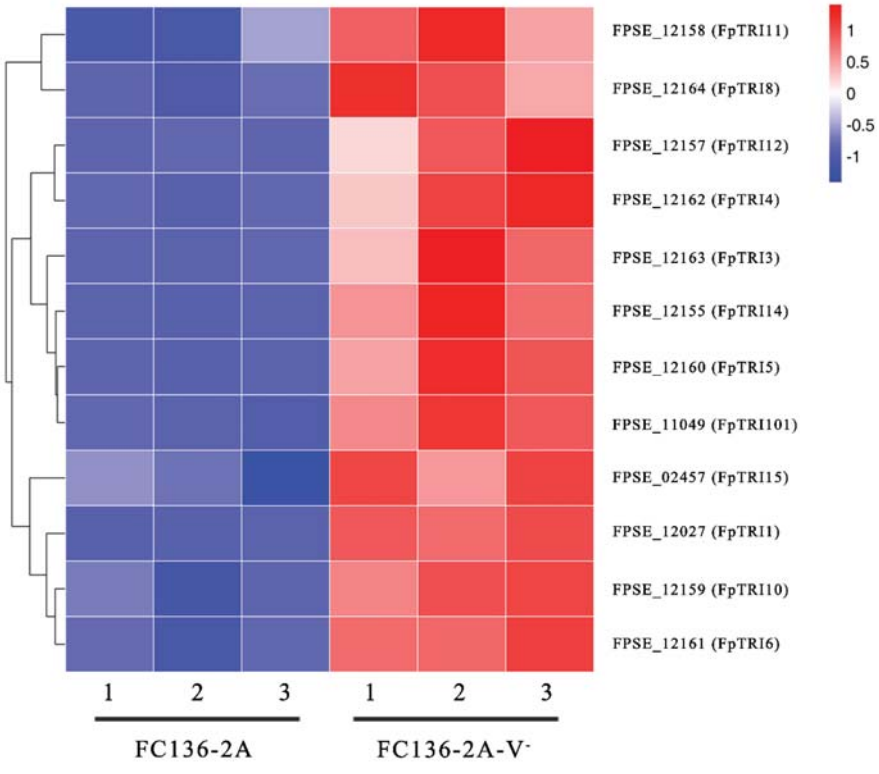

Figure 5. Heat map of TRI genes differentially expressed in F. pseudograminearum strain FC136-2A compared to FC136-2A-V^{-}.

2.5. Ergosterol Biosynthesis and Metabolism Were Inhibited by FpgMBV1

Fungal ergosterol content is significantly and positively correlated with DON content. In this study, ergosterol synthesis and metabolism were significantly enriched according to the results of GO enrichment of down-regulated genes (Figure 6A). In the PHI database annotation, four DEGs related to ergosterol synthesis were significantly down-regulated by FpgMBV1. They were FgERG4 (PHI:2728), FgERG5B (PHI:3038), FgERG5A (PHI:3037), and FgERG3B (PHI:3036) (Figure 6B). These results showed inhibition in ergosterol biosynthesis and metabolism in the FpgMBV1-containing strain FC136-2A.

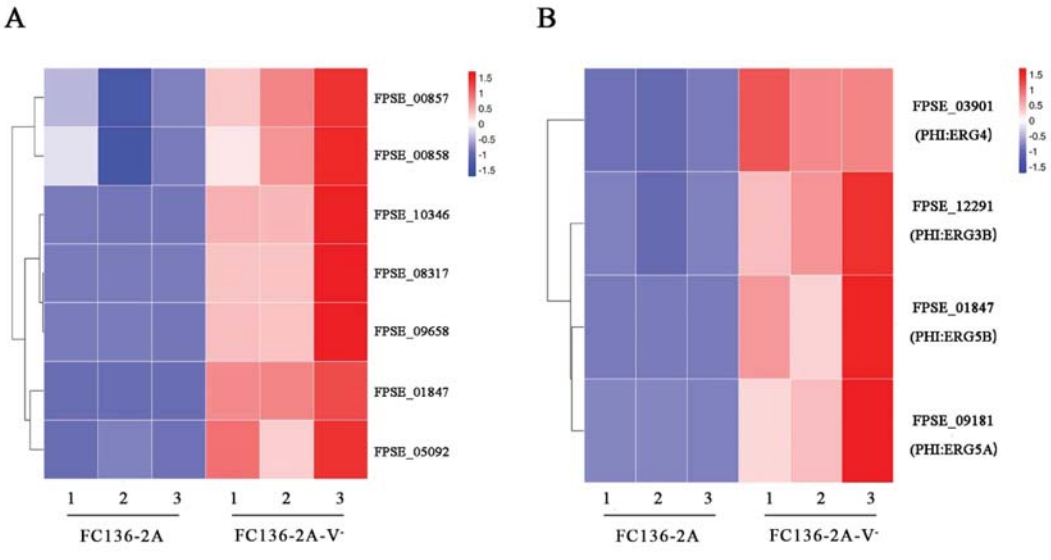

Figure 6. Heat map of genes related to ergosterol biosynthesis and metabolism differentially expressed in *F. pseudograminearum* strain FC136-2A compared to FC136-2A-V$^-$, including genes annotated as ergosterol biosynthesis and metabolism based on NCBI-NR database (**A**), and based on PHI database (**B**).

2.6. FpDicer1 and FpAGO1 Were Down-Regulated by FpgMBV1

Based the RNA-seq result of FC136-2A and FC136-2A-V$^-$, two Dicer (DCL) genes, two argonaute (AGO) genes, and one RNA-dependent RNA polymerase (RdR) gene were found differentially expressed. They were key genes in RNA silencing, which is an adaptive defense mechanism against foreign nucleic acids, especially viruses in animals, fungi, and plants [37]. Among them, FpDicer2(FPSE_06330), FpAGO2(FPSE_07737), and FpRdR1(FPSE_07737) were significantly up-regulated and FpDicer1(FPSE_07072) and FpAGO1(FPSE_00006) were down-regulated in the FpgMBV1-containing strain FC136-2A compared to the virus-free strain FC136-2A-V$^-$ (Figure 7). These results suggest that these RNA-silencing-related genes in *F. pseudograminearum* were involved in the defensive immunity against FpgMBV1.

2.7. Gene Expression Level by Quantitive Real-Time RT-PCR

Through quantitative real-time RT-PCR, the expression levels of 15 DEGs involved in metabolism, RNA silencing, virulence, and DON biosynthesis were confirmed. Primers are listed in Table S6. The expression levels of these representative genes were consistent with those in the transcriptomic data (Figure 8).

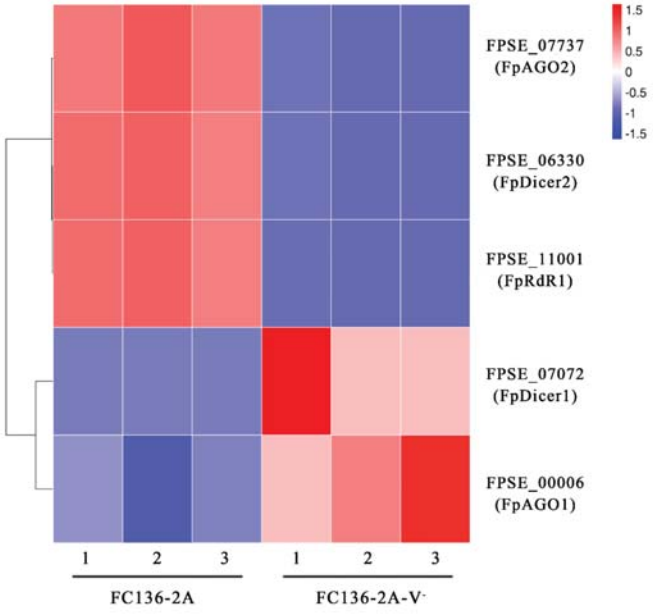

Figure 7. Heat map of RNA-silencing-related genes differentially expressed between *F. pseudograminearum* strain FC136-2A harboring FpgMBV1 and the isogenic virus-free strain FC136-2A-V⁻.

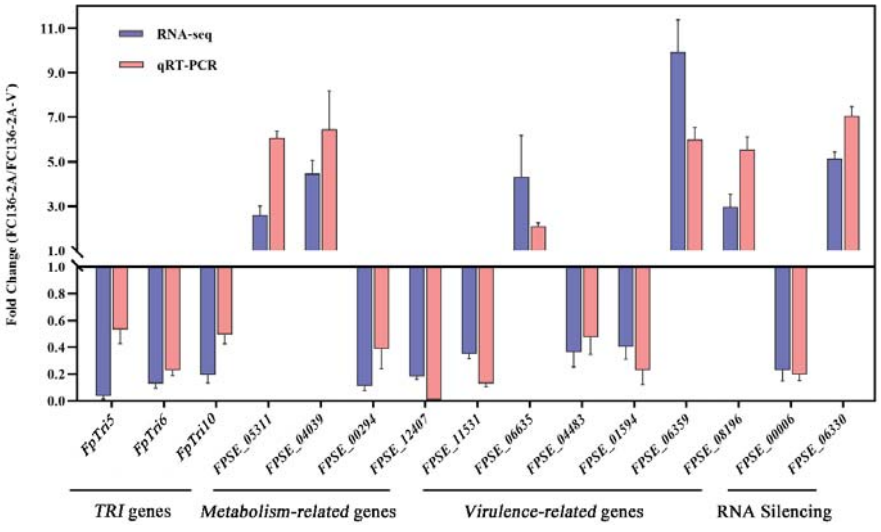

Figure 8. Gene expression comparison of some genes between *F. pseudograminearum* strain FC136-2A and FC136-2A-V⁻ by quantitative real-time RT-PCR (orange) and RNA-seq (blue).

3. Discussion

In this study, the production of key mycotoxins DON and 15-ADON was found to be inhibited by FpgMBV1 significantly. The expression of 12 out of 15 *TRI* genes was repressed in accordance with the HPLC-MS/MS data. Previously, mycovirus FgV1 was reported to cause decreased DON production (60-fold) in *F. graminearum* [26]. However, only the *TRI12* gene in the TRI gene cluster was differently expressed in the FgV1-containing strains [32].

For FgMTV1/SX64, another mycovirus reducing the DON concentration significantly in *F. graminearum*, whether *TRI* gene expression was regulated is unknown [31]. The global regulation of most *TRI* genes by a mycovirus was first reported for FpgMBV1. Two transcription regulators, *TRI6* and *TRI10,* were key regulators in the *TRI* gene cluster [17]. *TRI6* has been identified as a global transcription regulator, not only enhancing the expression of the genes in the DON biosynthetic pathway but also involved in the upstream isoprenoid pathway for trichothecene accumulation [38,39]. *TRI10* regulated the expression of *TRI1, TRI3, TRI8, TRI11, TRI12, TRI14,* and *TRI15* in *Fusarium* spp. [40]. In this study, the significant down-regulation of *TRI6* and *TRI10* might be the reason for the down-regulation of other *TRI* genes. The significant disruption of *TRI* gene expression resulted in the low contents of DON mycotoxin. This suggests an unrevealing mechanism underlying the repression of DON and *TRI* gene expression by mycovirus FpgMBV1, which would provide new methods in the detoxification of DON and reducing the yield loss in wheat.

Other genes of biosynthetic pathways were differentially expressed under the infection of FpgMBV1. For example, four genes encoding key enzymes in ergosterol synthesis were down-regulated. They were *FgERG3B*, *FgERG4*, *FgERG5A*, and *FgERG5B* [41,42]. It has been reported that ergosterol synthesis has a strong, positive correlation with the content of mycotoxin DON in the infected grains [43,44]. Moreover, ergosterol is an important constituent of fungal membranes [45]. Membranes are essential for many cellular processes, including the defensing response against viruses in fungi [46,47]. Another significantly down-regulated gene, HMG-CoA-reductase (*HMR1*), is the key enzyme in the mevalonate pathway. *HMR1* is involved in the biosynthesis of many primary and secondary metabolites [48]. Some mevalonate derivatives function in fungi–plant interaction, such as isoprenoids and gibberellins [49]. Another down-regulated gene, *FgVELB,* plays a critical role in regulating various cellular processes and acts as a negative regulator for lipid biosynthesis. The deletion mutant of the *FgVELB* gene in *F. graminearum* produces a very low level of DON [50,51]. These results demonstrated the specific genes involved in the regulation of DON production Further studies on these genes would clarify the virulence-related pathways in fungi, especially *Fusarium*.

In general, the gene expression profile of *F. pseudograminearum* was reprogrammed by FpgMBV1 with 2564 genes differentially expressed. The disrupted metabolism caused by FpgMBV1 included amino acid and lipid metabolism, ergosterol metabolic and biosynthetic processes, carbohydrate metabolism and biosynthesis. Some of these pathways were critical in the transcriptome of other fungi under the infection of mycoviruses. In *C. parasitica*, "biosynthesis of other secondary metabolites", "amino acid metabolism", "carbohydrate metabolism", and "translation" were enriched among the DEGs after CHV1 infection, demonstrating that virus infection resulted in massive but specific changes in primary and secondary metabolism. Some of the highly induced metabolites played key roles in the growth, development and pathogenicity of fungi [52]. The complex interaction between leucine metabolism and the global regulator of mycotoxin biosynthesis, *TRI6,* and virulence in *F. graminearum* has been explored [53]. In this study, the KEGG enrichment results showed that tryptophan, phenylalanine, tyrosine, glycine, serine, and threonine-related genes were differentially expressed under the infection of FpgMBV1. Further studies on the regulation mechanism of FpgMBV1 would help in revealing the crosstalk between some primary metabolic pathways and mycotoxin biosynthesis and virulence in *F. pseudograminearum*.

Mycoviruses were triggers and targets of RNA silencing. Three genes (*FpDCL2*, *FpAGO2*, and *FpRdR1)* were up-regulated and two genes (*FpDCL1* and *FpAGO1)* were down-regulated in *F. pseudograminearum* under the infection of FpgMBV1. They are genes for key components in the RNA-silencing machinery [54]. Gene expression of *DCL2* and *AGO2* were induced by CHV1 in *C. parasitica* [55]. Genes of *SsAgl2*, *SsDcl1*, and *SsDCl2* were essential in defending against viruses in *S. sclerotiorum* [56]. The expression of *FgDICER2* and *FgAGO2* were suppressed by FgV1 in *F. graminearum* [57]. Most RNA-silencing genes in *S. sclerotiorum* were repressed by SsHADV-1 [35]. Considering the high diversity of

these virus–fungi systems, the different regulation on the RNA-silencing pathway seems reasonable. The regulation network of FpgMBV1 is partially revealed in this study, while the underlying mechanism is to be explored.

4. Conclusions

Megabirnavirus FpgMBV1 significantly repressed the production of mycotoxin DON and the expression of 12 *TRI* genes in *F. pseudograminearum*. The expression of ergosterol biosynthesis and RNA-silencing-related genes and genes involved in metabolism were regulated by FpgMBV1(Figure 9). Prospectively, FpgMBV1 is valuable in the detoxification of DON and the management of diseases caused by *F. pseudograminearum*.

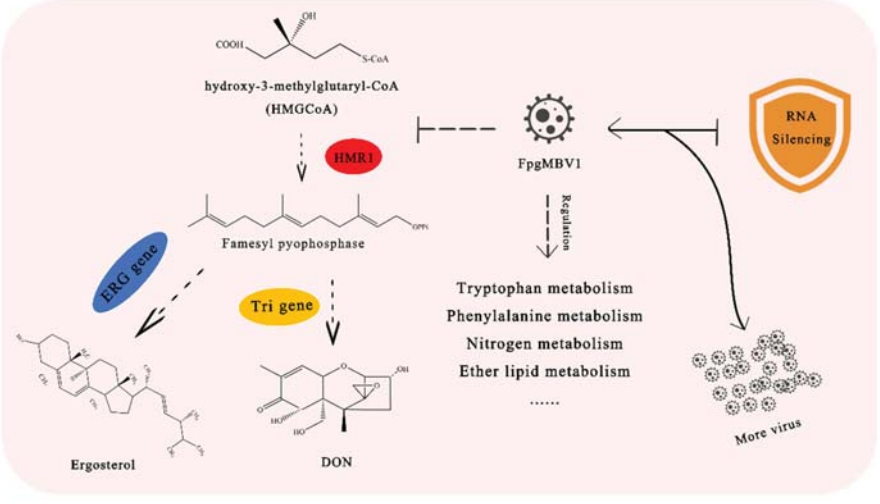

Figure 9. General view of genes and pathways regulated by FpgMBV1 in *F. pseudograminearum* revealed in this study.

5. Materials and Methods

5.1. Fungal Material and Growth Conditions

FpgMBV1-containing *F. pseudograminearum* strain FC136-2A and its isogenic FpgMBV1-free strain FC136-2A-V$^-$ were maintained in the laboratory, department of plant protection, Henan Agricultural University, Henan province, China [27]. For RNA sequencing, these two strains were grown at 25 °C in the dark on potato dextrose agar (PDA) medium (Becton, Dickinson, and Company, Sparks, MD, USA). For HPLC-MS/MS analysis, these strains were cultured in wheat grain media. Typically, 180 g of wheat seeds was soaked in distilled water for 12 h and boiled for 30 min then air-dried and autoclaved at 120 °C for 30 min in triangle flasks to complete the preparation of the wheat grain medium. Three-day-old PDA plugs of FC136-2A or FC136-2A-V$^-$ mycelia were cultured in wheat grain media for 30 days in the dark at 25 °C.

5.2. HPLC-MS/MS Analysis of Type B Trichothecene

Finely ground wheat grain (5.00 g) was weighted and extracted with 20 mL acetonitrile/water/acetic acid (70:29:1, *v*/*v*/*v*). The suspension was blended for 5 min at 2500 rpm using multi-tube vortexer UMV-2. The homogenized solution was centrifuged for 10 min after cooling (T = 4 °C, 8000 rpm). Then, 750 µL of the upper layer and 2 mL water were mixed in a 15 mL tube at 11,000 rpm for 10 min. The upper layer was cleaned via nylon filters and used for HPLC-MS/MS analysis.

HPLC analysis was performed using LC-MS-8060NX (Shimadzu, Japan) in gradient conditions. The separation of the toxin was performed using 100 nm × 2.1 mm, 1.9 µm (Thermo Fisher Scientific, Shanghai, China). The column temperature was set at 40 °C and the injection volume was 1 µL. Solvent A was 1 mmoL·L-1 ammonium formate in 0.1% formic acid and solvent B was methanol and 1 mmoL·L-1 ammonium formate in 0.1% formic acid. A gradient at a flow rate of 0.2 mL·min-1 was performed within 26 min (Table S7).

MS/MS was performed on an 8060NX triple quadrupole mass spectrometer equipped with a Turbo Ion-Spray electrospray ionization (ESI) source (Shimadzu, Japan) heated at 400 °C in the negative (DON, 3-ADON, and 15-ADON) and positive (ZEN, D3G, and NIV) ionization mode. Quantitation was performed using multiple-reaction monitoring (MRM) with a dwell time of 100 ms. The following transition reactions of DON, 3ADON,15ADON, ZEN, D3G, NIV, and the IS with the respective declustering potential (DP), collision energy (CE), and cell exit potential (CXP) in parentheses were recorded using the first mass transition for quantitation. DON: m/z 297.1 (DP −21.0 V, CE −11.0 V, CXP −25.0V), 3ADON: m/z 339.2 (DP −30V, CE −14V, CXP −25V), 15ADON: m/z 356.2 (DP −18V, CE −9.0V, CXP −23V), D3G: m/z 503.0 (DP +26V, CE +20V, CXP +29V), ZEN: m/z 317.2 (DP +16V, CE +24V, CXP +29V), and NIV: m/z 357.2 (DP +13V, CE +13V, CXP +28V).

Data are reported as mean values ± SD of three biological replications. Type B trichothecene (NIV, DON, FX, 3-ADON, and 15-ADON) yields are expressed as µg·kg-1 of dry fungal biomass. Values were compared at the 1% significance level using DPS software (control vs. treated).

5.3. Total RNA Extraction

The 0.5 mg mycelia of strains FC136-2A and FC136-2A-V$^-$ were harvested from PDA plates and ground in liquid nitrogen. Total RNA isolation was conducted using TRIzol (Invitrogen, Carlsbad, CA, USA). The extracted RNA was treated with RNase-free DNase I (Promega, Madison, WI, United Kingdom). The concentration of the extracted RNAs was determined with Nanodrop system (NanoDrop, Madison, WI, USA). The RNA integrity was examined by the RNA integrity number (RIN) using an Agilent 2100 bioanalyzer (Agilent, Santa Clara, CA, USA).

5.4. cDNA Library Preparation and Sequencing

MGI Easy RNA Library Preparation Kit (BGI-Shenzhen, China) and DNA Clean Beads MGI Easy DNA Cleanbeads Kit (BGI-Shenzhen, China) were used to purify mRNA and synthesize cDNA and PCR amplification; then, purification of the PCR product was carried out following the kit instructions. The product was validated on the Agilent Technologies 2100 bioanalyzer for quality control. The double-stranded PCR products from the previous step were heated, denatured, and circularized by splint oligo sequencing to obtain the final library. The single-stranded circular DNA was formatted as the last library and amplified with phi29 polymerase to make a DNA nanoball, with more than 300 copies per molecule. DNBs were loaded into the patterned nanoarray, and 100 paired base reads were generated on the BGI seq500 platform (BGI-Shenzhen, China).

5.5. RNA-Seq Data Analysis

The raw data were filtered with BGI's filtering software SOAPnuke (version: v1.4.0) to remove reads containing splices (splice contamination), reads with unknown base N content greater than 10%, and reads in which bases with a quality value of lower than 15 accounted for more than 20% of the total number of bases. Using HISAT2 software (version: v2.1.0; http://www.ccb.jhu.edu/software/hisat), the clean reads were mapped to the *F. pseudograminearum* CS3096 genome (Taxonomy ID: 1028729). Bowtie2 (version: v2.2.5; http://bowtie-bio.sourceforge.net/Bowtie2/index.shtml) was used to compare the reference gene sequences and RSEM (version: v1.2.8) was applied to calculate the expression levels of genes and transcripts. Pearson correlation coefficients between every two samples

were obtained using the core function in the R software, and principal component analysis (PCA) was performed using the princomp method. To identify significant virulence genes in fungus, DIAMOND software was used to annotate genes with query coverage of 50% and identity of 40% in the PHI database (version: V0.8.31). To improve the accuracy of DEGs, we defined genes with more than two-fold difference and Q-values ≤ 0.001 to be screened as significantly differentially expressed genes. Differential genes were functionally classified according to GO and KEGG annotation results and official classification. At the same time, enrichment analysis was performed using the phyper function in R software, with FDR correction for *p*-value, and functions with Q value ≤ 0.05 were considered significantly enriched.

5.6. Quantitative Real-Time RT-PCR (qRT-PCR) Analysis

Total RNA samples from FC136-2A and FC136-2A-V$^-$ were used for cDNA synthesis by Goldenstar® RT6 cDNA Synthesis kit ver.2 (Tsingke Biotechnology Co., Ltd., Beijing, China). The resulting cDNAs were used as templates for qRT-PCR.

The qRT-PCR was carried out in a QuantStudio 3 Real-Time PCR System (Thermo Fisher Scientific, Waltham, MA, USA) with 2×T5 Fast qPCR Mix (Tsingke Biotechnology Co., Ltd., Beijing, China). PCR amplification was performed under the following conditions: 95 °C for 1 min, followed by 40 cycles of 95 °C for 10 s, and 60 °C for 30 s. Meltcurve plots were analyzed for each gene tested after each PCR reaction. The ubiquitin gene of TEF1α (FPSE_11980) served as an internal reference gene. Primers for 15 of the DEGs were designed using Primer Premier 5 and are listed in Table S6.

Supplementary Materials: The following supporting information can be downloaded at: https://www.mdpi.com/article/10.3390/toxins14070503/s1, Figure S1: The virulence genes according to the PHI-base. (A) Heat map of reduced-virulence genes in DEGs. (B) Heat map of essential genes (according to PHI database) in DEGs, Figure S2: Accumulation of mycotoxin 15-ADON in wheat cultures of FC136-2A and FC136-2A-V$^-$. Table S1: Statistics of the transcriptome-sequencing results, Table S2: The GO enrichment analysis of the up-regulated genes, Table S3: The GO enrichment analysis of the down-regulated genes, Table S4: The KEGG enrichment analysis of the up-regulated genes, Table S5: The KEGG enrichment analysis of the down-regulated genes, Table S6: qRT-PCR primers used in this study, Table S7: Gradient elution conditions of mobile phase.

Author Contributions: Conceptualization, F.G. and X.Z.; data curation, X.P., Y.X. and X.Z.; formal analysis, K.L. and J.S.; funding acquisition H.L., J.L. and X.Z.; investigation X.P., S.Y. and D.L. (Dongmei Liu); methodology, F.G., D.L. (Dongmei Liu) and J.D.; resources, Y.X.; supervision, J.L.; validation, D.L. (Dongwei Liu) and Z.W.; writing—original draft, K.L.; writing—review and editing, X.Z. All authors have read and agreed to the published version of the manuscript.

Funding: This work was financially supported by the Major International (Regional) Joint Research NSFC-CGIAR Project (31961143018), Henan Province Agricultural Science and Technology Research Project (212102110138), Henan Agricultural University Science and Technology Innovation Project (KJCX2020A14), New discipline development project of Henan Academy of Agricultural Sciences (2020XK06, 2022XK08).

Institutional Review Board Statement: Not applicable.

Informed Consent Statement: Not applicable.

Data Availability Statement: The data presented in this study are available in Supplementary Materials Tables S1–S7 and Figures S1 and S2.

Acknowledgments: We thank the editor for editing assistance, and the anonymous reviewers for constructive and helpful comments. We also acknowledge the BGI database development team for technical support.

Conflicts of Interest: The authors declare no conflict of interest.

References

1. Burgess, L.; Bryden, W. *Fusarium*: A ubiquitous fungus of global significance. *Microbiology* **2012**, *33*, 22. [CrossRef]
2. Ma, L.J.; Geiser, D.M.; Proctor, R.H.; Rooney, A.P.; O'Donnell, K.; Trail, F.; Gardiner, D.M.; Manners, J.M.; Kazan, K. *Fusarium* pathogenomics. *Annu. Rev. Microbiol.* **2013**, *67*, 399–416. [CrossRef] [PubMed]
3. Dean, R.; Van Kan, J.A.L.; Pretorius, Z.A.; Hammond-Kosack, K.E.; Di Pietro, A.; Spanu, P.D.; Rudd, J.J.; Dickman, M.; Kahmann, R.; Ellis, J.; et al. The Top 10 fungal pathogens in molecular plant pathology. *Mol. Plant Pathol.* **2012**, *13*, 314–430. [CrossRef]
4. Rampersad, S. Pathogenomics and management of *Fusarium* diseases in plants. *Pathogens* **2020**, *9*, 340. [CrossRef] [PubMed]
5. Petronaitis, T.; Simpfendorfer, S.; Hüberli, D. Importance of *Fusarium spp.* in wheat to food security: A global perspective. In *Plant Pathology in the 21st Century*; Springer: Berlin/Hamburg, Germany, 2021; Volume 10. [CrossRef]
6. Li, H.L.; Yuan, H.X.; Fu, B.; Xing, X.P.; Sun, B.J.; Tang, W.H. First Report of *Fusarium pseudograminearum* Causing Crown Rot of Wheat in Henan, China. *Plant Dis.* **2012**, *103*, 18–19. [CrossRef]
7. Alahmad, S.; Simpfendorfer, S.; Bentley, A.R.; Hickey, L.T. Crown rot of wheat in Australia: *Fusarium pseudograminearum* taxonomy, population biology and disease management. *Australas. Plant Pathol.* **2018**, *47*, 285–299. [CrossRef]
8. Kazan, K.; Gardiner, D.M. *Fusarium* crown rot caused by *Fusarium pseudograminearum* in cereal crops: Recent progress and future prospects. *Mol. Plant Pathol.* **2018**, *19*, 1547–1562. [CrossRef]
9. Zhou, H.; He, X.; Wang, S.; Ma, Q.; Sun, B.; Ding, S.; Chen, L.; Zhang, M.; Li, H. Diversity of the *Fusarium* pathogens associated with crown rot in the Huanghuai wheat-growing region of China. *Environ. Microbiol.* **2019**, *21*, 2740–2754. [CrossRef]
10. Bragard, C.; Baptista, P.; Chatzivassiliou, E.; DiSerio, F.; Gonthier, P.; JaquesMiret, J.A.; Justesen, A.F.; MacLeod, A.; Magnusson, C.S.; Milonas, P.; et al. Pest categorisation of *Fusarium pseudograminearum*. *EFSA J.* **2022**, *29*, e07399. [CrossRef]
11. Perincherry, L.; Justyna, L.; Lukasz, S. *Fusarium*-Produced Mycotoxins in Plant-Pathogen Interactions. *Toxins* **2019**, *11*, 664. [CrossRef]
12. Borbély, M.; Sipos, P.; Pelles, F.; Győri, Z. Mycotoxin contamination in cereals. *J. Agroaliment. Process. Technol.* **2010**, *16*, 96–98. Available online: https://www.researchgate.net/publication/265178683 (accessed on 10 June 2010).
13. Lozowicka, B.; Iwaniuk, P.; Konecki, R.; Kaczynski, P.; Kuldybayev, N.; Dutbayev, Y. Impact of Diversified Chemical and Biostimulator Protection on Yield, Health Status, Mycotoxin Level, and Economic Profitability in Spring Wheat (*Triticum aestivum* L.) Cultivation. *Agronomy* **2022**, *12*, 258. [CrossRef]
14. Skrzydlewski, P.; Twarużek, M.; Grajewski, J. Cytotoxicity of Mycotoxins and Their Combinations on Different Cell Lines: A Review. *Toxins* **2022**, *14*, 244. [CrossRef]
15. Pierzgalski, A.; Bryła, M.; Kanabus, J.; Modrzewska, M.; Podolska, G. Updated Review of the Toxicity of Selected *Fusarium* Toxins and Their Modified Forms. *Toxins* **2021**, *13*, 768. [CrossRef]
16. Flynn, C.M.; Broz, K.; Jonkers, W.; Schmidt-Dannert, C.; Kistler, H.C. Expression of the *Fusarium graminearum* terpenome and involvement of the endoplasmic reticulum-derived toxisome. *Fungal Genet. Biol.* **2019**, *124*, 78–87. [CrossRef] [PubMed]
17. Seong, K.Y.; Pasquali, M.; Zhou, X.; Song, J.; Hilburn, K.; McCormick, S.; Dong, Y.; Xu, J.R.; Kistler, H.C. Global gene regulation by *Fusarium* transcription factors *Tri6* and *Tri10* reveals adaptations for toxin biosynthesis. *Mol. Microbiol.* **2009**, *72*, 354–367. [CrossRef]
18. Menke, J.; Dong, Y.N.; Kistler, H.C. *Fusarium graminearum Tri12p* influences virulence to wheat and trichothecene accumulation. *Mol. Plant-Microbe Interact.* **2012**, *25*, 1408–1418. [CrossRef] [PubMed]
19. Alexander, N.J.; McCormick, S.P.; Hohn, T.M. *TRI12*, a trichothecene efflux pump from *Fusarium sporotrichioides*: Gene isolation and expression in yeast. *Mol. Gen. Genet.* **1999**, *261*, 977–984. [CrossRef]
20. Kimura, M.; Tokai, T.; O'Donnell, K.; Ward, T.J.; Fujimura, M.; Hamamoto, H.; Shibata, T.; Yamaguchi, I. The trichothecene biosynthesis gene cluster of *Fusarium graminearum* F15 contains a limited number of essential pathway genes and expressed non-essential genes. *FEBS Lett.* **2003**, *539*, 105–110. [CrossRef]
21. Lee, T.; Lee, S.H.; Shin, J.Y.; Kim, H.K.; Yun, S.H.; Kim, H.Y.; Lee, S.; Ryu, J.G. Comparison of trichothecene biosynthetic gene expression between *Fusarium graminearum* and *Fusarium asiaticum*. *Plant Pathol. J.* **2014**, *30*, 33–42. [CrossRef]
22. Lin, H.; Lan, X.; Liao, H.; Parsley, T.B.; Nuss, D.L.; Chen, B. Genome Sequence, Full-Length Infectious cDNA Clone, and Mapping of Viral Double-Stranded RNA Accumulation Determinant of Hypovirus CHV1-EP721. *J. Virol.* **2007**, *81*, 1813–1820. [CrossRef] [PubMed]
23. Yu, X.; Li, B.; Fu, Y.; Jiang, D.; Ghabrial, S.A.; Li, G.; Peng, Y.; Xie, J.; Cheng, J.; Huang, J.; et al. A geminivirus-related DNA mycovirus that confers hypovirulence to a plant pathogenic fungus. *Proc. Natl. Acad. Sci. USA* **2010**, *107*, 8387–8392. [CrossRef] [PubMed]
24. Chiba, S.; Salaipeth, L.; Lin, Y.-H.; Sasaki, A.; Kanematsu, S.; Suzuki, N. A Novel Bipartite Double-Stranded RNA Mycovirus from the White Root Rot Fungus *Rosellinia necatrix*: Molecular and Biological Characterization, Taxonomic Considerations, and Potential for Biological Control. *J. Virol.* **2009**, *83*, 12801–12812. [CrossRef] [PubMed]
25. Li, P.; Bhattacharjee, P.; Wang, S.; Zhang, L.; Ahmed, I.; Guo, L. Mycoviruses in *Fusarium* species: An update. *Front. Cell. Infect. Microbiol.* **2019**, *9*, 257. [CrossRef]
26. Chu, Y.M.; Jeon, J.J.; Yea, S.J.; Kim, Y.H.; Yun, S.H.; Lee, Y.W.; Kim, K.H. Double-stranded RNA mycovirus from *Fusarium graminearum*. *Appl. Environ. Microbiol.* **2002**, *68*, 2529–2534. [CrossRef]
27. Darissa, O.; Adam, G.; Schäfer, W. A dsRNA mycovirus causes hypovirulence of *Fusarium graminearum* to wheat and maize. *Eur. J. Plant Pathol.* **2012**, *134*, 181–189. [CrossRef]

28. Li, P.; Zhang, H.; Chen, X.; Qiu, D.; Guo, L. Molecular characterization of a novel hypovirus from the plant pathogenic fungus *Fusarium graminearum*. *Virology* **2015**, *481*, 151–160. [CrossRef]
29. Zhang, X.; Gao, F.; Zhang, F.; Xie, Y.; Zhou, L.; Yuan, H.; Zhang, S.; Li, H. The complete genomic sequence of a novel megabirnavirus from *Fusarium pseudograminearum*, the causal agent of wheat crown rot. *Arch. Virol.* **2018**, *163*, 3173–3175. [CrossRef]
30. Xie, Y.; Wang, Z.; Li, K.; Liu, D.; Jia, Y.; Gao, F.; Dai, J.; Zhang, S.; Zhang, X.; Li, H. A megabirnavirus alleviates the pathogenicity of *Fusarium pseudograminearum* to wheat. *Phytopathology* **2021**, *112*, 1175–1184. [CrossRef]
31. Li, P.; Lin, Y.; Zhang, H.; Wang, S.; Qiu, D.; Guo, L. Molecular characterization of a novel mycovirus of the family Tymoviridae isolated from the plant pathogenic fungus *Fusarium graminearum*. *Virology* **2016**, *489*, 86–94. [CrossRef]
32. Cho, W.K.; Yu, J.; Lee, K.M.; Son, M.; Min, K.; Lee, Y.W.; Kim, K.H. Genome-wide expression profiling shows transcriptional reprogramming in *Fusarium graminearum* by Fusarium graminearum virus 1-DK21 infection. *BMC Genom.* **2012**, *13*, 173. [CrossRef]
33. Lee, K.M.; Cho, W.K.; Yu, J.; Son, M.; Choi, H.; Min, K.; Lee, Y.W.; Kim, K.H. A comparison of transcriptional patterns and mycological phenotypes following infection of *Fusarium graminearum* by four mycoviruses. *PLoS ONE* **2014**, *9*, e0100989. [CrossRef] [PubMed]
34. Wang, S.; Zhang, J.; Li, P.; Qiu, D.; Guo, L. Transcriptome-based discovery of *Fusarium graminearum* stress responses to FgHV1 infection. *Int. J. Mol. Sci.* **2016**, *17*, 1922. [CrossRef] [PubMed]
35. Qu, Z.; Fu, Y.; Lin, Y.; Zhao, Z.; Zhang, X.; Cheng, J.; Xie, J.; Chen, T.; Li, B.; Jiang, D. Transcriptional Responses of *Sclerotinia sclerotiorum* to the Infection by SsHADV-1. *J. Fungi* **2021**, *7*, 493. [CrossRef] [PubMed]
36. Chen, Y.; Kistler, H.C.; Ma, Z. *Fusarium graminearum* Trichothecene Mycotoxins: Biosynthesis, Regulation, and Management. *Annu. Rev. Phytopathol.* **2019**, *57*, 15–39. [CrossRef]
37. Ding, S.W.; Li, H.; Lu, R.; Li, F.; Li, W.X. RNA silencing: A conserved antiviral immunity of plants and animals. *Virus Res.* **2004**, *102*, 109–115. [CrossRef]
38. Nasmith, C.G.; Walkowiak, S.; Wang, L.; Leung, W.W.Y.; Gong, Y.; Johnston, A.; Harris, L.J.; Guttman, D.S.; Subramaniam, R. *Tri6* is a global transcription regulator in the phytopathogen *Fusarium graminearum*. *PLoS Pathog.* **2011**, *7*, e1002266. [CrossRef] [PubMed]
39. Proctor, R.H.; Hohn, T.M.; McCormick, S.P.; Desjardins, A.E. *Tri6* encodes an unusual zinc finger protein involved in regulation of trichothecene biosynthesis in *Fusarium sporotrichioides*. *Appl. Environ. Microbiol.* **1995**, *61*, 1923–1930. [CrossRef] [PubMed]
40. Peplow, A.W.; Tag, A.G.; Garifullina, G.F.; Beremand, M.N. Identification of new genes positively regulated by *Tri10* and a regulatory network for trichothecene mycotoxin production. *Appl. Environ. Microbiol.* **2003**, *69*, 2731–2736. [CrossRef]
41. Yun, Y.; Yin, D.; Dawood, D.H.; Liu, X.; Chen, Y.; Ma, Z. Functional characterization of *FgERG3* and *FgERG5* associated with ergosterol biosynthesis, vegetative differentiation and virulence of *Fusarium graminearum*. *Fungal Genet. Biol.* **2014**, *68*, 60–70. [CrossRef]
42. Liu, X.; Jiang, J.; Yin, Y.; Ma, Z. Involvement of *FgERG4* in ergosterol biosynthesis, vegetative differentiation and virulence in *Fusarium graminearum*. *Mol. Plant Pathol.* **2013**, *14*, 71–83. [CrossRef] [PubMed]
43. Gilbert, J.; Abramson, D.; Mccallum, B.; Clear, R. Comparison of Canadian *Fusarium graminearum* isolates for aggressiveness, vegetative compatibility, and production of ergosterol and mycotoxins. *Mycopathologia* **2002**, *153*, 209–215. [CrossRef] [PubMed]
44. Lamper, C.; Teren, J.; Bartok, T.; Komoroczy, R.; Mesterhazy, A.; Sagi, F. Predicting DON contamination in *Fusarium*-infected wheat grains via determination of the ergosterol content. *Cereal Res. Commun.* **2000**, *28*, 337–344. [CrossRef]
45. Rodrigues, M.L. The multifunctional fungal ergosterol. *mBio* **2018**, *9*, e01755-18. [CrossRef] [PubMed]
46. Jacob-Wilk, D.; Turina, M.; Van Alfen, N.K. Mycovirus Cryphonectria hypovirus 1 elements cofractionate with trans-Golgi network membranes of the fungal host *Cryphonectria parasitica*. *J. Virol.* **2006**, *80*, 6588–6596. [CrossRef]
47. Van De Sande, W.W.J.; Lo-Ten-Foe, J.R.; Van Belkum, A.; Netea, M.G.; Kullberg, B.J.; Vonk, A.G. Mycoviruses: Future therapeutic agents of invasive fungal infections in humans? *Eur. J. Clin. Microbiol. Infect. Dis.* **2010**, *29*, 755–763. [CrossRef]
48. Seong, K.; Li, L.; Hou, Z.; Tracy, M.; Kistler, H.C.; Xu, J.R. Cryptic promoter activity in the coding region of the HMG-CoA reductase gene in *Fusarium graminearum*. *Fungal Genet. Biol.* **2006**, *43*, 34–41. [CrossRef]
49. Stermer, B.A.; Bianchini, G.M.; Korth, K.L. Regulation of HMG-CoA reductase activity in plants. *J. Lipid Res.* **1994**, *35*, 1133–1140. [CrossRef]
50. Lee, J.; Myong, K.; Kim, J.E.; Kim, H.K.; Yun, S.H.; Lee, Y.W. FgVelB globally regulates sexual reproduction, mycotoxin production and pathogenicity in the cereal pathogen *Fusarium graminearum*. *Microbiology* **2012**, *158*, 1723–1733. [CrossRef]
51. Jiang, J.; Yun, Y.; Liu, Y.; Ma, Z. FgVeLB is associated with vegetative differentiation, secondary metabolism and virulence in *Fusarium graminearum*. *Fungal Genet. Biol.* **2012**, *49*, 653–662. [CrossRef]
52. Chun, J.; Ko, Y.H.; Kim, D.H. Transcriptome analysis of *Cryphonectria parasitica* infected with Cryphonectria hypovirus 1 (CHV1) reveals distinct genes related to fungal metabolites, virulence, antiviral RNA-silencing, and their regulation. *Front. Microbiol.* **2020**, *11*, 1711. [CrossRef] [PubMed]
53. Subramaniam, R.; Narayanan, S.; Walkowiak, S.; Wang, L.; Joshi, M.; Rocheleau, H.; Ouellet, T.; Harris, L.J. Leucine metabolism regulates *TRI6* expression and affects deoxynivalenol production and virulence in *Fusarium graminearum*. *Mol. Microbiol.* **2015**, *98*, 760–769. [CrossRef] [PubMed]
54. Leonetti, P.; Stuttmann, J.; Pantaleo, V. Regulation of plant antiviral defense genes via host RNA-silencing mechanisms. *Virol. J.* **2021**, *18*, 194. [CrossRef] [PubMed]

55. Nuss, D.L. Mycoviruses, RNA Silencing, and Viral RNA Recombination. *Adv. Virus Res.* **2011**, *80*, 25–48. [CrossRef]
56. Mochama, P.; Jadhav, P.; Neupane, A.; Marzano, S.Y.L. Mycoviruses as triggers and targets of RNA silencing in white mold fungus *Sclerotinia sclerotiorum*. *Viruses* **2018**, *10*, 214. [CrossRef]
57. Yu, J.; Park, J.Y.; Heo, J.I.; Kim, K.H. The ORF2 protein of Fusarium graminearum virus 1 suppresses the transcription of *FgDICER2* and *FgAGO1* to limit host antiviral defences. *Mol. Plant Pathol.* **2020**, *21*, 230–243. [CrossRef]

toxins

MDPI

Article

Preparation of Monoclonal Antibody against Deoxynivalenol and Development of Immunoassays

Hoyda Elsir Mokhtar, Aidi Xu, Yang Xu, Mohamed Hassan Fadlalla and Shihua Wang *

Fujian Key Laboratory of Pathogenic Fungi and Mycotoxins, and School of Life Sciences, Fujian Agriculture and Forestry University, Fuzhou 350002, China; elsirhoyda@gmail.com (H.E.M.); 1200514073@fafu.edu.cn (A.X.); xuyang1996@fafu.edu.cn (Y.X.); awnab3@gmail.com (M.H.F.)
* Correspondence: wshmail@m.fafu.edu.cn

Abstract: Fusarium toxins are the largest group of mycotoxins, which contain more than 140 known secondary metabolites of fungi. Deoxynivalenol (DON) is one of the most important compounds of this class due to its high toxicity and its potential to harm mankind and animals and a widespread contaminant of agricultural commodities, such as wheat, corn, barley, oats, bread, and biscuits. Herein, a hybridoma cell 8G2 secreting mAb against DON was produced by fusing the splenocytes with a tumor cell line Sp2/0. The obtained mAb had a high affinity (2.39×10^9 L/mol) to DON. An indirect competitive Enzyme-Linked Immunosorbent Assay (ic-ELISA) showed that the linear range for DON detection was 3.125–25 μg/mL, and the minimum inhibitory concentration (IC_{50}) was 18.125 μg/mL with a limit of detection (LOD) of 7.875 μg/mL. A colloidal gold nanoparticle (AuNP) with 20 nm in diameter was synthesized for on-site detection of DON within 10 min with vLOD of 20 μg/mL. To improve the limit of detection, the gold nanoflower (AuNF) with a larger size (75 nm) was used to develop the AuNF-based strip with vLOD of 6.67 μg/mL. Compared to the vLOD of a convectional AuNP-based strip, the AuNF-based strip was three times lower. Herein, three immunoassay methods (ic-ELISA and AuNP/AuNF-based strips) were successfully developed, and these methods could be applied for the DON detection in agricultural products.

Keywords: deoxynivalenol; monoclonal antibody; cell fusion; ELISA; immunochromatographic strips

Key Contribution: High affinity and specific monoclonal antibody was successfully obtained and used to develop immunoassay methods for detecting Deoxynivalenol in agricultural commodities.

Citation: Mokhtar, H.E.; Xu, A.; Xu, Y.; Fadlalla, M.H.; Wang, S. Preparation of Monoclonal Antibody against Deoxynivalenol and Development of Immunoassays. *Toxins* **2022**, *14*, 533. https://doi.org/10.3390/toxins14080533

Received: 21 June 2022
Accepted: 28 July 2022
Published: 3 August 2022

1. Introduction

Deoxynivalenol (DON) is a small molecule secondary metabolite, well known as vomitoxin, which is secreted by various *Fusarium* species [1]. The genus *Fusarium* produces diverse mycotoxins known as trichothecenes, and DON is one of the most important compounds of this class due to its high toxicity. DON is classified as a type III carcinogen [2]. Ingesting feed or food exposed to DON can lead to abdominal suffering, reduced feed or food consumption, depression, diarrhea, neurotoxic and immunotoxic effects, shock, and death, particularly in high doses [3] in both animals and humans [4,5]. Mycotoxin toxicity occurs at very low concentrations, therefore, sensitive and reliable methods for their detection are required [6]. Various kinds of instrument-based approaches for DON detection have been utilized, including High-Performance Liquid Chromatography (HPLC) [7], Liquid Chromatography connected with Mass Spectrometry (LC-MS) [4], Gas Chromatography (GC) [8], and Gas Chromatography connected with Mass Spectrometry (GC-MS) [9]. These instrument- based approaches are highly sensitive and appropriate for multiple mycotoxins detection [10]. However, the drawbacks include sophisticated instrumentation, personnel experience, time-consuming, and unsuitability for the rapid screening of numerous samples. Recently, pioneer technologies with high sensitivity have been developed for DON detection, including chemiluminescence enzyme immunoassays [11,12], Raman [13],

microfluidic method [14], electrochemical immunosensors [15], and lateral-flow devices (LFD). Compared to the sophisticated instrument-based method, immunoassays, such as enzyme-linked immunosorbent assay (ELISA) and lateral flow immunoassay (LFIA), have been broadly utilized for mycotoxins detection owing to attractive advantages including high sensitivity, simplicity, low commercial cost, and rapidity [16]. The lateral flow test, or immunochromatographic assay (ICA), is a direct visible detection method via naked eyes [17]. In addition, convectional LFIA was developed by integrating different nanoparticles as signal reporters to enhance their performance [18,19] with small surface area of 20–30 nm in diameter, such as gold nanosphere (AuNS) [20]. Gold nanoparticles remain most popular reporters for ICA due to their characteristics, such as easy of synthesis and modification [18]. The traditional colloidal gold-based ICA that use 20–40 nm colloidal gold (AuNP) as signal reporters has low sensitivity given the insufficient brightness of AuNP [21]. Hierarchical structures of gold nanoparticles with large and rough surface areas are more favorable for the strong absorption of antibodies than spherical AuNP [22]. Gold nanoflower (AuNF) possesses high optical brightness and strong target binding affinity because of its multibranched structure and large specific surface area. Thus, ICA with AuNF reporters has better sensitivity than ICA with conventional AuNP. Hierarchical flowerlike gold nanoparticles (AuNF) with a larger diameter (70 mm) of surface area provide higher signal intensity than conventional AuNS [23,24]. Kim et al. established ICA to detect both DON and ZEA, with vLOD of 50 ng/mL [25]. Herein, high affinity and specific monoclonal antibody (mAb) against DON was successfully developed, and based on obtained mAb, three immunoassay methods including ic-ELISA, AuNP-based strip, and AuNF-based strip, which could be applied for DON detection in agricultural commodities, were successfully developed.

2. Results

2.1. Animal Immunization and Hybridoma Screening

Eight-week old female Balb/c mice were immunized by DON-BSA conjugate. After four immunizations, sera were collected from immunized mice individually from the tail vein. Antibody titer was measured by the iELISA method using the DON-KLH conjugate to coat the plate. It was found that two immunized mice with complete conjugate (DON-BSA) showed higher antibody titer against standard DON toxin. The splenic cells of the immunized mouse with the highest antibody titer were isolated and fused with a tumor cell line Sp2/0. The hybridoma clones specific to DON were screened by a limited dilution method. Finally, two positive clones 4A4 and 8G2 secreting specific anti-DON mAb were successfully obtained in the study.

2.2. Isotypes and Chromosome Count

The subclass of obtained antibodies secreted by positive clones was assayed via a commercial iso-typing kit (IgA, IgGI, IgG2a, IgG2b, IgG3, IgM,). It was found that 4A4 and 8G2 secreting anti-DON mAb belonged to the IgG1 subtype as shown in Figure 1a. In the previously published paper, it was reported that the chromosome count of splenocyte was 66 ± 4, and a tumor Sp2/0 was 39 ± 1 [26]. The chromosome count of positive clone 4A4 and 8G2 was 95 ± 5 and 103 ± 5, respectively, as shown in Figure 1b. Hence, results of the chromosome count indicated that the number of chromosomes resulted from the fusion of the splenic cell of immunized mice and the tumor cell line Sp2/0.

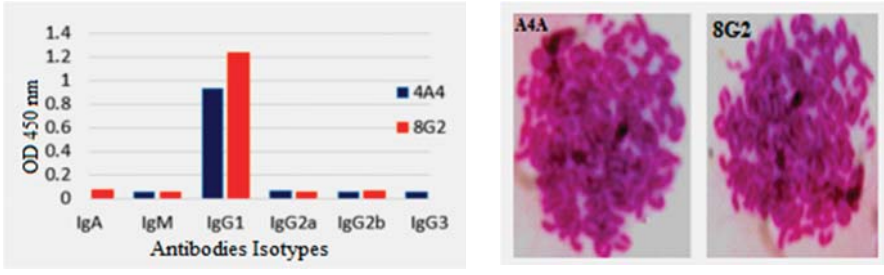

Figure 1. Isotype and chromosome assay: (**a**) Isotype assay of the hybridoma cells 4A4 and 8G2; (**b**) chromosome analysis of the hybridoma cells 4A4 and 8G2.

2.3. Purification of Positive mAb

The positive hybridoma of interest (4A4 and 8G2) were injected into the mice abdomens for ascites production. The ascites fluid was collected and directly purified using caprylic acid/ammonium sulfate procedure. The purified antibodies were assayed using Sodium dodecyl sulfate-polyacrylamide gel electrophoresis (SDS-PAGE). Figure 2a,b show that a band size of heavy and light chains for 4A4 and 8G2 were 50 kDa and 27 kDa, respectively, corresponding to the molecular weight of IgG. Subsequently, the titer of the purified antibodies was measured by iELISA. Figure 2c showed the actual titer of the purified antibodies, indicating that a high titer of the antibody was obtained. The concentrations of the target antibodies were measured by BCA protein assay, and the result showed that the concentrations of secreted antibodies of 4A4 and 8G2 were 1.41 mg/mL and 1.70 mg/mL, respectively.

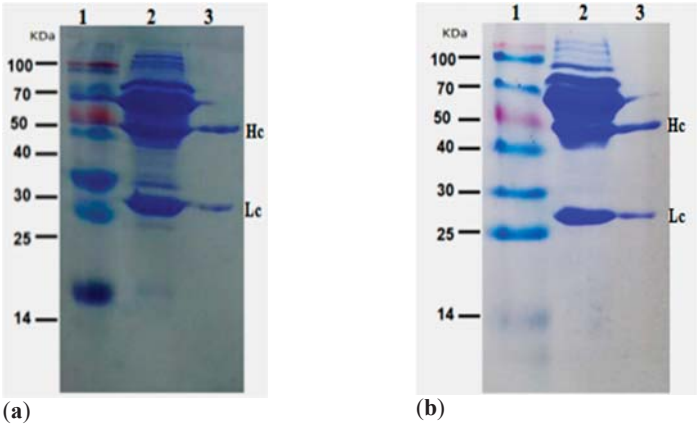

Figure 2. *Cont.*

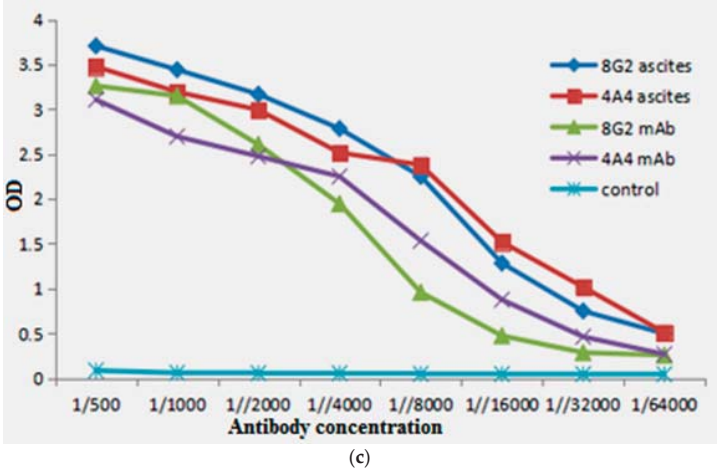

(**c**)

Figure 2. Purification and titer assay of ascites and the purified anti-DON mAb: (**a**) SDS-PAGE assay of ascites and the purified mAb for 4A4; (**b**) SDS-PAGE assay of ascites and the purified mAb for 8G2. lane 1: marker; lane 2: ascites; lane 3: purified antibody; Hc = heavy chain; Lc = light chain; (**c**) titer assay of ascites and purified mAb (4A4 and 8G2).

2.4. Affinity and Speciality of the Positive mAb

The affinity of hybridoma clones (4A4 and 8G2) against DON was characterized by iELISA assay using DON-KLH with different concentrations (1.25–10 μg/mL) to coat the ELISA plate, and serial dilutions of the purified antibody were added into the plate. Analysis of the affinity constants (*Kaff*) of 4A4 and 8G2 against the DON antigen were obtained using Origin 9.1 for data analysis. The results showed that the mAb secreted by the two clones 4A4 and 8G2 were sensitive to DON, and the (*Kaff)* for 4A4 and 8G2 were 3.9×10^8 L/mol and 2.39×10^9 L/mol, respectively (Figure 3a,b). Specificity assay of hybridoma clones (4A4 and 8G2) was carried out according to the previous method [27]. Different toxins other than DON, such as penicillic acid (PA), fumonisin B_1 (FB_1), ochratoxins A (OTA), aflatoxin B_1 (AFB_1), ocadic acid (OA), and citrinin (CTN) were used as competitor antigens for the hybridoma clones (4A4 and 8G2). From the results, the anti-DON mAb only reacted to DON without cross-reactivity to other tested toxins (Figure 3c,d). Because the affinity binding of anti-DON mAb secreted by 8G2 was higher than that of the 4A4 cell line, 8G2 was selected for further experiments.

2.5. Establishment of Standard Curve Based on ic-ELISA

The standard curve based on optimal conditions of the ic-ELISA method using the 8G2 anti-DON mAb was constructed. The relationship between DON concentration and its inhibition was analyzed using Origin 9.1 software (Figure 4a). The results showed the equation of logistic curve was $y = 0.3372 + (0.78529 - 0.33772)/(1 + x/18671)^{1.58782}$, and the correlation coefficient (R^2) was 0.98827. The linear equation was $y = 2.27178 - 0.40137x$, and the correlation coefficient (R^2) was 0.95542 (Figure 4b). In this study, IC_{50} was 18.125 μg/mL. The linear range was 3.125–25 μg/mL, and LOD was 7.875 μg/mL.

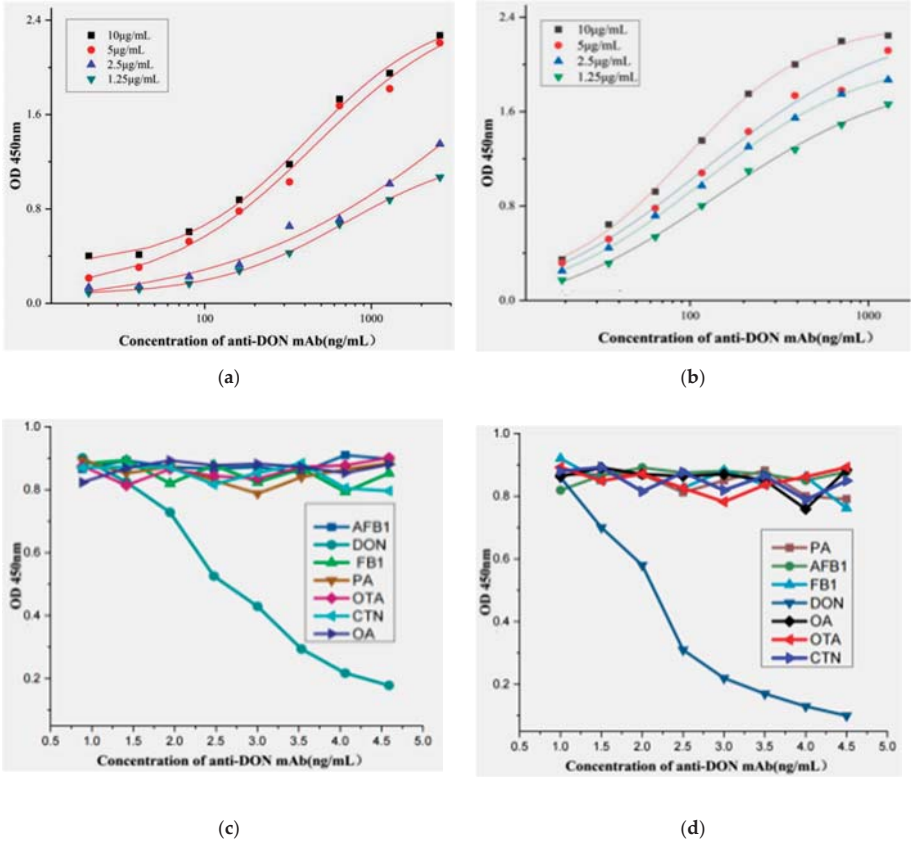

Figure 3. Affinity and cross-reactivity analysis of anti-DON mAb: (**a**) affinity determination of anti-DON mAb from 4A4; (**b**) affinity determination of anti-DON mAb from 8G2; (**c**) specificity of anti-DON mAb from 4A4; (**d**) specificity of anti-DON mAb from 8G2.

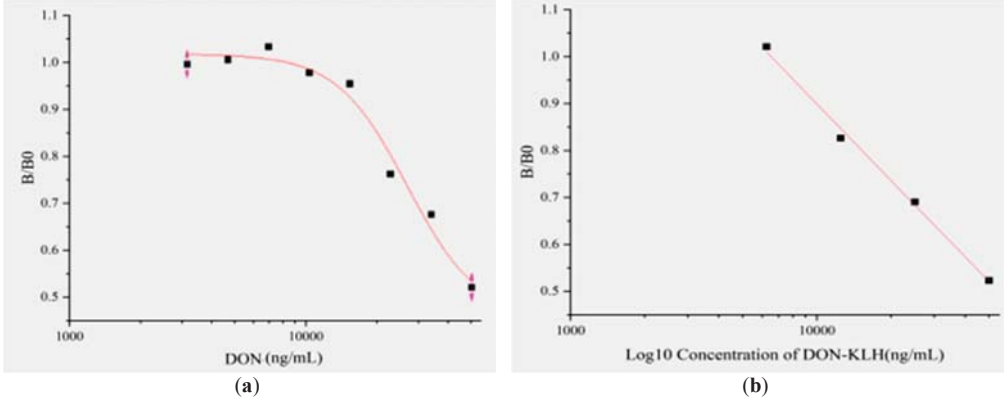

Figure 4. Development of ic-ELISA: (**a**) calibration curve of (B/B0) against DON concentration; (**b**) standard curve for DON determination by ic-ELISA.

2.6. Samples Detection

To assess the validity of the ic-ELISA method, the recovery test was performed, and four spike concentrations were selected (0.5, 5, 100, and 1000 ng/mL) for an artificially spiked DON-free corn sample. From results for intra assay, the recovery range was 87.80% to 96.53% with the average recovery of 91.46%, and the coefficient of variation (CV) range was 3.42% to 13.31%. The recovery range of inter assay was 92% to 96.61% with average recovery of 94.21%, and the CV range was 3.19% to 11.02% (Table 1). From the above results, the developed ELISA method in this study has a good stability and could be utilized for DON detection in real samples.

Table 1. Analysis of DON in spiked corn samples using the developed ic-ELISA (n = 3).

Sample	Spiked Level (ng/mL)	Intra Assay(n = 3) *				Inter Assay(n = 3) #			
		Measured Level (ng/mL)	Recovery (%)	SD	CV (%)	Measured Level (ng/mL)	Recovery (%)	SD	CV (%)
Corn	0.5	0.45	90.00	5.342	11. 87	0.46	92	4.54	9.88
	5	4.39	87.80	58.43	13.31	4.77	95.4	34.7	7.27
	100	96.53	96.53	330.1	3.42	96.61	96.61	308.2	3.19
	1000	951.2	91.52	3367.248	3.54	928.4	92.84	13.76	11.02
	Average		91.46				94.21		

Standard deviation (SD); coefficient of variation (CV); (n = 3) * within plate in one day; (n = 3) # between run in 6 days.

2.7. Development of AuNP-Based Strip for Determination of DON

Colloidal gold (AuNP) about 20 nm in diameter was prepared using the standard citrate reduction procedure, and the red solution of AuNP was obtained which was easy to be seen by the naked eye. The structure of the AuNP-based strip is shown in Figure 5a. The DON-KLH conjugate, and the Goat anti-mouse IgG were sprayed onto a nitrocellulose (NC) membrane to form a test line (T line) and a control line (C line), respectively. If the DON-free sample was subjected to the strip sample pad, the AuNP probe directly bound the DON-KLH conjugate integrated on the NC, and a red line was shown on the T line (negative). If the samples contained DON, the AuNP probe reacted with the DON from the samples, which blocked the binding to the DON-KLH conjugates on the T line. Hence, the C line on the AuNP-based strip becomes lighter (positive). If both T and C lines showed a red line, it indicates a negative result. If the T line showed the red line but the C line did not or both the C and T line did not show the red line, it indicates an invalid test (Figure 5b). For specificity assessment of the strip, different toxins including ochratoxins A (OTA), fumonisin B1 (FB1), aflatoxin G1 (AFG1), ocadic acid (OA), and penicillic acid (PA) were individually dropped onto the developed AuNP strip sample pad. The AuNP-based strip test showed a red line on both T and C line except in the case of DON. This finding shows that the AuNP-based strip was highly specific to DON without any cross-reactivity (Figure 5c). For sensitivity assessment of the AuNP-based strip, different DON toxin concentrations were added individually (4 to 100 μg/mL) to the sample pads of different AuNP-based strips. From the result, the vLOD was 20 μg/mL (Figure 5d). Real samples (wheat flour, corn flour, barely, and oats) were purchased from a supermarket and analyzed for DON contamination. From the results, the developed color of the tested samples on the strip was the same as the negative control (PBS), indicating that these samples were DON-free (Figure 5e).

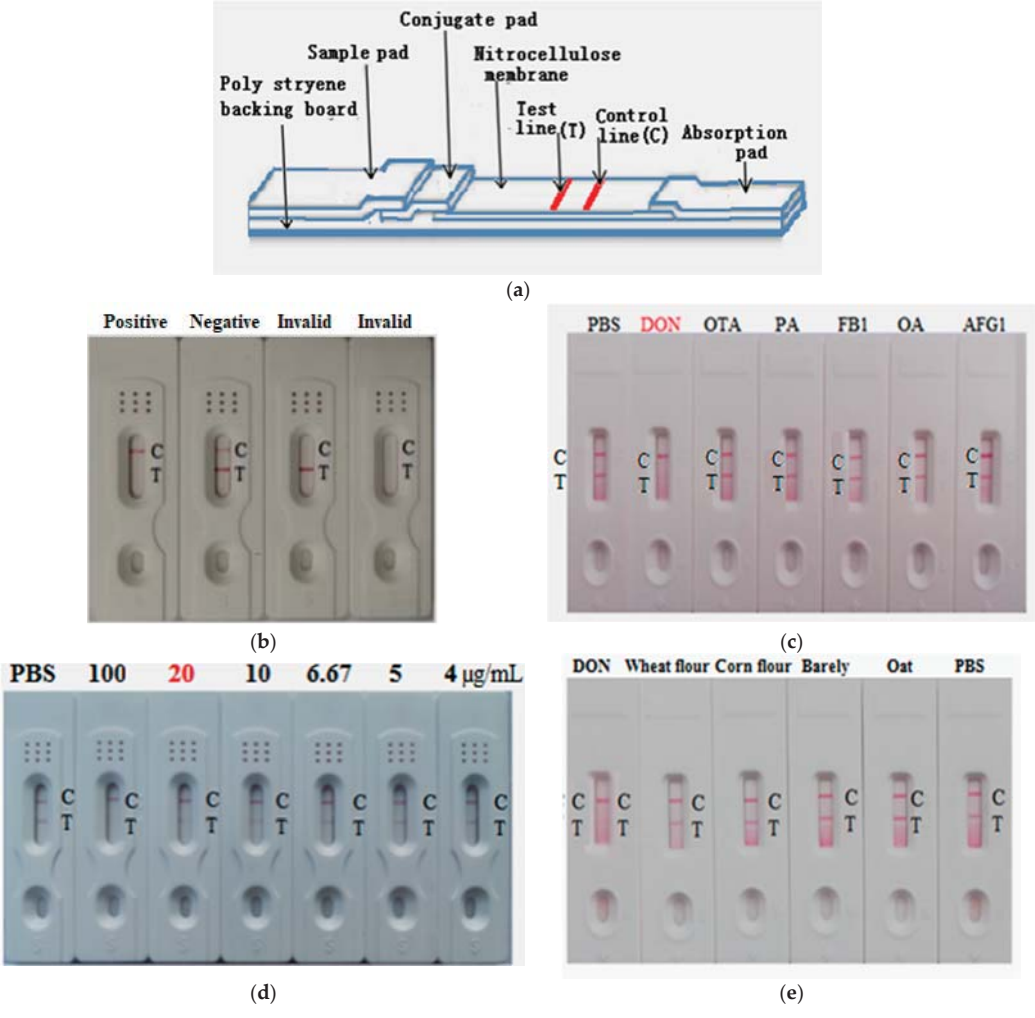

Figure 5. Construction of the AuNP-based strip for determination of DON: (**a**) AuNP strip model; (**b**) construction of the AuNP-based strip; (**c**) specificity of the AuNP-based strip; (**d**) sensitivity of the developed AuNP strip for DON toxin detection; (**e**) real samples were determined by the developed AuNP-based strip.

2.8. Preparation of AuNF Solution and AuNF-mAb Probe

To improve the detection limit of the conventional AuNP strip, the gold nanoflower (AuNF) with a large diameter of surface area was used [28], and the nanoparticles with different shape and size were also prepared [29]. For synthesis AuNF, the standard seeding growth method was used. It was reported that the reaction solution pH value together with the surface area of the AuNP influenced the antibody binding and adsorption. The prepared nanoflower solution was blue (Figure 6a). UV-vis absorption spectra showed that the peak of absorbance for the prepared AuNF solution was about 590 nm (Figure 6b). To synthesize the AuNF probe, the anti-DON mAb amount and AuNF reaction solution pH should be optimized. The optimal mount of anti-DON mAb for preparation of the AuNF probe was optimized to be 3 μL (6.12 μg) (Figure 6c). Moreover, the suitable pH of the

AuNF reaction solution adjusted with 0.1M K_2CO_3 was considered to be 9 μL (pH about 6.8) (Figure 6d). Then the AuNF probe was synthesized under the optimal conditions.

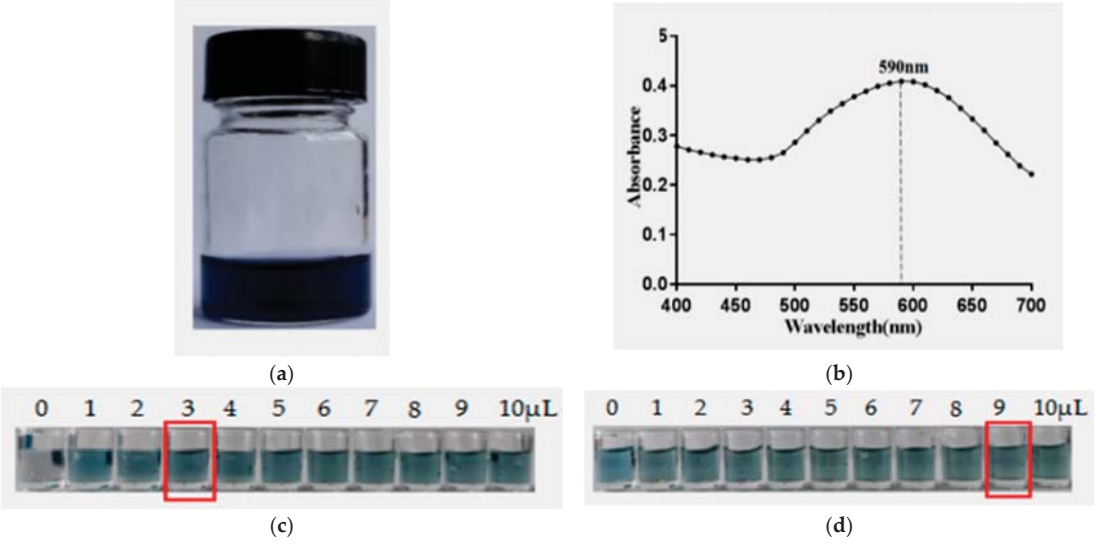

(**a**) (**b**)

(**c**) (**d**)

Figure 6. Preparation of the AuNF solution and the AuNF probe: (**a**) preparation of the AuNF solution; (**b**) the spectra of AuNF solution; (**c**) the optimal amount of anti-DON mAb for preparation of AuNF probe; (**d**) optimal volume of K_2CO_3 for preparation of the AuNF probe.

2.9. Construction and Characterization of the AuNF Strip

The AuNF strip just like the AuNP strip involved four components including sample pad (sample holder), absorption pad, and conjugate pad adhered to a nitrocellulose (NC) membrane. For sensitivity assessment of the AuNF strip, different concentrations of DON ranging from 4 to 100 μg/mL were added onto a sample pad of the developed AuNF strip. From the results, the blue on the strip (T line) became lighter with increased DON concentration (Figure 7A). Thus, the vLOD of the strip against DON was 6.67 μg/mL. For specificity evaluation of the developed AuNF strip, mycotoxins other than DON, such as AFB_1, AFB_2, and AFG_1, were individually dropped into the sample pad, and the result showed blue lines on both T and C line except for the DON toxin (Figure 7B), indicating that the AuNF strip was very specific to DON without any cross-reactivity. Likewise, real samples including rice, wheat, and corn were investigated for DON contamination. From the result in Figure 7C, the strip showed the same result as the negative control PBS, indicating that these samples were DON-free.

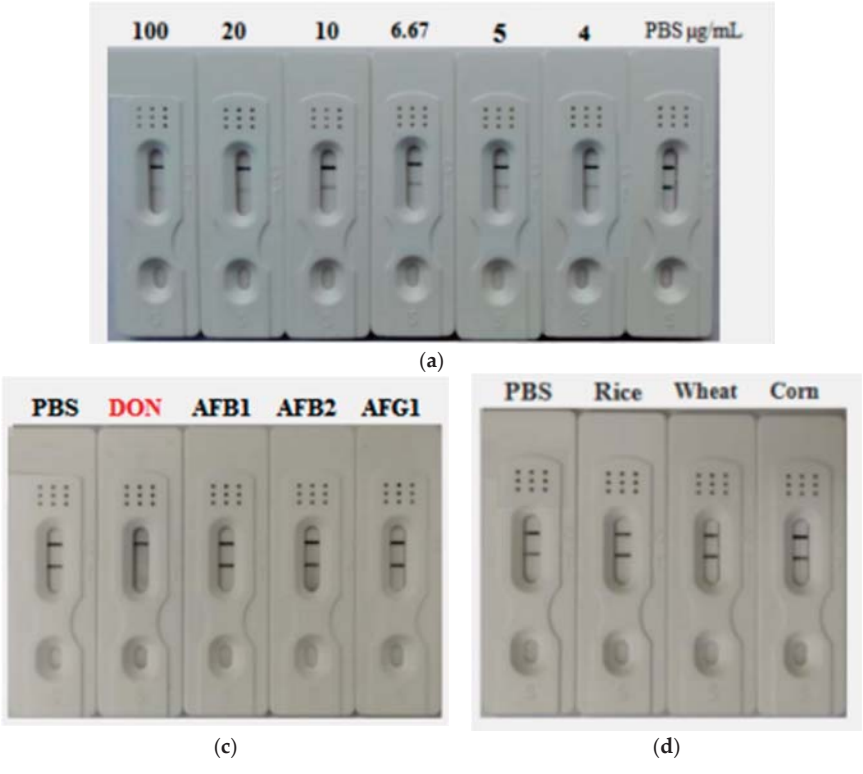

Figure 7. Construction and characterization of the AuNF strip: (**a**) sensitivity of the developed AuNF strip for DON toxin detection; (**b**) specificity of the AuNF strip; (**c**) detection of DON in real samples using the AuNF strip.

3. Discussion

DON is a secondary metabolite small molecule which cannot induce mouse immune response, thus it requires carrier proteins to enhance mouse immunity to produce a specific monoclonal antibody. In this study, high antibody titers were induced by injecting the DON-BSA conjugate into the female Balb/c mouse, then the splenic cells were isolated from injected mice and fused with their partner tumor cell line Sp2/0. The successful cell fusions were achieved, and average fusion was 86.74% and the positive fusion rate was 48.95%. According to the previously reported studies, the high average of cell fusion rates was appropriate for hybridoma production [29,30]. The cell fusion and development of hybridoma cells in this study produced several positive cell clones, and their anti-DON antibody titers were determined by iELISA. The sub-class of obtained mAb in this study was an IgG1, which showed high specificity to DON. After screening, two positive clones 4A4 and 8G2 were selected according to their high titer and then were injected into the mice abdomens for ascities production. The ascitic fluid carrying specific anti-DON mAb was withdrawn and purified using caprylic/ammonium sulfate, and the SDS-PAGE method was utilized for determination of the heavy and light chain molecular weight of target antibodies. The results showed that the A4A and 8G2 mAbs were successfully purified, and the weight of the heavy and the light chain of 4A4 and 8G2 were 50 kDa and 27 kDa, respectively, which matches the weight of the heavy and the light chain of IgG in agreement with the previous study [30]. On the other hand, the specificity of the mAbs secreted by the A4A and 8G2 hybridoma cell was measured by ic-ELISA, and the results indicated that the

anti-DON mAbs were specific to DON. In addition, an affinity constant value is essential for the antibody quality measuring the antigen–antibody reaction or binding quality, and the results showed that mAbs secreted by the two cell lines 4A4 and 8G2 were specific to DON, with an affinity constant 3.9×10^8 L/mol and 2.39×10^9 L/mol, respectively. According to the previously reported data, an antibody affinity within the range 10^7–10^{12} L/mol indicated a good antibody potency [31]. Therefore, the anti-DON mAb secreted by 8G2 clone was specific to DON with good affinity, which was higher than that in the previously reported studies [30]. Therefore, 8G2 was selected for further experiments.

Based on the constructed standard curve, the IC_{50} was 18.125 μg/mL, LOD was 7.875 μg/mL, and the ic-ELISA linear ranged 3.125–25 μg/mL which was characterized as the concentration of DON inhibition from 20% to 80%. This finding indicated that the obtained anti-DON mAb secreted by 8G2 could be utilized to prepare an assay kit for DON detection. The result from intra-assay showed that the recovery ranged from 87.80% to 96.53%, the average recovery was 91.46%, and the coefficient of variation (CV) ranged from 3.42% to 13.31%. In the inter-assay, the recovery ranged from 92% to 96.61% with a recovery average 94.21%, and CV ranged from 3.19% to 11.02%. The CVs of intra- and inter-assay were both <14%. According to the Codex Alimentarius guide (CAC/GL 71-2009, the World Health Organization and the Agriculture Food Organization, Italy), the satisfactory CV for intra-laboratory assaying is <15%. Thus, this finding confirmed that the prepared ELISA method has very good stability. Our data recommend that the ELISA method prepared in the present study could meet the requirement of quantitative analytical methods. On the other hand, a rapid ICA strip was prepared for DON detection. At the same time, anti-DON mAbs secreted by 8G2 were conjugated with colloidal gold nanoparticles (AuNP). The significant advantage of the method applied is that the AuNP can be used as a rapid and on-side detection system without any instrument, providing an important way for DON detection. For sensitivity assessment, different concentrations of standard DON (4–100 μg/mL) were assayed. From the results, the vLOD of AuNP strip was 20 μg/mL. To improve the limit of detection, the gold nanoflower (AuNF) with a larger size (75 nm) was used to develop the AuNF-based strip with LOD 6.67 μg/mL. Compared to the vLOD of a convectional AuNP-based strip, the AuNF-based strip was three times lower. All these finding indicated that the developed immuno-assays are accurate, rapid, and sensitive and could be applied for the analysis of DON residues in agricultural products.

4. Conclusions

In this work, the high affinity of monoclonal antibody (mAb) against DON (2.39×10^9 L/mol) secreted by the 8G2 cell line was obtained. Based on this mAb, three detection methods (ELISA, AuNP-based strip and AuNF-based strip) were developed. The linear range of ic-ELISA for DON detection was 3.125–25 μg/mL with LOD of 7.875 μg/mL, and the minimum inhibitory concentration (IC_{50}) was 18.125 μg/mL. Moreover, mAb was labeled with colloidal gold nanoparticles (about 20 nm) to establish the conventional AuNP-based strip, and the vLOD of the strip test was 20 μg/mL. To improve the vLOD of the conventional AuNP-based strip, the hierarchical flowerlike structure AuNF was synthesized and utilized as the reporter to produce AuNF-based strip. The AuNF strip showed vLOD of 6.67 μg/mL. These results indicated the immunological methods developed in this work could be applied for DON detection in agricultural products.

5. Materials and Methods

5.1. Material and Reagents

Balb/c female mice were obtained from Wushi animal laboratory (Shanghai, China). Standard deoxynivalenol toxin (DON), Goat anti-mouse-peroxidase conjugate (IgG- HRP), Keyhole limpet haemocyanin (KLH), Ovalbumin (OVA), DON-KLH conjugate, Bovine serum albumin (BSA), DON-BSA conjugate, Chloroauric acid ($HAuCl_4 \bullet 4H_2O$), Mouse monoclonal antibody isotyping kit (IgG1, IgG2a, IgG2b, IgG3, IgM, IgA), Fetal bovine

serum (FBS), and RPMI 1640 were purchased from Sigma-Aldrich Chemical (St. Louis, MO, USA). The murine yeloma cell line Sp2/0 was stocked in liquid nitrogen at our laboratory.

5.2. Immunization and Titer Determination

All the animal studies adhered to the Committee for Animal Ethics of Fujian Agriculture and Forestry University (FAFU) in China (C1017/23.Dec.2014). To obtain a highly sensitive as well as specific monoclonal antibody (mAb), the immunogen DON-BSA conjugate was used to immunize the 8-week old mice according to a previously published paper [32]. Equal volume of DON-BSA conjugate (100 μg) and Freund's complete adjuvant were mixed before animal injection. In the first injection of immunization, the mixer was administrated intraperitoneally. Then, an equal volume of DON-BSA conjugate (100 μg) and Freund's incomplete adjuvant were mixed for assist immunization, at 2-week intervals. After the fourth immunization, the blood was collected from the tail vein of the individual mouse and centrifuged at 5000 r/min for 35 min. Then the serum was stored at −20 °C for further use. The serum titer was measured by the iELISA method according to the previous publication [29].

5.3. Screening and Characterization of Hybridoma Cells

The positive hybridoma clones against DON were screened according to the published paper [33] with minor modifications. B-lymphocytes from the injected mouse were fused with its partner Sp2/0 myeloma cells at the ratio of 10:1 in the presence of PEG1450 [34]. Hybridoma cells were exhaustively cultivated into 96-well ELISA plates in the presence of feeder cells. Positive hybridoma were sub-cloned 3 times and isolated from the culture by limited dilution method. The positive hybridoma were cloned again for a second time and then hybridoma were characterized by the sub-class kit [35]. The chromosome number of hybridoma cells was measured using a Geimsa stain [27].

5.4. Purification and Characterization of mAb from Ascites

For ascites production, Balb/c mice were first injected with 500 μL of pristine intraperitoneally. One week later, the mice were injected with 8G2 hybridoma cells. At about 7 days, the produced ascites fluid was harvested. The ascites was purified by caprylic acid/ammonium sulfate precipitation methods. The purified mAb was assayed via SDS-PAGE [36], and antibody concentration was measured by BCA kit [37]. The affinity of target antibodies was determined based on the method previously described [24]. Different concentrations of the DON-KLH (1.25, 2.5, 5, and 10 μg/mL) were used to coat the ELISA microplate then incubated at 37 °C for 2 h, and a serial dilution of mAb in PBSM was dropped into the reaction. After washing and blocking steps, the HRP conjugated goat anti-mouse IgG (1:8000 dilutions) was finally added. The antibody affinity was evaluated using Origin 9.0 software [35]. For specificity assessment of the obtained mAbs, an ic-ELISA was conducted based on the previously published method [27], and different toxins, including ochratoxins A (OTA), fumonisin B_1 (FB_1), aflatoxin B_1 (AFB_1), citrinin (CTN), and penicillic acid (PA) with various concentrations (0.39, 0.78, 1.56, 3.13, 6.25, 12.5, 25, and 50 μg/mL) were applied as a competitor antigen to examine the cross reactivity of the obtained antibody [34].

5.5. Development of ic-ELISA and Standard Curve

Based on ic-ELISA and the optimal conditions, the standard curve was plotted [37,38]. In brief, the DON-KLH was diluted with coating buffer and used to coat the ELISA plate and incubated for 2 h at 37 °C to form a solidified antigen. Then the plate was washed and blocked with PBSM for 2 h at 37 °C. Then the blocking solution was removed, and the plate was triple-washed by PBST and then PBS, respectively. An equal volume of anti-DON mAb and standard DON toxin at different concentrations (0.39, 0.78, 1.56, 3.13, 6.25, 12.5, 25, and 50 μg/mL) were mixed and incubated at 37 °C for 30 min. After washing many times, the formed solidified antigen–antibody complex was retained on the microplate. The

HRP conjugated goat anti-mouse IgG (1:8000) was dropped into the plate and incubated for 1 h at 37 °C. The remaining solidified antigen–antibody complex reacted with the HRP conjugated secondary antibody to form a new antigen-antibody complex with enzyme activity. After an extra wash step, the substrate TMB was dropped into the plate and incubated at 37 °C for 20 min. Eventually, the H_2SO_4 (2 mol/L) was added to terminate the reaction, and the absorbance at 450 nm was measured [24]. Finally, the standard curve was constructed, and the inhibition concentration of standard DON toxin in relation to anti-DON mAb was measured using data analysis software Origin Pro 9.1 (OriginLab, Northampton, MA, USA) [27]. An actual corn sample was spiked with four concentrations of DON standard toxin (0.5, 5, 100, and 1000 ng/mL). The corn sample was crushed and soaked in 10 mL of 70% methanol (*v*/*v*) and homogenized for 35 min. After extracted and centrifuged at 1200 r/min for 20 min, the obtained supernatant was assayed by ic-ELISA. The recovery test was conducted and measured based on the constructed standard curve, and the coefficient variation (CV) together with the recovery test was measured in triplicate.

5.6. Construction and Characterization of AuNP-Based Strip

A colloidal gold particle (AuNP) was prepared by Masinde's methods [39]. The amount of antibody and optimal pH were optimized first. Then, AuNP was conjugated with anti-DON mAb to synthesize the AuNP-mAb (AuNP probe). The AuNP strip involved four components (sample pad, conjugate pad, absorbent pad, and nitrocellulose (NC) membrane). Goat anti-mouse IgG and DON-KLH coating antigen were sprayed onto the NC to form the control line (C line) and test line (T line), respectively. The AuNP probe was sprayed into the conjugate pad. To evaluate the specificity of the AuNP strip, different toxins including DON, OTA, PA, FB_1, OA, and AFG1 were, respectively, added into the individual AuNP strip. The visual results were obtained within 10 min. For the sensitivity test, different DON concentrations (4, 5, 6.67, 10, 20, and 50 μg/mL) were dropped into the individual AuNP strip, which was allowed to react with the DON-KLH coating antigen for the limited AuNP probe sprayed into the conjugate pad [33].

5.7. Preparation of Gold Nanoflower (AuNF) and AuNF Probe

The seeding growth method was conducted with some modification for synthesis of AuNF [29]. The conventional AuNP with diameter 20 nm was prepared according to the citrate reduction method [40] and used as gold seeds, whereas the $HAuCl_4$ solution and sodium hydroquinone citrate were utilized as the growth solution. Briefly, 750 μL of the hydroquinone (1 mol/L), 750 μL of $HAuCl_4$ solution (0.01%), and 100 μL of the prepared AuNP solution were placed into 100 mL of distilled water with continuous stirring. After reacting at room temperature for 35 min, the color of the solution was changed to blue, and the morphology of the obtained AuNF solution was characterized by transmission electron microscope (TEM). The preparation of the AuNF probe was conducted as Ji's method [37] with slight modification. The pH of the AuNF solution as well as the antibody amount was optimized for perfect performance of the AuNF probe. Then the anti-DON mAb was mixed by dropping into the AuNF solution under contentious gentle stirring for 35 min, and the obtained AuNF probe solution was centrifuged at 6000 r/min for 50 min, then suspended in 0.5 mL PBS and placed at 4 °C for further use.

5.8. Preparation and Characterization of AuNF-Based Strip

The AuNF strip has four components similar to the conventional AuNP strip. The AuNF probe was sprayed onto the conjugate pad. The goat anti-mouse IgG antibody and DON-KLH conjugate were integrated onto the NC membrane to form the C line and the T line, respectively. To assess specificity of the AuNF strip, different toxins such as DON, AFB_1, AFB_2, and AFG_1 were used to compete with the AuNF probe on the conjugate pad, and the visual result would be determined by the naked eyes within 7–10 min. For sensitivity, 1 mg/mL of the DON toxin standard solution was diluted into

suitable concentration (4, 5, 6.67, 10, 20, 50, and 100 μg/mL), and the sensitivity of the test strip was measured according to the experimental results (PBS as negative control).

5.9. Samples Detection

Real samples including rice, wheat, and corn samples received from a local market were assayed by the above established AuNP/AuNF -based strip tests. Briefly, 1 g of each sample was crushed and placed into a 50 mL centrifuge tube, then extracted with 2 mL aqueous solution (20% methanol). Then, the mixture was shaken for 25 min and centrifuged at 1000 r/min for 15 min, and the supernatant of each sample was collected and individually dropped into the sample pad of the constructed AuNP/AuNF -based strips, respectively.

5.10. Ethical Clearance and Animal Handle

All the animal studies adhered to the Animal Ethics Committee of the Fujian Agriculture and Forestry University, China (C1017/23.Dec.2014). The mice (female Balb/C) were handled under an appropriate condition. The room temperature was set at 25 ± 1 °C with humidity of 47–55%. The total health monitoring of the experimental mice was achieved regularly, and the mice room and cage were cleaned on a regular program.

Author Contributions: Conceptualization, S.W. and H.E.M.; methodology, A.X. and H.E.M.; validation, Y.X. and H.E.M.; formal analysis, H.E.M.; investigation, H.E.M. and M.H.F.; data curation, H.E.M.; writing—original draft preparation, H.E.M.; writing—review and editing, S.W.; supervision, S.W.; project administration, S.W. All authors have read and agreed to the published version of the manuscript.

Funding: This research received no external funding.

Institutional Review Board Statement: Not applicable.

Informed Consent Statement: Not applicable.

Data Availability Statement: Not applicable.

Conflicts of Interest: The authors declare no conflict of interest.

References

1. Zuo, H.G.; Zhu, J.X.; Shi, L.; Zhan, C.R.; Guo, P.; Wang, Y.; Zhang, Y.; Liu, J. Development of a novel immunoaffinity column for the determination of deoxynivalenol and its acetylated derivatives in cereals. *Food Anal. Methods* **2018**, *11*, 2252–2260. [CrossRef]
2. Luongo, D.; Severino, L.; Bergamo, P.; D'Arienzo, R.; Rossi, M. Trichothecenes NIV and DON modulate the maturation of murine dendritic cells. *Toxicon* **2010**, *55*, 73–80. [CrossRef] [PubMed]
3. Pestka, J.J. Mechanisms of deoxynivalenol-induced gene expression and apoptosis. *Food Addit. Contam.* **2008**, *25*, 1128–1140. [CrossRef] [PubMed]
4. Peng, Z.; Chen, L.; Nüssler, A.K.; Liu, L.; Yang, W. Current sights for mechanisms of deoxynivalenol-induced hepatotoxicity and prospective views for future scientific research: A mini review. *J. Appl. Toxicol.* **2017**, *37*, 518–529. [CrossRef]
5. Deng, C.; Li, C.; Zhou, S.; Wang, X.; Xu, H.; Wang, D.; Gong, Y.Y.; Routledge, M.N.; Zhao, Y.; Wu, Y. Risk assessment of deoxynivalenol in high-risk area of China by human biomonitoring using an improved high throughput UPLC-MS/MS method. *Sci. Rep.* **2018**, *8*, 3901. [CrossRef]
6. Rahmani, A.; Jinap, S.; Soleimany, F. Qualitative and quantitative analysis of mycotoxins. *Compr. Rev. Food Sci. Food Saf.* **2009**, *8*, 202–251. [CrossRef]
7. Rupp, H.S. Determination of Deoxynivalenol in Whole Wheat Flour and Whear Bran. *J. AOAC Int.* **2002**, *85*, 1355–1359. [CrossRef]
8. Eke, Z.; Kende, A.; Torkos, K. Simultaneous detection of A and B trichothecenes by gas chromatography with flame ionization or mass selective detection. *Microchem. J.* **2004**, *78*, 211–216. [CrossRef]
9. Jestoi, M.; Ritieni, A.; Rizzo, A. Analysis of the Fusarium mycotoxins fusaproliferin and trichothecenes in grains using gas chromatography− mass spectrometry. *J. Agric. Food Chem.* **2004**, *52*, 1464–1469. [CrossRef] [PubMed]
10. Wang, R.; Zeng, L.; Yang, H.; Zhong, Y.; Wang, J.; Ling, S.; Farhan Saeed, A.; Yuan, J.; Wang, S. Detection of okadaic acid (OA) using ELISA and colloidal gold immunoassay based on monoclonal antibody. *J. Hazard. Mater.* **2017**, *339*, 154–160. [CrossRef]
11. Zhang, R.; Zhou, Y.; Zhou, M. A sensitive chemiluminescence enzyme immunoassay for the determination of deoxynivalenol in wheat samples. *Anal. Methods* **2015**, *7*, 2196–2202. [CrossRef]
12. Li, L.; Xia, L.; Zhao, Y.; Wang, M.; Jiang, X. Immune-affinity monolithic array with chemiluminescent detection for mycotoxins in barley. *J. Sci. Food Agric.* **2017**, *97*, 2426–2435. [CrossRef]

13. Yuan, J.; Zhang, C.; Fang, S.; Zhuang, Z.; Ling, S.; Wang, S. A monoclonal antibody against F1-F0 ATP synthase beta subunit. *Hybridoma* **2012**, *31*, 352–357. [CrossRef] [PubMed]
14. Soares, R.; Santos, D.; Chu, V.; Azevedo, A.; Aires-Barros, M.; Conde, J. A point-of-use microfluidic device with integrated photodetector array for immunoassay multiplexing: Detection of a panel of mycotoxins in multiple samples. *Biosens. Bioelectron.* **2017**, *87*, 823–831. [CrossRef]
15. Lu, L.; Seenivasan, R.; Wang, Y.-C.; Yu, J.-H.; Gunasekaran, S. An electrochemical immunosensor for rapid and sensitive detection of mycotoxins fumonisin B1 and deoxynivalenol. *Electrochim. Acta* **2016**, *213*, 89–97. [CrossRef]
16. He, K.; Zhang, X.; Wang, L.; Du, X.; Wei, D. Production of a soluble single-chain variable fragment antibody against okadaic acid and exploration of its specific binding. *Anal. Biochem.* **2016**, *503*, 21–27. [CrossRef]
17. Rong-Hwa, S.; Shiao-Shek, T.; Der-Jiang, C.; Yao-Wen, H. Gold nanoparticle-based lateral flow assay for detection of staphylococcal enterotoxin B. *Food Chem.* **2010**, *118*, 462–466. [CrossRef]
18. Quesada-González, D.; Merkoçi, A. Nanoparticle-based lateral flow biosensors. *Biosens. Bioelectron.* **2015**, *73*, 47–63. [CrossRef]
19. Huang, X.; Aguilar, Z.P.; Xu, H.; Lai, W.; Xiong, Y. Membrane-based lateral flow immunochromatographic strip with nanoparticles as reporters for detection: A review. *Biosens. Bioelectron.* **2016**, *75*, 166–180. [CrossRef]
20. Parolo, C.; de la Escosura-Muñiz, A.; Merkoçi, A. Enhanced lateral flow immunoassay using gold nanoparticles loaded with enzymes. *Biosens. Bioelectron.* **2013**, *40*, 412–416. [CrossRef]
21. Ji, Y.; Ren, M.; Li, Y.; Huang, Z.; Shu, M.; Yang, H.; Xiong, Y.; Xu, Y. Detection of aflatoxin B1 with immunochromatographic test strips: Enhanced signal sensitivity using gold nanoflowers. *Talanta* **2015**, *142*, 206–212. [CrossRef] [PubMed]
22. Hamon, C.; Novikov, S.; Scarabelli, L.; Basabe-Desmonts, L.; Liz-Marzán, L.M. Hierarchical self-assembly of gold nanoparticles into patterned plasmonic nanostructures. *ACS Nano* **2014**, *8*, 10694–10703. [CrossRef]
23. Zhang, W.; Duan, H.; Chen, R.; Ma, T.; Zeng, L.; Leng, Y.; Xiong, Y. Effect of different-sized gold nanoflowers on the detection performance of immunochromatographic assay for human chorionic gonadotropin detection. *Talanta* **2019**, *194*, 604–610. [CrossRef] [PubMed]
24. Ling, S.; Zhao, Q.; Iqbal, M.N.; Dong, M.; Li, X.; Lin, M.; Wang, R.; Lei, F.; He, C.; Wang, S. Development of immunoassay methods based on monoclonal antibody and its application in the determination of cadmium ion. *J. Hazard. Mater.* **2021**, *411*, 124992. [CrossRef] [PubMed]
25. Kim, K.Y.; Shim, W.B.; Kim, J.S.; Chung, D.H. Development of a simultaneous lateral flow strip test for the rapid and simple detection of deoxynivalenol and zearalenone. *J. Food Sci.* **2014**, *79*, M2048–M2055. [CrossRef]
26. Zhou, Y.; Li, Y.; Pan, F.; Liu, Z.; Wang, Z. Identification of tetrodotoxin antigens and a monoclonal antibody. *Food Chem.* **2009**, *112*, 582–586. [CrossRef]
27. Ling, S.; Pang, J.; Yu, J.; Wang, R.; Liu, L.; Ma, Y.; Zhang, Y.; Jin, N.; Wang, S. Preparation and identification of monoclonal antibody against fumonisin B1 and development of detection by Ic-ELISA. *Toxicon* **2014**, *80*, 64–72. [CrossRef] [PubMed]
28. Shende, P.; Kasture, P.; Gaud, R. Nanoflowers: The future trend of nanotechnology for multi-applications. *Artif. Cells Nanomed. Biotechnol.* **2018**, *46*, 413–422. [CrossRef] [PubMed]
29. Zhang, Y.; Yang, J.; Lu, Y.; Ma, D.-Y.; Qi, M.G.; Wang, S. A competitive direct enzyme-linked immunosorbent assay for the rapid detection of deoxynivalenol: Development and application in agricultural products and feedstuff. *Food Agric. Immunol.* **2017**, *28*, 516–527. [CrossRef]
30. Zhou, S.; Xu, L.; Kuang, H.; Xiao, J.; Xu, C. Fluorescent microsphere immunochromatographic sensor for ultrasensitive monitoring deoxynivalenol in agricultural products. *Microchem. J.* **2021**, *164*, 106024. [CrossRef]
31. Maragos, C.; Busman, M.; Plattner, R. Development of monoclonal antibodies for the fusarin mycotoxins. *Food Addit. Contam.* **2008**, *25*, 105–114. [CrossRef] [PubMed]
32. Kong, T.; Hao, X.-Q.; Li, X.-B.; Liu, G.-W.; Zhang, Z.-G.; Yang, Z.-J.; Wang, Z.; Tang, J.; Yang, W.; Sun, J. Preparation of novel monoclonal antibodies against chelated cadmium ions. *Biol. Trace Elem. Res.* **2013**, *152*, 117–124. [CrossRef] [PubMed]
33. Fadlalla, M.H.; Ling, S.; Wang, R.; Li, X.; Yuan, J.; Xiao, S.; Wang, K.; Tang, S.; Elsir, H.; Wang, S. Development of ELISA and lateral flow immunoassays for ochratoxins (OTA and OTB) detection based on monoclonal antibody. *Front. Cell. Infect. Microbiol.* **2020**, *10*, 80. [CrossRef]
34. Cho, Y.-J.; Lee, D.-H.; Kim, D.-O.; Min, W.-K.; Bong, K.-T.; Lee, G.-G.; Seo, J.-H. Production of a monoclonal antibody against ochratoxin A and its application to immunochromatographic assay. *J. Agric. Food Chem.* **2005**, *53*, 8447–8451. [CrossRef]
35. Ling, S.; Chen, Q.-A.; Zhang, Y.; Wang, R.; Jin, N.; Pang, J.; Wang, S. Development of ELISA and colloidal gold immunoassay for tetrodotoxin detetcion based on monoclonal antibody. *Biosens. Bioelectron.* **2015**, *71*, 256–260. [CrossRef] [PubMed]
36. Di Girolamo, F.; Ponzi, M.; Crescenzi, M.; Alessandroni, J.; Guadagni, F. A simple and effective method to analyze membrane proteins by SDS-PAGE and MALDI mass spectrometry. *Anticancer Res.* **2010**, *30*, 1121–1129.
37. Jin, N.; Ling, S.; Yang, C.; Wang, S. Preparation and identification of monoclonal antibody against Citreoviridin and development of detection by Ic-ELISA. *Toxicon* **2014**, *90*, 226–236. [CrossRef]
38. Lenc, L.; Czecholiński, G.; Wyczling, D.; Turów, T.; Kaźmierczak, A. Fusarium head blight (FHB) and Fusarium spp. on grain of spring wheat cultivars grown in Poland. *J. Plant Prot. Res.* **2015**, *55*, 266–277. [CrossRef]

39. Masinde, L.A.; Sheng, W.; Xu, X.; Zhang, Y.; Yuan, M.; Kennedy, I.R.; Wang, S. Colloidal gold based immunochromatographic strip for the simple and sensitive determination of aflatoxin B1 and B2 in corn and rice. *Microchim. Acta* **2013**, *180*, 921–928. [CrossRef]
40. Zhan, L.; Guo, S.-z.; Song, F.; Gong, Y.; Xu, F.; Boulware, D.R.; McAlpine, M.C.; Chan, W.C.; Bischof, J.C. The role of nanoparticle design in determining analytical performance of lateral flow immunoassays. *Nano Lett.* **2017**, *17*, 7207–7212. [CrossRef]

toxins

MDPI

Article

Insights into the Underlying Mechanism of Ochratoxin A Production in *Aspergillus niger* CBS 513.88 Using Different Carbon Sources

Shan Wei [1,2], Chaojiang Hu [1,2], Ping Nie [1,2], Huanchen Zhai [1,2], Shuaibing Zhang [1,2], Na Li [1,2], Yangyong Lv [1,2,*] and Yuansen Hu [1,2,*]

[1] College of Bioengineering, Henan University of Technology, Zhengzhou 450001, China
[2] Henan Provincial Key Laboratory of Biological Processing and Nutritional Function of Wheat, Zhengzhou 450001, China
* Correspondence: lvyangyong@haut.edu.cn (Y.L.); huyuansen@haut.edu.cn (Y.H.)

Abstract: *Aspergillus niger* produces carcinogenic ochratoxin A (OTA), a serious food safety and human health concern. Here, the ability of *A. niger* CBS 513.88 to produce OTA using different carbon sources was investigated and the underlying regulatory mechanism was elucidated. The results indicated that 6% sucrose, glucose, and arabinose could trigger OTA biosynthesis and that 1586 differentially expressed genes (DEGs) overlapped compared to a non-inducing nutritional source, peptone. The genes that participated in OTA and its precursor phenylalanine biosynthesis, including *pks*, *p450*, *nrps*, *hal*, and *bzip*, were up-regulated, while the genes involved in oxidant detoxification, such as *cat* and *pod*, were down-regulated. Correspondingly, the activities of catalase and peroxidase were also decreased. Notably, the novel *Gal4*-like transcription factor An12g00840 (*AnGal4*), which is vital in regulating OTA biosynthesis, was identified. Deletion of *AnGal4* elevated the OTA yields by 47.65%, 54.60%, and 309.23% using sucrose, glucose, and arabinose as carbon sources, respectively. Additionally, deletion of *AnGal4* increased the superoxide anion and H_2O_2 contents, as well as the sensitivity to H_2O_2, using the three carbon sources. These results suggest that these three carbon sources repressed *AnGal4*, leading to the up-regulation of the OTA biosynthetic genes and alteration of cellular redox homeostasis, ultimately triggering OTA biosynthesis in *A. niger*.

Keywords: *Aspergillus niger*; ochratoxin A; secondary metabolism; redox homeostasis; carbon sources; *AnGal4*

Key Contribution: This study demonstrates that arabinose, sucrose, and glucose trigger OTA production in *A. niger* CBS 513.88 by repressing a *Gal4*-like transcription factor An12g00840 (*AnGal4*), leading to the up-regulation of the OTA biosynthetic genes and altered cellular redox homeostasis.

Citation: Wei, S.; Hu, C.; Nie, P.; Zhai, H.; Zhang, S.; Li, N.; Lv, Y.; Hu, Y. Insights into the Underlying Mechanism of Ochratoxin A Production in *Aspergillus niger* CBS 513.88 Using Different Carbon Sources. *Toxins* **2022**, *14*, 551. https://doi.org/10.3390/toxins14080551

Received: 12 July 2022
Accepted: 8 August 2022
Published: 12 August 2022

1. Introduction

Aspergillus and *Penicillium* frequently contaminate nuts and grapes and produce the "group 2B carcinogen" ochratoxin A (OTA), which is a serious threat to human health and causes huge economic losses worldwide [1,2]. In *Aspergillus*, OTA is dominantly produced by *Aspergillus carbonarius* and *A. ochraceus*, and recent studies reported that several *A. niger* strains produced OTA [3,4]. *A. niger* is an extremely well-studied and versatile organism, with widespread applications in the production of organic acids, industrial enzymes, and heterologous proteins. *A. niger* CBS 513.88 was found to have a putative OTA biosynthetic gene cluster by genome sequencing [5]. Further investigation of the OTA biosynthesis in *A. niger* CBS 513.88 could, therefore, provide the theoretical basis for the development of effective strategies to control mycotoxin contamination in the fermentation of industrial products.

OTA is a polyketide derivative formed by connecting a dihydrocoumarin moiety and L-phenylalanine by an amide bond [6,7]. The OTA biosynthetic pathway has been well characterized in *A. ochraceus* using comparative genomic analyses [3]. Four genes, *pks*, *p450*, *nrps*, *hal*, and the *bzip* gene for a transcription factor (TF), comprise this cluster [8]. Previous reports indicated that OTA biosynthesis is regulated by environmental factors, including carbon sources, nitrogen sources, temperature, water activities, pH, and other conditions [9,10].

The utilization of carbon sources affects fungal production of secondary metabolites, including mycotoxins such as aflatoxin [11], fumonisin [12], patulin [13] trichothecene [14], citrinin [15], and OTA [16]. However, apart from carbon catabolite repression (CCR) [17], the cAMP signaling pathway [18], and the flux rearrangement of primary metabolism [19], few studies have evaluated the regulatory mechanisms of secondary metabolite production. Therefore, the underlying mechanism of carbon sources regulating OTA production in *A. niger* needs to be further explored. Glucose, sucrose, and arabinose could be used as carbon sources in industrial fermentation of *A. niger* [20–22]. Elucidating the regulatory mechanism of OTA biosynthesis in response to different carbon sources will help in developing effective strategies for controlling OTA contamination.

In this study, to better understand the OTA production facilitating its prevention and control in *A. niger*, the effects of sucrose, glucose, and arabinose on growth, conidia formation, and OTA biosynthesis in *A. niger* CBS 513.88 were investigated, and its underlying mechanism was elucidated by transcriptome analyses. Notably, a significantly down-regulated fungal-specific *AnGal4*-like Zn(II)2Cys6 transcription factor in three OTA-inducing carbon sources was investigated, and its function in OTA biosynthesis and underlying regulatory mechanisms were further elucidated.

2. Results

2.1. Identification of the OTA-Producing Aptitude by A. niger CBS 513.88

To investigate whether the *A. niger* CBS 513.88 strain could produce OTA, the retention time of the OTA standard was determined by HPLC-FLD (Figure 1A). The corresponding peak was observed at a similar time in the methanolic extracts of *A. niger* CBS 513.88 that was cultured on YES solid media under the same chromatographic conditions (Figure 1B), so the peak was further analyzed using UHPLC-MS. The results confirmed that *A. niger* CBS 513.88 could produce OTA (Figure 1C,D).

2.2. Influence of Different Carbon Sources on Colony Morphology, Conidia Production, and OTA Biosynthesis of A. niger CBS 513.88

After 5.5 days of culture, colony morphology and sporulation ability were significantly changed in *A. niger* CBS 513.88 when grown on yeast extract containing different carbon sources (sucrose, glucose, and arabinose), when compared with peptone. As shown in Figure 2A, on YEP solid medium, colonies were covered by dense dark brown conidial heads in the center. In contrast, on YES, YEG, and YEA solid media, colonies were light yellow. The conidia productions on YES, YEG, and YEA solid media were significantly lower than that on YEP solid medium (Figure 2B). Moreover, the colony diameters on YES, YEG, and YEA solid media were larger than that on YEP solid medium (Figure 2C). Together, the results indicated that the growth rates of the strains grown on YES, YEG, and YEA solid media were higher than that on YEP solid medium.

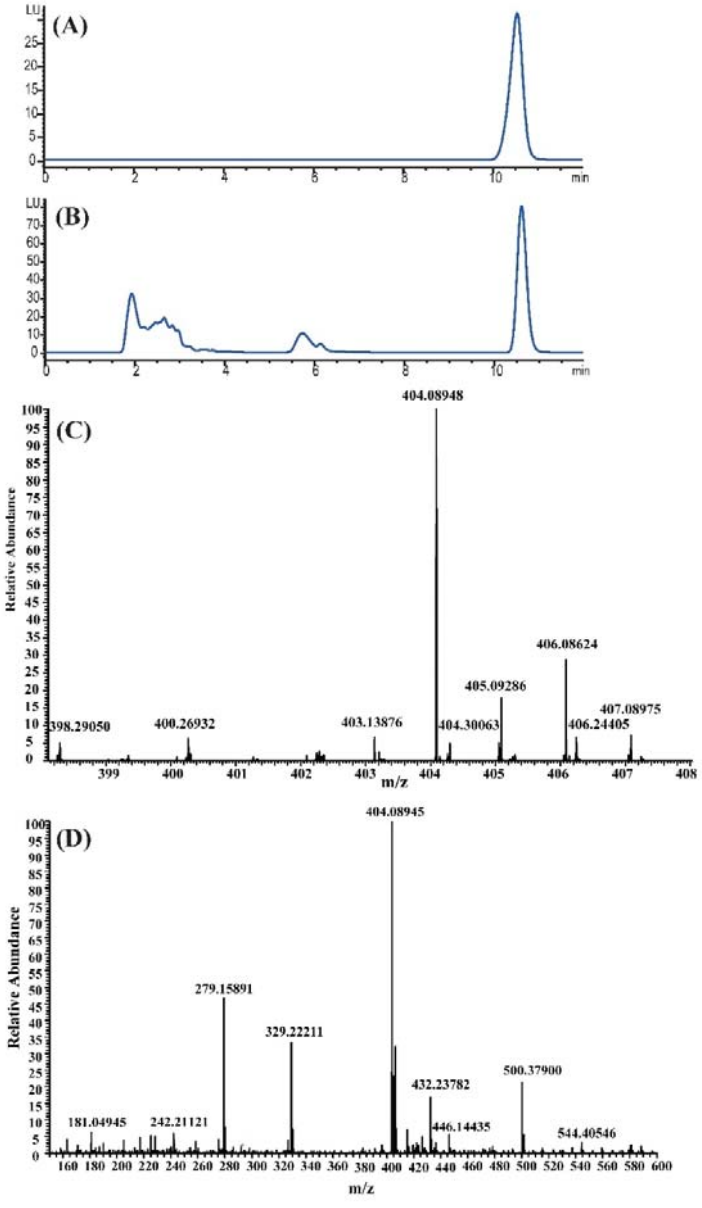

Figure 1. High-performance liquid chromatography with fluorescence detection (HPLC-FLD) chromatograms and ultra-high performance liquid chromatography mass spectrometry (UHPLC-MS) analysis of the methanolic extract of *A. niger* CBS 513.88. HPLC-FLD chromatograms of OTA standard (**A**) and the methanolic extract of *A. niger* CBS 513.88 (**B**), UHPLC-MS analysis of OTA standard (**C**) and the methanolic extract of *A. niger* CBS 513.88 (**D**) in the positive ion mode.

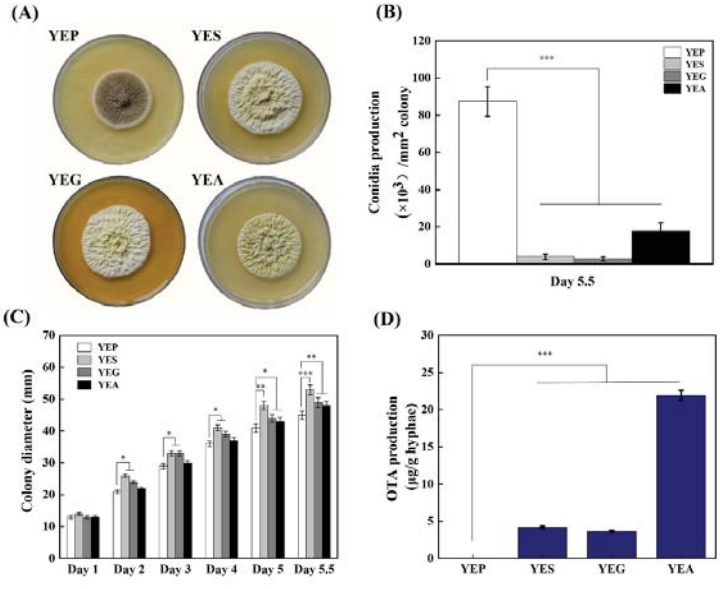

Figure 2. Colony view and phenotypic analysis of the *A. niger* CBS 513.88 strain inoculated on YEP, YES, YEG, and YEA media plates incubated at 30 °C for 5.5 days. (**A**) The colonies at 5.5 days. (**B**) Conidia production per mm^2 of colony at 5.5 days. (**C**) The colony diameters at days 1~5.5. (**D**) OTA production (μg/g dry hyphae). The error bars represent the standard deviation of three parallel biological experiments. * $t < 0.05$, ** $t < 0.01$, *** $t < 0.001$.

The influence of different carbon sources on OTA biosynthesis was further studied by HPLC-FLD. After 5.5 days of cultivation at 23 °C in the dark, the concentration of OTA reached around 4.19, 3.64, and 21.93 μg/g dry hyphae on YES, YEG, and YEA solid media, respectively. However, OTA was not detected on the YEP solid medium (Figure 2D). These results confirmed that arabinose was the best carbon source to produce OTA in *A. niger* CBS 513.88, followed by sucrose and glucose, while peptone inhibited OTA production. Arabinose, sucrose, and glucose were, therefore, defined as OTA-inducing carbon sources, and peptone as the non-inducing nutritional source.

2.3. Transcriptional Profiles and DEGs Analyses of A. niger CBS 513.88 Using Different Carbon Sources

To further reveal the mechanism of OTA production using different carbon sources, we performed transcriptome sequencing of the *A. niger* strain. Strains grown on YES, YEG, and YEA solid media were the test group, and YEP medium was the control group. We identified DEGs, which overlapped with the three OTA-inducing carbon sources and the non-inducing nutritional source, to narrow the scope of our studies. The samples were all analyzed at 5.5 days of incubation at 23 °C in the dark. Transcriptome analyses showed that 1778, 1618, and 1792 genes were significantly up-regulated on YES, YEG, and YEA solid media, respectively, whereas 1317, 1079, and 1579 genes were significantly down-regulated, respectively (Figure 3A). A total of 1586 DEGs overlapped on YES, YEG, and YEA solid media, of which 986 were up-regulated and 595 were down-regulated (Figure 3B). Among them, genes associated with the OTA precursor phenylalanine (An08g06800, An14g06010, and An15g02460) and OTA biosynthesis (*nrps*, *P450*, *hal*, and *bzip*) were significantly up-regulated (Table 1), which was confirmed by qRT-PCR analyses (Figure S1). Although the transcriptional level of *pks* was unchanged on YES and YEG media, it was significantly up-regulated on YEA medium with the highest OTA concentration. Together, the results

showed that carbon sources affected the OTA production of *A. niger* by controlling the levels of OTA and its precursor phenylalanine biosynthesis.

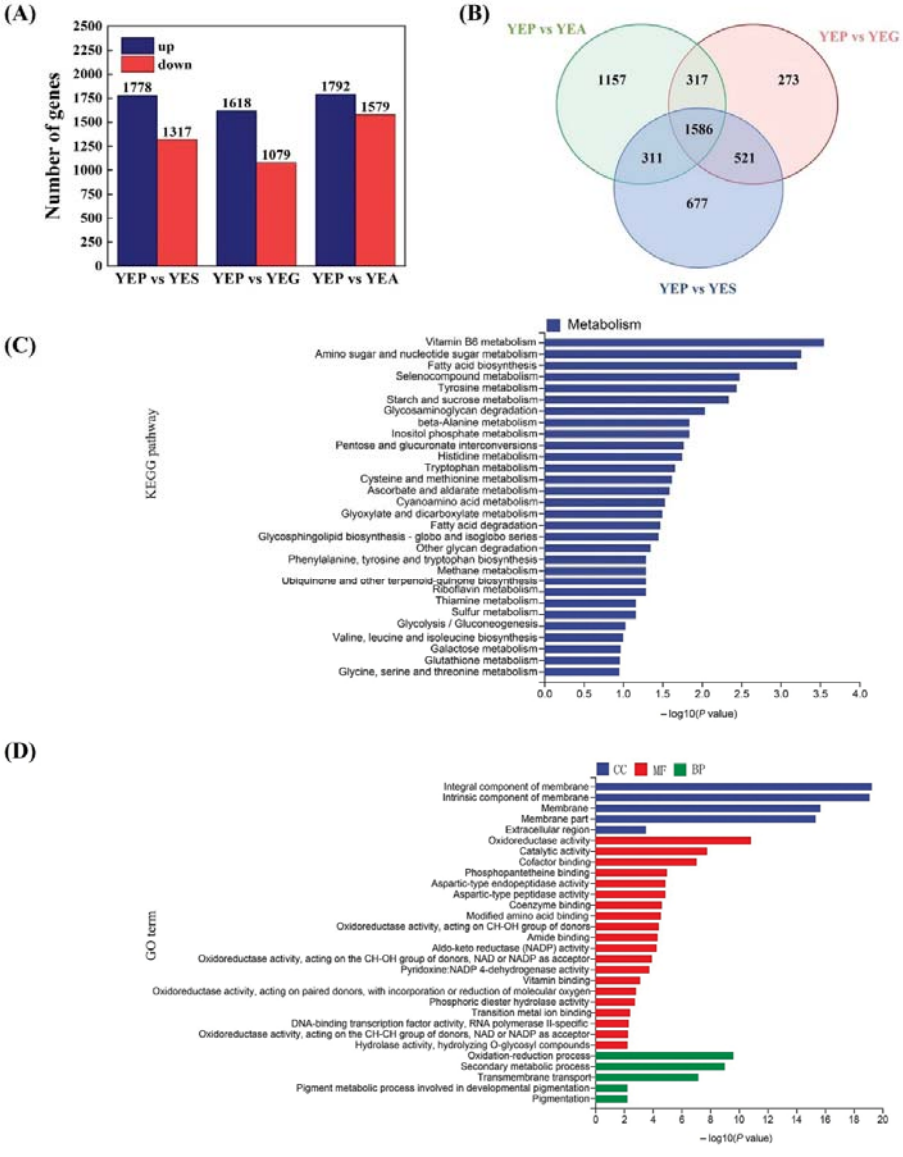

Figure 3. Analysis of differentially expressed genes in the presence of different carbon sources. (**A**) The number of up-and down-regulated genes on YES, YEG, and YEA solid media, when compared to that on YEP solid medium. (**B**) Venn diagram showing the overlaps on YEP vs. YES, YEP vs. YEG, and YEP vs. YEA. (**C**) Kyoto Encyclopedia of Genes and Genomes enrichment analysis of the overlapping differentially expressed genes (DEGs) on YES, YEG, and YEA solid media. (**D**) Gene Ontology enrichment analysis of the overlapping DEGs on YES, YEG, and YEA solid media.

Table 1. RNA-seq analysis of DEGs in *A. niger* CBS 513.88.

Gene ID	Function	Transcriptome Data (log_2(Fold Change))		
		YES/YEP	YEG/YEP	YEA/YEP
DEGs involved in conidiogenesis				
An01g10540	Regulatory protein (*brlA*)	−2.44 ***	−2.18 ***	−2.81 ***
DEGs involved in phenylalanine, histidine, tyrosine, tryptophan, and arginine biosynthesis				
An08g06800	5-Dehydroshikimate dehydrase	1.30 ***	1.06 ***	1.71 ***
An14g06010	Chorismate mutase	1.28 ***	1.57 ***	1.90 ***
An15g02460	L-kynurenine/alpha-aminoadipate aminotransfease	1.45 **	1.19	1.50 ***
An14g07210	Histidinol dehydrogenase 1	3.37 ***	2.58 *	2.17 ***
An16g02500	Tryptophan synthase	4.33 ***	3.87 ***	3.40 ***
An04g08100	Shikimate/quinate 5-dehydrogenase	5.49 ***	5.66 ***	4.53 ***
An15g02340	Argininosuccinate synthase	1.61 ***	1.05 ***	1.16 ***
DEGs involved in OTA biosynthesis				
An15g07920	Polyketide synthase (*pks*)	0.01	0.19	1.7 ***
An15g07900	Oxidoreductase activity (*p450*)	3.28 **	2.62	2.30 **
An15g07910	Nonribosomal peptide synthase (*nrps*)	3.43 *	2.96 *	3.28 ***
An15g07880	Oxidoreductase activity (*hal*)	3.55 *	3.19	3.59 ***
An15g07890	bZIP transcription factor (*bzip*)	2.32	2.29	1.53
DEGs involved in oxidative stress				
An08g08920	Catalase activity (*cat*)	−1.42 ***	−1.41 ***	−2.15 ***
An14g00690	Catalase activity (*cat*)	−2.65 ***	−2.04 ***	−3.21 ***
An09g00820	Predicted peroxidase activity (*pod*)	−2.04 ***	−2.40 ***	−2.75 ***
An16g00630	Predicted peroxidase activity (*pod*)	−2.16 **	−3.67 ***	−1.59 *

All data are the mean ± standard deviation of independent tests performed in triplicate. * $p < 0.05$, ** $p < 0.01$, *** $p < 0.001$.

KEGG pathway and GO analyses for the 1586 DEGs were also conducted. According to the KEGG pathway analyses, DEGs were involved in carbohydrate metabolism, containing glycolysis/gluconeogenesis, and starch/sucrose/galactose/amino acids metabolism (Figure 3C). Genes involved in phenylalanine, histidine, tyrosine, tryptophan, and arginine biosynthesis were up-regulated (Table 1). According to GO terms analyses, DEGs were primarily involved in oxidative stress. In the molecular functions and biological processes category, DEGs were mainly associated with oxidoreductase activity and oxidation-reduction processes, respectively (Figure 3D).

2.4. Carbon Sources Affect the Cellular Redox Homeostasis of A. niger CBS 513.88

The carbon source affects the cellular redox status in filamentous fungi, and OTA production is closely related to oxidative stress [3,10,12]. The generated H_2O_2 can be catalyzed by CAT and POD. In this study, the expression levels of An08g08920 and An14g00690 that encode CAT and An09g00820 and An16g00630 that encode POD, were all significantly down-regulated in three OTA-inducing conditions, when compared to non-inducing conditions (Figure 4A) (Table 1). Correspondingly, the activities of the two antioxidant enzymes of *A. niger* strains were detected (Figure 4B). Compared to that on YEP solid medium, the activities of CAT on YES, YEG, and YEA solid medium decreased by 75.6%, 69.5%, and 62.8%, respectively. Similarly, compared to that on the YEP solid medium, the activities of POD on YES, YEG, and YEA solid medium decreased by 40.4%, 48.0%, and 64.6%, respectively. Together, the results indicated that carbon sources may affect OTA biosynthesis by altering the homeostasis of cellular redox.

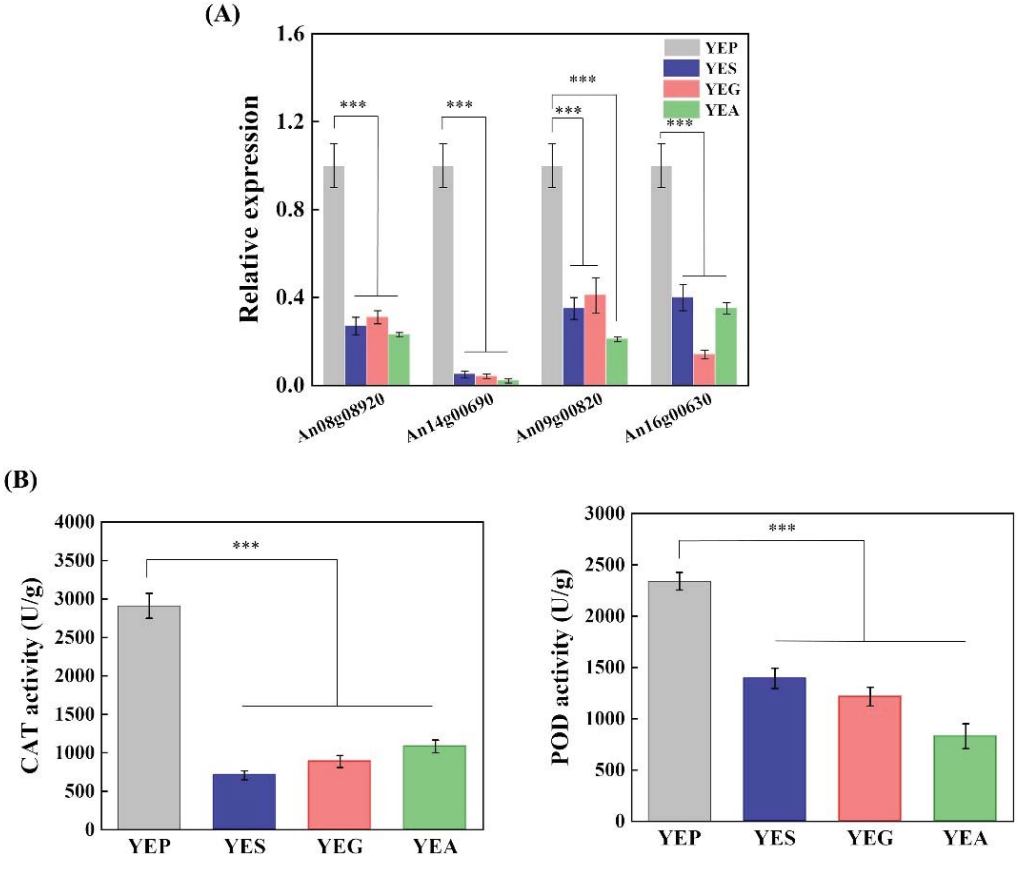

Figure 4. Effect of carbon sources on the cellular redox homeostasis of *A. niger* CBS 513.88. (**A**) The qRT-PCR results of differentially expressed genes associated with cellular oxidant detoxification. (**B**) The activities of antioxidant enzymes include catalase (CAT, U/g) and peroxidase (POD, U/g). All data are expressed as the mean ± standard deviation of independent tests performed in triplicate (*** $t < 0.001$).

2.5. Disruption of a Novel Gal4-like Transcription Factor Affects OTA Biosynthesis

Transcription factors (TFs) in gene regulatory networks have previously been reported to regulate intracellular metabolic processes in response to environmental changes [23]. There were 25 up-regulated TFs and 14 down-regulated TFs in the 3 OTA-inducing conditions (Table S1). Among them, 20 TFs had homologous genes in yeast and were annotated according to the *Saccharomyces* Genome Database, SGD (https://www.yeastgenome.org/, accessed on 1 December 2021). Using SGD annotation, these TF genes were shown to be involved in carbon metabolism, stress response, amino acid catabolism, sterol biosynthesis, etc. An12g00840, a fungal-specific *Gal4*-like Zn(II)2Cys6 transcription factor (*AnGal4*), was significantly down-regulated in three OTA-inducing carbon sources. To characterize the role of *AnGal4* in OTA biosynthesis, an *AnGal4* deletion strain was constructed (Figure 5A). The samples were collected after 5.5 days at 23 °C, when grown in the three OTA-inducing conditions. The results showed OTA yields of the Δ*AnGal4* strain increased by 47.65%, 54.60%, and 309.23% on YES, YEG, and YEA solid media, respectively (Figure 5B). Correspondingly, the transcript levels of OTA biosynthetic genes of the Δ*AnGal4* strain were all

obviously up-regulated in the presence of the three carbon sources (Figure 5C–E). Together, the results showed that *AnGal4* negatively regulated the OTA biosynthesis.

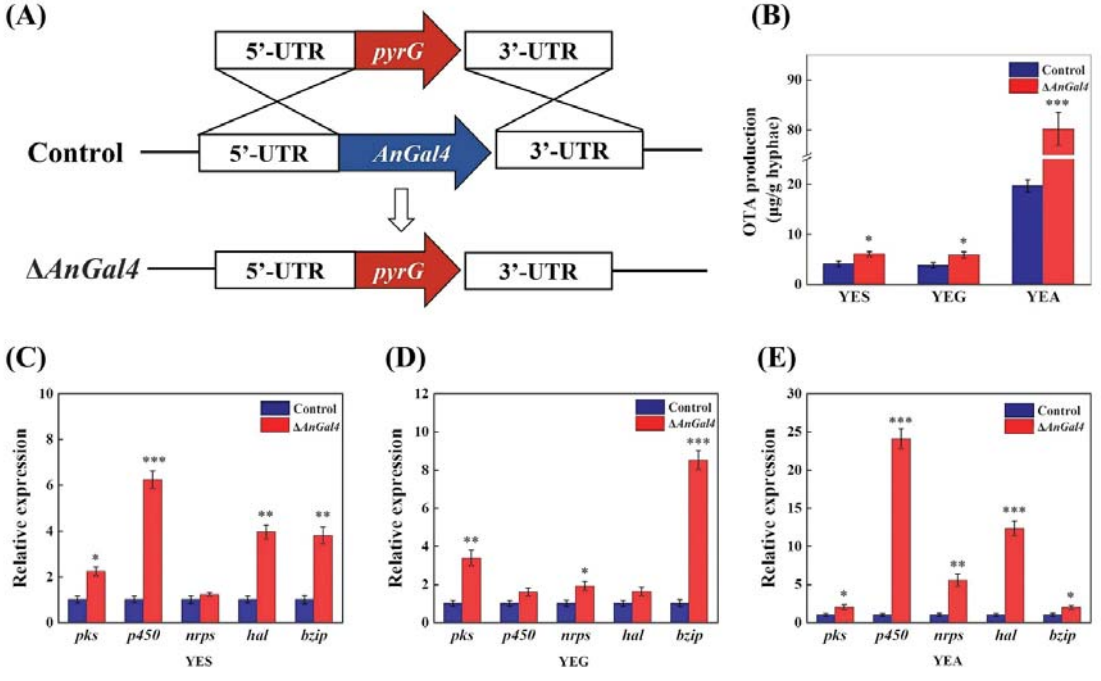

Figure 5. The effect of *AnGal4* deletion on the OTA yields and related gene expressions in the presence of three OTA-inducing carbon sources. Construction of the *AnGal4* deletion strain (**A**). The effect of *AnGal4* deletion on OTA yield (**B**). The effect of *AnGal4* deletion on the expressions of OTA biosynthetic genes on YES solid medium (**C**), on YEG solid medium (**D**), and on YEA solid medium (**E**). * $t < 0.05$, ** $t < 0.01$, *** $t < 0.001$.

2.6. AnGal4 Affects Cellular Redox Homeostasis of A. niger

To further investigate the correlation between *AnGal4* and oxidative stress, the O^{2-} and H_2O_2 contents, and the sensitivity to H_2O_2 in the Δ*AnGal4* strain using three carbon sources were determined. The results showed that the O^{2-} contents in the Δ*AnGal4* strain increased by 158.37%, 80.57%, and 27.07% on YES, YEG, and YEA solid media, respectively (Figure 6A). The H_2O_2 contents in Δ*AnGal4* strain increased by 11.94%, 25.77%, and 20.41% on YES, YEG, and YEA solid media, respectively (Figure 6B). In addition, although the growth was unchanged in the Δ*AnGal4* and control strains under unstressed conditions, the Δ*AnGal4* strain exhibited significant growth defects when supplemented with 10, 20 and 30 mM H_2O_2, with the defects especially pronounced at high concentrations, showing that deletion of Δ*AnGal4* increased the sensitivity to H_2O_2 (Figure 6C). Together, the results suggested that *AnGal4* affected the cellular redox homeostasis of *A. niger* and that the deletion of Δ*AnGal4* increased cellular oxidative stress.

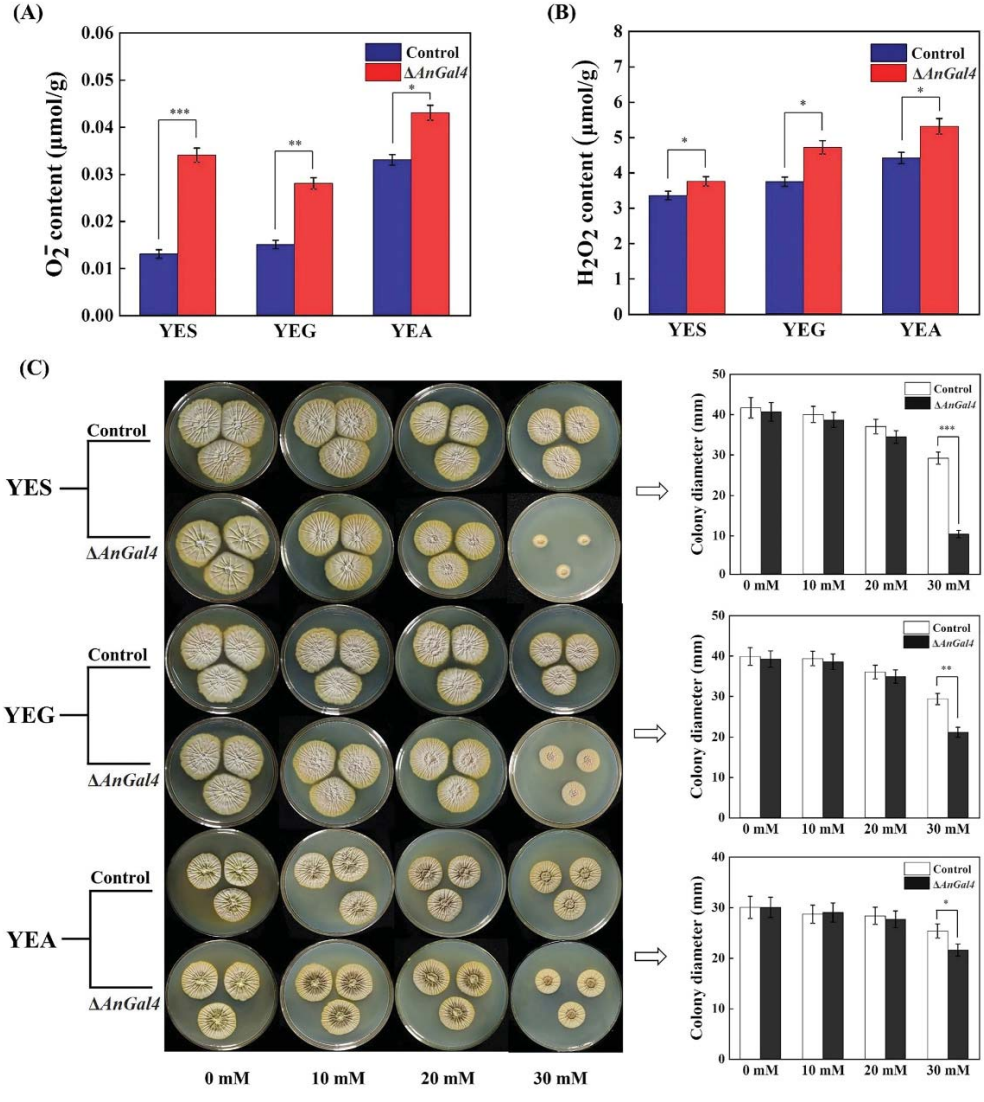

Figure 6. The effect of AnGal4 deletion on the cellular redox homeostasis of *A. niger* strain in the presence of three OTA-inducing carbon sources. (**A**) O^{2-} contents. (**B**) H_2O_2 contents. (**C**) The sensitivity to H_2O_2 at different concentrations and the effects of H_2O_2 on the growth of different strains. * $t < 0.05$, ** $t < 0.01$, *** $t < 0.001$.

3. Discussion

A. niger CBS 513.88 is a "generally recognized as safe" industrial fermentation strain, and previous reports showed the presence of potential OTA biosynthesis genes in its genome [5]. We found that CBS 513.88 produced OTA, and confirmed that arabinose was the suitable carbon source for OTA production, followed by glucose and sucrose. Our results are consistent with those of Hashem et al. [16], who reported that glucose and sucrose were favorable carbon sources for OTA production, but inconsistent with those of Wang et al. [24], who reported that arabinose repressed OTA production in *A. ochraceus*. The

differences might be attributable to the different physiological and genetic characteristics of the fungi [25]. In addition, we found that peptone suppressed OTA production. The inhibitory effect of peptone on mycotoxins may be attributed to the limited availability of malonyl-CoA or acetyl, because almost all of them were used for primary energy production rather than mycotoxin biosynthesis [26]. In *A. flavus*, YES medium induced aflatoxin biosynthesis, while YEP medium repressed it, consistent with OTA production in *A. niger*. Sequencing of the transcriptomes of the *A. niger* CBS 513.88 strain cultured in OTA-inducing conditions (YEA, YES, YEG) compared to non-inducing conditions (YEP) was performed. The common differences were investigated to elucidate the underlying regulatory mechanism.

The OTA biosynthetic pathway has been well characterized in *A. ochraceus* [3]. Four genes, *nrps*, *p450*, *hal*, and *bzip* in the OTA biosynthetic gene cluster, were all up-regulated when sucrose or glucose was used as the sole carbon source. More importantly, *pks*, the first and backbone gene in the OTA biosynthesis pathway, was significantly up-regulated with arabinose as the carbon source. The high expression of *pks* was an important reason for the highest OTA yield when arabinose was the carbon source in *A. niger.* The results indicated that carbon sources affected OTA biosynthesis by regulating the expression of OTA biosynthesis-associated genes in *A. niger*.

Medina et al. [25] and Abbas et al. [27] reported that amino acids, including phenylalanine, tyrosine, tryptophan, histidine, and arginine, induced OTA production. Phenylalanine, as the precursor for OTA biosynthesis, is sequentially synthesized via the shikimate and phenylalanine biosynthesis pathways [25]. Our results showed that An08g06800 (catalyzing steps two to six in the shikimate pathway), An14g06010 (catalyzing step eight of the phenylalanine biosynthesis), and An15g02460 (catalyzing step 10 of the phenylalanine biosynthesis), were all up-regulated in the presence of three OTA-inducing carbon sources. Additionally, the genes involved in tyrosine, tryptophan, histidine, and arginine biosynthesis were also up-regulated in the presence of three OTA-inducing carbon sources. Together, the results showed that carbon sources may affect OTA biosynthesis by regulating the biosynthesis of amino acids.

Oxidative stress is an important factor correlated with the biosynthesis of mycotoxins in fungi [1,28–31]. Reverberi et al. [32] suggested that oxidative stress agents, such as carbon tetrachloride or t-butyl hydroperoxide, induced OTA production in *A. ochraceus*, while antioxidants had the opposite effects [33]. In addition, oxidative stress can regulate OTA biosynthesis, which has been confirmed by the disruption of the oxidative stress-related genes, *Aoyap1* and *AoloxA* [33]. Our results showed that expression of the oxidant detoxification-related genes (*cat* and *pod*) and activities of the corresponding antioxidant enzymes (CAT and POD) on the three OTA-inducing carbon sources were lower overall than that on the non-inducing nutritional source. These results suggested that carbon sources may trigger OTA biosynthesis by altering cell redox homeostasis in *A. niger*, consistent with the observed association of mannose blocking fumonisin production with milder oxidative stress in *Fusarium proliferatum* [12].

A carbon source is a principal factor that regulates various metabolic processes via TFs [6,23]. We identified 39 significantly changed TFs that overlapped in the 3 OTA-inducing conditions (YEA, YES, YEG) compared to non-inducing conditions (YEP). These mainly included ZnCys, C_2H_2, NEG and the bZIP family (Table S1). Among them, *BrlA*, a transcriptional activator for conidiation [34], was significantly down-regulated in the presence of the three OTA-inducing carbon sources. The findings indicate that the conidiation was inhibited. In addition, Zn(II)2Cys6 proteins are always involved in the biosynthesis of fungal secondary metabolites. For example, Zn(II)2Cys6 proteins *AflR*, *Fum21*, *GliZ*, *MclR*, *CtnA*, and *Gip2* are transcriptional activators for the production of the fungal secondary metabolites aflatoxin [35], fumonisin [36], gliotoxin [37], compactin [38], citrinin [39], aurofusarin [40], respectively. Our transcriptome analysis indicated that An12g00840, a fungal specific transcription factor with a *Gal4*-like Zn(II)2Cys6 binuclear cluster DNA-binding domain (*AnGal4*), was significantly down-regulated in the presence of three OTA-inducing

carbon sources. Based on the above findings, we speculate that the *AnGal4* TF may be involved in the biosynthesis of OTA. Our results indicate that disruption of *AnGal4* significantly increased OTA yield, and the expressions of *pks*, *nrps*, *p450*, *bzip*, and *hal*, in three OTA-inducing carbon sources. Specifically, the OTA yields of the Δ*AnGal4* strain increased by 47.65%, 54.60%, and 309.23%, when sucrose, glucose, and arabinose were used as the sole carbon source, respectively. The results indicate that *AnGal4* activity mediated by the carbon source negatively regulated the OTA biosynthesis. There is only very limited information, including carbon catabolite repression (CCR) [17], cAMP signaling pathway [18], and the flux rearrangement of primary metabolism [19], concerning the involvement in the regulation of secondary metabolite production responding to different carbon sources. Among them, CCR genes *CreA* and *Cre1* regulate the production of several secondary metabolites, including cephalosporin C [41], lovastatin [42], aflatoxin [43], and OTA [24]. In our study, the novel TF *AnGal4* was identified for the first time and demonstrated to have a negative regulatory role in OTA biosynthesis responding to the different carbon sources in *A. niger*. In addition, a previous report suggested that *Gal4* of yeast bound to upstream activation sites of target genes with 5′-CGGN$_5$(T/A)N$_5$CCG-3′ in vivo, or (A/C)GGN$_{10–12}$CCG in vitro [43]. The promoters of the OTA biosynthesis genes of *A. niger* were predicted using a dedicated promoter prediction website (https://services.healthtech.dtu.dk, accessed on 1 February 2022). Notably, we found that *AnGal4* had direct binding sites on the promoters of the OTA biosynthesis genes *pks*, *nrps*, *p450*, *bzip*, and *hal*, in vivo or in vitro (Table S3). The results indicate that *AnGal4* may directly regulate OTA biosynthesis by binding to the OTA biosynthesis genes.

Previous reports indicated that the CCR gene *CreA* homologue gene *Mig1* is negatively correlated with the oxidative stress response [44]. We speculate that *AnGal4* regulated by the carbon source may be involved in the oxidative stress. Our results showed that deletion of *AnGal4* increased the contents of O_2^- and H_2O_2, as well as the sensitivity to H_2O_2 in the presence of the three selected carbon sources, demonstrating that *AnGal4* alters the cellular redox homeostasis in *A. niger*. The Δ*AnGal4* strain had the highest O_2^- and H_2O_2 concentrations in YEA medium, consistent with the highest OTA yield. The results suggest that carbon source-mediated *AnGal4* may regulate OTA biosynthesis by altering cellular redox homeostasis.

4. Conclusions

Our results confirm that arabinose, sucrose, and glucose contribute to OTA production in the industrial fermentation strain *A. niger* CBS 513.88, and characterize the novel *Gal4*-like TF An12g00840 (*AnGal4*). The results suggest that carbon sources repress *AnGal4*, leading to up-regulation of OTA biosynthetic genes and altered cellular redox homeostasis. These changes ultimately trigger OTA biosynthesis in *A. niger* CBS 513.88. This study clarifies the underlying regulatory mechanism of OTA biosynthesis responding to different carbon sources. The findings provide a theoretical basis for the development of effective strategies to control mycotoxin contamination in the fermentation of industrial products.

5. Materials and Methods

5.1. Construction of Strains and Cultivation Conditions

The strains and primers used in this study are listed in Table 2 and Supplementary Table S2, respectively. *A. niger* CBS 513.88 (provided by professor Li Pan, South China University of Technology) and *A. niger* CBS 513.88 (*kusA*$^-$, *pyrG*$^-$) (laboratory constructed) were grown on YEA (6% arabinose, 2% yeast extract, pH 5.8), YES (6% sucrose, 2% yeast extract, pH 5.8), YEG (6% glucose, 2% yeast extract, pH 5.8), and YEP (6% peptone, 2% yeast extract, pH 5.8) solid media that were not supplemented or supplemented with 10 mM uridine. In addition, the YEA, YES, YEG, and YEP solid media were also used for strain morphology and conidia assay, OTA production, enzyme activity assay, determinations of superoxide anion and hydrogen peroxide (H_2O_2) contents, and the H_2O_2 susceptibility assays. Czapek-Dox (CD) medium supplemented with or without uridine was used for

strain transformation. All strains were cultivated at 30 °C for 5.5 days for growth and at 23 °C for 5.5 days in the dark for OTA production.

Table 2. *A. niger* strains used in this study.

***A. niger* Strains**	**Description**	**Sources**
A.niger CBS 513.88	Wild-type strain	Provided by Li Pan
A. niger CBS 513.88 (*kusA*$^{-}$, *pyrG*$^{-}$)	*A. niger* CBS 513.88 derivative, Δ*kusA::ptrA*, Δ*pyrG::hygB*	Laboratory constructed
A. niger CBS 513.88 (*kusA*$^{-}$, *pyrG*$^{+}$) (Control)	*A. niger* CBS 513.88 derivative, Δ*kusA*, Δ*pyrG*, *pyrG-Com*	Laboratory constructed
Δ*AnGal4*	*A. niger* CBS 513.88 derivative, Δ*kusA*, Δ*pyrG*, Δ*AnGal4::pyrG*	This study

AnGal4 (An12g00840) gene knockout was performed by homologous recombination [45], and *A. niger* CBS 513.88 (*kusA*$^{-}$, *pyrG*$^{+}$) was the control strain. The *pyrG* gene expression cassette was used as the selection marker, which was cloned from plasmid ANIp7. Homologous fragments of 1.60 kb and 1.47 kb at either end of the *AnGal4* open reading frame (ORF) were amplified. The upstream and downstream homologous fragments and *pyrG* expression cassette were ligated into plasmid pMD20 using a one-step cloning kit (Novazyme, Nanjing, China) to yield pMD20-Δ*AnGal4*, which was transferred into the *A. niger* CBS 513.88 (*kusA*$^{-}$, *pyrG*$^{-}$) strain. The recombinant strain was screened using Czapek-Dox (CD) medium lacking uridine. The screening was verified by PCR using the genome of the correct transformants as a template.

5.2. Colony Morphology, Mycelial Growth, and Conidia Production

Conidia suspensions (5 μL, 10^6 spores/mL) were centrally spotted on YEA, YES, YEG, and YEP media and cultivated for 5.5 days at 23 °C. Colony morphology and colony diameters were observed and measured [46]. Conidia suspensions were viewed using a microscope and counted using a hemocytometer. All cultures were conducted in triplicate.

5.3. High-Performance Liquid Chromatography (HPLC) Analysis of OTA

Conidia suspensions (200 μL, 10^6 spores/mL) were spread evenly on YEA, YES, YEG, and YEP media and cultivated for 5.5 days at 23 °C in the dark. All mycelium and agar on plates were collected, and then were mashed and placed in an Erlenmeyer flask with 25 mL methanol, followed by shaking for 1 h in the dark. All cultures were conducted in triplicate. OTA was detected by HPLC with fluorescence detection (HPLC-FLD) (Agilent Technologies, San Jose, CA, USA) [47].

5.4. Ultra-High Performance Liquid Chromatography Mass Spectrometry (UHPLC-MS) Analysis

For UHPLC-MS analysis, the supernatant of the OTA extract was purified using an OTA immunoaffinity column (PriboFast, Beijing, China) and transferred to a 2 mL Eppendorf tube. The highly purified sample was detected using a Q-Orbitrap instrument system (Thermo Fisher Scientific, Waltham, MA, USA), equipped with a binary solvent delivery system. A C18 column (2.1 × 100 mm, 1.7 μm particle diameter; Thermo Fisher Scientific) was used for chromatography. The UHPLC-MS run used positive ESI. The details were performed as previously described [48].

5.5. Transcriptome Analysis

Conidia suspensions (200 μL, 10^6 spores/mL) were spread evenly on YEA, YES, YEG, and YEG media and cultivated for 5.5 days at 23 °C in the dark. Hyphae were collected, then frozen in liquid nitrogen and subjected to transcriptome analyses. We first extracted total RNA using a UNIQ-10 TRIzol RNA Purification Kit (Sangon Biotech, Shanghai, China), with three biological parallels for each sample, then sequenced it using a NovaSeq (Personalbio, Nanjing, China). Raw data showed significant differences between YES and YEP, YEG and YEP, and YEA and YEP, with a bioproject accession number of PRJNA765465. Significant differences were indicated by an absolute $\log_2$-fold change of 1.0 or greater, and p-values of 0.05 or less. All annotations were obtained according to NCBI

(https://www.ncbi.nlm.nih.gov/, accessed on 10 December 2021). Gene Ontology (GO) terms and Kyoto Encyclopedia of Genes and Genomes (KEGG) pathways were performed according to the reference [49], and were classified as significantly enriched among the differentially expressed genes (DEGs).

5.6. Real-Time Quantitative PCR (RT-qPCR) Analysis

The qPCR data were analyzed according to a previously described method [50]. After RNA extraction, we used a PrimeScript™ RT reagent Kit (TaKaRa Bio, Beijing, China) to obtain the cDNA. We then used *qgpdA* as the reference gene, and the equation $N = 2^{-\Delta\Delta Ct}$ to evaluate the relative transcription levels. The *t*-test was performed to assess the differences between samples.

5.7. Determination of Antioxidant Enzyme Activity, and Superoxide Anion and H_2O_2 Contents

Two hundred microliter aliquots of conidia suspensions containing 10^6 spores/mL were spread evenly on YEA, YES, YEG, and YEP media and cultivated for 5.5 days at 23 °C in the dark. The mycelia were collected, triturated with acetone, and the supernatant was collected by centrifugation at 4 °C. Catalase (CAT) and glutathione peroxidase (POD) were quantified using the corresponding detection kits (Solarbio, Beijing, China). The superoxide anion (O^{2-}) and H_2O_2 contents were also measured according to the corresponding detection kit instructions (Solarbio, Beijing, China).

5.8. Assay of H_2O_2 Susceptibility

Five microliter aliquots of conidia suspensions containing 10^6 spores/mL were spotted onto YEA, YES, YEG, and YEP media supplemented with H_2O_2 at different concentrations (0, 10, 20, and 30 mM), and cultivated for 5.5 days at 30 °C. The growth of strains on plates was then recorded.

5.9. Statistical Analysis

All experiments were repeated with three independent biological replicates. The data are expressed as the mean ± standard deviation of independent tests performed in triplicate. The differences were calculated with student's *t* test (*t*-test), and marked with *, **, and *** as $t < 0.05$, $t < 0.01$, and $t < 0.001$, respectively.

Supplementary Materials: The following supporting information can be downloaded at: https://www.mdpi.com/article/10.3390/toxins14080551/s1, Figure S1: qRT-PCR analyses of differentially expressed genes in OTA precursor phenylalanine and OTA biosynthesis; Table S1: The significantly changed TFs that overlapped in the three OTA-inducing conditions (YEA, YES, YEG) compared to non-inducing condition (YEP); Table S2: All primers used in this study; Table S3: Sequences of *Gal4* binding sites on the predicted promoter.

Author Contributions: S.W., Y.L. and Y.H. made the original plan. C.H. and P.N. performed the experiments. H.Z., S.Z. and N.L. performed the formal analysis. S.W. analyzed and integrated the data and wrote the manuscript. All authors have read and agreed to the published version of the manuscript.

Funding: This work was sponsored by grants from the High-level Talent Scientific Research Fund Project of Henan University of Technology (31401269), the National Natural Science Foundation of China (31972176, 31871852), the Innovative Funds Plan of Henan University of Technology (2020ZKCJ01), and the Cultivation Program for Young Backbone Teachers in Henan University of Technology (21420114).

Data Availability Statement: Data are available in a publicly accessible repository.

Conflicts of Interest: The authors declare no conflict of interest.

References

1. Gil-Serna, J.; Vázquez, C.; Patiño, B. Genetic regulation of aflatoxin, ochratoxin A, trichothecene, and fumonisin biosynthesis: A Review. *Int. Microbiol.* **2020**, *23*, 89–96. [CrossRef] [PubMed]
2. Visconti, A.; Perrone, G.; Cozzi, G.; Solfrizzo, M. Managing ochratoxin A risk in the grape-wine food chain. *Food Addit. Contam.* **2008**, *25*, 193–202. [CrossRef]
3. Wang, Y.; Wang, L.; Wu, F.; Liu, F.; Wang, Q.; Zhang, X.; Selvaraj, J.N.; Zhao, Y.; Xing, F.; Yin, W.B.; et al. A consensus ochratoxin A biosynthetic pathway: Insights from the genome sequence of *Aspergillus ochraceus* and a comparative genomic analysis. *Appl. Environ. Microbiol.* **2018**, *84*, e01009-18. [CrossRef] [PubMed]
4. Heussner, A.H.; Bingle, L.E. Comparative ochratoxin toxicity: A review of the available data. *Toxins* **2015**, *7*, 4253–4282. [CrossRef] [PubMed]
5. Pel, H.J.; de Winde, J.H.; Archer, D.B.; Dyer, P.S.; Hofmann, G.; Schaap, P.J.; Turner, G.; de Vries, R.P.; Albang, R.; Albermann, K.; et al. Genome sequencing and analysis of the versatile cell factory *Aspergillus niger* CBS 513.88. *Nat. Biotechnol.* **2007**, *25*, 221–231. [CrossRef]
6. Wang, Y.; Wang, L.; Liu, F.; Wang, Q.; Selvaraj, J.N.; Xing, F.; Zhao, Y.; Liu, Y. Ochratoxin A producing fungi, biosynthetic pathway and regulatory mechanisms. *Toxins* **2016**, *8*, 83. [CrossRef]
7. el Khoury, A.; Atoui, A. Ochratoxin A: General overview and actual molecular status. *Toxins* **2010**, *2*, 461–493. [CrossRef]
8. Gil-Serna, J.; García-Díaz, M.; González-Jaén, M.T.; Vázquez, C.; Patiño, B. Description of an orthologous cluster of ochratoxin A biosynthetic genes in *Aspergillus* and *Penicillium* species. A comparative analysis. *Int. J. Food Microbiol.* **2018**, *268*, 35–43. [CrossRef]
9. Passamani, F.R.; Hernandes, T.; Lopes, N.A.; Bastos, S.C.; Santiago, W.D.; Cardoso, M.D.G.; Batista, L.R. Effect of temperature, water activity, and pH on growth and production of ochratoxin A by *Aspergillus niger* and *Aspergillus carbonarius* from Brazilian grapes. *J. Food Prot.* **2014**, *77*, 1947–1952. [CrossRef]
10. Abarca, M.L.; Bragulat, M.R.; Castellá, G.; Cabañes, F.J. Impact of some environmental factors on growth and ochratoxin A production by *Aspergillus niger* and *Aspergillus welwitschiae*. *Int. J. Food Microbiol.* **2019**, *291*, 10–16. [CrossRef]
11. Wilkinson, J.R.; Yu, J.; Abbas, H.K.; Scheffler, B.E.; Kim, H.S.; Nierman, W.C.; Bhatnagar, D.; Cleveland, T.E. Aflatoxin formation and gene expression in response to carbon source media shift in *Aspergillus parasiticus*. *Food Addit. Contam.* **2007**, *24*, 1051–1060. [CrossRef] [PubMed]
12. Li, T.; Gong, L.; Jiang, G.; Wang, Y.; Gupta, V.K.; Qu, H.; Duan, X.; Wang, J.; Jiang, Y. Carbon sources influence fumonisin production in *Fusarium proliferatum*. *Proteomics* **2017**, *17*, 1700070. [CrossRef] [PubMed]
13. Zong, Y.; Li, B.; Tian, S. Effects of carbon, nitrogen and ambient pH on patulin production and related gene expression in *Penicillium expansum*. *Int. J. Food Microbiol.* **2015**, *206*, 102–108. [CrossRef] [PubMed]
14. Kawakami, A.; Nakajima, T.; Hirayae, K. Effects of carbon sources and amines on induction of trichothecene production by *Fusarium asiaticum* in liquid culture. *FEMS Microbiol. Lett.* **2014**, *352*, 204–212. [CrossRef]
15. Li, T.; Jiang, G.; Qu, H.; Wang, Y.; Xiong, Y.; Jian, Q.; Wu, Y.; Duan, X.; Zhu, X.; Hu, W.; et al. Comparative transcriptome analysis of *Penicillium citrinum* cultured with different carbon sources identifies genes involved in citrinin biosynthesis. *Toxins* **2017**, *9*, 69. [CrossRef]
16. Hashem, A.; Fathi Abd-Allah, E.; Sultan Al-Obeed, R.; Abdullah Alqarawi, A.; Alwathnani, H.A. Effect of carbon, nitrogen sources and water activity on growth and ochratoxin production of *Aspergillus carbonarius* (Bainier) Thom. *Jundishapur J. Microbiol.* **2015**, *8*, e17569. [CrossRef]
17. Ruiz, B.; Chávez, A.; Forero, A.; García-Huante, Y.; Romero, A.; Sánchez, M.; Rocha, D.; Sánchez, B.; Rodríguez-Sanoja, R.; Sánchez, S.; et al. Production of microbial secondary metabolites: Regulation by the carbon source. *Crit. Rev. Microbiol.* **2010**, *36*, 146–167. [CrossRef]
18. Miyake, T.; Zhang, M.Y.; Kono, I.; Nozaki, N.; Sammoto, H. Repression of secondary metabolite production by exogenous camp in *Monascus*. *Biosci. Biotechnol. Biochem.* **2006**, *70*, 1521–1523. [CrossRef]
19. Fan, Y.; Gao, Y.; Zhou, J.; Wei, L.; Chen, J.; Hua, Q. Process optimization with alternative carbon sources and modulation of secondary metabolism for enhanced ansamitocin P-3 production in *Actinosynnema pretiosum*. *J. Biotechnol.* **2014**, *192 Pt A*, 1–10. [CrossRef]
20. Liu, P.; Wang, S.; Li, C.; Zhuang, Y.; Xia, J.; Noorman, H. Dynamic response of *Aspergillus niger* to periodical glucose pulse stimuli in chemostat cultures. *Biotechnol. Bioeng.* **2021**, *118*, 2265–2282. [CrossRef]
21. Veana, F.; Fuentes-Garibay, J.A.; Aguilar, C.N.; Rodríguez-Herrera, R.; Guerrero-Olazarán, M.; Viader-Salvadó, J.M. Gene encoding a novel invertase from a xerophilic *Aspergillus niger* strain and production of the enzyme in *Pichia pastoris*. *Enzym. Microb. Technol.* **2014**, *63*, 28–33. [CrossRef] [PubMed]
22. de Groot, M.J.; Prathumpai, W.; Visser, J.; Ruijter, G.J. Metabolic control analysis of *Aspergillus niger* L-arabinose catabolism. *Biotechnol. Prog.* **2005**, *21*, 1610–1616. [CrossRef] [PubMed]
23. Wei, S.; Liu, Y.; Wu, M.; Ma, T.; Bai, X.; Hou, J.; Shen, Y.; Bao, X. Disruption of the transcription factors Thi2p and Nrm1p alleviates the post-glucose effect on xylose utilization in *Saccharomyces cerevisiae*. *Biotechnol. Biofuels* **2018**, *11*, 112. [CrossRef]
24. Wang, G.; Wang, Y.; Yang, B.; Zhang, C.; Zhang, H.; Xing, F.; Liu, Y. Carbon catabolite repression gene aocrea regulates morphological development and ochratoxin A biosynthesis responding to carbon sources in *Aspergillus ochraceus*. *Toxins* **2020**, *12*, 697. [CrossRef]

25. Medina, A.; Mateo, E.M.; Valle-Algarra, F.M.; Mateo, F.; Mateo, R.; Jiménez, M. Influence of nitrogen and carbon sources on the production of ochratoxin A by ochratoxigenic strains of *Aspergillus* Spp. isolated from grapes. *Int. J. Food Microbiol.* **2008**, *122*, 93–99. [CrossRef]
26. Fountain, J.C.; Bajaj, P.; Pandey, M.; Nayak, S.N.; Yang, L.; Kumar, V.; Jayale, A.S.; Chitikineni, A.; Zhuang, W.; Scully, B.T.; et al. Oxidative stress and carbon metabolism influence *Aspergillus flavus* transcriptome composition and secondary metabolite production. *Sci. Rep.* **2016**, *6*, 38747. [CrossRef]
27. Abbas, A.; Valez, H.; Dobson, A.D. Analysis of the effect of nutritional factors on OTA and OTB biosynthesis and polyketide synthase gene expression in *Aspergillus ochraceus*. *Int. J. Food Microbiol.* **2009**, *135*, 22–27. [CrossRef] [PubMed]
28. Zhu, Z.; Yang, M.; Bai, Y.; Ge, F.; Wang, S. Antioxidant-related catalase *CTA1* regulates development, aflatoxin biosynthesis, and virulence in pathogenic fungus *Aspergillus flavus*. *Environ. Microbiol.* **2020**, *22*, 2792–2810. [CrossRef] [PubMed]
29. Tolaini, V.; Zjalic, S.; Reverberi, M.; Fanelli, C.; Fabbri, A.A.; Del Fiore, A.; De Rossi, P.; Ricelli, A. Lentinula edodes enhances the biocontrol activity of *Cryptococcus laurentii* against *Penicillium expansum* contamination and patulin production in apple fruits. *Int. J. Food Microbiol.* **2010**, *138*, 243–249. [CrossRef] [PubMed]
30. Ponts, N.; Pinson-Gadais, L.; Verdal-Bonnin, M.N.; Barreau, C.; Richard-Forget, F. Accumulation of deoxynivalenol and its 15-acetylated form is significantly modulated by oxidative stress in liquid cultures of *Fusarium graminearum*. *FEMS Microbiol. Lett.* **2006**, *258*, 102–107. [CrossRef]
31. Montibus, M.; Ducos, C.; Bonnin-Verdal, M.N.; Bormann, J.; Ponts, N.; Richard-Forget, F.; Barreau, C. The bzip transcription factor Fgap1 mediates oxidative stress response and trichothecene biosynthesis but not virulence in *Fusarium graminearum*. *PLoS ONE* **2013**, *8*, e83377. [CrossRef] [PubMed]
32. Reverberi, M.; Gazzetti, K.; Punelli, F.; Scarpari, M.; Zjalic, S.; Ricelli, A.; Fabbri, A.A.; Fanelli, C. Aoyap1 Regulates Ota Synthesis by Controlling Cell Redox Balance in *Aspergillus Ochraceus*. *Appl. Microbiol. Biotechnol.* **2012**, *95*, 1293–1304. [CrossRef] [PubMed]
33. Reverberi, M.; Punelli, F.; Scarpari, M.; Camera, E.; Zjalic, S.; Ricelli, A.; Fanelli, C.; Fabbri, A.A. Lipoperoxidation affects ochratoxin A biosynthesis in *Aspergillus ochraceus* and its interaction with wheat seeds. *Appl. Microbiol. Biotechnol.* **2010**, *85*, 1935–1946. [CrossRef] [PubMed]
34. Twumasi-Boateng, K.; Yu, Y.; Chen, D.; Gravelat, F.N.; Nierman, W.C.; Sheppard, D.C. Transcriptional profiling identifies a role for brla in the response to nitrogen depletion and for stua in the regulation of secondary metabolite clusters in *Aspergillus fumigatus*. *Eukaryot. Cell* **2009**, *8*, 104–115. [CrossRef]
35. Wang, P.; Xu, J.; Chang, P.K.; Liu, Z.; Kong, Q. New Insights of transcriptional regulator AflR in *Aspergillus flavus* physiology. *Microbiol. Spectr.* **2022**, *10*, e0079121. [CrossRef]
36. Brown, D.W.; Butchko, R.A.; Busman, M.; Proctor, R.H. The *Fusarium verticillioides* Fum gene cluster encodes a Zn(Ii)2cys6 protein that affects fum gene expression and pumonisin production. *Eukaryot. Cell* **2007**, *6*, 1210–1218. [CrossRef]
37. Bok, J.W.; Chung, D.; Balajee, S.A.; Marr, K.A.; Andes, D.; Nielsen, K.F.; Frisvad, J.C.; Kirby, K.A.; Keller, N.P. Gliz, a transcriptional regulator of gliotoxin biosynthesis, contributes to *Aspergillus fumigatus* virulence. *Infect. Immun.* **2006**, *74*, 6761–6768. [CrossRef]
38. Abe, Y.; Ono, C.; Hosobuchi, M.; Yoshikawa, H. Functional analysis of MlcR, a regulatory gene for Ml-236b (compactin) biosynthesis in *Penicillium citrinum*. *Mol. Genet. Genom.* **2002**, *268*, 352–361. [CrossRef]
39. Shimizu, T.; Kinoshita, H.; Nihira, T. Identification and in vivo functional analysis by gene disruption of *ctnA*, an activator gene involved in citrinin biosynthesis in *Monascus purpureus*. *Appl. Environ. Microbiol.* **2007**, *73*, 5097–5103. [CrossRef]
40. Kim, J.E.; Jin, J.; Kim, H.; Kim, J.C.; Yun, S.H.; Lee, Y.W. Gip2, a putative transcription factor that regulates the aurofusarin biosynthetic gene cluster in *Gibberella zeae*. *Appl. Environ. Microbiol.* **2006**, *72*, 1645–1652. [CrossRef]
41. Jekosch, K.; Kück, U. Loss of glucose repression in an *Acremonium chrysogenum* beta-lactam producer strain and its restoration by multiple copies of the *Cre1* gene. *Appl. Microbiol. Biotechnol.* **2000**, *54*, 556–563. [CrossRef]
42. Hajjaj, H.; Niederberger, P.; Duboc, P. Lovastatin biosynthesis by *Aspergillus terreus* in a chemically defined medium. *Appl. Environ. Microbiol.* **2001**, *67*, 2596–2602. [CrossRef] [PubMed]
43. Vashee, S.; Xu, H.; Johnston, S.A.; Kodadek, T. How do "Zn2 cys6" proteins distinguish between similar upstream activation sites? Comparison of the DNA-binding specificity of the Gal4 protein in vitro and in vivo. *J. Biol. Chem.* **1993**, *268*, 24699–24706. [CrossRef]
44. Yao, Y.; Tsuchiyama, S.; Yang, C.; Bulteau, A.L.; He, C.; Robison, B.; Tsuchiya, M.; Miller, D.; Briones, V.; Tar, K.; et al. Proteasomes, Sir2, and Hxk2 form an interconnected aging network that impinges on the Ampk/Snf1-regulated transcriptional repressor Mig1. *PLoS Genet.* **2015**, *11*, e1004968. [CrossRef] [PubMed]
45. Yao, L.; Ban, F.; Peng, S.; Xu, D.; Li, H.; Mo, H.; Hu, L.; Zhou, X. Exogenous iron induces nadph oxidases-dependent ferroptosis in the conidia of *Aspergillus flavus*. *J. Agric. Food Chem.* **2021**, *69*, 13608–13617. [CrossRef] [PubMed]
46. Jia, K.; Yan, L.; Jia, Y.; Xu, S.; Yan, Z.; Wang, S. Afln Is Involved in tbiosynthesis of aflatoxin and conidiation in *Aspergillus flavus*. *Toxins* **2021**, *13*, 831. [CrossRef]
47. Zhang, J.; Zhu, L.; Chen, H.; Li, M.; Zhu, X.; Gao, Q.; Wang, D.; Zhang, Y. A polyketide synthase encoded by the gene An15g07920 is involved in the biosynthesis of ochratoxin A in *Aspergillus niger*. *J. Agric. Food Chem.* **2016**, *64*, 9680–9688. [CrossRef]
48. Tsagkaris, A.S.; Prusova, N.; Dzuman, Z.; Pulkrabova, J.; Hajslova, J. Regulated and non-regulated mycotoxin detection in cereal matrices using an ultra-high-performance liquid chromatography high-resolution mass spectrometry (UHPLC-HRMS) method. *Toxins* **2021**, *13*, 783. [CrossRef]

49. Young, M.D.; Wakefield, M.J.; Smyth, G.K.; Oshlack, A. Gene ontology analysis for RNA-seq: Accounting for selection bias. *Genome Biol.* **2010**, *11*, 1–12. [CrossRef]
50. Livak, K.J.; Schmittgen, T.D. Analysis of relative gene expression data using real-time quantitative PCR and the 2(-Delta Delta C(T)) Method. *Methods* **2001**, *25*, 402–408. [CrossRef]

toxins

MDPI

Article

GTPase Rac Regulates Conidiation, AFB1 Production and Stress Response in Pathogenic Fungus *Aspergillus flavus*

Ling Qin †, Lan Yang †, Jiaru Zhao, Wanlin Zeng, Minxuan Su, Shihua Wang * and Jun Yuan *

Key Laboratory of Pathogenic Fungi and Mycotoxins of Fujian Province, Key Laboratory of Biopesticide and Chemical Biology of Education Ministry, School of Life Sciences, Fujian Agriculture and Forestry University, Fuzhou 350002, China

* Correspondence: wshyyl@sina.com (S.W.); yjmail2008@126.com (J.Y.)

† These authors contributed equally to this work.

Abstract: As a member of the Rho family, Rac plays important roles in many species, including proliferation, differentiation, apoptosis, DNA damage responses, metabolism, angiogenesis, and immunosuppression. In this study, by constructing *Rac*-deleted mutants in *Aspergillus flavus*, it was found that the deletion of *Rac* gene led to the decline of growth and development, conidia production, AFB1 toxin synthesis, and seed infection ability of *A. flavus*. The deletion of *Rac* gene also caused the disappearance of *A. flavus* sclerotium, indicating that *Rac* is required for sclerotium formation in *A. flavus*. The sensitivity of *Rac*-deficient strains responding to cell wall stress and osmotic pressure stress increased when compared to *A. flavus* WT. The Western blot result showed that mitogen-activated serine/threonine-protein kinase Slt2 and mitogen-activated protein kinase Hog1 proteins were no longer phosphorylated in *Rac*-deficient strains of *A. flavus*, showing that Rac may be used as a molecular switch to control the Slt2-MAPK cascade pathway and regulate the osmotic Hog-MAPK cascade pathway in *A. flavus* in response to external stress. Altogether, these results indicated that Rac was involved in regulating the growth and development, conidia formation and AFB1 synthesis, and response to cell wall stress and osmotic pressure stress in *A. flavus*.

Keywords: *A. flavus*; Rac; conidiation; aflatoxins; stress response

Key Contribution: In this study, the function of Rac in *A. flavus* was studied for the first time, and the possible role of Rac in the filamentous fungus *A. flavus* was discussed, which expanded a new idea for the study of Rac GTPase.

Citation: Qin, L.; Yang, L.; Zhao, J.; Zeng, W.; Su, M.; Wang, S.; Yuan, J. GTPase Rac Regulates Conidiation, AFB1 Production and Stress Response in Pathogenic Fungus *Aspergillus flavus*. *Toxins* **2022**, *14*, 581. https://doi.org/10.3390/toxins14090581

Received: 1 August 2022
Accepted: 18 August 2022
Published: 24 August 2022

1. Introduction

Aspergillus flavus, as a common saprophytic filamentous fungus, is widely distributed all over the world. It is not only a plant pathogenic fungus, but also a conditional human and animal pathogenic fungus. Many secondary metabolites are produced during the growth and development of *A. flavus*, among which aflatoxins are produced from polyketones [1]. *A. flavus* produces aflatoxins by infecting cereal crops, including corn, peanut, and wheat [2], which causes a variety of harm to humans and animals, such as hepatotoxicity [3], carcinogenicity [4] and immunotoxicity [5]. Aflatoxin-contaminated cereal crops pose serious health risks in developing countries [6], as well as significant economic losses to the United States and other developed countries [7]. Therefore, the study of *A. flavus* is of more practical significance under the current situation of food security and shortage in many countries.

Rho family proteins belong to one of the important members of the Ras superfamily, including the Rho, Rac, and Cdc subfamilies. Members of this family have the inherent activity of hydrolyzing GTPases, so they are accustomed to being called Rho GTPases. As a molecular switch, Rho GTPases almost participate in the basic cellular process. The

GTP binding state is activated, and the GDP binding state is inactivated [8]. Rho GTPase can regulate actin cytoskeleton [9], cell cycle progression [10], and signal network of gene expression, thus regulating normal cell proliferation, differentiation and apoptosis, and is closely related to tumor occurrence and metastasis.

As one of the most studied proteins in the Rho family, Rac plays an extremely important role in many species. As early as 1955, Rac was proved to regulate the production of reactive oxygen in macrophages in response to the attack of pathogens [11]. In *Drosophila melanogaster*, Rac not only plays an important role in neuron development [12] but also participates in axon growth and myoblast fusion [13]. Rac seems to activate LIM kinase to inhibit axon growth via the effector kinase PAK, but may also activate a PAK-independent pathway that promotes axon growth [12,14]. In fungi, such as *Aspergillus nidulans*, *Rac*-deficient mutants showed slow growth and development, but there is no obvious difference in mycelium morphogenesis. However, the conidia had various defects, such as the appearance of vesicles without conidia, shortening of stalk and vesicle branches, irregular shape of vesicles, and reduction in the number of conidia and vesicles [15]. The *RacA* gene was found to play an important role in the growth and pathogenesis of *Aspergillus fumigatus*. The absence of *RacA* in *A. fumigatus* reduced the production of reactive oxygen but had little effect on virulence [16]. In dimorphic plant pathogenic fungus *Ustilago maydis*, it was found that *Rac1* deletion resulted in the loss of virulence, affecting cell morphology and interfering with mycelium growth [17]. Unlike the other Rho GTPases, Rac orthologs were not found in unicellular yeasts such as *Saccharomyces cerevisiae* and *Schizosaccharomyces pombe*, suggesting that the *Rac* gene might have evolved with the increase in cell complexity [18]. However, the function of Rac in *A. flavus* has not been explored until now. Therefore, this paper focused on the Rac biofunctions in *A. flavus*, and the main results were shown as follows.

2. Result

2.1. Biological Analysis of Rac

Blast comparison was carried out with *A. nidulans* Rac protein (XP_662347.1) in NCBI to identify homologous protein AflRac (XP_002384152.1) in *A. flavus*. Then, AflRac was compared with Rac proteins of other four fungi to study whether Rac proteins from fungi are conserved. Since Rac protein also plays an important role in the development of animal nerves, we compared Rac homologous proteins in two vertebrates. We used MEGA7 to map the phylogenetic tree based on the protein sequences blasted in NCBI. The result showed that Rac protein sequences are highly homologous in fungi and vertebrates (Figure 1A), indicating that the Rac protein is highly conserved in the process of evolution. We used DOG2.0 software (Jian Ren, Hefei, China) to draw the domain diagram of the proteins mentioned above and found that all these proteins have a Rac-like domain (Figure 1B), indicating that the Rac protein domain is also highly conserved in these species.

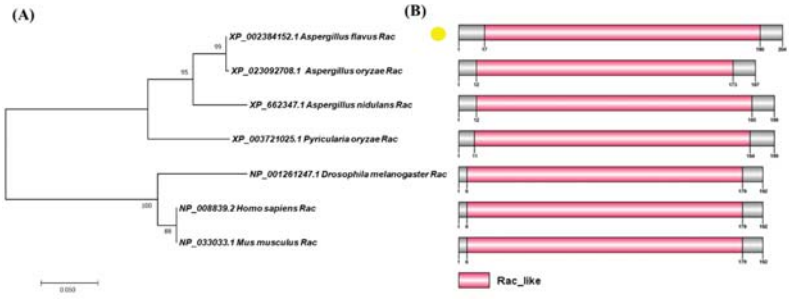

Figure 1. Bioinformatics analysis of Rac protein. (**A**) The phylogenetic relationship of Rac in selected eukaryotes was analyzed and visualized by MEGA7.0 software (Mega Limited, Auckland, New Zealand). (**B**) The domain of Rac protein was identified and visualized by SMART/(http://smart.embl-heidelberg.de) and DOG2.0 software (Jian Ren, Hefei, China).

2.2. Rac from *A. flavus* Is a GTPase

After systematic prediction, sequence alignment showed that *A. flavus* Rac (XP_00238-4152.1) had high homology with *A. nidulans* Rac (XP_662347.1, 90.69% identification) and they two showed highly conserved three-dimensional protein structures (Figure 2A). In order to confirm whether AflRac has GTPase activity, we cloned the coding sequence of AflRac using the cDNA of *A. flavus* wild type (WT) as template and ligated it into the pET28a vector. After sequencing and twice transformation, the Rac protein expression strain was successfully constructed. After induction by IPTG, it was purified by a Ni^{2+}-NTA column (Figure 2B). GTP enzyme activity was detected *in vitro*, and it was found that the AflRac protein had GTP enzyme activity (Figure 2C). The above results proved that AflRac has GTPase activity in *A. flavus*. Thus, in this paper, we directly define the protein XP_002384152.1 in *A. flavus* as Rac.

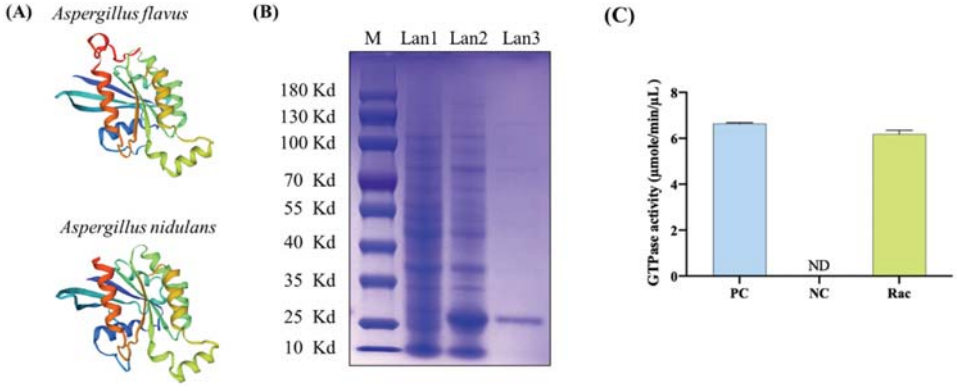

Figure 2. Expression and GTPase activity assay. (**A**) *A. flavus* Rac (XP_002384152.1) sequence is similar to *A. nidulans* Rac (XP_662347.1; 90.69% identify), and they had highly conserved three-dimensional protein structure. (**B**) SDS-PAGE assay of the expressed recombinant protein and purification result. Line 1: the expressed recombinant plasmid pET28a-*Rac* without IPTG, line 2: the expressed recombinant plasmid pET28a-*Rac* with IPTG induction, line 3: the purified recombinant protein. (**C**) GTPase activities of Rac protein. PC = positive control, NC = negative control.

2.3. Rac Is Involved in Vegetative Growth and Conidiation

To study the function of Rac in *A. flavus*, we constructed *Rac*-deleted mutant strains. Using the principle of gene recombination, we replaced *Rac* in *A. flavus* wild type with *AfupyrG* to construct *Rac* deletion mutants (Δ*Rac*) (Figure 3A). At the same time, we constructed *Rac* complementary strains (Rac^C). Then, PCR (Figure 3B), RT-PCR (Figure 3C), qPCR (Figure 3D), and Southern blot (Figure 3E) results verified that Δ*Rac* and Rac^C were successfully constructed. The above-constructed strains were diluted to the same multiple and inoculated in two kinds of rich media (CM and PDA) and two kinds of basic media (GMM and MM) for culture (Figure 4A). By observing the colony growth, it was found that the diameter of Δ*Rac* in all media was significantly smaller than that of WT and Rac^C (Figure 4B), which indicates that Rac participates in the vegetative growth process of *A. flavus*. During the observation, we also found that the color of Δ*Rac* was obviously white, as the green color on the strains was conidia of *A. flavus*. Therefore, a rich medium (PDA) and a basic medium (GMM) were selected to culture all the above strains, and the conidia were eluted to count the number with a blood cell counter under an optical microscope. The results showed that the conidia production of Δ*Rac* was significantly lower than that of WT and Rac^C (Figure 4C). The decrease in conidia made us wonder whether it was related to the decrease in conidiophore. Therefore, we observed the conidiophore and found that the number of conidiophore of Δ*Rac* was significantly decreased than that of WT and Rac^C (Figure 4D), indicating that Rac was very important for the formation of conidiophores of

A. flavus. We also verified the key genes related to conidia formation in *A. flavus* by qPCR and found that the expression levels of genes *abaA* and *brlA* were significantly decreased in Δ*Rac* (Figure 4E), which further indicated that Rac regulates the expression of genes related to conidiation, thus affecting the conidia formation of *A. flavus*.

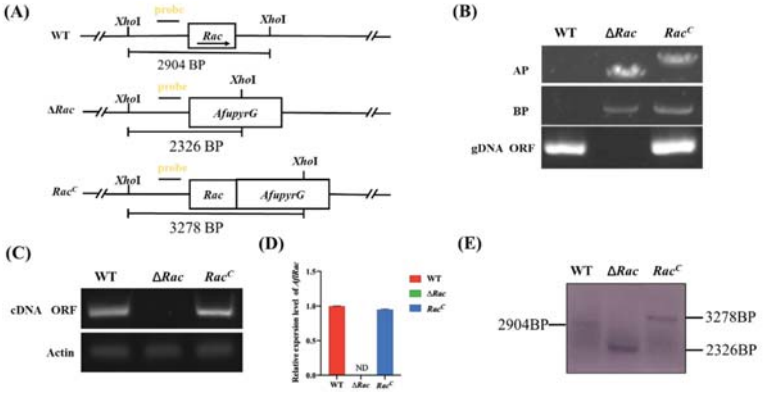

Figure 3. Generation of deletion and complementation strains. (**A**) The deletion mutant was constructed by homologous recombination. (**B**) The construction was verified by routine PCR with gDNA as template. (**C**) RT-PCR was used to verify the construction with cDNA as template. (**D**) The expression level of *Rac* gene was verified by qPCR. (**E**) Southern blot proved that Δ*Rac* strain and strain Rac^C were successfully constructed. The length of the WT fragment cut out by *Xho*I was 2904 bp, Δ*Rac* strain was 2326 bp, and Rac^C was 3278 bp.

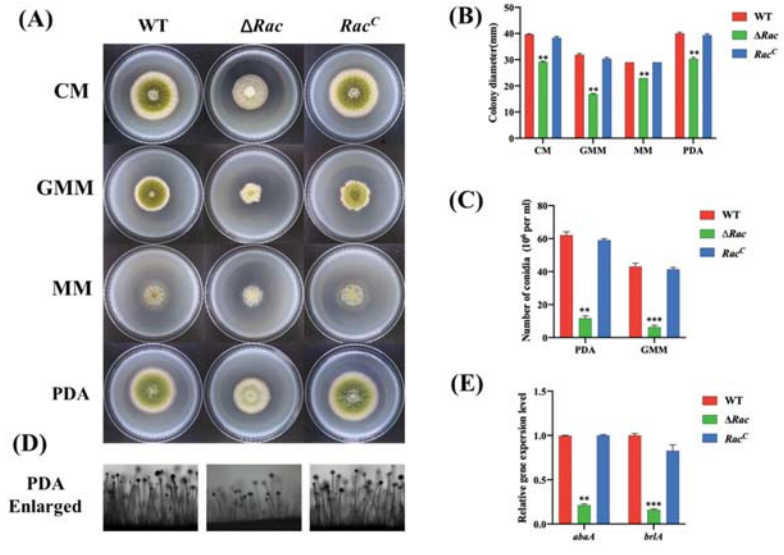

Figure 4. *Rac* was involved in vegetative growth and conidiation in *A. flavus*. (**A**) WT, Δ*Rac* and Rac^C were cultured in two kinds of rich media (CM, PDA) and two kinds of basic media (GMM, MM) at 37 °C for 3 days. (**B**) GraphPad Prism8 was used to analyze the growth diameter of colonies. (**C**) Spores number of these strains on the rich medium (PDA) and basic medium (GMM). (**D**) Amplification of conidiophore cultured on PDA medium. (**E**) qPCR verified the expression level of genes *abaA* and *brlA* in these strains. ** mean $p < 0.05$, *** means $p < 0.0001$.

2.4. Rac Is Required for Sclerotial Formation in A. flavus

Sclerotium is another form of *A. flavus* reproduction, so the effect of Rac on the sclerotium formation of *A. flavus* deserves our study. We cultured the strains in CM medium for 7 days to observe the sclerotium formation, and the results showed that the Δ*Rac* did not produce sclerotium at all, but WT and Rac^C of *A. flavus* produced normal sclerotium (Figure 5A,B). qPCR result showed that the expression of *nadC* and *nsdD*, the key genes of sclerotium formation, was decreased markedly in Δ*Rac* when compared to WT and Rac^C (Figure 5C), which indicated that *Rac* was involved in sclerotium formation in *A. flavus*. This implies that Rac may act as a molecular switch to regulate the expression of genes related to the sclerotium formation pathway. When *Rac* was deleted, the sclerotium formation process was blocked and sclerotium disappeared due to the lack of control switch in *A. flavus*. All the above results showed that Rac is involved in the development and reproduction of *A. flavus*.

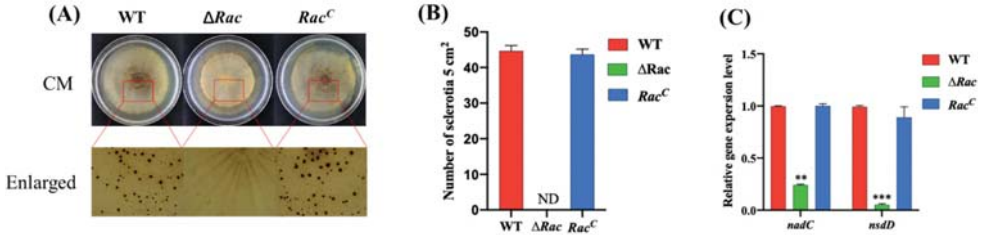

Figure 5. *Rac* is required for sclerotial formation in *A. flavus*. (**A**) The strain was cultured in CM medium at 37 °C for 7 days and then observed. (**B**) Number of sclerotia of these strains. (**C**) qPCR verified the expression level of genes *nsdC* and *nsdD* in these strains. ** means $p < 0.05$, *** means $p < 0.0001$.

2.5. Effect of Rac on Aflatoxin Biosynthesis in A. flavus

AFB1 is the most harmful secondary metabolite produced by *A. flavus*. To study the role of Rac in AFB1 production, all strains were cultured in liquid medium, and TLC and HPLC were used to detect the aflatoxin production. The result showed that the ability of *Rac* mutant to produce toxin AFB1 was impaired significantly compared to WT and Rac^C (Figure 6A–C). To explore the reason for the significant decrease of AFB1 in Δ*Rac*, we amplified secondary metabolism-related genes and regulatory genes in the aflatoxin formation gene cluster by qPCR. It was found that the expression of secondary metabolism regulatory genes *veA* and *laeA* was decreased, and the expression of genes in the toxin formation gene cluster (*aflR*, *aflC*, *aflD*, *aflJ*, *aflK*, *aflL*, *aflN*, *aflO*, *aflP*, *aflQ*, *aflR*, *aflS*, *aflY*) was also downregulated (Figure 6D). It could be speculated that Rac might regulate the expression of genes related to toxin synthesis, thereby affecting the toxin synthesis ability in *A. flavus*.

2.6. Role of Rac in Seed Infection

In order to explore the ability of Δ*Rac* to infect seeds and produce aflatoxin in the process of infecting the host, we conducted an in vitro infection experiment. The same amount of conidia was inoculated to corn and peanut seeds and cultured for 7 days, and it was found that the conidia produced by Δ*Rac* in the process of infecting seeds decreased significantly when compared to WT and Rac^C (Figure 7A,B,E), and the toxins produced by Δ*Rac* in the infecting process were significantly reduced when compared to WT and Rac^C (Figure 7C,D,F). All the above results showed that *Rac* also played an important role in the process of *A. flavus* infecting seeds.

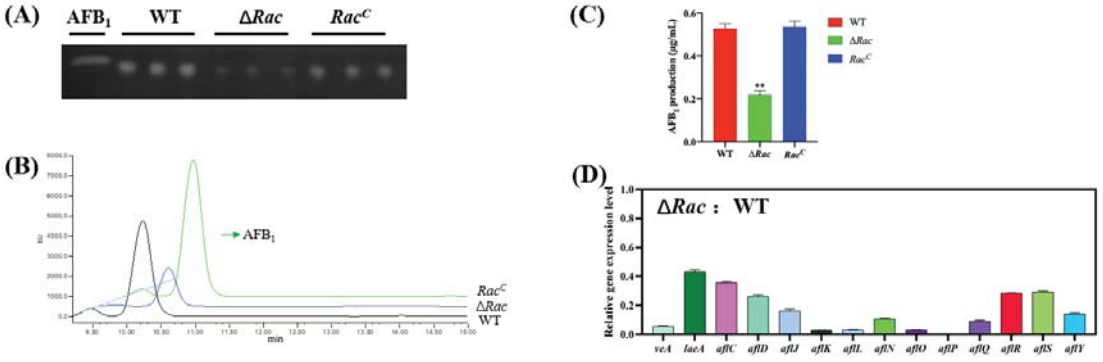

Figure 6. Effect of *Rac* on aflatoxin biosynthesis in *A. flavus.* (**A**) TLC was used to observe AFB1 production of the strains. (**B**) Determination of AFB1 production by HPLC. (**C**) According to the HPLC data, the amount of AFB1 produced in the strains was calculated, and the histogram was drawn and analyzed by GraphPad Prism8. ** means $p < 0.05$. (**D**)The expression level of toxin synthesis-related and regulatory genes in Δ*Rac* was calculated, and the histogram was drawn and analyzed by GraphPad Prism8.

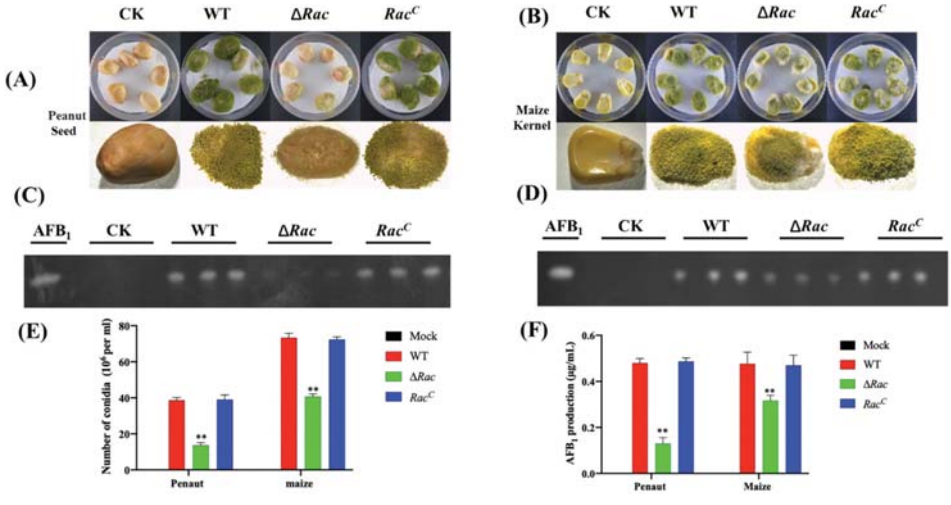

Figure 7. Role of Rac in seed infection. (**A**) Peanut was infected with uniformly diluted 1×10^6 conidia solution and cultured at 29 °C for 7 days. (**B**) The corn was infected with the uniformly diluted 1×10^6 conidia solution and cultured at 29 °C for 7 days. (**C**) Detection of aflatoxin production by infected peanut by TLC. (**D**) Detection of aflatoxin production by infected corn by TLC. (**E**) Spore number from infected peanut and corn. (**F**) Amount of toxin produced by infected peanut and corn. ** means $p < 0.05$.

2.7. Rac Contributes to Cell Wall and Osmotic Stress Response

It was found that when 1.2 M calcofluor white (CFW) was added to the culture medium (Figure 8A), the inhibition rate of cell wall stress to Δ*Rac* was higher than that to WT and Rac^C (Figure 8B), indicating that the sensitivity of Δ*Rac* to respond to cell wall stress increased. Western blot results indicated that Slt2 could not be phosphorylated after *Rac* deletion (Figure 8C), showing that Rac may be used as the switch for the Slt2-MAPK cascade in *A. flavus* to control the pathway. When 1.2 M sorbitol was added into the culture medium (Figure 8D), the results showed that the inhibition rate of Δ*Rac* was also

increased when compared to WT and Rac^C (Figure 8E), indicating the sensitivity of Δ*Rac* responding to osmotic stress was increased. Western blot results found that Hog could not be phosphorylated after *Rac* was deleted (Figure 8F), which indicated that Rac could be used as the switch of the osmotic glycerol pathway in *A. flavus* to regulate the Hog-MAPK cascade to cope with osmotic stress.

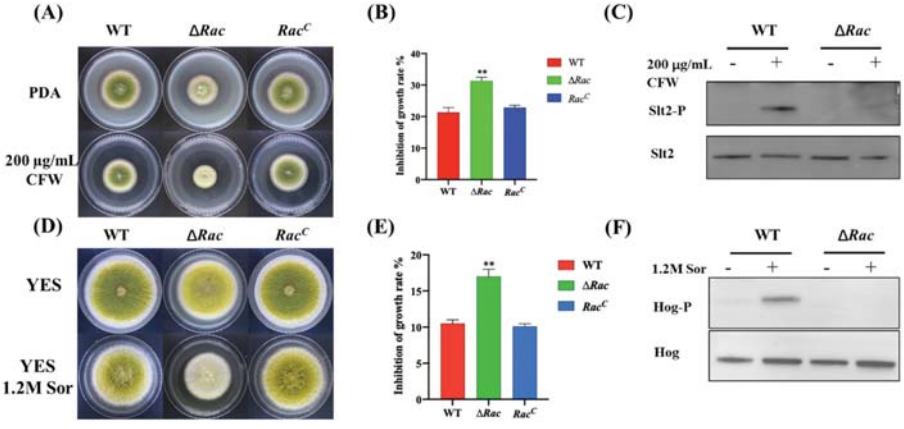

Figure 8. *Rac* contributes to cell wall stress and osmotic stress. (**A**) CFW was added to PDA culture medium, and strains with the same dilution ratio were cultured at 37 °C for 3 days. (**B**) The inhibition rate was calculated by the ratio of the absolute value of the growth diameter of the stressed strain to that of the unstressed strain. (**C**) Western blot assay of Slt2 and Slt2-P proteins in WT and Δ*Rac* were studied by Slt2- and Slt2-P-specific antibodies. (**D**) Sorbitol was added into PDA culture medium and cultured at 37 °C for 3 days. (**E**) The inhibition rate was calculated in these strains. (**F**) Western blot of Hog and Hog-P proteins in WT and Δ*Rac* by using Hog and Hog-P-specific antibodies. ** means $p < 0.05$.

3. Discussion

In plants, Rac orthologs are thought to be involved in the regulation of pollen tube growth, which shares several features with filamentous growth [19]. As the first Rac homologous gene studied in fungi, the deletion of *YlRAC1* resulted in the morphological changes of dimorphic yeast *Yarrowia lipolytica* cells, suggesting that the function of YlRAC1 may be related to some aspects of cell growth polarization [20]. In filamentous fungi, it was reported that the absence of *RacA* in *Aspergillus niger* leads to hyper-branched reproductive tubes and hyphae, which are short in length but wide in hyphal diameter. The frequent branching leads to tighter colonies on solid media, and the diameter of colonies becomes smaller due to the slow elongation at the tip [21]. In this study, we found that in *A. flavus*, when *Rac* was absent, the elongation rate of the apical hypha was low, the colony diameter was obviously reduced, and the strain morphology and development defects were serious, which was very similar to the phenotype of *A. niger*. Therefore, Rac in *A. flavus* may affect the hypha extension by acting on cell polarization and finally, affect the colony diameter.

Both *A. nidulans* and *A. fumigatus*, which are currently known to be sequenced, have been found to contain a plethora of clustered genes specifically for the production of secondary metabolites [22]. In *A. nidulans*, *aflR* and *stcU* were not expressed when *laeA* was deleted. However, when *aflR* is deleted, it does not affect the transcription level of *laeA*. When *aflR* is overexpressed, the expression of *laeA* decreases. This indicates that *laeA* can regulate the key gene *aflR* in the production of aflatoxins [23]. In *A. parasiticus* and *A. flavus*, *veA* was necessary for the transcription of the key genes of toxin production *aflR* and *aflJ* [24,25]. In this study, we found that the expression level of *veA* and *laeA* in Δ*Rac* was decreased compared with WT. The expression of the AFB1 synthesis gene cluster was

decreased, and the AFB1 production ability of Δ*Rac* also declined. Therefore, we suspect that Rac may regulate the key genes *aflR* and *aflS* to control the other toxin production gene cluster to participate in toxin synthesis. It can also regulate the expression level of *laeA* and *veA*, which are involved in the switch toward secondary metabolism, thus regulating aflatoxin synthesis.

It is known in previous reports that not only aflatoxin production is regulated by veA, but also *veA* is a necessary gene for sclerotium formation in *A. flavus* [26]. In this study, it was found that Δ*Rac* did not produce sclerotium. The qPCR results also showed that compared with WT, the expression of *veA* of Δ*Rac* was extremely low, which was consistent with the previously reported results. It is not difficult to speculate that Rac may control the expression of *veA* in *A. flavus*, thus affecting sclerotium formation.

Compared with *A. fumigatus*, the virulence of RacA-deleted mutant is unchanged [16], but in *U.maydis*, the deletion of Rac1 leads to the loss of virulence [17]. In *Claviceps purpurea*, it was found that after *Rac* was deleted, its pathogenicity was completely lost [27]. The *Rac*-deleted mutant cannot penetrate the plant surface, which due to the serious cytoskeleton defects of the mutant, thus it cannot produce the mechanical force required for penetration. Unlike the absence of *RacA* in *A. fumigatus* [16], we found that the infectivity of *A. flavus Rac*-deleted mutant was greatly reduced compared with that of WT. Therefore, we suggested that when Rac is absent, the mutant strains have serious cytoskeleton defects, and the mechanical force required for penetration in *A. flavus* is low, which leads to the decline of infection ability.

It has been reported that under high osmotic pressure, Rac-induced activation of the PAK2 subtype leads to its phosphorylation and translocation to the intercellular junction, where it locally promotes the phosphorylation of MLC [28], which is a cascade reaction of cells to external osmotic pressure. According to our research results, the absence of Rac made Slt2 and Hog no longer phosphorylated, and the sensitivity of the strain to cope with cell wall stress and osmotic stress increased. It could be concluded that Rac is indeed involved in the pathway of *A. flavus* responding to external cell wall stress and osmotic stress. Combining with the reports [29], we speculated that Rac may play its molecular switch function as a member of the Rho family, and control the phosphorylation process of Slt2 and Hog, thus opening the communication path of the strain against environmental stress.

4. Materials and Methods

4.1. Strains and Media

All strains used in the experiment are listed in Table 1. *A. flavus* CA14 PTS (Δ*ku70*Δ*pyrG*, uracil auxotrophic) was used as the parent strain for transformation. The strains in this study were cultured on yeast extract sucrose (YES), minimal medium (MM), potato dextrose agar (PDA), glucose minimal medium (GMM), and complete medium (CM) for conidia culture and mycelial growth [30]. The sclerotia-inducing Wickerham (WKM) medium was used for sclerotia formation. YES liquid medium was used for AFB1 production. Each experiment was repeated at least 3 times.

Table 1. Strains used in this study.

Strains	Genotype Descripion	Source
A. flavus CA14	Δ*ku70*, Δ*pyrG*	Purchased from FGSC (Manhattan, NY, USA)
Wild-type (WT)	Δ*ku70*, Δ*pyrG*::*AfpyrG*	This study
Δ*AflRac*	Δ*ku70*, Δ*pyrG*::*AfpyrG*, Δ*AflRac*	This study
Δ*AflRacC*	Δ*ku70*, Δ*Aflmsb2*:: *Aflmsb2*, *pyrG*	This study
E. coil DH5α		Takara
E. coil Rosetta		Takara

4.2. Domain and Phylogenetic Tree Analysis

The sequence of *A. flavus* Rac (XP_002384152.1) was downloaded from NCBI and compared to the gene sequences of human, mouse, and other fungi. The phylogenetic tree was established with MEGA 7.0 software [31]. The protein domain was predicted by SMART [32] (http://smart.embl-heidelberg.de/) software and plotted by DOG2.0 software [33].

4.3. Expression of Recombinant Protein and Detection of GTPase Activity

The Rho GTPase *Rac* gene was cloned by PCR using special primers which include restriction sites of *EcoR* I and *Hind* III. The pET28a vector and *Rac* gene fragment were digested by *EcoR* I and *Hind* III, and then ligated by T4 ligase. Positive plasmid pET28a-*Rac* was extracted and transformed into an expression strain of *E. coli* Rosetta, grown in liquid LB medium, and further incubated at 37 °C for 4–5 h until the OD value reached 0.5. Isopropyl-β-D-thiogalactopyranoside (IPTG, 0.4 mM) was added into the medium for inducing target protein expression. After 4 h induction, cells were collected and then sonicated on ice. Cell lysates were centrifuged at 13,000 r/min until no significant precipitation. The supernatant was loaded into a Ni^{2+}-NTA column for purification [34]. GTPase activities were measured using the ATPase/GTPase Activity Assay Kit (MAK-113, Sigma-Aldrich, St. Louis, MO, USA) according to the manufacturer's instructions.

4.4. Construction of Mutant Strains

The *Rac* gene deletion mutants (Δ*Rac*) were constructed by homologous recombination [35]. The primers used in this study were listed in Table 2. PCR amplification was used to generate a gene deletion cassette, and the PCR product was transformed into *A. flavus* CA14 protoplast. Positive transformants were screened and verified by diagnostic PCR [36] and Southern blot. Then, the two-step method was used to construct the complementary strains (Rac^C) [37], and positive transformants were verified by PCR verification.

Table 2. Primers used in this study.

Primer	Sequence (5′-3′)	Characteristics
Rac-p1	GGTTTCCTCAACGGTGTT	For amplifying
Rac-p3	GGGTGAAGAGCATTGTTTGAGGC TCTTTCAGAATCTGCGATAT	5′UTR of Δ*Rac*
Rac-p6	GCATCAGTGCCTCCTCTCAGA	For amplifying
Rac-p8	CAATTTTCTCCCGACTATAA CATCATTCCTAATGTGCTT	3′ UTR of Δ*Rac*
Rac-p2	GTTGGGAAAGAGGTGTCG	For fusion PCR
Rac-p7	GTCTCAGTGCGTGTTGCT	of Δ*Rac*
pyrG-F	GCCTCAAACAATGCTCTTCACCC	For amplifying
pyrG-R	GTCTGAGAGGAGGCACTGATGC	*A. fumigatus* pyrG
Rac-p9	CGGCTAATAGACGACCAAT	For validating ORF
Rac-p10	AGACGCTCTTCAGATTACG	
Rac-C-p1	GATTGTTCCCTTATCATTG	For amplifying
Rac-C-p2	CGAACAAGGTGTATAGTCT	ORF of *RacC*
Rac-C-p3	GATTGTTCCCTTATCATTG	
Rac-C-p4	GGGTGAAGAGCATTGTTTGAG	For amplifying
Rac-C-p5	GCCTACAGAATCAGACATTTGCTCTTC GCATCAGTGCCTCCTCTCAGA	5′UTR of Rac^C For amplifying
Rac-C-p6	CATCGATTCTTATAATTTTCTCCCGA CGAACAAGGTGTATAGTCT	3′UTR of Rac^C
Rac-C-O1	CCTGCCTTGTGGTATTTC	For fusion PCR
Rac-C-O2	ATGCTTTGCTGACGCTAT	of Rac^C
Rac-S-O1	ACCAGCCATTCAGTGTTC	For Southern blot
Rac-S-O2	AATTGCAGTGACAAGAGATG	
pyrG-907-F	ATGACGGCGATGTAGGGA	For screening Δ*Rac* mutant
pyrG-919-R	CGACATCCTCACCGATTTCA	
Rac-G-O1	AATGGGTCGCGGATCCCTGGAAGTTC TGTTCCAGGGGCCCATGGCGACCGGT	For amplifying
Rac-G-O2	GGTGGTGGTGGTGGTGCTCGAGCTACAGA ATCAGACATTTGCTC	complete *Rac* gene

4.5. Mycelial Growth, Conidiation and Sclerotia Analysis

The phenotypes of WT, Δ*Rac*, and *Rac*^{C} strains were observed and analyzed in different media. The mycelium growth and development, conidia formation, and sclerotium formation were analyzed according to the methods described previously [38].

4.6. Aflatoxins Analysis

In order to produce aflatoxin, 10 μL conidia suspensions of WT, Δ*Rac*, and *Rac*^{C} strains (1×10^7 conidia/mL) were inoculated into 7.5 mL YES liquid medium, respectively, and cultured at 29 °C in the dark for 7 days. Thin-layer chromatography (TLC) was used to detect aflatoxin products [39]. All the culture toxin medium was transferred to a 50 mL centrifuge tube, and an equal volume of chloroform was added and mixed well. After shaking and extraction for 30 min, the lower layer of chloroform was taken and volatilized. The mycelium was filtered and dried to obtain the dry weight of mycelium. Chloroform lytic toxin was added according to the proportion of dry weight of mycelium. TLC developing agent (volume ratio, chloroform: acetone = 9:1) was poured into the chromatography cylinder, and then 10 μL of each sample was added to the TLC plate. After completion, the samples were air-dried and placed under the UV gel imaging system for toxin detection. In order to quantitatively analyze the yield of aflatoxin, the aflatoxin extract was further analyzed by high-performance liquid chromatography (HPLC). Aflatoxin was detected by fluorescence detector (Water, Milford, MA, USA) with excitation wavelength and emission wavelength of 365 nm and 455 nm, respectively. Each experiment was repeated 3 times [29].

4.7. Seeds Infections

The ability of WT, Δ*Rac*, and *Rac*^{C} strains to infect plant seeds was tested by previous methods [40]. Seeds were inoculated with conidia suspension and cultured at 29 °C; then, 700 μL of sterile water was added to keep the culture filter paper in a moist state. After 6 days of culture, the infected seeds were collected and placed into a 50 mL centrifuge tube, and then 15 mL sterile water and 7.5 mL dichloromethane were added. In order to make the conidia fully suspend in the liquid, the tube was shaken violently for 5 min. The number of conidia was counted, and aflatoxin was extracted according to the previous method [41]. Each experiment was repeated at least 3 times.

4.8. Cell Wall Stress and Osmotic Pressure Stress

Two hundred μg/mL CFW was added to PDA medium to construct cell wall stress medium, and 1.2 mol/mL sorbitol was added to YES medium to construct osmotic stress medium. The strains with the same dilution ratio were cultured at 37 °C for 3 days [42].

4.9. Western Blot Analysis

The conidia (6×10^5) of WT, Δ*Rac* and *Rac*^{C} strains were inoculated into YES liquid medium, respectively, and cultured for 48 h. Whole-cell extraction and Western blot were carried out according to our previous publication [43]. Anti-Hog1 (Santa Cruz Biotechnology Company, Dallas, TX, USA) and anti-AflSlt2 antibodies (prepared by our laboratory) were used. Enhanced chemiluminescence (ECL) substrate was used for Western blot analysis, and chemiluminescence was determined by G-box Chemi XT4 (Syngene, Hong Kong, China).

4.10. Quantitative RT-PCR Analysis

The mycelia of WT, Δ*Rac*, and *Rac*^{C} strains were harvested on YES medium at 37 °C. Total RNA of mycelium was extracted by an RNA extraction kit (Tianmo Bio, Beijing, China), and reverse transcription cDNA was obtained by gene synthesis SuperMix (Transgen Biotech, Beijing, China). On the ThermoFisher Scientific real-time PCR system, SYBR Green qPCR Mix (Guangzhou Dongsheng Biotechnology, Guangzhou, China) was used for qRT-PCR. The *actin* gene of *A. flavus* was used as the reference gene, and the relative expression

of the target gene was calculated by the $2^{-\Delta\Delta Ct}$ method [44]. The qRT-PCR primers were listed in Table 3. All qRT-PCR tests were performed in triplicate for each sample, and each experiment was repeated at least 3 times.

Table 3. qPCR primers used in this study.

Primer	Sequence (5′-3′)	Characteristics
abaA-qRT-F	TCTTCGGTTGATGGATGATTTC	For amplifying *abaA*
abaA-qRT-R	CCGTTGGGAGGCTGGGT	
brlA-qRT-F	GCCTCCAGCGTCAACCTTC	For amplifying *brlA*
brlA-qRT-R	TCTCTTCAAATGCTCTTGCCTC	
nsdC-qRT-F	GCCAGACTTGCCAATCAC	For amplifying *nsdC*
nsdC-qRT-R	CATCCACCTTGCCCTTTA	
nsdD-qRT-F	GGACTTGCGGGTCGTGCTA	For amplifying *nsdD*
nsdD -qRT-R	AGAACGCTGGGTCTGGTGC	
veA -qRT-F	TATCATTCCGTGGCTCAAT	For amplifying *veA*
veA -qRT-R	GAGAGGTACTGCTGGATG	
laeA -qRT-F	TTGTTGGGGTTGACCTTGCT	For amplifying *laeA*
laeA -qRT-R	GCCATCCCATCACACTTCCA	
aflC-qRT-F	TTACGCTGCGATCAGTTCCTC	For amplifying *aflC*
aflC-qRT-R	CGACTCGCATTACAGCATCTAAC	
aflD-qRT-F	GTGGTGGTTGCCAATGCG	For amplifying *aflD*
aflD-qRT-R	CTGAAACAGTAGGACGGGAGC	
aflJ-qRT-F	CGGCGTATGAGGAGAATG	For amplifying *aflJ*
aflJ-qRT-R	CTTCATCAACCTGGCATCA	
aflK-qRT-F	GAGCGACAGGAGTAACCGTAAG	For amplifying *aflK*
aflK-qRT-R	CCGATTCCAGACACCATTAGCA	
aflL-qRT-F	GGCTGCGGAACTGTATTG	For amplifying *aflL*
aflL-qRT-R	TGTGGAGTGCTGGAAGAG	
aflN-qRT-F	TTCATTCCTGAGCGATGG	For amplifying *aflN*
aflN-qRT-R	CGTATGCTGGCGTAATATC	
aflO-qRT-F	GATTGGGATGTGGTCATGCGATT	For amplifying *aflO*
aflO-qRT-R	GCCTGGGTCCGAAGAATGC	
aflP-qRT-F	ACGAAGCCACTGGTAGAGGAGATG	For amplifying *aflP*
aflP-qRT-R	GTGAATGACGGCAGGCAGGT	
aflQ-qRT-F	GTCGCATATGCCCCGGTCGG	For amplifying *aflQ*
aflQ-qRT-R	GGCAACCAGTCGGGTTCCGG	
aflR-qRT-F	AAAGCACCCTGTCTTCCCTAAC	For amplifying *aflR*
aflR-qRT-R	GAAGAGGTGGGTCAGTGTTTGTAG	
aflS-qRT-F	AAGCTAAGGCCGAGTCTGG	For amplifying *aflS*
aflS-qRT-R	CAGGTTGTGTTGCTGTTGATAG	
aflY-qRT-F	AGGCAGACTTTCTAACACT	For amplifying *aflY*
aflY-qRT-R	CCTTCAGTTCCACACCAA	
Rac -qRT-p9	GGTGACGGTGCTGTTGGA	
Rac -qRT-p10	CGGGTCGTGGATTGAGAA	
actin-qRT-F	ACGGTGTCGTCACAAACTGG	For amplifying *actin*
actin -qRT-R	CGGTTGGACTTAGGGTTGATAG	

4.11. Statistical Analysis

GraphPad Prism8 [45] (https://www.graphpad.com) was used for statistical analysis. T-test was used for comparison between the two groups, and ANOVA was used for comparison among multiple groups.

Author Contributions: Conceptualization, L.Q. and L.Y.; methodology, J.Z.; software, W.Z.; validation, M.S.; writing—original draft preparation, L.Y.; writing—review and editing, S.W. and J.Y.; project administration, J.Y.; funding acquisition, J.Y. All authors have read and agreed to the published version of the manuscript.

Funding: This research was funded by [National Natural Science Foundation of China] grant number [No. 31600118].

Institutional Review Board Statement: Not applicable.

Informed Consent Statement: Not applicable.

Data Availability Statement: Not applicable.

Conflicts of Interest: The authors declare that they have no known competing financial interests or personal relationships that could have appeared to influence the work reported in this paper.

References

1. Kumar, P.; Mahato, D.K.; Kamle, M.; Mohanta, T.K.; Kang, S.G. Aflatoxins: A Global Concern for Food Safety, Human Health and Their Management. *Front. Microbiol.* **2016**, *7*, 2170. [CrossRef] [PubMed]
2. Amaike, S.; Keller, N.P. Aspergillus flavus. *Annu. Rev. Phytopathol.* **2011**, *49*, 107–133. [CrossRef] [PubMed]
3. Kensler, T.W.; Roebuck, B.D.; Wogan, G.N.; Groopman, J.D. Aflatoxin: A 50-year odyssey of mechanistic and translational toxicology. *Toxicol. Sci.* **2011**, *120* (Suppl. S1), S28–S48. [CrossRef] [PubMed]
4. Roze, L.V.; Hong, S.Y.; Linz, J.E. Aflatoxin biosynthesis: Current frontiers. *Annu. Rev. Food Sci. Technol.* **2013**, *4*, 293–311. [CrossRef]
5. Arenas-Huertero, F.; Zaragoza-Ojeda, M.; Sánchez-Alarcón, J.; Milić, M.; Šegvić Klarić, M.; Montiel-González, J.M.; Valencia-Quintana, R. Involvement of Ahr Pathway in Toxicity of Aflatoxins and Other Mycotoxins. *Front. Microbiol.* **2019**, *10*, 2347. [CrossRef]
6. Strosnider, H.; Azziz-Baumgartner, E.; Banziger, M.; Bhat, R.V.; Breiman, R.; Brune, M.N.; DeCock, K.; Dilley, A.; Groopman, J.; Hell, K.; et al. Workgroup report: Public health strategies for reducing aflatoxin exposure in developing countries. *Environ. Health Perspect.* **2006**, *114*, 1898–1903. [CrossRef]
7. Robens, J.; Cardwell, K. The Costs of Mycotoxin Management to the USA: Management of Aflatoxins in the United States. *Toxin Rev.* **2003**, *22*, 139–152. [CrossRef]
8. Vigil, D.; Cherfils, J.; Rossman, K.L.; Der, C.J. Ras superfamily GEFs and GAPs: Validated and tractable targets for cancer therapy? *Nat. Rev. Cancer* **2010**, *10*, 842–857. [CrossRef]
9. Heasman, S.J.; Ridley, A.J. Mammalian Rho GTPases: New insights into their functions from in vivo studies. *Nat. Rev. Mol. Cell Biol.* **2008**, *9*, 690–701. [CrossRef]
10. Mittnacht, S.; Paterson, H.; Olson, M.F.; Marshall, C.J. Ras signalling is required for inactivation of the tumour suppressor pRb cell-cycle control protein. *Curr. Biol.* **1997**, *7*, 219–221. [CrossRef]
11. Bokoch, G.M. Regulation of the phagocyte respiratory burst by small GTP-binding proteins. *Trends Cell Biol.* **1995**, *5*, 109–113. [CrossRef]
12. De Curtis, I. Functions of Rac GTPases during neuronal development. *Dev. Neurosci.* **2008**, *30*, 47–58. [CrossRef] [PubMed]
13. Luo, L.; Liao, Y.J.; Jan, L.Y.; Jan, Y.N. Distinct morphogenetic functions of similar small GTPases: Drosophila Drac1 is involved in axonal outgrowth and myoblast fusion. *Genes Dev.* **1994**, *8*, 1787–1802. [CrossRef] [PubMed]
14. Ng, J.; Luo, L. Rho GTPases regulate axon growth through convergent and divergent signaling pathways. *Neuron* **2004**, *44*, 779–793. [CrossRef] [PubMed]
15. Virag, A.; Lee, M.P.; Si, H.; Harris, S.D. Regulation of hyphal morphogenesis by cdc42 and rac1 homologues in Aspergillus nidulans. *Mol. Microbiol.* **2007**, *66*, 1579–1596. [CrossRef] [PubMed]
16. Li, H.; Barker, B.M.; Grahl, N.; Puttikamonkul, S.; Bell, J.D.; Craven, K.D.; Cramer, R.A., Jr. The small GTPase RacA mediates intracellular reactive oxygen species production, polarized growth, and virulence in the human fungal pathogen Aspergillus fumigatus. *Eukaryot. Cell* **2011**, *10*, 174–186. [CrossRef]
17. Mahlert, M.; Leveleki, L.; Hlubek, A.; Sandrock, B.; Bölker, M. Rac1 and Cdc42 regulate hyphal growth and cytokinesis in the dimorphic fungus Ustilago maydis. *Mol. Microbiol.* **2006**, *59*, 567–578. [CrossRef]
18. Boyce, K.J.; Hynes, M.J.; Andrianopoulos, A. Control of morphogenesis and actin localization by the Penicillium marneffei RAC homolog. *J. Cell Sci.* **2003**, *116*, 1249–1260. [CrossRef]
19. Kost, B.; Lemichez, E.; Spielhofer, P.; Hong, Y.; Tolias, K.; Carpenter, C.; Chua, N.H. Rac homologues and compartmentalized phosphatidylinositol 4, 5-bisphosphate act in a common pathway to regulate polar pollen tube growth. *J. Cell Biol.* **1999**, *145*, 317–330. [CrossRef]
20. Hurtado, C.A.; Beckerich, J.M.; Gaillardin, C.; Rachubinski, R.A. A rac homolog is required for induction of hyphal growth in the dimorphic yeast Yarrowia lipolytica. *J. Bacteriol.* **2000**, *182*, 2376–2386. [CrossRef]
21. Kwon, M.J.; Nitsche, B.M.; Arentshorst, M.; Jørgensen, T.R.; Ram, A.F.; Meyer, V. The transcriptomic signature of RacA activation and inactivation provides new insights into the morphogenetic network of Aspergillus niger. *PLoS ONE* **2013**, *8*, e68946. [CrossRef] [PubMed]
22. Kale, S.P.; Milde, L.; Trapp, M.K.; Frisvad, J.C.; Keller, N.P.; Bok, J.W. Requirement of LaeA for secondary metabolism and sclerotial production in Aspergillus flavus. *Fungal Genet. Biol.* **2008**, *45*, 1422–1429. [CrossRef] [PubMed]
23. Bok, J.W.; Keller, N.P. LaeA, a regulator of secondary metabolism in Aspergillus spp. *Eukaryot. Cell* **2004**, *3*, 527–535. [CrossRef] [PubMed]

24. Calvo, A.M. The VeA regulatory system and its role in morphological and chemical development in fungi. *Fungal Genet. Biol.* **2008**, *45*, 1053–1061. [CrossRef]
25. Du, W.; Obrian, G.R.; Payne, G.A. Function and regulation of aflJ in the accumulation of aflatoxin early pathway intermediate in Aspergillus flavus. *Food Addit. Contam.* **2007**, *24*, 1043–1050. [CrossRef]
26. Duran, R.M.; Cary, J.W.; Calvo, A.M. Production of cyclopiazonic acid, aflatrem, and aflatoxin by Aspergillus flavus is regulated by veA, a gene necessary for sclerotial formation. *Appl. Microbiol. Biotechnol.* **2007**, *73*, 1158–1168. [CrossRef]
27. Rolke, Y.; Tudzynski, P. The small GTPase Rac and the p21-activated kinase Cla4 in Claviceps purpurea: Interaction and impact on polarity, development and pathogenicity. *Mol. Microbiol.* **2008**, *68*, 405–423. [CrossRef]
28. Di Ciano-Oliveira, C.; Thirone, A.C.; Szászi, K.; Kapus, A. Osmotic stress and the cytoskeleton: The R(h)ole of Rho GTPases. *Acta Physiol.* **2006**, *187*, 257–272. [CrossRef]
29. Qin, L.; Li, D.; Zhao, J.; Yang, G.; Wang, Y.; Yang, K.; Tumukunde, E.; Wang, S.; Yuan, J. The membrane mucin Msb2 regulates aflatoxin biosynthesis and pathogenicity in fungus Aspergillus flavus. *Microb. Biotechnol.* **2021**, *14*, 628–642. [CrossRef]
30. Lan, H.; Wu, L.; Fan, K.; Sun, R.; Yang, G.; Zhang, F.; Yang, K.; Lin, X.; Chen, Y.; Tian, J.; et al. Set3 Is Required for Asexual Development, Aflatoxin Biosynthesis, and Fungal Virulence in Aspergillus flavus. *Front. Microbiol.* **2019**, *10*, 530. [CrossRef]
31. Wang, Y.; Wang, S.; Nie, X.; Yang, K.; Xu, P.; Wang, X.; Liu, M.; Yang, Y.; Chen, Z.; Wang, S. Molecular and structural basis of nucleoside diphosphate kinase-mediated regulation of spore and sclerotia development in the fungus Aspergillus flavus. *J. Biol. Chem.* **2019**, *294*, 12415–12431. [CrossRef]
32. Available online: http://smart.embl-heidelberg.de/ (accessed on 20 August 2022).
33. Ren, J.; Wen, L.; Gao, X.; Jin, C.; Xue, Y.; Yao, X. DOG 1. *0: Illustrator of protein domain structures. Cell Res.* **2009**, *19*, 271–273. [CrossRef]
34. Lan, H.; Wu, L.; Sun, R.; Keller, N.P.; Yang, K.; Ye, L.; He, S.; Zhang, F.; Wang, S. The HosA Histone Deacetylase Regulates Aflatoxin Biosynthesis Through Direct Regulation of Aflatoxin Cluster Genes. *Mol. Plant Microbe Interact.* **2019**, *32*, 1210–1228. [CrossRef]
35. Lan, H.; Sun, R.; Fan, K.; Yang, K.; Zhang, F.; Nie, X.Y.; Wang, X.; Zhuang, Z.; Wang, S. The Aspergillus flavus Histone Acetyltransferase AflGcnE Regulates Morphogenesis, Aflatoxin Biosynthesis, and Pathogenicity. *Front. Microbiol.* **2016**, *7*, 1324. [CrossRef]
36. Yang, K.; Liu, Y.; Wang, S.; Wu, L.; Xie, R.; Lan, H.; Fasoyin, O.E.; Wang, Y.; Wang, S. Cyclase-Associated Protein Cap with Multiple Domains Contributes to Mycotoxin Biosynthesis and Fungal Virulence in Aspergillus flavus. *J. Agric. Food Chem.* **2019**, *67*, 4200–4213. [CrossRef]
37. Jia, K.; Yan, L.; Jia, Y.; Xu, S.; Yan, Z.; Wang, S. aflN Is Involved in the Biosynthesis of Aflatoxin and Conidiation in Aspergillus flavus. *Toxins* **2021**, *13*, 831. [CrossRef]
38. Tan, C.; Deng, J.L.; Zhang, F.; Zhu, Z.; Yan, L.J.; Zhang, M.J.; Yuan, J.; Wang, S.H. CWI pathway participated in vegetative growth and pathogenicity through a downstream effector AflRlm1 in Aspergillus flavus. *iScience* **2021**, *24*, 103159. [CrossRef]
39. Yang, M.; Zhu, Z.; Bai, Y.; Zhuang, Z.; Ge, F.; Li, M.; Wang, S. A novel phosphoinositide kinase Fab1 regulates biosynthesis of pathogenic aflatoxin in Aspergillus flavus. *Virulence* **2021**, *12*, 96–113. [CrossRef]
40. Yang, K.; Liang, L.; Ran, F.; Liu, Y.; Li, Z.; Lan, H.; Gao, P.; Zhuang, Z.; Zhang, F.; Nie, X.; et al. The DmtA methyltransferase contributes to Aspergillus flavus conidiation, sclerotial production, aflatoxin biosynthesis and virulence. *Sci. Rep.* **2016**, *6*, 23259. [CrossRef]
41. Mengjuan, Z.; Guanglan, L.; Xiaohua, P.; Weitao, S.; Can, T.; Xuan, C.; Yanling, Y.; Zhenhong, Z. The PHD transcription factor Cti6 is involved in the fungal colonization and aflatoxin B1 biological synthesis of Aspergillus flavus. *IMA Fungus* **2021**, *12*, 12. [CrossRef]
42. Yuan, J.; Chen, Z.; Guo, Z.; Li, D.; Zhang, F.; Shen, J.; Zhang, Y.; Wang, S.; Zhuang, Z. PbsB Regulates Morphogenesis, Aflatoxin B1 Biosynthesis, and Pathogenicity of Aspergillus flavus. *Front. Cell Infect. Microbiol.* **2018**, *8*, 162. [CrossRef]
43. Zhu, Z.; Yang, M.; Bai, Y.; Ge, F.; Wang, S. Antioxidant-related catalase CTA1 regulates development, aflatoxin biosynthesis, and virulence in pathogenic fungus Aspergillus flavus. *Environ. Microbiol.* **2020**, *22*, 2792–2810. [CrossRef]
44. Livak, K.J.; Schmittgen, T.D. Analysis of relative gene expression data using real-time quantitative PCR and the 2(-Delta Delta C(T)) Method. *Methods* **2001**, *25*, 402–408. [CrossRef]
45. Available online: https://www.graphpad.com (accessed on 20 August 2022).

toxins

MDPI

Article

Glutamine Synthetase Contributes to the Regulation of Growth, Conidiation, Sclerotia Development, and Resistance to Oxidative Stress in the Fungus *Aspergillus flavus*

Sen Wang †, Ranxun Lin †, Elisabeth Tumukunde , Wanlin Zeng, Qian Bao, Shihua Wang * and Yu Wang *

State Key Laboratory of Ecological Pest Control for Fujian and Taiwan Crops, Key Laboratory of Pathogenic Fungi and Mycotoxins of Fujian Province, and School of Life Sciences, Fujian Agriculture and Forestry University, Fuzhou 350002, China

* Correspondence: wshyyl@sina.com (S.W.); wangyu@fafu.edu.cn (Y.W.); Tel.: +86-591-87984471 (S.W.)

† These authors contributed equally to the work.

Abstract: The basic biological function of glutamine synthetase (Gs) is to catalyze the conversion of ammonium and glutamate to glutamine. This synthetase also performs other biological functions. However, the roles of Gs in fungi, especially in filamentous fungi, are not fully understood. Here, we found that conditional disruption of glutamine synthetase (AflGsA) gene expression in *Aspergillus flavus* by using a xylose promoter leads to a complete glutamine deficiency. Supplementation of glutamine could restore the nutritional deficiency caused by AflGsA expression deficiency. Additionally, by using the xylose promoter for the downregulation of *AflgsA* expression, we found that AflGsA regulates spore and sclerotic development by regulating the transcriptional levels of sporulation genes *abaA* and *brlA* and the sclerotic generation genes *nsdC* and *nsdD*, respectively. In addition, AflGsA was found to maintain the balance of reactive oxygen species (ROS) and to aid in resisting oxidative stress. AflGsA is also involved in the regulation of light signals through the production of glutamine. The results also showed that the recombinant AflGsA had glutamine synthetase activity in vitro and required the assistance of metal ions. The inhibitor molecule L-α-aminoadipic acid suppressed the activity of rAflGsA in vitro and disrupted the morphogenesis of spores, sclerotia, and colonies in *A. flavus*. These results provide a mechanistic link between nutrition metabolism and glutamine synthetase in *A. flavus* and suggest a strategy for the prevention of fungal infection.

Keywords: *Aspergillus flavus* (*A. flavus*); glutamine synthetase; reactive oxygen species (ROS); L-α-aminoadipic acid

Key Contribution: AflGsA contributes to the regulation of growth, conidiation, sclerotia development, and resistance to oxidative stress in *A. flavus*. L-α-aminoadipic acid suppressed the activity of rAflGsA in vitro and disrupted the morphogenesis of spores, sclerotia, and colonies in *A. flavus*.

Citation: Wang, S.; Lin, R.; Tumukunde, E.; Zeng, W.; Bao, Q.; Wang, S.; Wang, Y. Glutamine Synthetase Contributes to the Regulation of Growth, Conidiation, Sclerotia Development, and Resistance to Oxidative Stress in the Fungus *Aspergillus flavus*. *Toxins* **2022**, *14*, 822. https://doi.org/10.3390/toxins14120822

Received: 25 October 2022
Accepted: 21 November 2022
Published: 23 November 2022

1. Introduction

Aspergillus flavus (*A. flavus*) is a saprophytic, pathogenic, and conditional plant fungus that invades important crops such as peanuts and corn during storage and transportation [1–3]. *A. flavus* is not only a plant pathogenic fungus but also causes invasive aspergillosis, threatening human life [4,5]. In addition, this fungus produces toxic secondary metabolites (aflatoxins) that have been recognized as notorious carcinogenic natural contaminants since their discovery [6–8]. Aflatoxin B1 (AFB1) has strong carcinogenic, teratogenic, and genotoxic properties [9]. Understanding the mechanisms of development and toxin synthesis of *A. flavus* can greatly improve the control strategies for fungal contamination. Therefore, how to effectively prevent and inhibit the infestation of *A. flavus* has become a major challenge.

Nitrogen metabolism is an important part of an organism's metabolism. Glutamine synthetase (Gs) is one of the key central enzymes in the nitrogen metabolic pathway [10] that catalyzes the conversion of glutamate and ammonium to glutamine via an ATP-dependent reaction [11]. Although Gs performs a variety of divergent cellular functions such as nitrogen metabolism and amino acid production [12–15], its biological function is not limited to glutamine synthesis. In wheat (*Triticum aestivum* L.), Gs controls the nitrogen cycle during plant growth and development [16]. Surprisingly, suppression of the Gs gene causes impaired photosynthesis and photorespiration, leading to a significant accumulation of reactive oxygen species (ROS) [17] in *Amaranthus palmeri* (*A. palmeri*). The Gs gene promotes organism repair via cellular nucleotide synthesis after DNA damage [18] and maintains osmotic homeostasis [19]. In *Schizosaccharomyces pombe* (*S. pombe*) and *Aspergillus nidulans* (*A. nidulans*), the inactivation of Gs leads to growth and developmental retardation via glutamine-dependent malnutrition [20,21]. Gs loss of function affects the primary and secondary metabolites' synthesis in the phytopathogenic fungus *Gibberella fujikuroi* (*G. fujikuroi*) [15].

In addition, glutamine synthetase has emerged as a new target for drug discovery and design. Methionine sulfoximine is used as a classical inhibitor for Gs protein activity in bacteria [11]. In plants, the role of Gs makes it an important target for the herbicide glufosinate [22]. Generally, Gs is classified into three types based on molecular weight and 3D spatial structure: GsI, GsII, and GsIII [23]. The Gs-encoding genes in filamentous fungi are usually identified as belonging to the GsII family [24]. Although the amino acid sequences are quite different for the three types of Gs enzymes, these proteins share similar tetrameric geometric structures consisting of two oligomeric rings in a duplex symmetry [25–28]. This oligomerization of Gs indicates that the protein may interact with other molecules and perform their functions in vivo. Indeed, a series of small molecules have been reported to decrease Gs activity, including amino acids, carbamoyl phosphate, and glucosamine-6-phosphate [11,29].

Here, we report that the AflGsA protein is important for colony growth, conidia production, and sclerotia development in *A. flavus*. Furthermore, AflGsA is involved in balancing ROS and resisting oxidative stress. L-α-aminoadipic acid, a potent inhibitor of rAflGsA, was effective in inhibiting growth, spore, and sclerotia production in *A. flavus*. These results provide detailed and comprehensive information concerning the regulatory mechanism of AflGsA in *A. flavus*.

2. Results

2.1. Identification of AflGsA in A. flavus

The sequence of the *A. flavus* Gs (AflGsA) protein was obtained from the NCBI gene database (AFLA_051930), which exhibited 63% similarity to GsA in *Saccharomyces cerevisiae* (*S. cerevisiae*). All of the analyzed proteins contained two conserved domains (Figure 1A). The phylogenetic tree analysis based on AflGsA and other homologous proteins showed that AflGsA was highly conserved in *Aspergillus* spp. (Figure 1B). The expression profiles of *AflgsA* were monitored by quantitative real-time PCR (qRT-PCR) at vegetative growth (VG), conidial development (CON), aflatoxin synthesis (AS), and sclerotial development (SD) stages [30]. The transcript level of *AflgsA* was the highest in the AS stage, whereas the lowest transcript level was reached in the SD stage (Figure 1C). The differences in expression patterns suggest that *AflgsA* may perform different functions at different stages in *A. flavus*.

2.2. AflgsA Is an Essential Gene for the Growth of A. flavus

To investigate the function of *AflgsA* in *A. flavus*, we first tried to obtain the *AflgsA* deletion strain by homologous recombination but failed. A better alternative strategy is to construct a xylose promoter mutant strain (^{xylP}*AflgsA*) for *AflgsA* functional verification (Figure 2A). After confirmation by PCR (Figure 2B) and DNA sequencing (Figure S1), the mutant strain and WT strain were incubated in YXT medium (containing xylose) and

YGT medium (without xylose) for four days at 37 °C in the dark. The mutant strain was completely unable to grow in the xylose-free medium, while growth was partially restored after the addition of xylose (Figure 2C,D). Additionally, a gradient increase in the colony diameter, mycelial tip, and conidial gemination of ^{xylP}*AflgsA* strain was found with an increasing concentration of xylose (Figure S2). These results suggest that glutamine synthetase is essential for the growth of *A. flavus*.

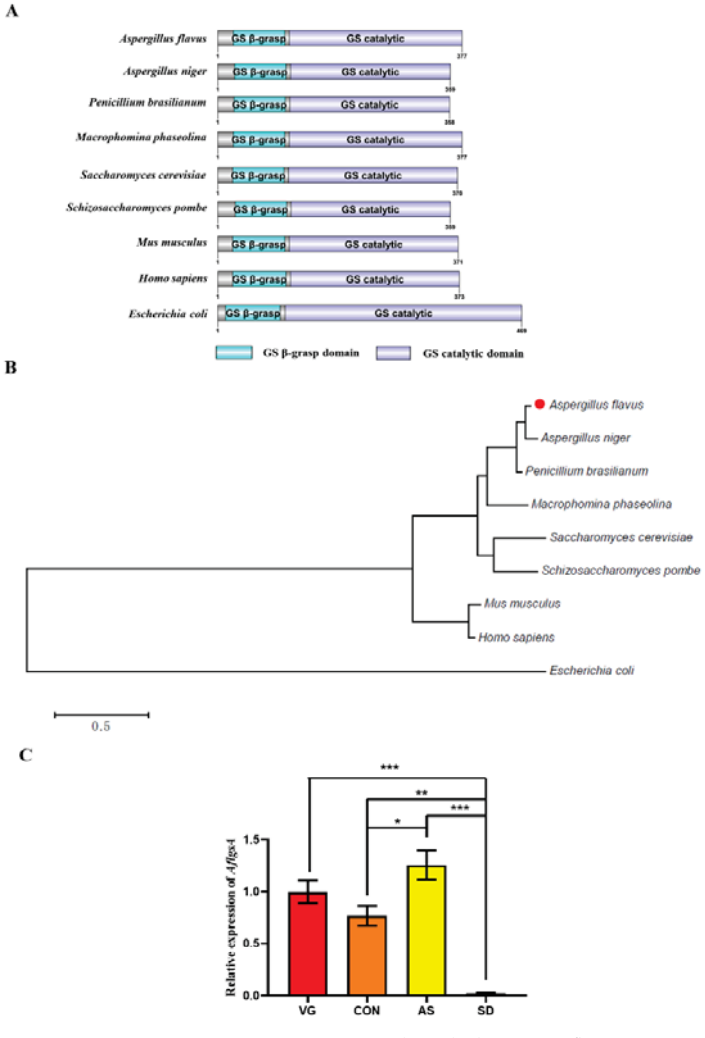

Figure 1. Sequence analysis and expression profiles of AflGsA in *A. flavus*. (**A**) Domain structure analysis of AflGsA from *A. flavus* and other species (*Aspergillus niger*, *Penicillium brasilianum*, *Macrophomina phaseolina*, *S. cerevisiae*, *S. pombe*, *Mus musculus*, *Homo sapiens*, and *Escherichia coli*). (**B**) Phylogenetic tree of AflGsA from different species. (**C**) Expression patterns of *AflgsA* were tested by qRT-PCR at vegetative growth (VG), conidial development (CON), aflatoxin synthesis (AS), and sclerotial development (SD) stages. * indicates a significance level of $p < 0.05$, ** indicates a significance level of $p < 0.01$, and *** indicates a significance level of $p < 0.001$ based on one-way ANOVA with three biological replicates.

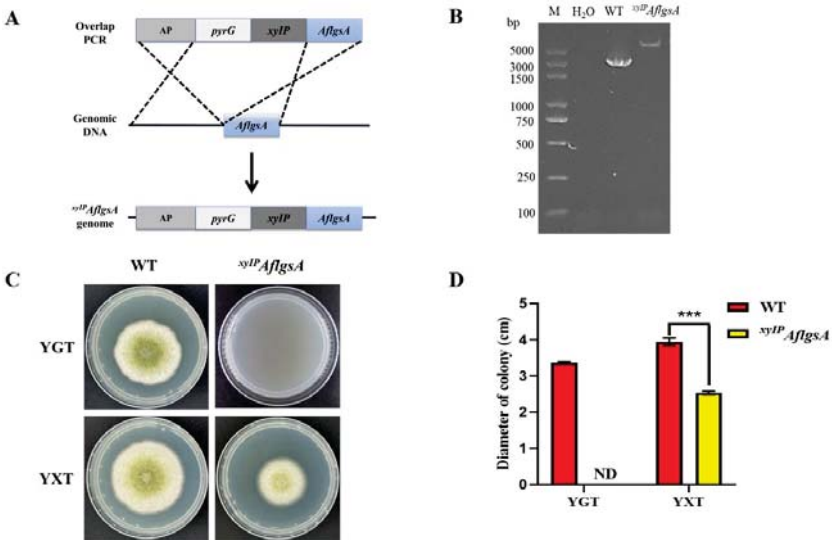

Figure 2. Construction and validation of the ^{xylP}*AflgsA* strain of *A. flavus*. (**A**) The gene replacement strategy for the construction of ^{xylP}*AflgsA*. (**B**) PCR validation of the ^{xylP}*AflgsA* strain. (**C**) Phenotypic observations of the growth for WT and the ^{xylP}*AflgsA* strain in YGT and YXT media in the dark at 37 °C for four days. (**D**) Statistical analysis of the colony diameters of the indicated *A. flavus* strains (panel (**C**)). ND indicates no detection. *** indicates a significance level of $p < 0.001$ based on *t*-tests with three replicates.

2.3. Glutamine Restores the Growth Defect of the ^{xylP}AflgsA Strain

We found that the addition of glutamine (GluN) to the xylose-free or xylose medium restored the growth of the ^{xylP}*AflgsA* strain (Figures 3A,B and S3). Meanwhile, the ammonium tartrate (NH_4^+) or glutamate (Glu) supplement was unable to promote colony growth (Figures 3A,B and S4). This suggested that the growth defect of the mutant strain was caused by the lack of glutamine synthetase. However, the ^{xylP}*AflgsA* strain showed different colony color compared to the WT strain after GluN supplementation (Figure 3A). Moreover, the growth of the ^{xylP}*AflgsA* strain was also inhibited by adding both GluN and NH_4^+ (Figure 3B,C). This phenomenon may be due to competition or inhibition of GluN uptake by excess NH_4^+ [21]. The mechanisms concerning the type of nitrogen sources that mediate the absorption pathway by *AflgsA* in the cell need to be further explored.

2.4. AflGsA Is Important for Conidia Development of A. flavus

To further determine the effect of *AflgsA* on *A. flavus*, we monitored the transcript level of *AflgsA* in the ^{xylP}*AflgsA* strain and found that it was less than half that in the WT (Figure 4A). In addition, the ^{xylP}*AflgsA* strain exhibited smaller spore heads of the child seat and sparser peduncles by microscopic observation (Figure 4B). Statistical analysis also showed a significant reduction in the number of spores in the ^{xylP}*AflgsA* strain compared to that in the WT strain (Figure 4C). Further analysis showed that the transcript levels of both regulatory genes for conidia, *brlA*, and *abaA*, were reduced by about half in the ^{xylP}*AflgsA* strain compared to that in WT (Figure 4D). These results suggest that *AflgsA* may be involved in the upstream regulation of *abaA* and *brlA* genes during spore development of *A. flavus*, and this further regulates the production of conidia.

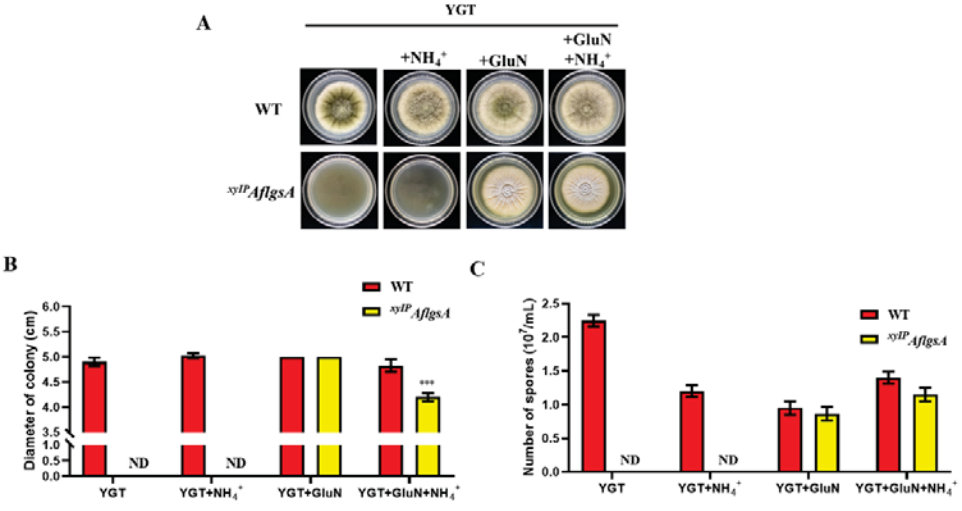

Figure 3. Analysis of the growth of WT and ^{xylP}*AflgsA* strains. (**A**) The colony morphology of the WT and ^{xylP}*AflgsA* strains on YGT medium containing 10 mM glutamine (GluN) or/and ammonium tartrate (NH_4^+) as nitrogen sources. (**B**) Statistical analysis of the diameter from panel (**A**). (**C**) The number of conidia produced by the above two *A. flavus* strains. ND indicates no detection. *** indicates a significance level of $p < 0.001$ based on *t*-tests with three replicates.

2.5. AflGsA Contributes to the Production of Sclerotia but Not to Toxin Synthesis in A. flavus

Sclerotia are important reproductive structures of *Aspergillus flavus*, and they aid in survival under harsh conditions. The sclerotia produced by the ^{xylP}*AflgsA* strain were significantly fewer compared to those in the WT strain (Figure 5A,B). In addition, the transcript levels of the sclerotia-related genes *nsdC* and *nsdD* were significantly lower in the ^{xylP}*AflgsA* strain compared to those in the WT strain, only about half of those in the WT strain (Figure 5C). In addition, the sclerotium production defect in the ^{xylP}*AflgsA* strain could not be recovered by the addition of a GluN supplement (Figure S5). These results suggest that AflGsA is important for sclerotia production, and its coding gene may influence sclerotia production by being involved in the upstream regulation of *nsdC* and *nsdD*. We also investigated the production of the toxic secondary metabolite AFB1 in *A. flavus* and found no significant differences in toxin production between the ^{xylP}*AflgsA* strain and the WT (Figure 5D,E). This suggests that *AflgsA* is not involved in the regulation of aflatoxin production.

2.6. AflGsA Balances ROS and Resists Oxidative Stress in A. flavus

A high concentration of ROS causes oxidative damage, disrupting cell metabolism and causing apoptosis. It was found that more ROS were produced in the low-expression state of *AflgsA* (Figure 6A). When adding hydrogen peroxide to simulate the oxidative stress state, the inhibition rate of the ^{xylP}*AflgsA* strain was significantly higher than that of the WT (Figure 6B,C), but this situation was significantly restored by the addition of GluN (Figure 6B,C). A similar phenotype was also shown in the addition of tBOOH to simulate the oxidative stress state (Figure S6). Further study revealed that there was no significant change in the transcript level of superoxide dismutase gene *sod*. However, the transcript level of the catalase gene *cat* was significantly lower in the ^{xylP}*AflgsA* strain compared to that in the WT strain (Figure 6D). These results suggest that GluN, the catalytic product of AflGsA, plays an important role in resistance to oxidative stress.

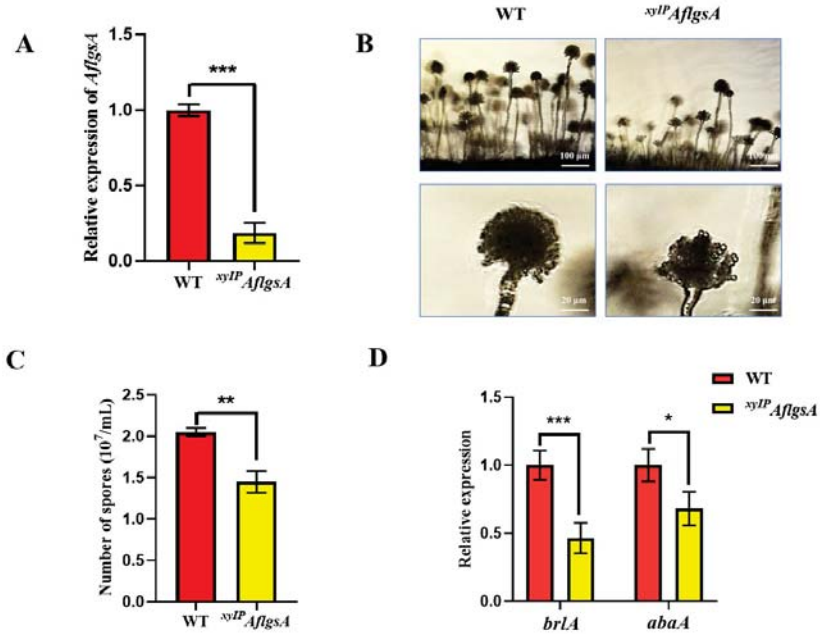

Figure 4. The role of AflGsA in conidia development in *A. flavus*. (**A**) qRT-PCR analysis of *AflgsA* expression in the WT and ^{xylP}*AflgsA* strains in YXT medium. (**B**) Microscopic view of conidiophore formation of the above two *A. flavus* strains in YXT medium. (**C**) The number of conidia produced by the above two *A. flavus* strains in YXT medium. (**D**) Relative expression of the *brlA* and *abaA* genes in the two above strains in YXT medium with three biological replicates. * indicates a significance level of $p < 0.05$, ** indicates a significance level of $p < 0.01$, and *** indicates a significance level of $p < 0.001$ based on *t*-tests with three biological replicates. The growth conditions of the above strains are described in Sections 5.4 and 5.6.

2.7. AflGsA Is Involved in Light Signaling Pathways in A. flavus

The colony diameter of *A. flavus* at 37 °C in the light was significantly smaller than that in the dark (Figure 7A). We also found that the ^{xylP}*AflgsA* strain exhibited significantly higher inhibition rates under light relative to those of the WT strain (Figure 7A,B), but this inhibition of growth was restored with the addition of glutamine (Figure 7A,B). Further studies found that *A. flavus* produced more ROS under light (Figure 7C), indicating that AflGsA could regulate ROS production under light conditions.

2.8. Recombinant AflGsA (rAflGsA) Has Glutamine Synthetase Activity

The recombinant protein rAflGsA (rAflGsA with 6× His tag, 6× His-rAflGsA) was successfully expressed and then purified by Ni-NTA column chromatography (Figure 8A). Recombinant protein activity was measured using the classical Gs enzymatic activity assay (see Section 5), and the results showed that rAflGsA has glutamine synthetase activity (Figure 8B). We further analyzed whether divalent metal ions affected the enzyme activity of rAflGsA. Based on the results of activity assays, the highest activity was observed with Mg^{2+} ions (control), while the activities with Mn^{2+} and Ca^{2+} ions were 81% and 72%, respectively (Figure 8C). Glutamine synthetase activity with the addition of Cu^{2+} ions was only 18% (Figure 8C). From the results above, it appears that the activity of rAflGsA requires the assistance of specific metal ions.

2.9. L-α-Aminoadipic Acid Is a Potential Inhibitor for rAflGsA and A. flavus

L-α-aminoadipic acid is a specific gliotoxin in vitro, and this chemical was reported to inhibit Gs activity in rats [31]. In this study, we found that the inhibitor L-α-aminoadipic acid suppressed the activity of rAflGsA with an IC_{50} value of 288.1 μM in vitro (Figure 8D). The results also showed that L-α-aminoadipic acid prevented the growth and conidial gemination of *A. flavus* with increasing concentrations (Figures 9A,B and S7). The morphology of conidia was influenced by an increasing concentration, and the spore heads became smaller (Figure 9C). The statistics revealed a gradient decrease in the number of spores of *A. flavus* with an increasing concentration of L-α-aminoadipic acid (Figure 9D). When observing the effect of L-α-aminoadipic acid on the production of sclerotia, we found a significant decrease in the number of sclerotia when 1.6 mg/mL of L-α-aminoadipic acid was added (Figure 9E,F). In contrast, the amount of aflatoxin did not change with an increasing concentration of added L-α-aminoadipic acid (Figure 9G,H). In view of the results above, it is clear that L-α-aminoadipic acid is an effective inhibitor of rAflGsA and consequently for *A. flavus*. Therefore, we speculate that AflGsA in *A. flavus* is an ideal candidate target for the L-α-aminoadipic acid inhibitor.

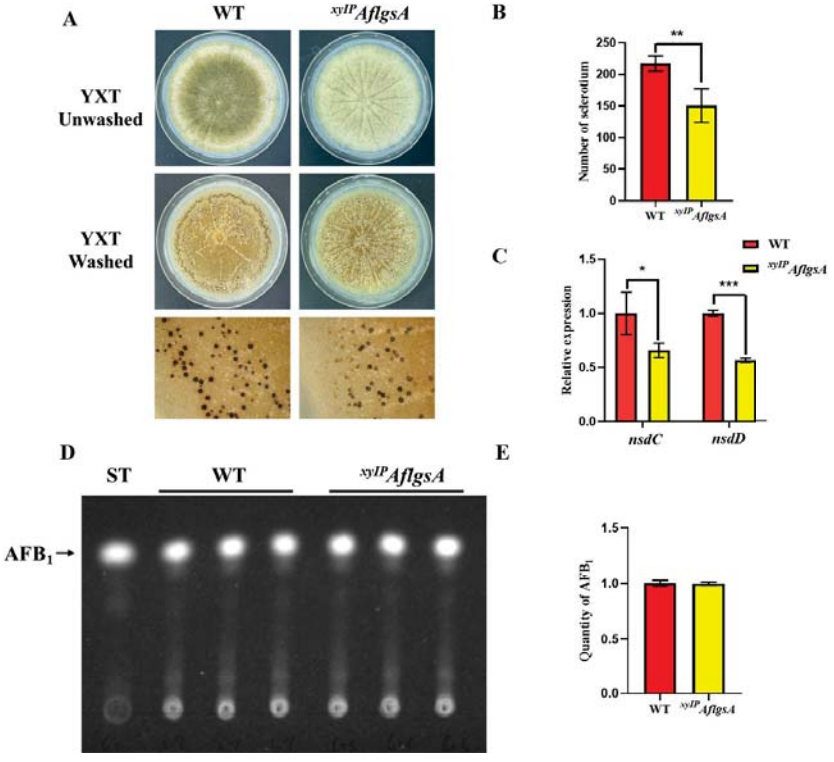

Figure 5. AflGsA regulates sclerotia formation in *A. flavus*. (**A**) Phenotypic observation of sclerotia formation in WT and *xylP AflgsA* strains on YXT medium. (**B**) The number of sclerotia produced by the above two *A. flavus* strains. (**C**) Relative expression of the *nsdC* and *nsdD* genes in the two strains. (**D**) TLC analysis of AFB1 production in *A. flavus* WT and *xylP AflgsA* strains on YXT medium containing 1 g/L $MgSO_4 \cdot 7H_2O$. (**E**) Optical density analysis of AFB1 production (as in panel (**D**)). * indicates a significance level of $p < 0.05$, ** indicates a significance level of $p < 0.01$, and *** indicates a significance level of $p < 0.001$ based on *t*-tests with three biological replicates.

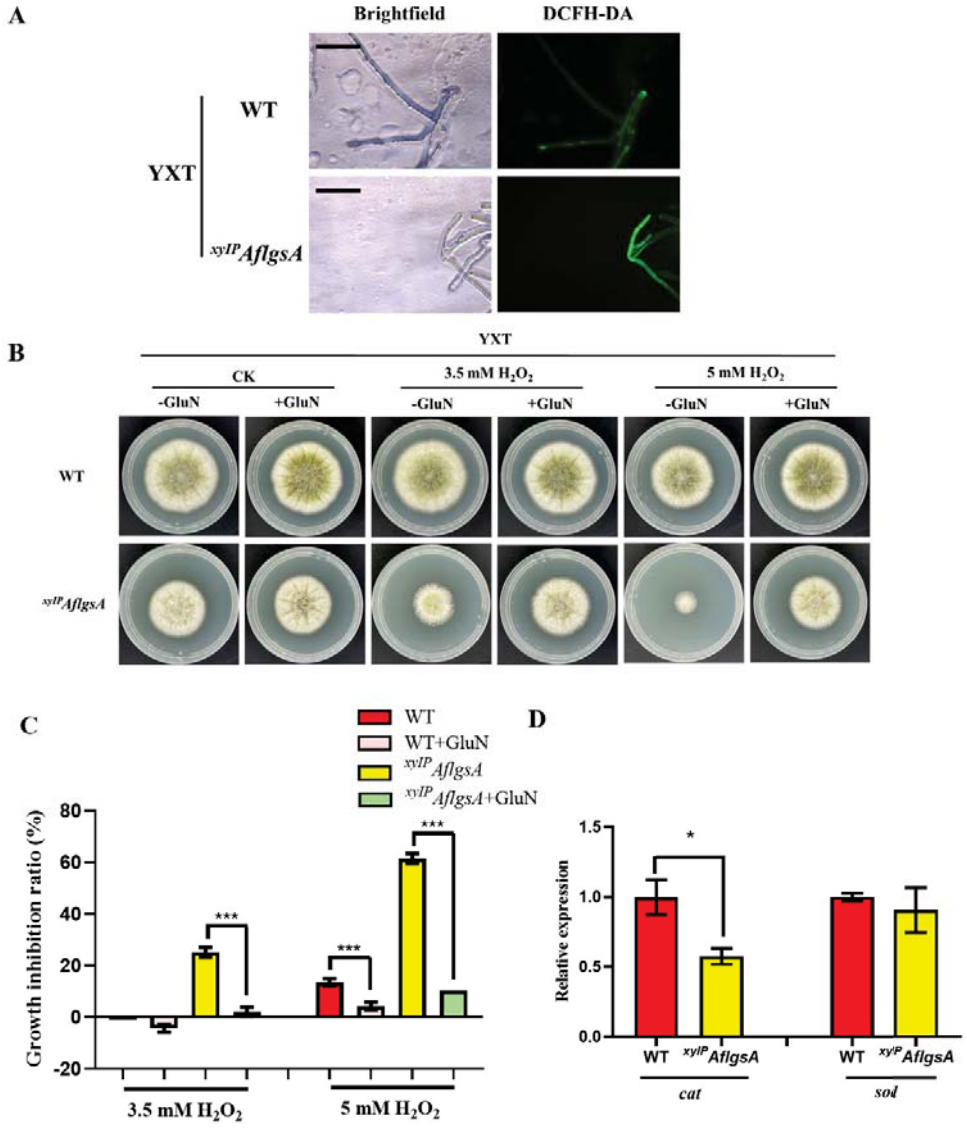

Figure 6. The role of AflGsA in the regulation of ROS and resistance to oxidative stress in *A. flavus*. (**A**) The ROS content of the WT and *xylP AflgsA* strains was detected using fluorescence microscopy. (**B**) Growth phenotype of the WT and *xylP AflgsA* strains cultured in medium (with or without GluN) with oxidative stress. (**C**) The growth inhibition rate of different strains in media under oxidative stress (as in panel (**B**)). *** indicates a significance level of $p < 0.001$ based on one-way ANOVA with three replicates. (**D**) Relative expression of the *cat* and *sod* genes in the WT and *xylP AflgsA* strains. * indicates a significance level of $p < 0.05$ based on *t*-tests with three replicates. The growth conditions of the above strains are described in Sections 5.4–5.6.

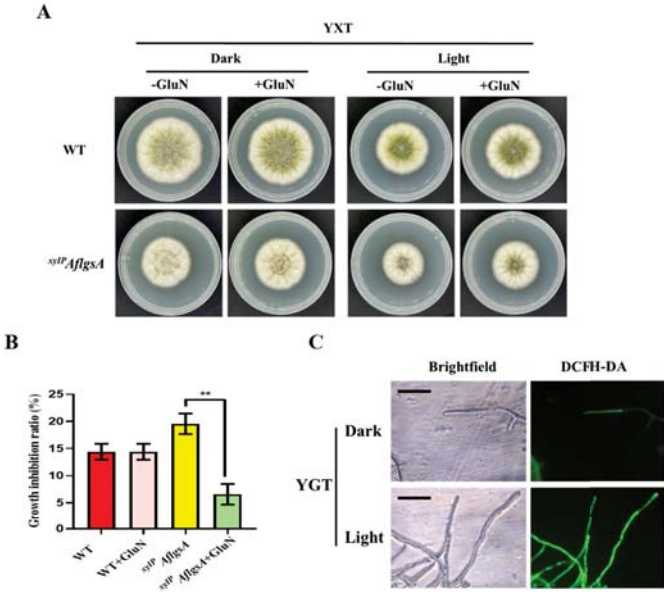

Figure 7. AflGsA is involved in light regulation in *A. flavus*. (**A**) Growth phenotype of the WT and ^{xylP}*AflgsA* strains cultured in YXT (with GluN or without GluN) in dark or light. (**B**) Growth inhibition rate of different strains in media with light (panel (**A**)). (**C**) ROS content of the WT in dark or light. ** indicates a significance level of $p < 0.01$ based on one-way ANOVA with three replicates.

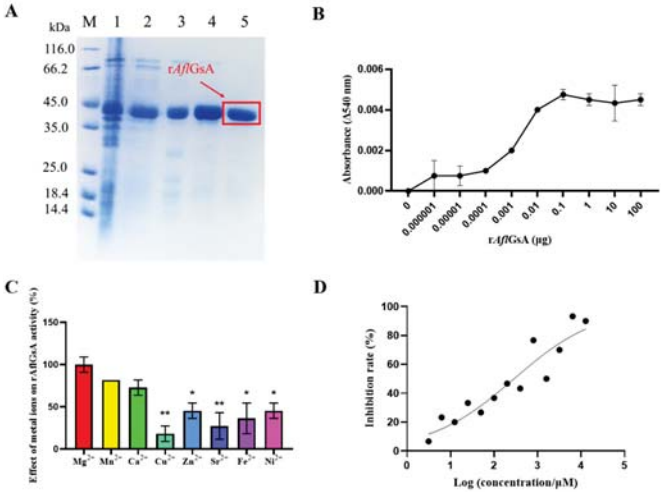

Figure 8. Enzymatic activity assay of recombinant AflGsA. (**A**) rAflGsA with a 6× His label was purified using Ni-NTA column chromatography. Line M: Marker; lane 1: supernatant; lane 2: wash fraction with 50 mM imidazole; lane 3: wash fraction with 100 mM imidazole; lanes 4 and 5: wash fraction with 300 mM imidazole. (**B**) Enzymatic assay of rAflGsA. (**C**) Effect of metal ions on rAflGsA activity. The activity assays were performed after incubation of the purified enzymes with 10 mM concentration of different metal chlorides for 30 min. (**D**) IC_{50} assay of L-α-aminoadipic acid on rAflGsA in vitro. * indicates a significance level of $p < 0.05$, and ** indicates a significance level of $p < 0.01$ based on one-way ANOVA with three biological replicates.

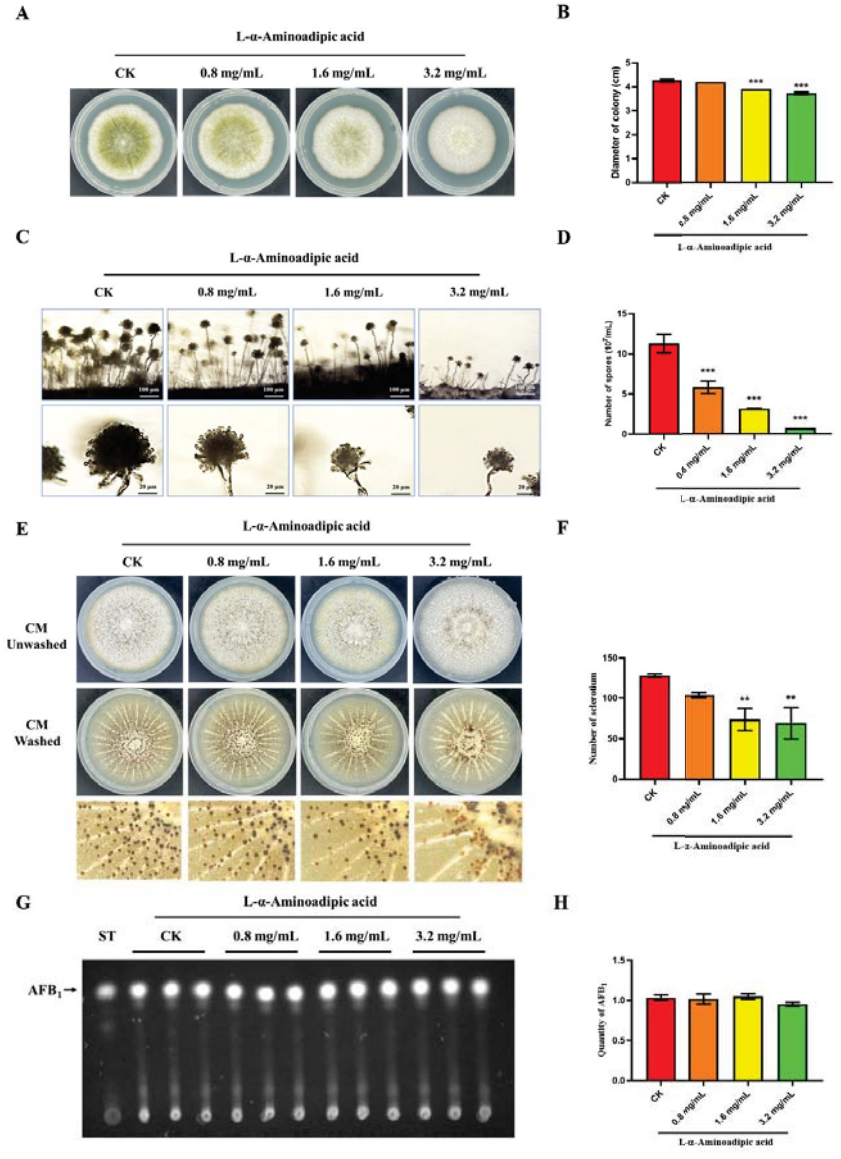

Figure 9. Effect of L-α-aminoadipic acid on growth, conidia production, and sclerotia formation in *A. flavus*. (**A**) The growth of the *A. flavus* WT strain was inhibited by L-α-aminoadipic acid (0–3.2 mg/mL). (**B**) Statistical analysis of the colony diameters of the WT strains treated with the inhibitor (as in panel (**A**)). (**C**) Microscopic view of conidiophore formation of the WT treated with L-α-aminoadipic acid. (**D**) The number of conidia produced by the WT strains treated with L-α-aminoadipic acid. (**E**) Phenotypic observation of sclerotia formation in the WT strains treated with different concentrations of L-α-aminoadipic acid. (**F**) The number of sclerotia produced by the WT strains (as in panel (**E**)). (**G**) TLC analysis of AFB1 production of the WT strains treated with L-α-aminoadipic acid. (**H**) Optical density analysis of AFB1 production (as in panel (**G**)). ** indicates a significance level of $p < 0.01$, and *** indicates a significance level of $p < 0.001$ based on one-way ANOVA with three biological replicates.

3. Discussion

Glutamine synthetase is responsible for catalyzing the conversion of glutamine from ammonium and glutamate as well as being the central enzyme for nitrogen assimilation [32]. Unlike *Rhizobium meliloti* (*R. meliloti*) [33] and *Magnaporthe oryzae* (*M. oryzae*) [24], which have three Gs proteins, we identified only one putative glutamine synthetase (AflGsA) in *A. flavus*. Furthermore, a previous report on *R. meliloti* stated that only simultaneous knockdown of all three Gs genes could cause a complete glutamine nutritional defect [33]. In *A. flavus*, only one protein has glutamine synthetase activity, and there is no alternative pathway for glutamine synthesis. To study the biofunction of glutamine synthetase in *A. flavus*, we constructed the ^{xylP}*AflgsA* mutant strain that has a complete glutamine nutrient-deficient mutation in the YGT medium.

In *A. flavus*, the addition of glutamine to the YGT medium partially restored the growth defect of the ^{xylP}*AflgsA* strain. However, in contrast to the pigmented colonies with conidia produced in *A. nidulans* [21], the addition of glutamine to the *A. flavus* mutant strain resulted in the formation of pigmentation defects similar to *M. oryzae* and *G. fujikuroi* [15,24]. This suggests that the glutamine synthetase regulated the production of *A. flavus* pigments, unlike that in *A. nidulans*. In addition, the phenotype after glutamine addition was inhibited by the addition of NH_4^+, which may be due to the competitive inhibition of GluN by NH_4^+ [21]. The transcript level of *ghd* gene encoding glutamate dehydrogenase was elevated in the ^{xylP}*AflgsA* strain compared to that in WT (Figure S8A). Glutamate dehydrogenase also plays an important role in ammonium assimilation. This may be a balancing mechanism for nitrogen regulation in *A. flavus*.

Like many pathogenic fungi, conidia production and sclerotia formation are important steps in the life cycle of *A. flavus*. It was found that the *AflgsA* of *A. flavus* plays an important role in the production of conidia. Further results also showed that *AflgsA* regulates spore production by regulating the transcript levels of the regulatory genes *brlA* and *abaA* for the production of conidia. Similarly to Δ*Mogln2* in *M. oryzae* [24], the inhibition of *AflgsA* function in *A. flavus* was followed by a reduction in the number of conidial peduncles and a smaller head of child seats compared to those in the WT, which may be a reason for the reduction of *A. flavus* spores. In addition, *AflgsA* in *A. flavus* regulates sclerotia formation by affecting the sclerotia-production-related genes *nsdC* and *nsdD*. All these results suggest that the sophisticated role of *AflgsA* in multiple developmental stages of *A. flavus* is related to its glutaminyl transferase activity. Glutamine synthetase in *G. fujikuroi* affects the synthesis of gibberellin (GA) and bikaverin metabolites [15]. In contrast, our study showed that both the ^{xylP}*AflgsA* mutant and the inhibitor-treated strains produced aflatoxin normally, revealing that *AflgsA* is not involved in aflatoxin synthesis in *A. flavus*.

ROS is an unavoidable and harmful by-product of oxidative metabolism, and ROS dynamic balance is essential for the development of the fungus [34,35]. The inhibition of glutamine synthetase or light irradiance led to more ROS production and had an inhibitory feedback effect on growth in *A. flavus* that was restored by the addition of glutamine. Photorespiration in plants leads to high production of ROS [36], and inhibition of Gs in *A. palmeri* leads to impaired function of photorespiration accompanied by cell apoptosis [17,22]. Therefore, we hypothesized that glutamine synthetase regulated ROS-mediated inhibition of the growth of *A. flavus* under light conditions. Furthermore, glutamine synthetase can regulate the metabolism in relation to oxidative stress in cyanobacteria [37]. In *M. oryzae*, the Δ*Mogln2* strain also results in a high sensitivity to H_2O_2 [24]. In this study, the *AflgsA* mutant strain of *A. flavus* was highly sensitive to oxidative stress, and this sensitivity was restored by supplementing glutamine. Further studies showed that the transcript level of catalase was significantly reduced in the *AflgsA* mutant strain, suggesting that the glutamine synthetase pathway resists oxidative stress by regulating the transcriptional level of catalase.

We obtained the rAflGsA protein from *E. coli* with a purity of up to 95% and confirmed that it had glutamate synthase activity. Reports show that glutamine synthetase has positive cooperativity with different cofactors and metal ions [38,39]. Our further study clarified that the glutamine synthesis activity of rAflGsA is dependent on divalent metal ions and that the highest enzyme activity is achieved by the addition of Mg^{2+} and Mn^{2+} ions. This finding was consistent with the results of cation preference towards recombinant glutamine synthetase from *Psychrotrophic Bacterium* [40] and *Mangrove* [41].

L-α-aminoadipic acid is a specific gliotoxin in vitro [42] and is a neuroexcitatory metabolite that reduces extracellular kynurenic acid levels in a dose-dependent manner [43]. However, it is not mentioned in other studies whether L-α-aminoadipic acid has antifungal activity. Our study showed that L-α-aminoadipic acid is an inhibitor for rAflGsA in vitro, and that it also prevents the growth, spore production, and sclerotia formation of *A. flavus* in vivo. In agreement with the phenotype of the ^{xylP}*AflgsA* strain, the addition of L-α-aminoadipic acid had no effect on aflatoxin synthesis. In addition, lower concentrations of L-α-aminoadipic acid (0.8 mg/mL and 1.6 mg/mL) did not affect the transcript level of *AflgsA*, but a higher dosage (3.2 mg/mL) seemed to decrease its transcriptional (Figure S8B). This suggests that L-α-aminoadipic acid may also have other unknown targets in *A. flavus*. Overall, these results suggest that L-α-aminoadipic acid is a potential inhibitor of *A. flavus*, and thus AflGsA may be an ideal target for L-α-aminoadipic acid in *A. flavus*. The study of the inhibition mechanism of L-α-aminoadipic acid against *A. flavus* is important for the prevention of *A. flavus*. This may be a very meaningful research direction in the future.

4. Conclusions

At present, many studies have attempted to elucidate the function of glutamine synthetase in organisms. However, the understanding of the biofunctional diversity of glutamine synthetase in filamentous fungi, especially in *A. flavus*, seems to have been relatively neglected. In this study, we found that AflGsA performed its activity as a glutamine synthetase and that it played a divergent role in the conidia production and sclerotia formation in *A. flavus*. It has an important role in the homeostasis of ROS and resistance to oxidative stress in *A. flavus*. In addition, L-α-aminoadipic acid inhibited both rAflGsA and *A. flavus* and thus was considered as a potential antifungal candidate for further study.

5. Materials and Methods

5.1. Strains and Culture Conditions

E. coli DH5a and BL21 (DE3) were used for plasmid DNA preparation and expression of the recombinant AflGsA (rAflGsA) protein, respectively. *A. flavus* WT and ^{xylP}*AflgsA* strains were cultured in YGT (5 g/L yeast extract, 20 g/L glucose, and 1 mL/L trace elements) and YXT (5 g/L yeast extract, 20 g/L xylose, and 1 mL/L trace elements) media at 37 °C in the dark. Then, 1.5% agar was added to obtain solid media. To study aflatoxin production, YXT medium containing 1 g/L $MgSO_4 \cdot 7H_2O$ was used at 29 °C.

5.2. Sequence Analysis

The NCBI database was used to search for the *AflgsA* sequence of *A. flavus* (AFLA_051930). The homologous protein sequence of AflGsA from *A. flavus* was retrieved by BLAST. The retrieved homologous protein sequences were analyzed by domain analysis using Uniprot Tools and mapped using DOG 2.0 software. The MAGE 7.0 software was used for multiple sequence alignment of the protein sequences, and the maximum likelihood method was used to construct the phylogenetic tree.

5.3. Construction and Identification of Mutant Strain

All of the primers used in this study were shown in Table S1. To obtain the ^{xylP}*AflgsA* mutant strain, we followed the method previously described in the literature [44]. An *AflgsA* xylose promoter mutant cassette was fused by overlapping extension PCR (*gsA*-

xolap-F and *gsA-xolap-R* primers were used) to an upstream fragment of *AflgsA*, a marker gene (*A. fumigatus pyrG*), the *xyIP* xylose conditional promoter [45], and the *AflgsA* CDS fragment. *A. flavus* CA14 was used as a starting strain during the preparation of protoplasts [46]. The *AflgsA* gene's promoter was converted to a xylose promoter by homologous recombination [44]. The *gsA-A-F* and *gsA-CDS-R* primers were used in the identification of ^{xylP}*AflgsA* transformants by PCR. The *AflgsA-F* and *AflgsA-R* primers were used to identify the sequence by qRT-PCR.

5.4. Analysis of the Growth, Conidial Production, and Sclerotia Formation of A. flavus

For colony diameter evaluation, YGT and YXT containing 10 mM glutamine (GluN) or ammonium tartrate (NH_4^+) were points inoculated with 10^6 conidia and incubated in the dark at 37 °C for four days. Spores were eluted with 2 mL of spore eluate and counted under a microscope using a hemocytometer plate to determine the number of spores after incubation in the dark at 37 °C for four days [44]. To observe conidiophore formation, 10^6 conidia were incubated in YXT medium at 37 °C in the dark for two days, and the surface mycelium was scraped off. The colonies were cut out and placed on cover breaks and incubated for 12 h at 37 °C, then observed using a microscope. For sclerotia production analysis, 10^6 conidia were incubated in YXT medium at 37 °C in the dark for seven days, and the morphology of sclerotia was recorded by rinsing off the mycelium with 75% ethanol [47]. For aflatoxin extraction, 10^6 conidia were incubated in YXT containing 1 g/L $MgSO_4 \cdot 7H_2O$ at 29 °C in the dark for five days. The toxin in the medium was extracted using chloroform and detected using TLC [44].

5.5. Detection of ROS in A. flavus

To detect the ROS in *A. flavus*, WT and ^{xylP}*AflgsA* strains were incubated in YXT liquid medium at 37 °C for 24 h. Mycelia were washed three times with a phosphate-buffered saline (PBS) buffer. The collected mycelia were incubated with a 10 µM DCFH-DA fluorescent probe (Beyotime, Nantong, China) for 30 min at 37 °C. After washing three times with PBS, the mycelium was placed on a slide, and ROS content was identified by microscopy. Fluorescence emission of DCFH-DA was excited at 488 nm.

5.6. Quantitative Real-Time PCR

The mycelia of the strains of *A. flavus* were collected after 48 h of incubation. The collected mycelia were ground in liquid nitrogen, and total RNA was extracted with the TRIzol (Biomarker Technologies, Beijing, China) reagent. RNA was translated into cDNA using a reverse transcription kit (Thermo Scientific, Waltham, MA, USA). The cDNA was then used as a template for quantitative PCR with specific primers [48].

5.7. Purification of Recombinant rAflGsA Protein and Determination of Enzyme Activity

The cDNA of *AflgsA* from *A. flavus* was expanded and cloned into the pET-28a expression vector. The expressed recombinant AflGsA (rAflGsA) protein was purified using Ni-NTA column chromatography [44]. The activity of rAflGsA was then measured at 540 nm using the classical glutamine synthetase enzyme activity assay [40]. Different divalent metal ions were added to assay the enzyme activity with a final concentration of 20 mM. Enzyme activity was measured after reacting at 37 °C for one hour.

5.8. Statistical Analysis

GraphPad Prism 5.0 (GraphPad Software, San Diego, CA, USA) was used for data statistics and analysis. All of the analyses had at least three biological replicates if not specifically indicated.

Supplementary Materials: The following supporting information can be downloaded at: https://www.mdpi.com/article/10.3390/toxins14120822/s1, Table S1: Oligonucleotide primers used in this study; Figure S1: Genome sequencing validation of the ^{xylP}*AflgsA* strain of *A. flavus*. *AflgsA* AP is the upstream noncoding region of the *AflgsA* gene. The mutations in the *AflgsA* CDS are synonymous mutations; Figure S2: Analysis of the growth, mycelial morphology, conidial germination, and conidiophore formation of WT and ^{xylP}*AflgsA* strains. (A) The mycelial morphology of WT and ^{xylP}*AflgsA* strains on the medium containing 10 g/L and 20 g/L xylose. (B) The colony morphology of WT and ^{xylP}*AflgsA* strains. (C) Statistical analysis of the diameter from panel (B). (D) Conidial germination of WT and ^{xylP}*AflgsA* strains. (E) Statistical analysis of the conidial germination rate from panel (D). (F) Microscopic view of the conidiophore formation of the above two *A. flavus* strains. (G) The number of conidia produced by the above two *A. flavus* strains. ND indicates no detection. ** indicates a significance level of $p < 0.01$, and *** indicates a significance level of $p < 0.001$ based on *t*-tests with three replicates. The medium containing 10 g/L xylose: 5 g/L yeast extract, 10 g/L glucose, 10 g/L xylose, 1 mL/L trace elements, and 1.5% agar. The medium containing 20 g/L xylose (YXT medium): 5 g/L yeast extract, 20 g/L xylose, 1 mL/L trace elements, and 1.5% agar; Figure S3: Analysis of the growth of WT and ^{xylP}*AflgsA* strains. (A) The colony morphology of the WT and ^{xylP}*AflgsA* strains on YXT medium containing 10 mM glutamine (GluN) or/and ammonium tartrate (NH_4^+) as nitrogen sources. (B) Statistical analysis of the diameter from panel (A). *** indicates a significance level of $p < 0.001$ based on *t*-tests with three replicates; Figure S4: Analysis of the growth of WT and ^{xylP}*AflgsA* strains. (A) The colony morphology of the WT and ^{xylP}*AflgsA* strains on YGT medium containing 10 mM glutamate (Glu) or on YXT medium. (B) Statistical analysis of the diameter from panel (A). ND indicates no detection. *** indicates a significance level of $p < 0.001$ based on *t*-tests with three replicates; Figure S5: AflGsA regulates sclerotia formation in *A. flavus*. (A) Phenotypic observation of sclerotia formation in WT and ^{xylP}*AflgsA* strains on YXT medium containing 10 mM glutamine (GluN). (B) The number of sclerotia produced by the above two *A. flavus* strains. ND indicates no detection. * indicates a significance level of $p < 0.05$ based on *t*-tests with three replicates; Figure S6: The role of AflGsA in resistance to oxidative stress in *A. flavus*. (A) Growth phenotype of the WT and ^{xylP}*AflgsA* strains cultured in medium (with or without GluN) with 0.8 mM tBOOH oxidative stress. (B) The growth inhibition rate of different strains in media under oxidative stress (as in panel (A)). *** indicates a significance level of $p < 0.001$ based on one-way ANOVA with three replicates; Figure S7: Effect of L-α-aminoadipic acid on mycelial morphology and conidial germination in *A. flavus*. (A) The mycelial morphology of the *A. flavus* WT strain was inhibited by L-α-aminoadipic acid (0–3.2 mg/mL). (B) The conidial germination of the *A. flavus* WT strain was inhibited by L-α-aminoadipic acid (0–3.2 mg/mL). (C) Statistical analysis of the conidial germination rate from panel B. ND indicates no detection. * indicates a significance level of $p < 0.05$, ** indicates a significance level of $p < 0.01$, and *** indicates a significance level of $p < 0.001$ based on one-way ANOVA with three replicates; Figure S8: Relative expression of the genes in different strains. (A) Relative expression of the *ghd* gene in the WT and ^{xylP}*AflgsA* strains. (B) Relative expression of the *AflgsA* gene of the WT strains treated with the inhibitor. * indicates a significance level of $p < 0.05$ based on *t*-tests or one-way ANOVA with three replicates.

Author Contributions: Conceptualization, S.W. and Y.W.; formal analysis, R.L.; funding acquisition, S.W. (Shihua Wang) and Y.W.; methodology, S.W. (Sen Wang); project administration, S.W. (Shihua Wang); supervision, S.W. (Shihua Wang) and Y.W.; validation, S.W. (Sen Wang), R.L., W.Z. and Q.B.; visualization, Y.W.; writing—original draft, S.W. (Sen Wang); writing—review and editing, E.T., S.W. (Shihua Wang) and Y.W. All authors have read and agreed to the published version of the manuscript.

Funding: This research was funded by the Scientific Research Foundation of the Graduate School of Fujian Agriculture and Forestry University (324-1122yb054) and the Science and Technology Innovation Fund of Fujian Agriculture and Forestry University (CXZX2020051A).

Institutional Review Board Statement: Not applicable.

Informed Consent Statement: Not applicable.

Data Availability Statement: Not applicable.

Conflicts of Interest: The authors declare no conflict of interest.

References

1. Bennett, J.W.; Klich, M.A. *Aspergillus*: Biology and industrial applications. *Biotechnology* **1992**, *23*, 1.
2. Samson, R.A. Current taxonomic schemes of the genus *Aspergillus* and its teleomorphs. *Biotechnology* **1992**, *23*, 355–390.
3. Amaike, S.; Keller, N.P. *Aspergillus flavus*. *Annu. Rev. Phytopathol.* **2011**, *49*, 107–133. [CrossRef] [PubMed]
4. Krishnan, S.; Manavathu, E.K.; Chandrasekar, P.H. *Aspergillus flavus*: An emerging non-fumigatus *Aspergillus* species of significance. *Mycoses* **2009**, *52*, 206–222. [CrossRef] [PubMed]
5. Kousha, M.; Tadi, R.; Soubani, A.O. Pulmonary aspergillosis: A clinical review. *Eur. Respir. Rev. Off. J. Eur. Respir. Soc.* **2011**, *20*, 156–174. [CrossRef]
6. Mehl, H.L.; Jaime, R.; Callicott, K.A.; Probst, C.; Garber, N.P.; Ortega-Beltran, A.; Grubisha, L.C.; Cotty, P.J. *Aspergillus flavus* diversity on crops and in the environment can be exploited to reduce aflatoxin exposure and improve health. *Ann. N. Y. Acad. Sci.* **2012**, *1273*, 7–17. [CrossRef]
7. Lim, C.W.; Yoshinari, T.; Layne, J.; Chan, S.H. Multi-mycotoxin screening reveals separate occurrence of aflatoxins and ochratoxin a in Asian rice. *J. Agric. Food Chem.* **2015**, *63*, 3104–3113. [CrossRef]
8. Leung, M.C.; Díaz-Llano, G.; Smith, T.K. Mycotoxins in pet food: A review on worldwide prevalence and preventative strategies. *J. Agric. Food Chem.* **2006**, *54*, 9623–9635. [CrossRef]
9. Choi, K.C.; Chung, W.T.; Kwon, J.K.; Yu, J.Y.; Jang, Y.S.; Park, S.M.; Lee, S.Y.; Lee, J.C. Inhibitory effects of quercetin on aflatoxin B1-induced hepatic damage in mice. *Food Chem. Toxicol. Int. J. Publ. Br. Ind. Biol. Res. Assoc.* **2010**, *48*, 2747–2753. [CrossRef]
10. Lam, H.M.; Coschigano, K.T.; Oliveira, I.C.; Melo-Oliveira, R.; Coruzzi, G.M. The molecular-genetics of nitrogen assimilation into amino acids in higher plants. *Annu. Rev. Plant Physiol. Plant Mol. Biol.* **1996**, *47*, 569–593. [CrossRef]
11. Eisenberg, D.; Gill, H.S.; Pfluegl, G.M.; Rotstein, S.H. Structure-function relationships of glutamine synthetases. *Biochim. Biophys. Acta* **2000**, *1477*, 122–145. [CrossRef]
12. Christa, L.; Simon, M.T.; Flinois, J.P.; Gebhardt, R.; Brechot, C.; Lasserre, C. Overexpression of glutamine synthetase in human primary liver cancer. *Gastroenterology* **1994**, *106*, 1312–1320. [CrossRef]
13. Caizzi, R.; Bozzetti, M.P.; Caggese, C.; Ritossa, F. Homologous nuclear genes encode cytoplasmic and mitochondrial glutamine synthetase in Drosophila melanogaster. *J. Mol. Biol.* **1990**, *212*, 17–26. [CrossRef]
14. Avisar, N.; Shiftan, L.; Ben-Dror, I.; Havazelet, N.; Vardimon, L. A silencer element in the regulatory region of glutamine synthetase controls cell type-specific repression of gene induction by glucocorticoids. *J. Biol. Chem.* **1999**, *274*, 11399–11407. [CrossRef]
15. Teichert, S.; Schönig, B.; Richter, S.; Tudzynski, B. Deletion of the Gibberella fujikuroi glutamine synthetase gene has significant impact on transcriptional control of primary and secondary metabolism. *Mol. Microbiol.* **2004**, *53*, 1661–1675. [CrossRef]
16. Kichey, T.; Le Gouis, J.; Sangwan, B.; Hirel, B.; Dubois, F. Changes in the cellular and subcellular localization of glutamine synthetase and glutamate dehydrogenase during flag leaf senescence in wheat (*Triticum aestivum* L.). *Plant Cell Physiol.* **2005**, *46*, 964–974. [CrossRef]
17. Takano, H.K.; Beffa, R.; Preston, C.; Westra, P.; Dayan, F.E. A novel insight into the mode of action of glufosinate: How reactive oxygen species are formed. *Photosynth. Res.* **2020**, *144*, 361–372. [CrossRef]
18. Fu, S.; Li, Z.; Xiao, L.; Hu, W.; Zhang, L.; Xie, B.; Zhou, Q.; He, J.; Qiu, Y.; Wen, M.; et al. Glutamine Synthetase Promotes Radiation Resistance via Facilitating Nucleotide Metabolism and Subsequent DNA Damage Repair. *Cell Rep.* **2019**, *28*, 1136–1143.e1134. [CrossRef]
19. Kim, C.; Kültz, D. An osmolality/salinity-responsive enhancer 1 (OSRE1) in intron 1 promotes salinity induction of tilapia glutamine synthetase. *Sci. Rep.* **2020**, *10*, 12103. [CrossRef]
20. Sasaki, Y.; Kojima, A.; Shibata, Y.; Mitsuzawa, H. Filamentous invasive growth of mutants of the genes encoding ammonia-metabolizing enzymes in the fission yeast *Schizosaccharomyces pombe*. *PLoS ONE* **2017**, *12*, e0186028. [CrossRef]
21. Margelis, S.; D'Souza, C.; Small, A.J.; Hynes, M.J.; Adams, T.H.; Davis, M.A. Role of glutamine synthetase in nitrogen metabolite repression in *Aspergillus nidulans*. *J. Bacteriol.* **2001**, *183*, 5826–5833. [CrossRef] [PubMed]
22. Takano, H.K.; Dayan, F.E. Biochemical Basis for the Time-of-Day Effect on Glufosinate Efficacy against *Amaranthus palmeri*. *Plants* **2021**, *10*, 2021. [CrossRef] [PubMed]
23. Rodríguez-Herrero, V.; Payá, G.; Bautista, V.; Vegara, A.; Cortés-Molina, M.; Camacho, M.; Esclapez, J.; Bonete, M.J. Essentiality of the *glnA* gene in *Haloferax mediterranei*: Gene conversion and transcriptional analysis. *Extrem. Life Extrem. Cond.* **2020**, *24*, 433–446. [CrossRef]
24. Aron, O.; Wang, M.; Lin, L.; Batool, W.; Lin, B.; Shabbir, A.; Wang, Z.; Tang, W. MoGLN2 Is Important for Vegetative Growth, Conidiogenesis, Maintenance of Cell Wall Integrity and Pathogenesis of *Magnaporthe oryzae*. *J. Fungi* **2021**, *7*, 463. [CrossRef] [PubMed]
25. Almassy, R.J.; Janson, C.A.; Hamlin, R.; Xuong, N.H.; Eisenberg, D. Novel subunit—Subunit interactions in the structure of glutamine synthetase. *Nature* **1986**, *323*, 304–309. [CrossRef]
26. Valentine, R.C.; Shapiro, B.M.; Stadtman, E.R. Regulation of glutamine synthetase. XII. Electron microscopy of the enzyme from *Escherichia coli*. *Biochemistry* **1968**, *7*, 2143–2152. [CrossRef]
27. van Rooyen, J.M.; Abratt, V.R.; Belrhali, H.; Sewell, T. Crystal structure of Type III glutamine synthetase: Surprising reversal of the inter-ring interface. *Structure* **2011**, *19*, 471–483. [CrossRef]

28. Chen, Y.; Xu, W.; Yu, S.; Ni, K.; She, G.; Ye, X.; Xing, Q.; Zhao, J.; Huang, C. Assembly status transition offers an avenue for activity modulation of a supramolecular enzyme. *eLife* **2021**, *10*, e72535. [CrossRef]
29. Woolfolk, C.A.; Stadtman, E.R. Regulation of glutamine synthetase: III. Cumulative feedback inhibition of glutamine synthetase from *Escherichia coli*. *Arch. Biochem. Biophys.* **1967**, *118*, 736–755. [CrossRef]
30. Lan, H.; Wu, L.; Sun, R.; Keller, N.P.; Yang, K.; Ye, L.; He, S.; Zhang, F.; Wang, S. The HosA histone deacetylase regulates aflatoxin biosynthesis through direct regulation of aflatoxin cluster genes. *Mol. Plant-Microbe Interact.* **2019**, *32*, 1210–1228. [CrossRef]
31. McBean, G.J. Inhibition of the glutamate transporter and glial enzymes in rat striatum by the gliotoxin, alpha aminoadipate. *Br. J. Pharmacol.* **1994**, *113*, 536–540. [CrossRef]
32. Bao, A.; Zhao, Z.; Ding, G.; Shi, L.; Xu, F.; Cai, H. The Stable Level of Glutamine synthetase 2 plays an important role in Rice growth and in Carbon-Nitrogen metabolic balance. *Int. J. Mol. Sci.* **2015**, *16*, 12713–12736. [CrossRef]
33. Shatters, R.G.; Liu, Y.; Kahn, M.L. Isolation and characterization of a novel glutamine synthetase from *Rhizobium meliloti*. *J. Biol. Chem.* **1993**, *268*, 469–475. [CrossRef]
34. Aguirre, J.; Ríos-Momberg, M.; Hewitt, D.; Hansberg, W. Reactive oxygen species and development in microbial eukaryotes. *Trends Microbiol.* **2005**, *13*, 111–118. [CrossRef]
35. Gessler, N.N.; Aver'yanov, A.A.; Belozerskaya, T.A. Reactive oxygen species in regulation of fungal development. *Biochem. Biokhimiia* **2007**, *72*, 1091–1109. [CrossRef]
36. Apel, K.; Hirt, H. Reactive oxygen species: Metabolism, oxidative stress, and signal transduction. *Annu. Rev. Plant Biol.* **2004**, *55*, 373–399. [CrossRef]
37. Robles-Rengel, R.; Florencio, F.J.; Muro-Pastor, M.I. Redox interference in nitrogen status via oxidative stress is mediated by 2-oxoglutarate in cyanobacteria. *New Phytol.* **2019**, *224*, 216–228. [CrossRef]
38. Montanini, B.; Betti, M.; Márquez, A.J.; Balestrini, R.; Bonfante, P.; Ottonello, S. Distinctive properties and expression profiles of glutamine synthetase from a plant symbiotic fungus. *Biochem. J.* **2003**, *373*, 357–368. [CrossRef]
39. Sakakibara, H.; Shimizu, H.; Hase, T.; Yamazaki, Y.; Takao, T.; Shimonishi, Y.; Sugiyama, T. Molecular identification and characterization of cytosolic isoforms of glutamine synthetase in maize roots. *J. Biol. Chem.* **1996**, *271*, 29561–29568. [CrossRef]
40. Gong, C.; You, X.; Zhang, S.; Xue, D. Functional analysis of a glutamine biosynthesis protein from a psychrotrophic Bacterium, *Cryobacterium soli GCJ02*. *Indian J. Microbiol.* **2020**, *60*, 153–159. [CrossRef]
41. Zhao, W.; Yang, J.; Tian, Y.; Fu, X.; Zhu, B.; Xue, Y.; Gao, J.; Han, H.J.; Peng, R.; Yao, Q.H. Expression, purification, and characterization of recombinant mangrove glutamine synthetase. *Mol. Biol. Rep.* **2014**, *41*, 7575–7583. [CrossRef] [PubMed]
42. Huck, S.; Grass, F.; Hörtnagl, H. The glutamate analogue alpha-aminoadipic acid is taken up by astrocytes before exerting its gliotoxic effect *in vitro*. *J. Neurosci. Off. J. Soc. Neurosci.* **1984**, *4*, 2650–2657. [CrossRef] [PubMed]
43. Wu, H.Q.; Ungerstedt, U.; Schwarcz, R. L-alpha-aminoadipic acid as a regulator of kynurenic acid production in the hippocampus: A microdialysis study in freely moving rats. *Eur. J. Pharmacol.* **1995**, *281*, 55–61. [CrossRef] [PubMed]
44. Wang, Y.; Wang, S.; Nie, X.; Yang, K.; Xu, P.; Wang, X.; Liu, M.; Yang, Y.; Chen, Z.; Wang, S. Molecular and structural basis of nucleoside diphosphate kinase-mediated regulation of spore and sclerotia development in the fungus *Aspergillus flavus*. *J. Biol. Chem.* **2019**, *294*, 12415–12431. [CrossRef]
45. Zadra, I.; Abt, B.; Parson, W.; Haas, H. *xylP* promoter-based expression system and its use for antisense downregulation of the Penicillium chrysogenum nitrogen regulator NRE. *Appl. Environ. Microbiol.* **2000**, *66*, 4810–4816. [CrossRef]
46. Chang, P.K.; Scharfenstein, L.L.; Wei, Q.; Bhatnagar, D. Development and refinement of a high-efficiency gene-targeting system for *Aspergillus flavus*. *J. Microbiol. Methods* **2010**, *81*, 240–246. [CrossRef]
47. Zhang, F.; Geng, L.; Deng, J.; Huang, L.; Zhong, H.; Xin, S.; Fasoyin, O.E.; Wang, S. The MAP kinase AflSlt2 modulates aflatoxin biosynthesis and peanut infection in the fungus *Aspergillus flavus*. *Int. J. Food Microbiol.* **2020**, *322*, 108576. [CrossRef]
48. Yang, K.; Liu, Y.; Wang, S.; Wu, L.; Xie, R.; Lan, H.; Fasoyin, O.E.; Wang, Y.; Wang, S. Cyclase-associated protein Cap with multiple domains contributes to mycotoxin biosynthesis and fungal virulence in *Aspergillus flavus*. *J. Agric. Food Chem.* **2019**, *67*, 4200–4213. [CrossRef]

toxins

MDPI

Article

The Potential of *Alternaria* Toxins Production by *A. alternata* in Processing Tomatoes

Qiaomei Qin [1,2,†], Yingying Fan [2,†], Qinlan Jia [1,2], Shuaishuai Duan [1,2], Fengjuan Liu [2], Binxin Jia [2], Guangquan Wang [3], Wanhui Guo [2] and Cheng Wang [1,2,*]

[1] College of Life Science and Technology, Xinjiang University, Urumqi 830049, China
[2] Key Laboratory of Agro-products Quality and Safety of Xinjiang, Laboratory of Quality and Safety Risk Assessment for Agri-products (Urumqi), Institute of Quality Standards & Testing Technology for Agri-products, Xinjiang Academy of Agricultural Sciences, Urumqi 830091, China
[3] College of Biology and Geography Sciences, Yili Normal University, Yining 835000, China
* Correspondence: wangcheng312@xaas.ac.cn
† These authors contributed equally to this work.

Abstract: As a filamentous and spoilage fungus, *Alternaria* spp. can not only infect processing tomatoes, but also produce a variety of mycotoxins which harm the health of human beings. To explore the production of *Alternaria* toxins in processing tomatoes during growth and storage, four main *Alternaria* toxins and four conjugated toxins were detected by ultrahigh-performance liquid chromatography-tandem mass spectrometry (UPLC-MS/MS) and ultra-performance liquid chromatography-ion mobility quadrupole time-of-flight mass spectrometry (UPLC-IMS QToF MS) in processing tomatoes on different days after being inoculated with *A. alternata*. The results show that the content of *Alternaria* toxins in an in vivo assay is higher than that under field conditions. Tenuazonic acid (TeA) is the predominant toxin detected in the field (205.86~41,389.19 μg/kg) and in vivo (7.64~526,986.37 μg/kg) experiments, and the second-most abundant toxin is alternariol (AOH). In addition, a small quantity of conjugated toxins, AOH-9-glucoside (AOH-9-Glc) and alternariol monomethyl ether-3-glucoside (AME-3-Glc), were screened in the in vivo experiment. This is the first time the potential of *Alternaria* toxins produced in tomatoes during the harvest period has been studied in order to provide data for the prevention and control of *Alternaria* toxins.

Keywords: *Alternaria* toxins; conjugated mycotoxins; field experiment; in vivo experiment; processing tomatoes

Key Contribution: This paper first reports the potential of *Alternaria* toxins produced by *A. alternata* in processing tomatoes during the harvest period, and the results show that the diversity and quantity of *Alternaria* toxins in the in vivo experiment are greater than those presented in the field assay.

Citation: Qin, Q.; Fan, Y.; Jia, Q.; Duan, S.; Liu, F.; Jia, B.; Wang, G.; Guo, W.; Wang, C. The Potential of *Alternaria* Toxins Production by *A. alternata* in Processing Tomatoes. *Toxins* **2022**, *14*, 827. https://doi.org/10.3390/toxins14120827

Received: 16 September 2022
Accepted: 22 November 2022
Published: 24 November 2022

1. Introduction

Processing tomato is a cultivated type of common tomatoes that received its name from its thick skins, which is resistant to transport damage and suitable for processing. Xinjiang, the valley region of California, and the Mediterranean region of Europe are known as the three major centers of tomato cultivation and processing in the world. However, during the growth and storage processes, processing tomatoes are susceptible to attack by various pathogenic and spoilage micro-organisms, which reduce their yield and quality during the growth period [1,2]. Among these fungi, *Alternaria* spp. can infect processing tomatoes and contribute to devastating fungal diseases, such as tomato early blight and black spot disease [3]. The latter disease mainly occurs after the coloring period. *A. alternata* enter the host tissue (tomato fruit) through wounds or natural openings during the harvest or pre-harvest periods [4], lurk for several days, and then appear as black spots causing *Alternaria* rot [5]. These spots appear as sunken lesions, and are mostly observed near the

blossom-end or peduncle of the fruit, leading to fruit spoilage that limits the product's marketability, in addition to causing considerable post-harvest losses [6].

Alternaria spp. is not only a filamentous and spoilage fungus that survives in a wide range of temperatures and attacks a wide range of economically important plants (for example, apple [7,8], tomato [8,9], pear [7,10], wheat [11], etc.), but also produces a variety of secondary metabolites with toxic properties, named as *Alternaria* toxins [12], including alternariol (AOH), alternariol monomethyl ether (AME), tenuzonic acid (TeA), tentoxin (TEN), etc [13]. In addition, these toxins can primarily be bound to sulfates or glucosides, forming the conjugated mycotoxins present in the plant host [14]. Additionally, these conjugated mycotoxins release the free toxin after being hydrolyzed during metabolism, potentially endangering the health of human beings [15]. The research conducted on *Alternaria* toxins dates back to the 1960s–1970s, when some metabolites produced by *Alternaria* spp. Were first reported to exert toxic effects [16]. A limited in vivo study showed that TeA exerted mild toxic effects on mammalian cells [17,18]. Both AOH and AME have repeatedly been reported to possess cytotoxic and, of particular concern, genotoxic properties in micromolar concentrations [19,20]. In 2011, according to the EFSA, the tolerable upper intake level, using threshold of toxicological concern (TTC) was 2.5 ng/kg body weight (b.w.) for AOH and AME and 1500 ng/kg b.w. for TeA and TEN [13]. In 2022, the European Union (EU) issued proposal 202/553 to amend regulation (EC) No 401/2006 for the monitoring of *Alternaria* toxins in food, and set limits for the toxins present in processed tomato products, in which AOH, AME, and TeA do not exceed 10, 5, and 500 μg/kg, respectively [21].

A survey conducted in Brazil revealed that neither AME nor AOH was detected in 80 samples, but TeA was observed in 7 tomato pulp (39~111 μg/kg) and 4 tomato puree (29~76 ng/kg) samples [22]. In contrast, AOH was found at levels of 13 μg/kg with high frequency in tomato (93% of 44 samples) products, reported by Ackerman et al. [23]. Approximately 60% of Argentinian tomato pulp samples were contaminated with TeA, AME, and AOH at levels up to 4021 μg/kg (29% of 80 samples), 1734 μg/kg (26% of 80 samples), and 8756 μg/kg (6% of 80 samples), respectively [24]. A survey conducted on the Swiss market in 2010 showed that TeA was found most frequently in tomato products (81 out of 85 samples) and in the highest levels of up to 790 μg/kg, while AOH and AME were found in lower concentrations, ranging from <1 to 33 μg/kg for AOH and <5 to 9 μg/kg for AME [25]. In an expanded follow-up survey, conjugated mycotoxins AOH-3-sulfate (AOH-3-S) and AME-3-sulfate (AME-3-S) were detected in 9% and 34% of tomato sauces collected in retail markets in Austria, Croatia, and Italy, and their contents were up to 2.1 μg/kg and 17.5 μg/kg, accounting for 7~100% of their parent toxin concentrations [26]. A total of 17 *Alternaria* toxins, including AOH-3-glucoside (AOH-3-Glc), AOH-9-glucoside (AOH-9-Glc), AOH-3-S, AME-3-glucoside (AME-3-Glc), and AME-3-S, were investigated in tomato sauce, sunflower seed oil, and wheat flour, and interestingly, the results determined that concentrations of AOH-9-Glc and AME-3-S were in similar to their parent toxins in a naturally contaminated tomato sauce sample [27]. These observations highlight the importance to include *Alternaria* toxins in analytical methods for food surveillance, and due to the detection of excessive *Alternaria* toxins in most tomato products, attention should be paid to the production of *Alternaria* toxins in tomato fruits.

There are only a few studies addressing the production and transformation of mycotoxins. An experiment about the infection process of *Fusarium culmorum* in wheat spikes after spray and single spikelet inoculations was presented by Kang and Buchenauer [28], who observed that the pathogen was extended in the rachis in upward and downward directions by inter- and intra- cellular growths inside and outside of the vascular bundles of the rachis. Wang et al. [29] investigated the interaction between *Penicillium expansum* and wounded apple fruit tissues during the early stages of the infection, using a Pannoramic MIDI slide scanner to determine the key time points to collect samples for the transcriptomic analysis. In 2018, Xie et al. [30] simultaneously quantified the pathway metabolites of aflatoxin biosynthesis in culture medium and revealed the dynamic changes in the biosyn-

thesis pathway by orbitrap fusion mass spectrometry and a D-optimal mixture design method. To date, in relation to the complex mechanisms in plants leading to various factors affecting the production of mycotoxins, different types of culture medium have been used to study the transformation and metabolism of toxins. Generally, ultra-performance liquid chromatography-high resolution mass spectrometry (UPLC-HRMS) is used to identify the metabolic intermediates of mycotoxins.

Over the years, most of the current studies on the toxicity and mechanism of *Alternaria* toxins have mainly focused on the in vivo investigations and generation mechanism, and the transformation pathway of *A. alternata* in the host has not been determined. This is mainly limited by instrument conditions and toxin standards. Many standards of *Alternaria* toxins, including conjugated toxins, are lacking developed research and availability of commercial products, which require UPLC-HRMS to perform a qualitative analysis. Therefore, in this study, the potential of *Alternaria* toxins production in processing tomatoes is evaluated via ultra-high-performance liquid chromatography–tandem mass spectrometry (UPLC-MS/MS) and ultra-performance liquid chromatography–ion mobility quadrupole time-of-flight mass spectrometry (UPLC-IMS QToF MS). Moreover, the changes in *Alternaria* toxin species and contents are compared in processing tomatoes during the growth and storage periods. This study provides the basic data for the further study of the production and metabolism of *Alternaria* toxins in processing tomatoes, which is of great significance to control the quantity of *Alternaria* toxins in tomato products.

2. Results

2.1. The Lesion Diameter Affected by A. alternata

The lesion diameter was measured using the cross crossing method. From Figure 1 EG (a), we can observe that the diameter of the spots in the experimental group present a significant change in the tomatoes, accompanied by the deepening of the color of the spots, while there were no changes visible in the tomatoes in the control group (Figure 1 CK). Three days post inoculation, sunken areas could be observed around the inoculation sites, and on the 5th day, the sunken areas had enlarged and turned into black lesions. In the view of the section plot (Figure 1, EG (b)), it is observed that the spread of disease spots in the in vivo experiment was more rapid than that in field experiments, and essentially penetrated the whole tomato fruit on the 11th day. Figure 2 also demonstrates that the in vivo experiment conducted on the same day appears to present slightly more plaque than the field experiment, as there is a difference in the lesion diameter (43.44 mm) relative to that of the field experiment (33.63 mm) at 13 days post-inoculation.

Figure 1. Observation of lesion diameter of tomatoes ((**a**): in field experiment; (**b**): in vivo experiment; CK: control group; EG: experimental group; from left to right in CK and EG (**a**), sunken areas can be observed on the 1st, 3rd, 5th, 7th, 9th, 11th, and 13th day post-inoculation; those in the EG (**b**) are the section plots on 5th, 7th, 9th, 11th, and 13th day post-inoculation of tomatoes).

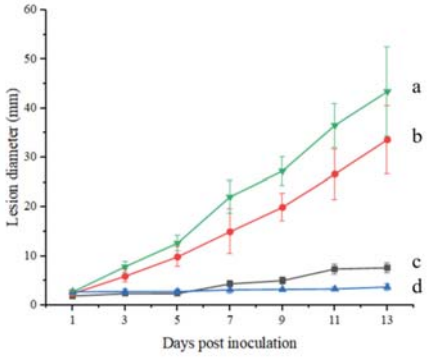

Figure 2. The change in lesion diameter after being inoculated (a: experimental group in in vivo experiment; b: experimental group in field experiment; c: control group in field experiment; d: control group in in vivo experiment).

2.2. Alternaria Toxins Produced in Processing Tomatoes in the Field Experiment

2.2.1. Analysis of Alternaria Toxins

The production of *Alternaria* toxins in the field trials was analyzed using UPLC-MS/MS. In fact, only TeA and AOH were detected, and neither AME nor TEN was detected either in the experimental or control groups. It can clearly be observed in Figure 3 that the concentrations of all the toxins in the experimental group were almost higher than those in the control group. In the experimental group, the highest accumulation rates of TeA (41,389.19 μg/kg) and AOH (2.33 μg/kg) were presented on the 9th day post-inoculation. During the 13 days post-inoculation, the range of TeA was 205.86~41,389.19 μg/kg with the accumulation increasing from the 1st day post-inoculation to the 9th day, and then rapidly decreasing within two days. The range of AOH was <0.26~2.33 μg/kg and the change in AOH content was consistent with that of TeA, except for a sharp increase on the last two days. In the control group, the concentrations of TeA and AOH were 32.97~1494.37 μg/kg and <0.26~0.6 μg/kg, respectively, which presented a similar trend as the experimental group. TeA was the predominant toxin produced, and was significantly higher ($p < 0.01$) than the other toxins in the two groups.

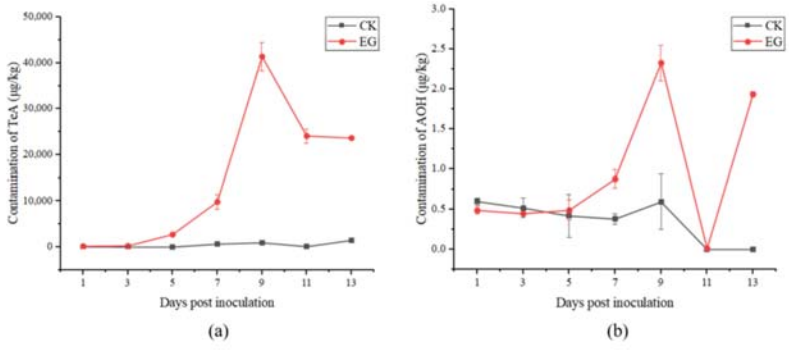

Figure 3. Production of tenuazonic acid (TeA) (**a**) and alternariol (AOH) (**b**) in tomatoes field experiments (CK: control group; EG: experimental group).

2.2.2. Analysis of Conjugated Alternaria Toxins

As the standards of conjugated *Alternaria* toxins were not available, UPLC-IMS QToF MS was used to screen the conjugated *Alternaria* toxins, including AOH-3-S, AOH-3-S,

AME-3-Glc, and AOH-9-Glc. As can be observed in Figure 4, the four conjugated toxins, except AME-3-Glc, were not detected. AME-3-Glc was detected post-inoculation, and the peak area in the control group was always larger than that in the experimental group. In the experimental group, the largest peak area of AME-3-Glc was 8579.93 on the 5th day post-inoculation, then decreased until the 11st day, and then slightly increased again. The largest peak area of AME-3-Glc in the control group was 16,412.85 on the third day post-inoculation and changed in a manner similar to that in the experimental group.

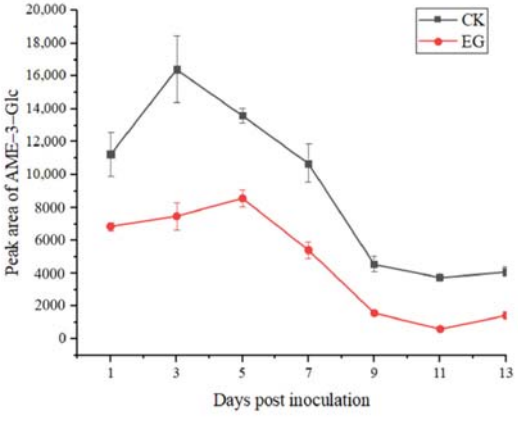

Figure 4. Production of alternariol monomethyl ether-3-glucoside (AME-3-Glc) in tomato field experiments (CK: control group; EG: experimental group).

2.3. Alternaria Toxins Produced in Processing Tomato in In Vivo Experiment

2.3.1. Analysis of Alternaria Toxins

The results of the toxins (TeA, AOH, AME, TEN) concentrations in the tomatoes in vivo experiments are presented in Figure 5. In the experimental group, TeA continued to accumulate after inoculation, achieving a peak on the 11th day (526,986.37 μg/kg), and then it decreased. The variation trends of AOH and AME were very similar, and from the 5th day post inoculation, the toxin sharply increased, and reached the peak on the 7th day (18.02 μg/kg and 1.10 μg/kg) then sharply decreased and began to increase on the 11th day. TEN showed an overall upward trend, the highest toxin concentration was on the 13th day (0.94 μg/kg). In the control group, the toxin levels in the tomatoes inoculated with sterile water were much lower than those in the experimental group, but the changes in toxin levels were similar to those in the experimental group. Comparing the four *Alternaria* toxins, the concentration of TeA was much higher than that of the other toxins, followed by AOH. AME and TEN had lower concentrations, either in the experimental or control groups.

2.3.2. Analysis of Conjugated Alternaria Toxins

The results of detecting conjugated toxins in the in vivo experiment with UPLC-IMS QToF MS are presented in Figure 6. It can be observed from Figure 6a that in the experimental group, following inoculation, the highest peak area of AOH-9-Glc was detected on the 1st day (3384.52), sharply decreased on the third day, and then increased until the 7th day, and the peak area was 2918.14. In the control group, the change in AOH-9-Glc was similar to that in the experimental group, which can be clearly observed from the 5th to 13th day post-inoculation, with the highest peak area for AOH-9-Glc on the 7th day (3535.80). It can be observed in Figure 6b that the concentration of AME-3-Glc decreased until the last day post-inoculation in the experimental group, while in the control group, the peak area of AME-3-Glc present an irregular change and the highest peak area was on the 3rd day (16,006.58) post-inoculation. From Figure 6, it can be observed that the in vivo experiment,

there was a downward trend of the conjugated toxins of AOH-9-Glc and AME-3-Glc as a whole.

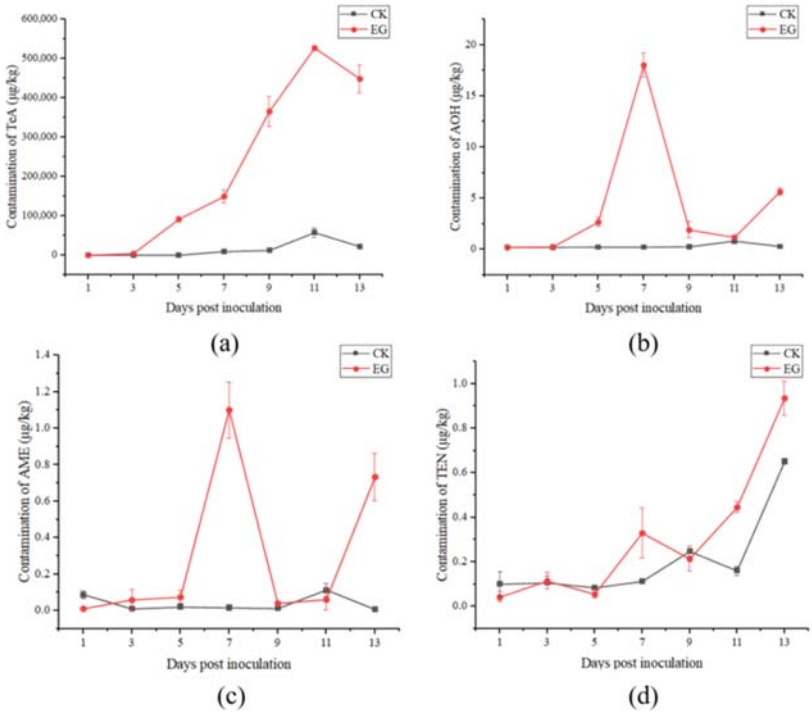

Figure 5. Production of TeA (**a**), AOH (**b**), alternariol monomethyl ether (AME) (**c**), and tentoxin (TEN) (**d**) in tomato in vivo experiments (CK: control group; EG: experimental group).

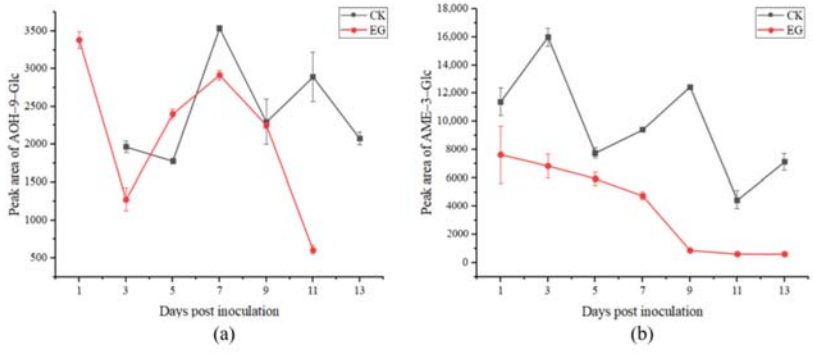

Figure 6. Production of alternariol-9-glucoside (AOH-9-Glc) (**a**) and AME-3-Glc (**b**) in tomato vivo experiments (CK: control group; EG: experimental group).

3. Discussion

3.1. Virulence of A. alternata in the Inoculation of Tomatoes

Artificial inoculation efficiently mimics a spontaneous mold contamination. Based on the observation of tomato disease spots in the field and in vivo experiments, it was easy to observe that when the tomato was infected with *A. alternata*, it spread from the lesion center to all sides, indicating that all of the tissues in the tomato could become a medium

for the growth of *A. alternata*. The change in lesions was highly consistent with black spot disease, and the research conducted by Rizwana et al. also confirmed this assessment [31].

3.2. Varying Potential of Alternaria Toxins Production between Field and In Vivo Experiments

In this study, we conducted field and in vivo experiments on the changes in secondary metabolites in tomatoes infected with *A. alternata*, and the wide variability of mycotoxins produced was observed in the field and in vivo experiments. Comparing the two experiments, the content of all the toxins in the in vivo experiments were more varied than that in the field experiment; a possible explanation might be that plucked tomatoes may be more susceptible to *Alternaria* infection due to senescence [32]. The great variability among *Alternaria* toxins was observed both in the field and in vivo experiments. The most frequently occurring toxin was TeA, and it was observed in significantly high levels. The range of TeA detected in the present study was 18.20~526,986.37 μg/kg, which was higher than the results for whole tomatoes (10,700~139,000 μg/kg) in Pennsylvania detected by Stinson et al. [33]. The amount of TeA was the highest in whole tomatoes and was at most four orders of magnitude higher than that of other *Alternaria* toxins, however, the highest amount of TeA was inconsistent for the variety difference of tomatoes and *Alternaria* strains. AOH and AME were produced in much lower quantities in our study, and most of the tomatoes did not contain detectable amounts of the two toxins in the other studies [33]. Sanzani et al. [34] also reported that AOH and AME were detected in few fresh tomatoes, to a lesser extent, by AME (10.2~18.3 μg/kg) and AOH (16.4 μg/kg), which had lower quantities than TeA (11~4560 μg/kg). It is understood that AOH and AME are the most important types of *Alternaria* toxins, since the toxicity of these mycotoxins can be emphasized by the combination of sulfates and glucosides produced by *Alternaria* spp. cultured on tomatoes; however, there are few data addressing the natural occurrence of AOH and AME in tomatoes in our study and other studies [35,36].

In this study, the amount of four *Alternaria* toxins in the field experiment were less than that in the in vivo experiment, but the standard deviation was higher, possibly owing to the fact that the in vivo experiment broke away from the uncertainty of the environmental factor in the field experiment. Under the conditions of appropriate temperature and water activity, the change in *Alternaria* toxin content was more obvious than that in the field experiment, but the toxin contained in the tomatoes themselves could not be excluded. The growth of and decline in *Alternatia* toxins in tomatoes can be preliminarily judged by comparing the experimental group with the control group.

3.3. The Production of Conjugated Mycotoxins

In this study, AOH-9-Glc, AME-3-Glc, AOH-3-S, and AME-3-S were identified by UPLC-IMS QToF MS. As shown in Figure 7, as part of their metabolism, plants are capable of transforming phytotoxins into conjugated forms. AOH and AME can be efficiently conjugated, especially with glucose or sulfates by cultured plant cells. In this study, AOH-9-Glc and AME-3-Glc were detected alone with AOH and AME in tomatoes. It can be observed that the amount of the two conjugated toxins in the control group was higher than that in the experimental group, which is similar to the result obtained by Sebastian et al. [37], who observed that non-infected tomatoes were able to generate glucosides but not sulfates of AOH and AME, whereas *A. alternata* produced sulfates but a small quantity of glucosides. The probable reason for the low amounts of glucosides observed in the study is the fact that the analyzed specimens contained mostly fungal material and very little intact tomato tissue. Many relatively new reports suggest that conjugated mycotoxins are of relevance for exposure and risk assessments, and further studies should aim to identify additional, to-date-unknown conjugates using new technology.

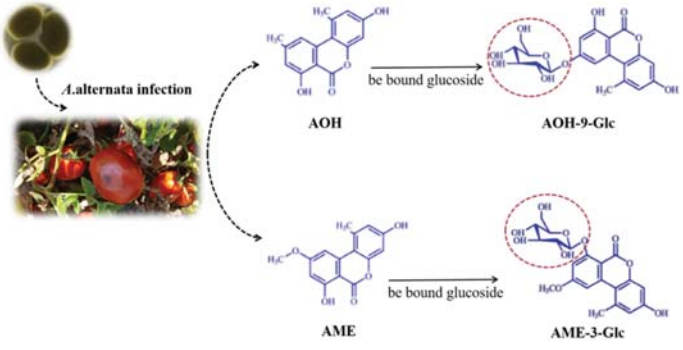

Figure 7. Transformation of *Alternaria* toxins in tomatoes.

4. Conclusions

Our results revealed a toxin production discrepancy after being infected by *A. alternata* between detached fruit and whole plant assays. In this study, four kinds of *Alternaria* toxins (AOH, AME, TeA, and TEN) and four conjugated mycotoxins (AOH-3-S, AME-3-Glc, AOH-9-Glc, and AME-3-S) were detected and investigated in processing tomatoes inoculated with *A. alternata* during harvest and storage periods. TeA was found to be the predominant toxin both in the field and in vivo experiments, then AOH and AME were detected in low levels. Through the screening of the conjugated mycotoxins, AME-3-Glc was detected both in the field and in vivo experiments, while AOH-9-Glc was only detected in the in vivo experiment. We propose that the content of all forms of *Alternaria* toxins detected in tomatoes may not be very accurate because the conjugated toxins can escape detection. Therefore, it is necessary to further study this more extensively to accurately understand the pollution of *Alternaria* toxins in tomatoes prior to harvesting.

5. Material and Methods

5.1. Chemical and Reagents

Anhydrous magnesium sulfate ($MgSO_4$) and sodium chloride (NaCl) were purchased from Sinopharm Chemical Reagent Co., Ltd. (Shanghai, China). LC-MS grades of acetonitrile, formic acid, and acetic acid were purchased from Thermo Fisher Scientific (Waltham, MA, USA). Ultra-pure water was provided by the Watsons Group (Hong Kong) Ltd. Standard TeA, AOH, AME, and TEN were purchased from Romar Labs Division Holding GmbH (Getzersdorf, Austria), and individual standard solutions of each mycotoxin were prepared at ~100 μg/mL in acetonitrile and stored at −20 °C. Leucine enkephalin was acquired from Waters Corporation (Milford, MA, USA).

5.2. Instruments

The samples were weighed on an XSE 204 balance (Mettler-Toledo, Greinfesee, Switzerland), homogenized with a T13 basic ultraturrax (IKA, Staufen, Germany), and mixed in an automatic horizontal shaker (Hannuo Instruments, Shanghai, China). Centrifugation was performed using a Sorvall biofuge Stratos system (Thermo Fisher Scientific, Waltham, MA, USA).

5.3. Tomato, A. alternata and Spore Suspension

H1015 tomatoes were grown in an experimental field in Changji, Xinjiang Province. Sowing was performed on 1 May 2021, and a single test field that consisted of 70 to 80 6-m rows spaced 40 cm apart was used. Seeds were sown 80 cm apart in the row, resulting in a population of approximately 600 plants. *A. alternata* isolate H10, being isolated from diseased tomatoes and identified, was obtained by single-spore isolation in our laboratory and cultivated in potato dextrose agar (PDA). To obtain a spore suspension of *A. alternata*

isolate H10, sterile distilled water was added to the fully overgrown PDA plates and the spore suspension was adjusted to 1×10^5 conidia/mL using a hemocytometer. Suspension was used directly after preparation for the different experiments.

5.4. Field Experiment

The tomatoes were inoculated approximately 15 days before harvest, washed, and sanitized with 75% ethanol. Using a sterilized toothpick, uniform cuts 3 mm deep and 3 mm wide were made in both sides of the epidermis of the fruit in the equatorial region. A quantity of 15 µL of spore suspension was then inoculated into each cut, and tomatoes inoculated with sterile water were used as controls. Samples were obtained the following day after inoculation, 7 times in total.

5.5. In Vivo Experiment

Healthy, non inoculated, and uniform-sized tomatoes free of disease spots were selected for the experiment. After being washed with water and sanitized with 75% ethanol, using a sterilized toothpick, uniform cuts 3 mm deep and 3 mm wide were made on both side of the epidermis of the fruit in the equatorial region. A quantity of 15 µL of a spore suspension and 15 µL of sterile water were inoculated into each cut of the experimental and control groups. The fruits were stored at 25 °C (±2 °C) in sterilized, breathable boxes for 13 d, and the samples were obtained the following day after inoculation.

5.6. Lesion Diameter Measurement

A total of 7 samples were obtained from the experimental and control groups respectively, in both the field test and in vivo experiment, and the diameters of the spots were measured.

5.7. Extraction of Alternaria Toxins

The homogenized samples (5 g) were placed in 50 mL centrifugal tubes, followed by the successive addition of 10 mL of water and 10 mL of acetonitrile containing 1% acetic acid. The mixtures were shaken on an automatic horizontal shaker at 2500 rpm for 5 min to fully disperse the sample. Subsequently, 4 g anhydrous $MgSO_4$ and 1 g NaCl were immediately added while vigorously shaking the tube to prevent the agglomeration of the salts. After centrifugation at 5000× *g* for 5 min, the supernatant was evaporated to near dryness (approximately 1 mL of residue remained) under a stream of nitrogen at 40 °C. Finally, 1 mL of the combined solution (acetonitrile/methanol/formic acid, 70:29:1, *v*/*v*/*v*) was added to the residue, which was vortexed, filtered through a 0.22 µm PTEE filter, and injected into the UPLC-IMS QToF MS system.

5.8. Alternaria Toxins Detection

The detection of *Alternaria* toxins (TeA, AOH, AME, and TEN) was performed on a Waters Acquity UPLC tandem quadrupole (TQD) mass spectrometer (Waters, Milford, MA, USA), which contained an Acquity UPLC HSS C18 (1.7 µm, 2.1 × 100 mm) column for separation. Column temperature was set at 40 °C. The mobile phase comprised methanol as eluent A and 0.1 mM ammonium carbonate as eluent B. A gradient elution was applied as follows: 20% A was initially used and linearly increased to 100% within 4 min, then maintained for 1.5 min, then decreased to 20% within 0.5 min, then maintained for 2 min, after which, column re-equilibration occurred, leading to a total run time of 8 min. The flow rate was set at 0.3 mL/min.

The MS/MS analysis was operated in the negative mode at a capillary voltage of 2.5 kV, a desolvation temperature of 600 °C, a source block temperature of 125 °C, a desolvation gas of 1000 L h^{-1}, and a cone nitrogen gas flow of 150 L h^{-1}. The ion chromatogram for each *Alternaria* toxin was obtained in MS^2 mode of the full-scan chromatogram. The accurate masses of TeA, AOH, AME, and TEN were 197.10, 258.05, 272.07, and 414.18, respectively, in the negative mode; the ionized form of *Alternaria* toxins in $[M-H]^-$; and

the accurate masses of these ionized *Alternaria* toxins were 196.10, 257.05, 271.07, and 413.18, respectively. From the scan filter, each mycotoxin was detected, along with the peak times: TeA, 1.8 min; AOH, 3.98 min; AME, 5.42 min; and TEN, 5.00 min.

The four conjugated *Alternaria* toxins (AOH-3-S, AME-3-S, AOH-9-Glc, and AME-3-Glc) were screened using a Waters Acquity UPLC VION^{TM} ion mobility quadrupole time-of-flight mass spectrometer (Water, Milford, MA, USA), which contained an Acquity UPLC HSS T3 (1.8 µm, 2.1 × 100 mm) column for separation. The column temperature was set at 40 °C. The mobile phase comprised acetonitrile, containing 0.1% (*v*/*v*) formic acid as eluent A, and ultra-pure water, containing 0.1% (*v*/*v*) formic acid, as eluent B. A gradient elution was applied as follows: 5% of mobile phase A was initially used and linearly increased to 80% within 2.5 min and 90% within 2 min and then maintained for 1.5 min. Then, column re-equilibration was performed, resulting in a total run time of 6 min. The flow rate was set to 0.3 mL/min.

The IMS QToF MS analysis for the conjugated toxins was conducted in negative ion mode (ESI$^-$) at a capillary voltage of 2.5 kV, a desolvation temperature of 350 °C, a source temperature of 125 °C, a desolvation gas flow of 800 L/h, and a cone nitrogen gas flow of 50 L/h. Argon was used as the collision gas at a pressure of 4×10^{-3} mbar. The injection volume was 3 µL. High-definition mass spectrometry (HDMS^E) was used as the acquisition mode with low- and high-collision energies set to 6 eV and 30–60 eV, respectively. The data were acquired between 50 and 1000 m/z. Lock mass correction was performed by infusing a leucine enkephalin solution (0.2 ng/L) into the ion source every 5 min (m/z 554.2615 used as the reference ion in the negative mode). Ion mobility and mass calibration were determined using a Major Mix IMS/ToF Calibration Kit (Waters Corporation). The other parameters for data acquisition and processing were set according to the manufacture's guidelines and performed using UNIFI 1.8.2 software (Waters Corporation).

5.9. Statistical Analysis

The results of this study were analyzed with Microsoft Office Excel 2010, and a line chart was plotted using Origin 2018. The data shown in the results are the means of triplicate (or more) values and expressed as ± SD (standard deviation) for the lesion diameter and mycotoxin content. Statistical analysis was performed using SPSS statistical package 18.0. One-way analysis of variance (ANOVA) and Turkey's HSD test were performed to determine the significance of the main factors and their interactions. $p < 0.01$ was considered statistically significant.

Author Contributions: Conceptualisation and methodogy, Q.Q. and Y.F.; writing-original draft, Q.Q., Y.F., Q.J., S.D., F.L., B.J., G.W. and W.G.; writing-review & editing, Y.F., F.L. and C.W. All authors have read and agreed to the published version of the manuscript.

Funding: This research was funded by National Key Research and Development Program of China (2019YFC1604502), Open fund project of Key Laboratory of Agro-Products Quality and Safety of Xinjiang (XJAQS-2022-01) and National Natural Science Foundation of China (32260634).

Institutional Review Board Statement: Not applicable.

Informed Consent Statement: Not applicable.

Data Availability Statement: Not applicable.

Conflicts of Interest: The authors declare no conflict of interest.

References

1. Prusky, D.; Eshel, D.; Kobiler, I.; Yakoby, N.; Moualem, D.B.; Ackerman, M.; Zuthji, Y.; Arie, R.B. Postharvest chlorine treatments for the control of the persimmon black spot disease caused by *Alternaria alternata*. *Postharvest Biol. Technol.* **2001**, *22*, 271–277. [CrossRef]
2. Smith, J.E.; Mengesha, B.; Tang, H.; Mengiste, T.; Bluhm, B.H. Resistance to *Botrytis cinerea* in *Solanum lycopersicoides* involves widespread transcriptional reprogramming. *BMC Genom.* **2014**, *15*, 334. [CrossRef] [PubMed]

3. Derbalah, A.; Shenashen, M.; Hamza, A.; Mohamed, A.; Safty, S.E. Antifungal activity of fabricated mesoporous silica nanoparticles against early blight of tomato. *Egypt. J. Basic Appl. Sci.* **2018**, *5*, 145–150. [CrossRef]
4. Pearson, R.C. Factors affecting the occurrence and severity of blackmold of ripe tomato fruit caused by *Alternaria alternata* [Fungus diseases]. *Phytopathology* **1975**, *65*, 1352. [CrossRef]
5. Troncoso, R.R.; Tiznado, H.M.E. Chapter 5—*Alternaria alternata* (Black Rot, Black Spot). *Postharvest Decay.* **2014**, 147–187. [CrossRef]
6. Prusky, D.; Alkan, N.; Mengiste, T.; Fluhr, R. Quiescent and necrotrophic lifestyle choice during postharvest disease development. *Annu. Rev. Phytopathol.* **2013**, *51*, 155–176. [CrossRef]
7. Thomma, B.P.H.J. *Alternaria* spp.: From general saprophyte to specific parasite. *Mol. Plant Pathol.* **2003**, *4*, 225–236. [CrossRef]
8. Ozcelik, S.; Ozcelik, N.; Beuchat, L.R. Toxin production by *Alternaria alternata* in tomatoes and apples stored under various conditions and quantitation of the toxins by high-performance liquid chromatography. *Int. J. Food Microbiol.* **1990**, *11*, 187–194. [CrossRef]
9. Mukesh, M.; Andleeb, Z.; Dubey, M.K.; Mohd, A.; Gupta, V.K.; Upadhyay, R.S. Comparative evaluation of biochemical changes in tomato (*Lycopersicon esculentum* mill.) infected by *Alternaria alternata* and its toxic metabolites (TeA, AOH, and AME). *Front. Plant Sci.* **2016**, *7*, 1408.
10. Woudenberg, J.H.C.; Seidl, M.F.; Groenewald, J.Z.; Vries, M.D.; Stielow, J.B.; Thomma, B.P.H.J.; Crous, P.W. Alternaria section Alternaria: Species, formae speciales or pathotypes? *Stud. Mycol.* **2015**, *82*, 1–21. [CrossRef]
11. Patriarca, A.; Azcarate, M.P.; Terminiello, L.; Pinto, V.F. Mycotoxin production by Alternaria strains isolated from Argentinean wheat. *Int. J. Food Microbiol.* **2007**, *119*, 219–222. [CrossRef]
12. Dall, A.C.; Cirlini, M.; Falavigna, C. Chapter three-mycotoxins from Alternaria: Toxicological implications. *Adv. Mol. Toxicol.* **2014**, *8*, 107–121.
13. Chain, E. Scientific opinion on the risks for animal and public health related to the presence of Alternaria toxins in feed and food. *EFSA J.* **2011**, *9*, 2407.
14. Michele, S. Recent advances on Alternaria mycotoxins. *Curr. Opin. Food Sci.* **2017**, *17*, 57–61.
15. Rychlik, M.; Humpf, H.U.; Marko, D.; Dänicke, S.; Mally, A.; Berthiller, F.; Klaffke, H.; Lorenz, N. Proposal of a comprehensive definition of modified and other forms of mycotoxins including "masked" mycotoxins. *Mycotoxin Res.* **2014**, *30*, 197–205. [CrossRef]
16. Pero, R.W.; Posner, H.; Blois, M.; Harvan, D.; Spalding, J.W. Toxicity of metabolites produced by the "Alternaria". *Environ. Health Persp.* **1973**, *4*, 87–94. [CrossRef]
17. Kang, Y.; Feng, H.W.; Zhang, J.X.; Chen, S.G.; Valverde, B.E.; Qiang, S. TeA is a key virulence factor for *Alternaria alternata* (Fr.) Keissler infection of its host. *Plant Physiol. Biochem.* **2017**, *115*, 73–82. [CrossRef]
18. Vejdovszky, K.; Warth, B.; Sulyok, M.; Marko, D. Non-synergistic cytotoxic effects of Fusarium and Alternaria toxin combinations in Caco-2 cells. *Toxicol. Lett.* **2016**, *241*, 1–8. [CrossRef]
19. Bensassi, F.; Gallerne, C.; Sharaf, E.D.O.; Hajlaoui, M.R.; Bacha, H.; Lemaire, C. Cell death induced by the *Alternaria mycotoxin* alternariol. *Toxicol. In Vitro* **2012**, *26*, 915–923. [CrossRef]
20. Pfeiffer, E.; Eschbach, S.; Metzler, M. Alternaria toxins: DNA strand-breaking activity in mammalian cellsin vitro. *Mycotoxin Res.* **2007**, *23*, 152–157. [CrossRef]
21. Commission Recommendation (EU) 2022/553 of 5 April 2022 on Monitoring the Presence of Alternaria Toxins in Food. 2022. Available online: https://op.europa.eu/en/publication-detail/-/publication/1bd43c13-b544-11ec-b6f4-01aa75ed71a1/language-en (accessed on 20 November 2022).
22. Motta, S.D.; Soares, L.M.V. Survey of Brazilian tomato products for alternariol, alternariol monomethyl ether, tenuazonic acid and cyclopiazonic acid. *Food Addit. Contam.* **2001**, *18*, 630–634. [CrossRef] [PubMed]
23. Ackermann, Y.; Curtui, V.; Dietrich, R.; Gross, M.; Latif, H.; Märtlbauer, E.; Usleber, E. Widespread occurrence of low levels of alternariol in apple and tomato products, as determined by comparative immunochemical assessment using monoclonal and polyclonal antibodies. *J. Agric. Food Chem.* **2011**, *59*, 6360–6368. [CrossRef]
24. Terminiello, L.; Patriarca, A.; Pose, G.; Pinto, V.F. Occurrence of alternariol, alternariol monomethyl ether and tenuazonic acid in Argentinean tomato puree. *Mycotoxin Res.* **2006**, *22*, 236–240. [CrossRef]
25. Noser, J.; Schneider, P.; Rother, M.; Schmutz, H. Determination of six Alternaria toxins with UPLC-MS/MS and their occurrence in tomatoes and tomato products from the Swiss market. *Mycotoxin Res.* **2011**, *27*, 265–271. [CrossRef] [PubMed]
26. Puntscher, H.; Cobankovic, L.; Marko, D.; Warth, B. Quantitation of free and modified Alternaria mycotoxins in European food products by LC-MS/MS. *Food Control* **2019**, *102*, 157–165. [CrossRef]
27. Puntscher, H.; Kütt, M.L.; Marko, D.; Warth, B.; Skrinjar, P.; Mikula, H.; Frhlich, J.; Podlech, J. Tracking emerging mycotoxins in food: Development of an LC-MS/MS method for free and modified Alternaria toxins. *Anal. Bioanal. Chem.* **2018**, *410*, 4481–4494. [CrossRef]
28. Kang, Z.; Buchenauer, H. Ultrastructural and cytochemical studies on the infection of wheat spikes by *Fusarium culmorum* as well as on degradation of cell wall components and localization of mycotoxins in the host tissue. *Mycotoxin Res.* **2000**, *16*, 1–5. [CrossRef]

29. Wang, K.L.; Zheng, X.F.; Zhang, X.Y.; Zhao, L.N.; Yang, Q.Y.; Boateng, N.A.S.; Ahima, J.; Liu, J.; Zhang, H.Y. Comparative transcriptomic analysis of the interaction between *Penicillium expansum* and apple fruit (*Malus pumila* mill.) during early stages of infection. *Microorganisms* **2019**, *7*, 495. [CrossRef]
30. Xie, H.L.; Wang, X.P.; Zhang, L.X.; Wang, T.; Zhang, W.; Jiang, J.; Chang, P.K.; Chen, Z.Y.; Bhatnagar, D.; Zhang, Q. Monitoring metabolite production of aflatoxin biosynthesis by orbitrap fusion mass spectrometry and a D-optimal mixture design method. *Anal. Chem.* **2018**, *90*, 14331–14338. [CrossRef]
31. Rizwana, H.; Bokahri, N.A.; Alsahli, S.A.; Showiman, A.S.A.; Alzahrani, R.M.; Aldehaish, H.A. Postharvest disease management of Alternaria spots on tomato fruit by Annona muricata fruit extracts. *Saudi J. Biol. Sci.* **2021**, *28*, 2236–3344. [CrossRef]
32. Miller, B.L.; Huffaker, R.C. Differential induction of endoproteinases during senescence of attached and detached barley leaves. *Plant Physiol.* **1985**, *78*, 442–446. [CrossRef]
33. Stinson, E.E.; Osman, S.F.; Heisler, E.G.; Siciliano, J.; Bills, D.D. Mycotoxin production in whole tomatoes, apples, oranges, and lemons. *J. Agric. Food Chem.* **1981**, *29*, 790–792. [CrossRef]
34. Sanzani, S.M.; Gallone, T.; Garganese, F.; Caruso, A.G.; Amenduni, M.; Ippolito, A. Contamination of fresh and dried tomato by Alternaria toxins in southern Italy. *Food Addit. Contam.* **2019**, *36*, 789–799. [CrossRef]
35. Patricia, L.; Dini, V.; Hans, M.; Martien, S.; Joyce, D.S.; Erika, P.; Monique, D.N. Alternaria toxins and conjugates in selected foods in the Netherlands. *Food Control* **2016**, *69*, 153–159.
36. Walravens, J.; Mikula, H.; Rychlik, M.; Asam, S.; Devos, T.; Ediage, E.N.; Mavungu, J.D.D.; Jacxsens, L.; Landschoot, A.V.; Vanhaecke, L.; et al. Validated UPLC-MS/MS methods to quantitate free and conjugated Alternaria toxins in commercially available tomato products, fruit and vegetable juices in belgium. *J. Agric. Food Chem.* **2016**, *64*, 5101–5109. [CrossRef]
37. Sebastian, T.S.; Beate, N.K.; Erika, P.; Rolf, G.; Manfred, M.; Mirko, B.; Sabine, E.K. Sulfoglucosides as novel modified forms of the mycotoxins alternariol and alternariol monomethyl ether. *J. Agric. Food Chem.* **2016**, *64*, 8892–8901.

toxins

MDPI

Article

Genetic Interaction of Global Regulators AflatfA and AflatfB Mediating Development, Stress Response and Aflatoxins B1 Production in *Aspergillus flavus*

Xiuna Wang, Wenjie Zha, Bin Yao, Lan Yang and Shihua Wang *

Key Laboratory of Pathogenic Fungi and Mycotoxins of Fujian Province, College of Life Sciences, Fujian Agriculture and Forestry University, Fuzhou 350002, China
* Correspondence: wshmail@m.fafu.edu.cn or wshyyl@sina.com

Abstract: *Aspergillus flavus* produces carcinogenic and mutagenic aflatoxins, which cause economic losses and risk of food safety by contaminating grains, food and feed. In this study, we characterized two bZIP transcription factors, AflatfA and AflatfB, and their genetic interaction. Compared to the wild type (WT), *AflatfA* deletion and *AflatfA* and *AflatfB* double deletion both caused retarded vegetative growth of mycelia. Relative to WT, the *AflatfA* deletion strain (Δ*AflatfA*) and *AflatfA* and *AflatfB* double deletion strain (Δ*AflatfA*Δ*AflatfB*) produced more sclerotia, whereas the *AflatfB* deletion strain (Δ*AflatfB*) produced less sclerotia. After 4 °C preservation and incubation at 50 °C, conidia viability dramatically decreased in the Δ*AflatfA* and Δ*AflatfA*Δ*AflatfB* but Δ*AflatfB* mutants, whereas conidia viability of the Δ*AflatfA*Δ*AflatfB* strain was higher after storage at 4 °C than in *AflatfA* mutant. Conidia of Δ*AflatfA*, Δ*AflatfB* and Δ*AflatfA*Δ*AflatfB* strains significantly increased in sensitivity to H_2O_2 in comparison with WT. Compared to WT, the mycelium of Δ*AflatfA* and Δ*AflatfB* strains were more sensitive to H_2O_2; conversely, the Δ*AflatfA*Δ*AflatfB* strain showed less sensitivity to H_2O_2. Δ*AflatfA* and Δ*AflatfA*Δ*AflatfB* strains displayed less sensitivity to the osmotic reagents NaCl, KCl and Sorbitol, in comparison with WT and Δ*AflatfB* strains. When on YES medium and hosts corn and peanut, Δ*AflatfA* and Δ*AflatfA*Δ*AflatfB* strains produced less aflatoxin B1 (AFB1) than Δ*AflatfB*, and the AFB1 yield of Δ*AflatfB* was higher than that of WT. When WT and mutants were inoculated on corn and peanut, the Δ*AflatfA* and Δ*AflatfA*Δ*AflatfB* but not Δ*AflatfB* mutants produced less conidia than did WT. Taken together, this study reveals that AflatfA controls more cellular processes, and the function of AflatfA is stronger than that of AflatfB when of the same process is regulated, except the response to H_2O_2, which might result from the effect of AflatfA on the transcriptional level of AflatfB.

Keywords: *Aspergillus flavus*; bZIP transcription factor; AflatfA; AflatfB; aflatoxin B1; development; stress response

Key Contribution: The transcription of AflatfB is regulated by AflatfA; however, AflatfA and AflatfB have no over-lapping functions. Relative to AflatfB, AflatfA involves more cellular processes and plays decisive roles.

Citation: Wang, X.; Zha, W.; Yao, B.; Yang, L.; Wang, S. Genetic Interaction of Global Regulators AflatfA and AflatfB Mediating Development, Stress Response and Aflatoxins B1 Production in *Aspergillus flavus*. *Toxins* **2022**, *14*, 857. https://doi.org/10.3390/toxins14120857

Received: 31 October 2022
Accepted: 2 December 2022
Published: 4 December 2022

Publisher's Note: MDPI stays neutral with regard to jurisdictional claims in published maps and institutional affiliations.

1. Introduction

Several transcription factors (TF) as global regulators are found to regulate secondary metabolism, virulence, stress response and development [1]. Among them, basic leucine zipper (bZIP) transcription factors are critical global regulators [2]. The family of the bZIP transcription factor is not only one of the largest but also the most conserved TF families across eukaryotes [3]. This family of transcription factors contains the conserved basic leucine zipper domain, which is responsible for dimerization, DNA binding and nuclear import. bZIP transcription factors are classified into various subfamilies, such as the ATF/CREB (activating transcription factor/cAMP-responsive element-binding protein) family. Among them, Atf1/AtfA is one of most well-studied TFs. As is known, Atf1/AtfA

acts downstream of the stress-activated mitogen-activated protein kinase (SAPK) cascade. The function and regulatory mechanism of Atf1 protein from fission yeast has been studied extensively. Activated and stabilized via phosphorylation by Sty1, the transcription factor Atf1 regulates genes involved in stress responses [4]. In *Schizosaccharomyces pombe*, Atf1 lowers the transition barrier for nucleosome-mediated establishment of heterochromatin, activates the *fbp1* gene transcription induced upon glucose starvation and modulates meiotic recombination and heterochromatin formation [5–10]. Atf1 frequently forms heterodimers with other bZIP TF Pcr1, and the interaction of Atf1 and Pcr1 regulates not only stress response genes but also cyclin expression during G2/M transition [8,11,12]. Moreover, Atf1 is a target for the ubiquitin-proteasome system and that its degradation is dependent upon an SCF E3 ligase containing the F box protein Fbh1 [13]. The binding of the transcription factor Atf1 to promoters serves as a barrier to phase nucleosome arrays and avoids cryptic transcription [14].

Orthologs of *S. pombe* Atf1are conserved in filamentous fungi, however, the functions and regulatory mechanisms are heterogeneous, including regulation of vegetative growth and development, a broad spectrum of stress responses, secondary metabolism and virulence. Deletion of *atf1* affects vegetative growth in *Aspergillus nidulans*, *Aspergillus oryzae*, *Botrytis cinerea*, *Magnaporthe oryzae* and *Fusarium verticillioides* [15–19]. Atf1/AtfA is found to regulate the sexual development of several fungi, including *Neurospora crassa* and *Fusarium graminearum* [20–22]. Many Atf1/AtfA orthologs, from *A. nidulans*, *Aspergillus fumigatus*, *F. verticillioides* and *Verticillium dahliae*, are involved in conidium production [15,19,23]. In *Claviceps purpurea* and *B. cinerea*, the formation of sclerotia is also mediated by Atf1/AtfA orthologs [17,24]. AtfA transcription factors also contribute to a variety of stress responses. The response of AtfA to oxidative stress is most universal in fungi, including *A. nidulans*, *A. fumigatus*, *A. oryzae*, *Penicillium marneffei* (*Talaromyces marneffei*), *M. oryzae*, *F. graminearum*, and *F. verticillioides* and *Fusarium oxysporum* [16,18,19,21,22,25–32]. The coordination of AtfA orthologs with oxidative stress response of fungi is related with both types of chemical reagents and morphological forms of fungi. An osmotic stress-sensitive phenotype has also been characterized in fungi, including *N. crassa*, *A. nidulans*, *A. fumigatus* and *F. graminearum* [20–22,27,33]. It is noteworthy that Atf1/AtfA orthologs, from *N. crassa*, *A. nidulans* and *A. fumigatus*, are also involved in the fungicide resistance [33–35]. Moreover, Atf1/AtfA orthologs are critical in cell wall integrity in *A. fumigatus*, *F. graminearum*,and *F. verticillioides* [19,22,36]. Furthermore, conidia of Δ*AtfA* strains show decreased viability after long-term storage at 4 °C as well as heat treatment in *A. nidulans* and *A. fumigatus* [26,27]. In addition, AtfA is involved in the response of conidia to heavy metal in *A. nidulans* [37], and AtfA affects conidia germination after dessication under vacuum in *A. fumigatus* [27]. A novel function is revealed that nitrosative stress response is controlled by AtfA in *V. dahliae* [38]. Atf1/AtfA orthologs, as global regulators, are also important players in the regulation of secondary metabolite biosynthesis in *A. nidulans*, *A. fumigatus* and *Aspergillus terreus*, *Mucor circinelloides*, *B. cinerea*, *F. graminearum* and *F. verticillioides* [17,19,21,22,29,39–41]. However, the regulation mechanism is complex, which is not only related with fungal species but also types of secondary metabolites and the host of pathogens. Atf1/AtfA orthologs as critical virulence factord affect pathogenicity in almost all pathogenic fungi, including human pathogens (*A. fumigatus*, *P. marneffei*, *M. circinelloidesa*, and *Cryptococcus neoformans*) and plant pathogens (*B. cinerea*, *F. graminearum*, *F. verticillioides*, *M. oryzae*, *C. purpurea* and *F. oxysporum*) [15,17–19,21,22,24,27,31,32,36,41,42].

Among the bZIP/CREB family, a novel homologous gene is firstly found in *A. oryzae*, which is shorter in the N-terminal region than AtfA [43]. *A. oryzae atfB* regulates the response of conidia and mycelium to H_2O_2 stress and conidia formation under hyperosmotic stress, whereas the conidia of Δ*atfB* increase in sensitivity to heat-shock [43]. Roze et al. (2004) found that a novel cAMP-response element, CRE1, modulates expression of the aflatoxin biosynthetic gene nor-1 in *Aspergillus parasiticus*, and that protein p32 with an approximate molecular mass of 32 kD binds CRE1 and physically interacts with the aflatoxin pathway regulator AflR [44]. A further study reveals that this protein shares 96% of

its identity with the *A. oryzae* bZIP protein AtfB, and *atfB* is not only related with stress response but also integrates secondary metabolisms with an oxidative stress response in *Aspergilli* [45]. AtfB binds at the aflatoxin biosynthetic gene promoters that carry a CRE motif, and the five nucleotides upstream from CRE1, AGCC(G/C) are highly conserved [45]. The expression of the gene *atfB* is positively influenced by a master regulator *veA*, and the normal formation of DNA-protein complexes in the *cat1* promoter is dependent on AtfB in *A. flavus* [46]. By gene silencing, AtfB controls virulence-associated processes in *A. parasiticus* [47].

Mycotoxins cause serious harm to human health by food or feed safety [48–50]. Among them, aflatoxins are the most notorious, especially AFB1, which is one of the most carcinogenic and mutagenic natural producers [51]. It is known that the opportunistic phytopathogen *Aspergillus flavus* is the main producer of aflatoxins, which infects oil seed crops such as corn, peanut, tree nuts and cotton [52]. Importantly, *A. flavus* is also an opportunistic human pathogen [52]. *A. flavus's* pathogenicity and aflatoxins-producing capability are coupled to environmental stress response, spore production, vegetative growth and so on [53]. Therefore, it is an advanced strategy to control *A. flavus* and aflatoxins by environment and development [51]. In *A. flavus*, RNA-seq analysis indicates that AtfA could regulate the inhibition of piperine on aflatoxins B1 production by modulating fungal oxidative stress response [54], and expression of AtfA is significantly decreased by the inhibitor of aflatoxins B1 epigallocatechin gallate (EGCG) [55]. Meanwhile, transcriptional level analyses demonstrate that AtfB could regulate different water activities and both processes of the inhibition of methyl jasmonate and inhibition of piperine on aflatoxins B1 in *A. flavus* [54,56,57].

In the *A. flavus* strain NRRL3357, AtfA and AtfB have impacts on growth, conidiation production, sclerotia formation, aflatoxin biosynthesis on artificial medium and oxidative stress response, whereas only AtfA affects cell wall stress response and pathogenicity [58]. Under stress, the *atfA* gene is controlled by the HogA (SakA) SAPK pathway in *A. nidulans* and *A. fumigatus* [33,35]. Intriguingly, deletion of *AtfA* has no effect on osmotic stress response in the *A. flavus* strain NRRL3357 [58]. Meanwhile, the genetic interaction of AflatfA and AflatfB is not clear. In this study, *AflatfA* and *AflatfB* were firstly deleted in the recipient strain (PTSΔ*ku70*Δ*pyrG*), and then *AflatfA* and *AflatfB* were complemented and *AflatfB* was deleted in the *AflatfA* strain to construct the double deletion strain. To characterize the functions of AtfA and AtfB in *A. flavus*, unlike the deletion strain containing the RFP gene and recipient strain NRRL3357 without the RFP gene [58], we compared the deletion strains with the WT strain but not the recipient strain, both of which contain the selective gene *pyrG*. We revealed the genetic interaction of AflatfA and AflatfB, and found several novel and different functions. Our results indicate that AflatfA positively regulates the transcription of the *AflatfB* gene, and more biological processes are meditated by *AflatfA* than by *AflatfB*, whereas *AflatfA* plays a decisive role and *AflatfA* and *AflatfB* have no overlapping functions.

2. Results

2.1. AflatfA and AflatfB Are ATF/CREB Homologous Genes in A. flavus

Using the ATF/CREB homologs AtfA and AtfB amino acid sequences of *A. oryzae* as the query, respectively, the searches of the *A. flavus* genome database were performed, and the genes AFLA_031340 and AFLA_094010 were identified with the greatest similarity to AtfA (66.87%) and AtfB (99.69%), respectively. Then, AFLA_031340 and AFLA_094010 in *A. flavus* were named AflatfA and AflatfB, respectively. Bioinformatic analysis showed that AFLA_031340 encodes 512 amino acids with two introns (438 bp and 53 bp), and AFLA_094010 encodes 318 amino acids with no intron. The re-sequence of *AflatfA* ORF and cDNA identified that the *AflrsmA* gene consists of two introns, 53 and 438 bp. Moreover, a highly conserved bZIP domain was in the C-terminal of the Atf1 homologs, and OSM, HRA and HRR domains were conserved in AflatfA in comparison with the Atf1 homologs in filamentous fungi except *B. cinerea* and budding yeast *S. pombe* (Figure 1). There is only

one bZIP domain in the AtfB from *A. flavus* and the compared fungi, including filamentous fungi and budding yeast. The phylogenetic tree based on the bZIP domain sequence showed that AflatfA is the most closely related to the AtfA homologs bZIP from *A. oryzae* (Figure 1).

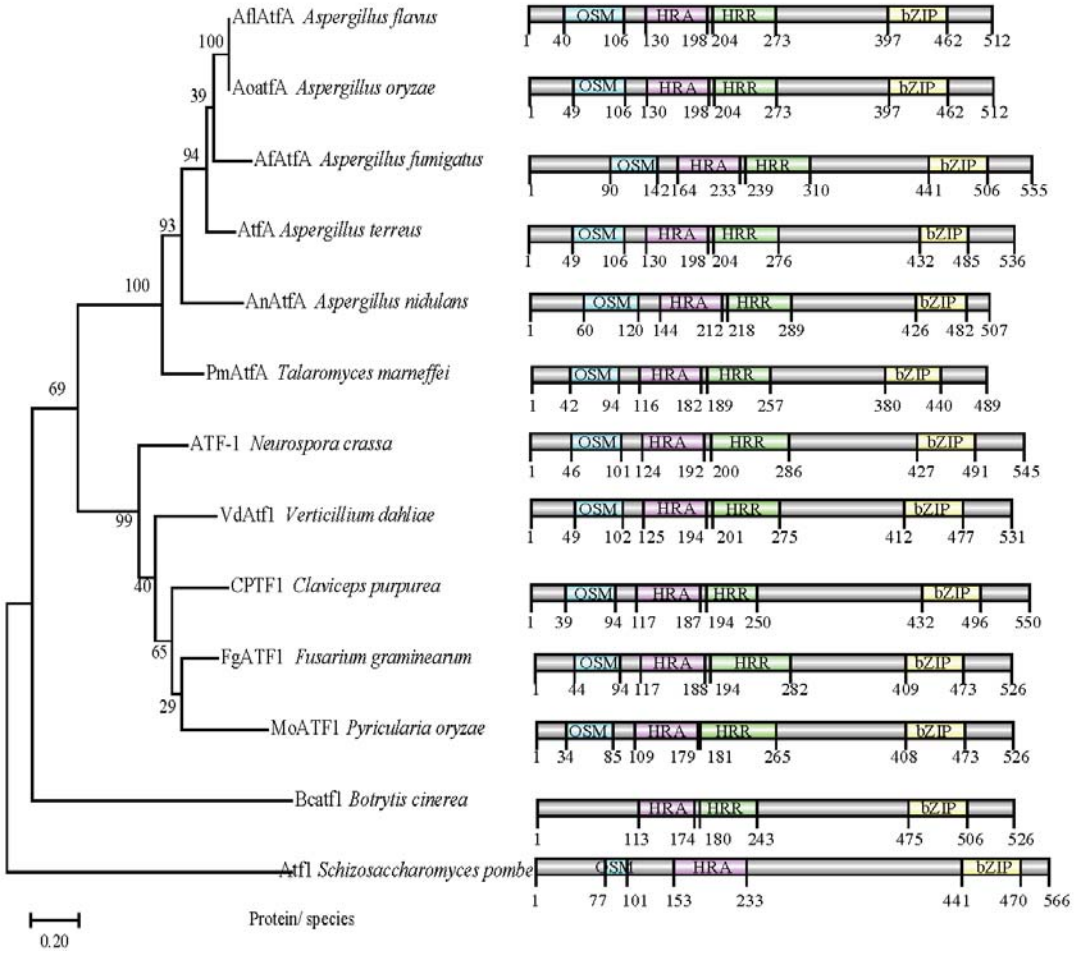

Figure 1. The phylogenetic analysis and functional domain of *Aspergillus flavus* transcription factor AflAtfA. Phylogenetic analysis of bZIP-type TF AtfA/ATF-1 from *A. flavus* and AtfA/ATF-1 orthologs that have been functionally verified in different fungi (Left). The protein sequences were aligned with Clustal X and the maximum likelihood tree was generated using MEGA X software. AtfA from *A. flavus* is in bold. *S. pombe* Atf1 (BAA09841.1), *A. oryzae* AoatfA (XP_001819834.1), *A. fumigatus* AfatfA (XP_754486.2), AtfA from *A. terreus* (EAU35111.1), *A. nidulans* AnAtfA (ANN75015.1), *T. marneffei* PmAtfA (KFX50645.1), *N. crassa* ATF-1 (KFX50645.1), *V. dahliae* VdATF-1 from (XP_009621680.1), *C. purpurea* CPTF1 (CCE33955.1), *F. graminearum* FgATF1 (XP_011319081.1), *P. oryzae* MoATF1 (ELQ67298.1) and *B. cinerea* Bcatf1 (XP_024550682.1) were used. The functional domain of *A. flavus* transcription factor *AflatfA* (Right). bZIP: basic leucine zipper domain; OSM: osmotic stress domain; HRA: domain that activates reorganization during meiosis; HRR: domain that inhibits reorganization during meiosis. The numbers at both ends of the protein indicate the length of each protein, whereas the numbers in the middle of the protein indicate the position of the domains. The protein domains are manually annotated with InterProScan on the EBI website.

2.2. The Generation of Mutants and Expression of AflatfB Was Impacted by AflatfA

In order to study the possible functions of AflatfA and AflatfB in *A. flavus* using reverse forward genetics, *AflatfA* and *AflatfB* were firstly deleted. Then, using a gene-replacement approach, the *AflatfA* and *AflatfB* genes were deleted via PEG-mediated transformation of the *A. flavus* strain protoplast (Figure 2A). The putative knockout strains were then screened by diagnostic polymerase chain reaction (PCR). Furthermore, the putative deleted mutants were confirmed by Southern blot. When hybridized with a probe amplified from the homologous arm of *AflatfA* or *AflatfB* r, two *AflatfB* mutants showed an expected signal, but among the two *AflatfA* mutants, one T1 showed an expected signal, whereas the other had two more brands besides the expected 8533 bp brand (Figure 2B,C). The result indicated that there is an ectopic integration in the *AflatfA* mutant T2. Furthermore, the complementary strains were created by reintroducing the *AflatfA* or *AflatfB* ORF sequence into *AflatfA* T1 and *AflatfB* T1 (Figure 2D,E). To investigate the relationship of *AflatfA* and *AflatfB*, the *AflatfB* gene was replaced by the selected gene *pTRA*, through transformation of the *AflatfA* deletion strain T1 (Figure 2A). Diagnostic PCR confirmed that *pTRA* was integrated in the *AflatfB* locus in the genome of the *AflatfA* mutant (Figure 2F,G).

To provide the insight of the relation between *AflatfA* and *AflatfB*, the transcription level was determined by RT-PCR. Compared with the WT strain, the transcriptional level of AflatfB was lower in the genome of the *AflatfA* deletion strain, but deletion of *AflatfB* has no impact on the transcriptional level of *AflatfA* (Figure 2H). Thus, *AflatfA* positively regulates the expression of *AflatfB* in *A. flavus*.

2.3. The Impact of AflatfA and AflatfB on Vegetative Growth and Sclerotia Formation of A. flavus

To investigate the function of AflatfA and AflatfB on mycelium growth in *A. flavus*, WT, Δ*AflatfA*, Δ*AflatfB*, Δ*AflatfA*Δ*AflatfB* and complementary strains were simultaneously incubated on the PDA medium. When grown on the PDA medium after five days, Δ*AflatfA* and Δ*AflatfA*Δ*AflatfB* were both significantly reduced in mycelium growth (Figure 3A,B) compared with the WT, Δ*AflatfB* and complementary strains. As a result, AflatfA positively regulates vegetative growth, whereas AflatfB is not involved in the regulation of colony growth.

To survive in adverse environmental conditions, *A. flavus* produces the resistant structure sclerotia. Therefore, we investigated whether sclerotia formation was affected by *AflatfA* and *AflatfB*. WT, *AflatfA* and *AflatfB* mutants were inoculated on a modified Wickerham medium, and then the number of sclerotia was counted after 12 d. Compared to WT and corresponding complementary strains, the *AflatfA* deletion strain produced more sclerotia; however, the number of sclerotia from the Δ*AflatfB* strain had significantly decreased (Figure 3C,D). Interestingly, the number of sclerotia produced by the Δ*AflatfA*Δ*AflatfB* strain was significantly increased, which is similar to that in the *AflatfA* mutant (Figure 3C,D). The above results indicate that AflatfA negatively regulates sclerotia formation, but AflatfB positively regulates sclerotia formation, and AflatfA has a stronger function than AflatfB for sclerotia formation.

2.4. The Decline of AFB1 Yield from ΔAflatfA, ΔAflatfB and ΔAflatfAΔAflatfB Strains on Artificial Medium YES

To confirm whether *AflatfA* and *AflatfB* regulate the biosynthesis of aflatoxins, equal amounts of spore from WT and mutant strains were inoculated on a YES medium and cultured at 29 °C for 5 d in the dark. TLC analysis showed that the yield of aflatoxin AFB1 produced by Δ*AflatfA*, Δ*AflatfB* and Δ*AflatfA*Δ*AflatfB* strains were significantly lower than that by WT, but that of *AflatfB* mutant was significantly higher than that of Δ*AflatfA* and Δ*AflatfA*Δ*AflatfB* strains (Figure 4). Interestingly, there is no difference in AFB1 production between Δ*AflatfA* and Δ*AflatfA*Δ*AflatfB* strains (Figure 4). The data showed that AflatfA and AflatfB both positively regulate the biosynthesis of AFB1, and the function of AflatfA is more powerful than that of AflatfB. However, *AflatfA* and *AflatfB* have no additive effect on AFB1 production.

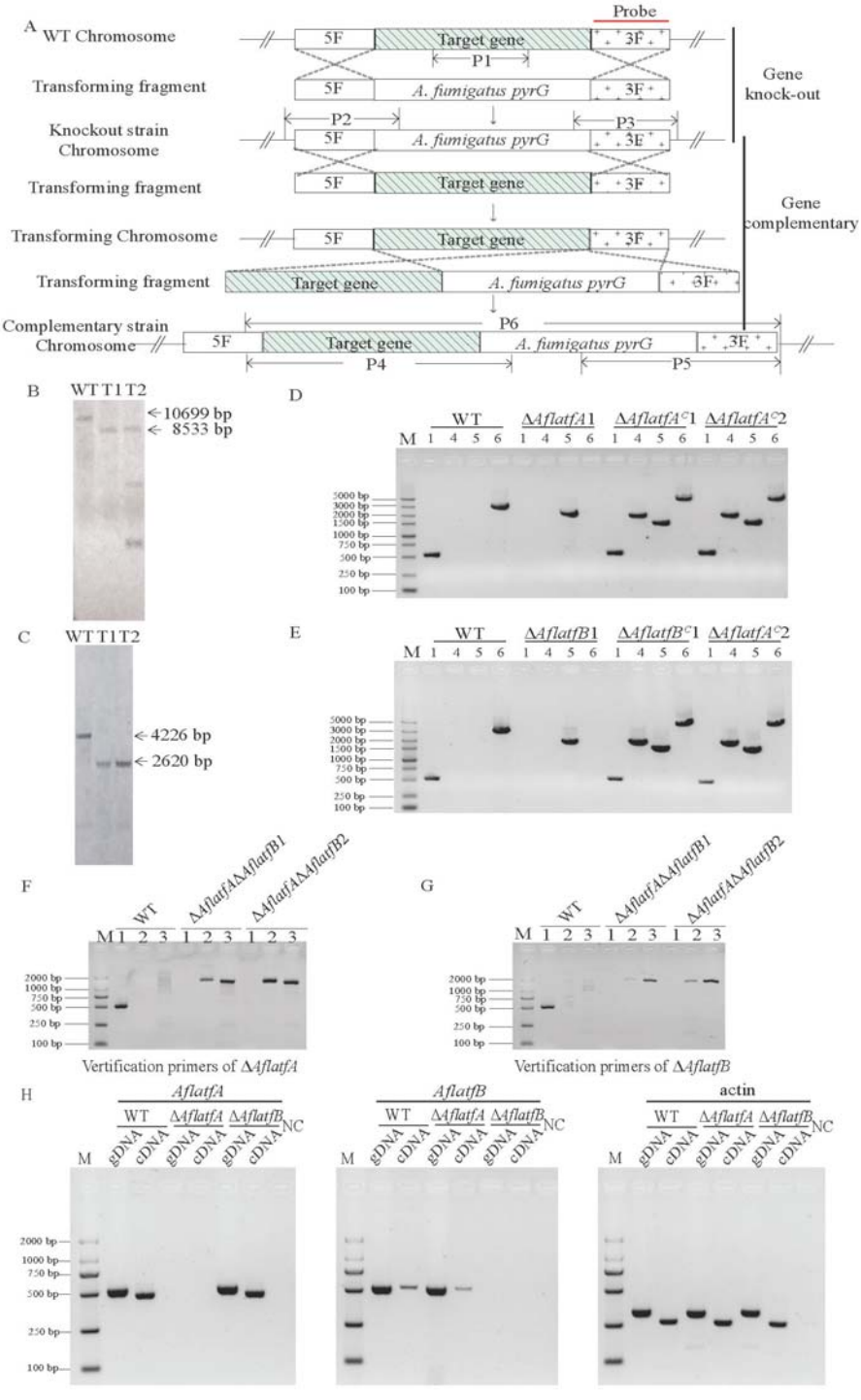

Figure 2. Construction of *AflatfA* and *AflatfB* mutant strains and analysis of the relationship between

bZIP transcription factors *AflAtfA* and *AflAtfB*. (**A**) Construction strategy of *AflatfA* and *AflatfB* mutants and schematic diagram of PCR identification. The pair of primers P1_F/R was used to amplify the target gene. The pairs of primers P2_F/R and P3_F/R were used to amplify the knock-out mutants. The pairs of primers P4_F/R, P5_F/R and P6_F/R were used to amplify the complementary strains. (**B**) Southern blot verification of *AflatfA* deletion strains using 3′ flanking region as a probe. Genomic DNA from wild type and mutant strains were digested with *Kpn* I. The expected size is 10 699 bp and 8 533 bp for WT and mutant strains, respectively. (**C**) Southern blot verification of *AflatfB* deletion strains. The 3′ flanking region is used as a probe, and genomic DNA from wild type and mutant strains are digested with *Hind* III. The expected size is 4226 bp and 2620 bp for WT and mutant strains, respectively. (**D**) PCR was carried out to confirm the complementary strains of *AflatfA*. (**E**) PCR was carried out to confirm the complementary strains of *AflatfB*. (**F**,**G**) PCR verification of Δ*AflatfA*Δ*AflatfB* double knock strain using primers to verify Δ*AflatfA* and Δ*AflatfB* strains (**H**) Transcription levels of *AflatfA* and *AflatfB* genes and internal reference gene actin were analyzed in WT, Δ*AflatfA* and Δ*AflatfB* genomes by RT-PCR. gDNA, genomic DNA; cDNA, reverse transcribed DNA; NC, negative control; the letter M indicates DNA marker. The number from Figure 2D–G indicates the primer pair marked in Figure 2A.

2.5. The ΔAflatfA Strain Has a Defect in the Conidia Response to Temperature Stress

The bZIP TF AtfA homologous genes from the *A. nidulans* and *A. fumigatus* function in the conidia response to heat stress and 4 °C preservation [26,27], and the contribution of *AflatfA* and *AflatfB* to the conidia response to temperature stress were determined. The conidia of WT and mutants were preserved at 4 °C for 7 d and 14 d, and then conidia viability was tested by the germinating rate. The viability of Δ*AflatfA* and Δ*AflatfA*Δ*AflatfB* strains were both significantly lower than that of the WT strain (Figure 5A,B). However, the conidia viability at 4 °C preservation showed no change among Δ*AflatfB*, WT and the two complementary strains (Figure 5A,B). Thus, AflatfA but not AflatfB mediates the conidial viability after long-term storage at 4 °C.

To investigate the functions of *AflatfA* and *AflatfB* in response to heat stress, the conidia of WT and mutants were treated at 50 °C for 1 h, and then the germinating rate was analyzed. The optimum growth temperature at 29 °C and heat stress both could result in the germinating rate of Δ*AflatfA* and Δ*AflatfA*Δ*AflatfB* conidia significantly being reduced compared with that of the WT strain (Figure 5C,D). However, heat stress made the germinating rate of WT conidia drop by 4.5%, whereas that of Δ*AflatfA* and Δ*AflatfA*Δ*AflatfB* conidia were reduced by up to 79.2% and 77.7%, respectively (Figure 5C,D). Compared to that of WT, the germinating rate of the conidia of Δ*AflatfB* and the two complementary strains were not different (Figure 5C,D). These observations implied that AflatfA but not AflatfB is required for response to heat stress in *A. flavus*.

2.6. Deletion of AflatfA and AflatfB Increases Sensitivity to Oxidative Stress

The bZIP transcription factors AtfA and AtfB play important roles in response to oxidative stress in *Aspergillus* spp. [26,30,33]. The cause of the H_2O_2 inhibitory action on *A. flavus* may be that H_2O_2 impact conidia germination. To test this hypothesis, conidia were firstly treated by 200 mM H_2O_2 for 20 min, and then two hundred spores were inoculated on YES to examine the germinating rate of conidia. Without H_2O_2, the germinating rate of Δ*AflatfA* and Δ*AflatfA*Δ*AflatfB* strains significantly decreased compared to WT; however, the germinating rate of Δ*AflatfB* and WT had no significant difference (Figure 6A,B). After H_2O_2 treatment, the germinating rate of Δ*AflatfA* and Δ*AflatfA*Δ*AflatfB* reduced by 42% and 44% respectively, whereas the germinating rate of WT reduced by 32% (Figure 6A,B). Germinating rate assays demonstrated that Δ*AflatfB* conidia was more sensitive to H_2O_2 than WT (Figure 6A,B). Therefore, *A. flavus* AflatfA and AflatfB are both required for oxidative stress tolerance in conidia.

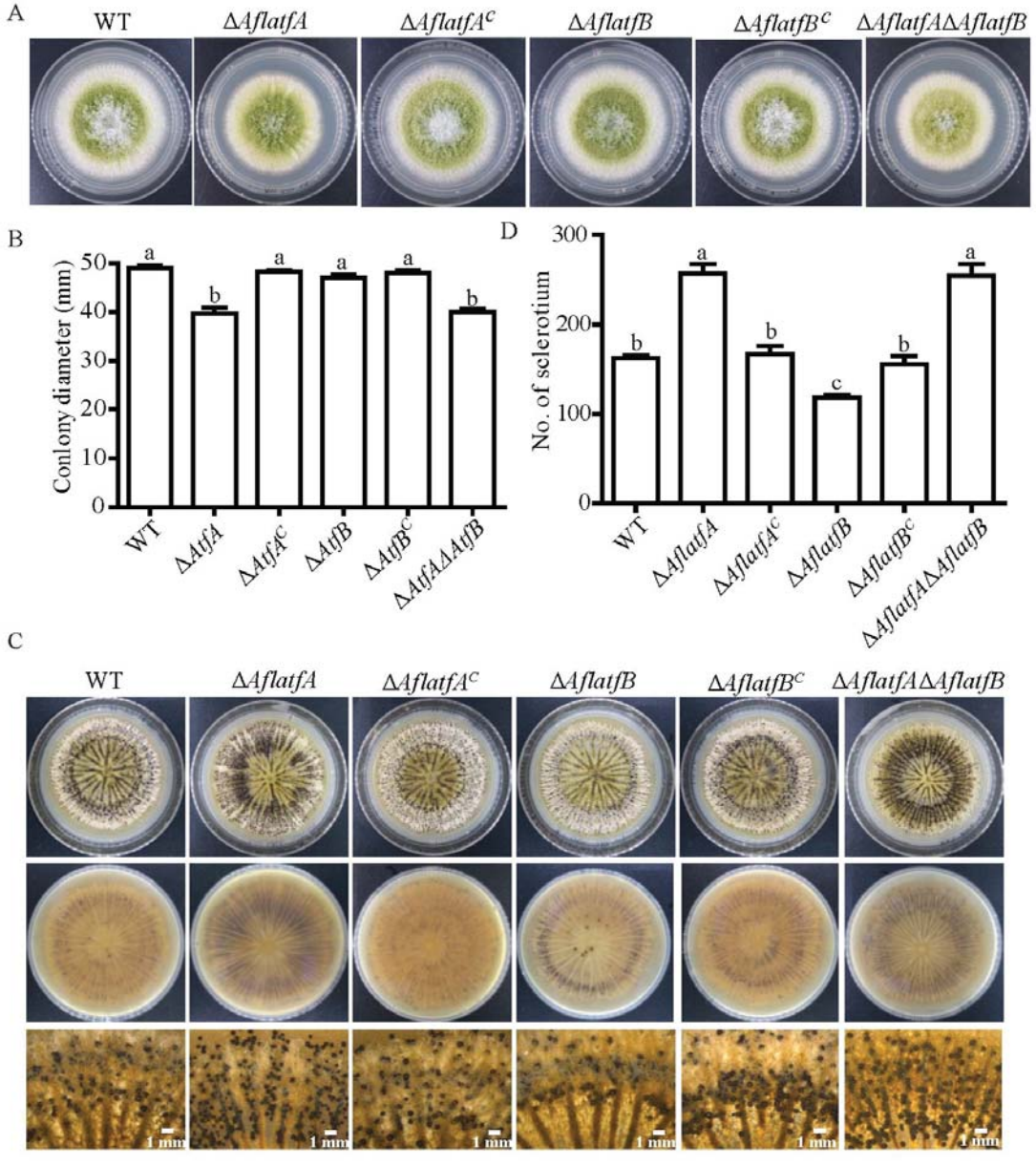

Figure 3. The function of AflatfA and AflatfB on mycelial growth and the production of sclerotia in *Aspergillus flavus*. (**A**) Mycelial growth of wild type, AflatfA and AflatfB mutant strains. Two hundred conidia of WT and mutants were cultured on PDA medium at 29 °C for 5 d. (**B**) Comparison of colony diameter between wild type and mutant strains on the fifth day. (**C**) Visual phenotype of sclerotia produced by wild type, *AflatfA* and *AflatfB* mutants. 10^3 conidia/plate was incubated on Wickerham medium and cultured at 37 °C for 12 d. (**D**) Statistical analysis of sclerotia yield from wild type and mutant strains. Two independent biological experiments were performed with three replicates each time. Error bars represent the standard deviations. The different lowercase letter means that the difference between treatments is significant at $p < 0.05$.

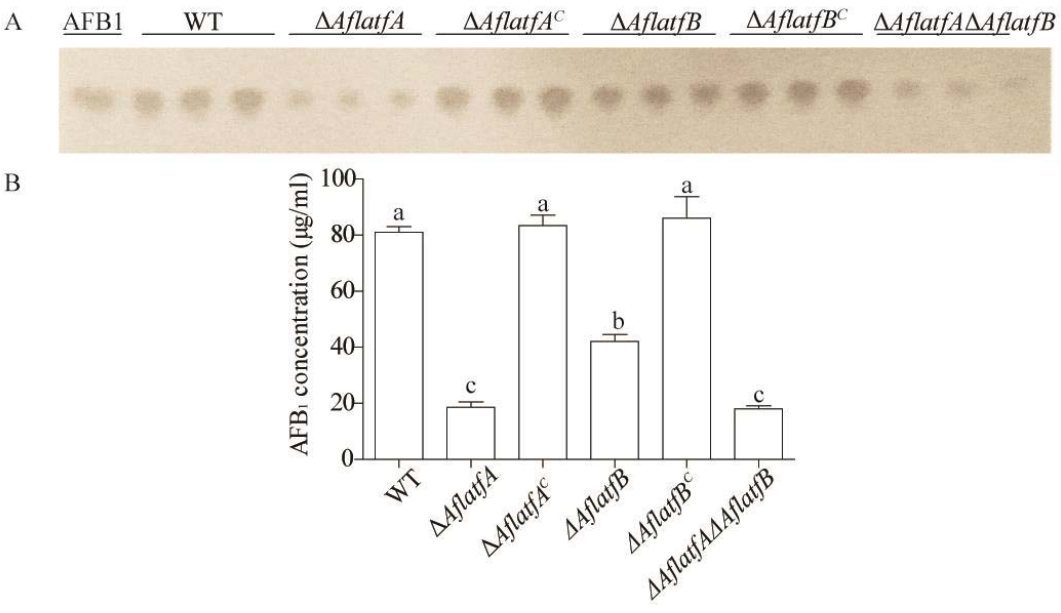

Figure 4. The bZIP transcription factors AflatfA and AflatfB in *Aspergillus flavus* positively regulate the production of aflatoxin B1. (**A**) Thin layer chromatography analysis of aflatoxin B1 produced by wild type, *AflatfA* and *AflatfB* mutant strains on artificial YES medium. AFB1 = aflatoxin B1 standard. (**B**) Statistical analysis of aflatoxins B1 produced by wild type, *AflatfA* and *AflatfB* mutants on YES artificial medium. Two independent biological experiments were performed with three replicates each time. Error bars represent the standard deviations. The different lowercase letter means that the difference is significant at $p < 0.05$.

To study mycelia tolerance to oxidative stress, two hundred spores per strain were inoculated on the 2 mm cellophane plated on the YES medium. After 24 h, the cellophane containing spores were transferred to the YES medium containing 10 mM H_2O_2. As determined by the inhibition rate, Δ*AflatfA* and Δ*AflatfB* strains were more sensitive to H_2O_2 than to the WT strain (Figure 6C,D). Intriguingly, the sensitivity of the Δ*AflatfA*Δ*AflatfB* strain was lower than that of WT. However, there were no differences in inhibition rates among WT, Δ*AflatfA*^{C} and Δ*AflatfB*^{C} strains (Figure 6C,D). Taken together, AflatfA and AflatfB play critical roles in mycelium respose to oxidative stress.

2.7. AflatfA but AflatfB Contributes to Osmotic Stress Response

As is known, bZIP transcription factor AtfA is a target gene that is regulated by the HOG pathway and plays an important role in the response to osmotic stress. To study the function of *AtfA* and *AtfB* homologs in *A. flavus* response to osmotic stress, WT and mutant strains were cultured on a GMM medium containing various osmotic reagents. Without an osmotic reagent, the colony diameter of Δ*AflatfA* and Δ*AflatfA*Δ*AflatfB* strains were smaller than that of the WT strain (Figure 7). Compared to that of WT, the colony diameter of Δ*AflatfA* and Δ*AflatfA*Δ*AflatfB* were significantly increased with 1.5 M NaCl, 1.8 M KCl or 1.4 M Sorbitol (Figure 7). However, there is no difference in colony diameter between Δ*AflatfB* and WT strains with or without osmotic reagents (Figure 7). The above results showed that *AflatfA* but not *AflatfB* regulates the osmotic stress response in *A. flavus*.

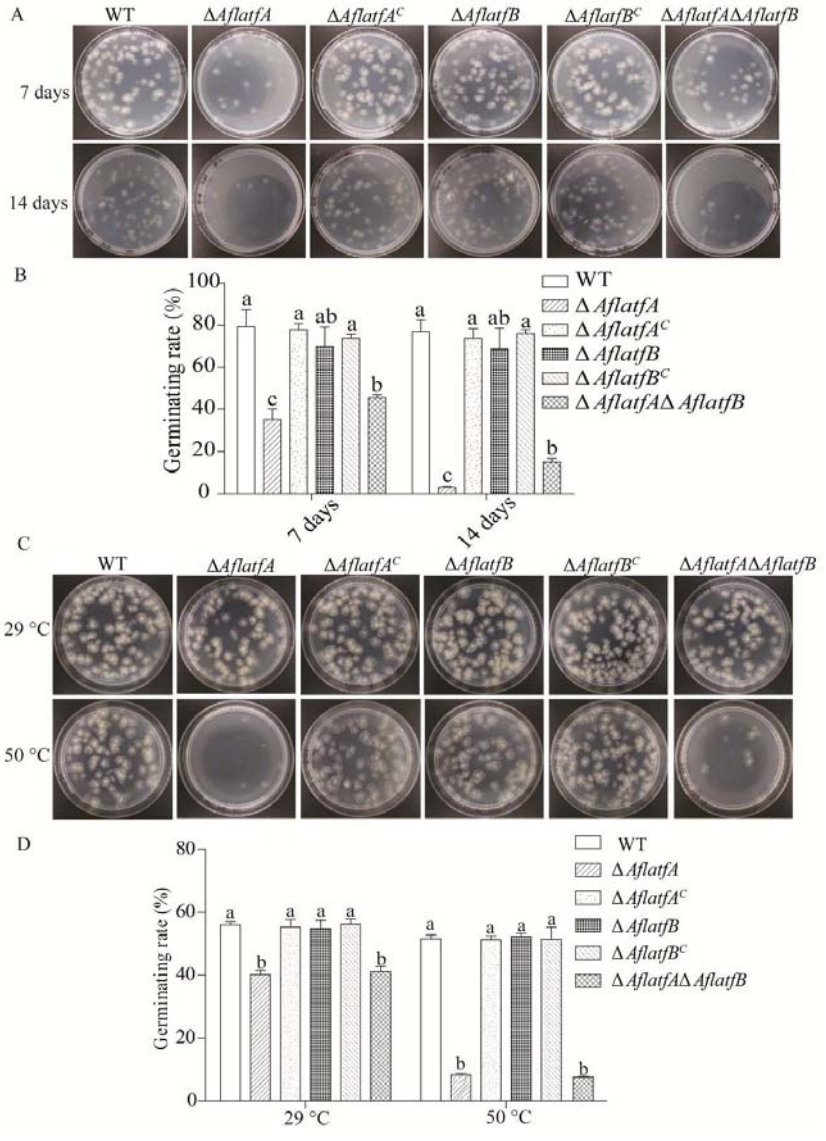

Figure 5. The effect of AflatfA and AflatfB genes on the survival rate of *Aspergillus flavus* stored at 4 °C and treated by high temperature. (**A**) Germination of wild type, *AflatfA* and *AflatfB* mutants after storage at 4 °C for 7 d or 14 d. Two hundred conidia were spread on GMM medium and cultured for 48 h. (**B**) Statistical analysis of survival rates of conidia of wild type and mutant strains after storage at 4 °C for 7 d or 14 d. (**C**) The stress tolerance against heat stress was examined. Conidia suspensions were heated at 55 °C or incubated at 29 °C as control for 1 h. Two hundred conidia were plated onto GMM plates, and visible colonies were counted after incubation at 29 °C for 48 h. (**D**) Statistical analysis of germination rates of conidia after heat treatment. Two independent biological experiments were performed with three replicates each time. Error bars represent the standard deviations. The different lowercase letter means that the difference is significant at $p < 0.05$.

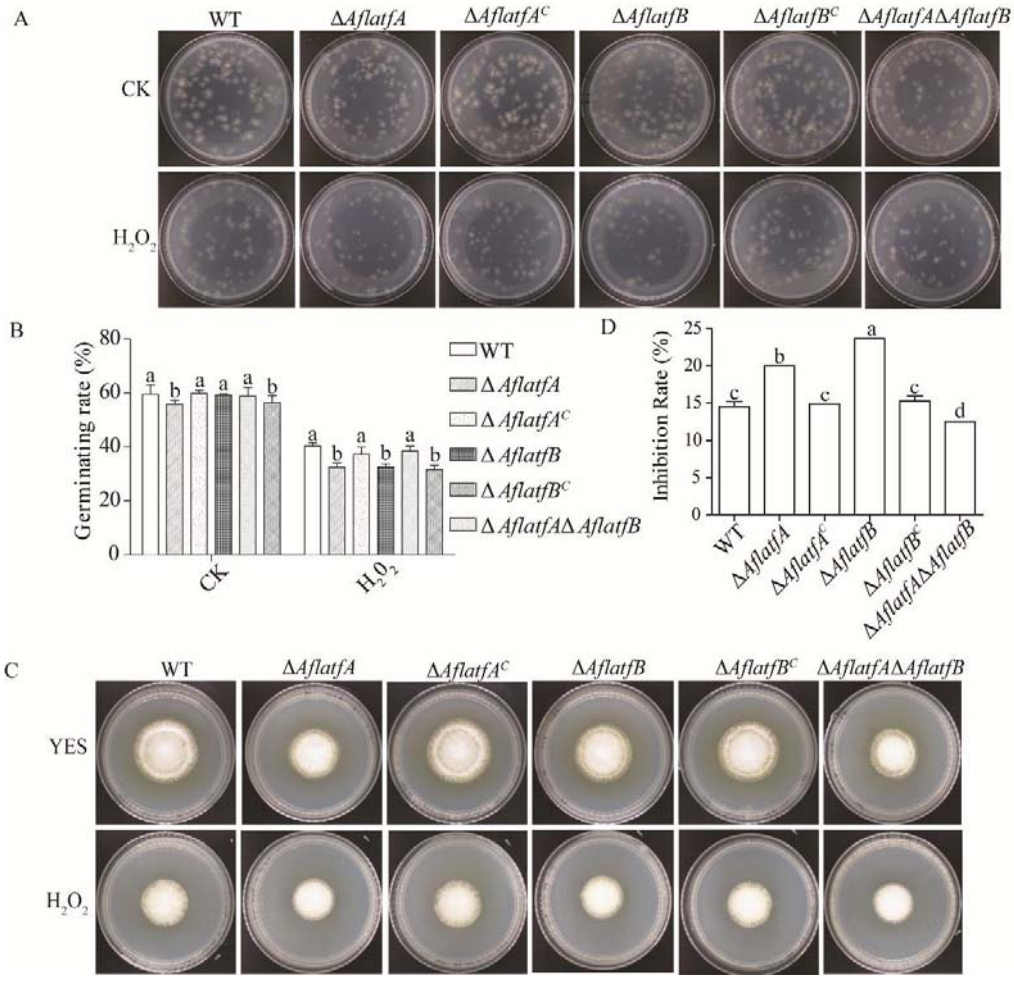

Figure 6. Hypersensitivity of *AflatfA* and *AflatfB* mutants to oxidative stress. (**A**) The stress tolerance of conidia against oxidative stress was examined. Conidia suspensions were incubated at room temperature with 200 mM H_2O_2 for 20 min. Two hundred of conidia were plated onto GMM plates, and visible colonies were counted after incubation at 29 °C for 48 h. (**B**) Statistical analysis of germinating rate of conidia from WT and mutants on YES under oxidative stress. (**C**) The stress tolerance of mycelium against oxidative stress was examined. Equal conidia were pipetted onto cellophane sheets on the YES plates and cultured at 29 °C for 24 h. Mycelial mates with sheets were transferred onto fresh YES plate with or without 10 mM H_2O_2 and cultured at 29 °C for 3 d. (**D**) Statistical analysis of mycelium growth of WT and mutants on YES under oxidative stress. Measurements of growth inhibition rate are relative to growth rate of each untreated control. Two independent biological experiments were performed with three replicates each time. Error bars represent the standard deviations. The different lowercase letter means that the difference is significant at $p < 0.05$.

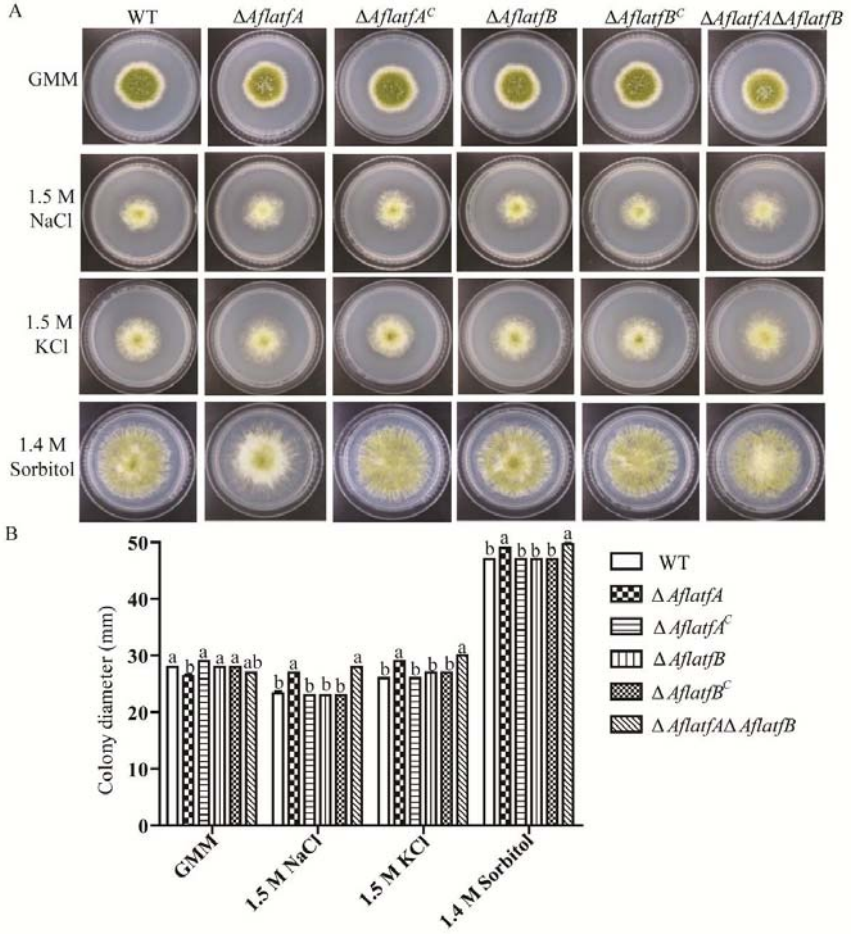

Figure 7. AflatfA response to osmotic stress. (**A**) Mycelia growth of the *A. flavus* wild type and *AflatfA* and *AflatfB* mutants under osmotic stress. Two hundred conidia of *A. flavus* WT and mutants were cultured on GMM media supplemented with or without NaCl (1.5 M), KCl (1.5 M) or Sorbitol (1.4 M) at 29 °C for 5 d. (**B**) Statistical analysis of colony diameter of the testing strains measured on the 5th day. Each treatment included three replicates. Error bars represent the standard deviations. The different lowercase letter means that the difference between treatments is significant at $p < 0.05$.

2.8. Effect of AflatfA and AflatfB on Pathogenicity of A. flavus

We performed topical infection with corn and peanut to examine the effect of *AflatfA* and *AflatfB* on *A. flavus* pathogenicity. After infecting corn and peanut for 5 d, the sporulation and AFB1 yield were estimated and compared among the WT and mutant strains. Compared to the WT strain, Δ*AflatfA* and Δ*AflatfA*Δ*AflatfB* produced less conidia (Figure 8A,B). However, the difference in sporulation was not significant between WT and Δ*aflatfB* (Figure 8A,B). These results indicated that *AflatfA* but not *AflatfB* positively regulates conidia production.

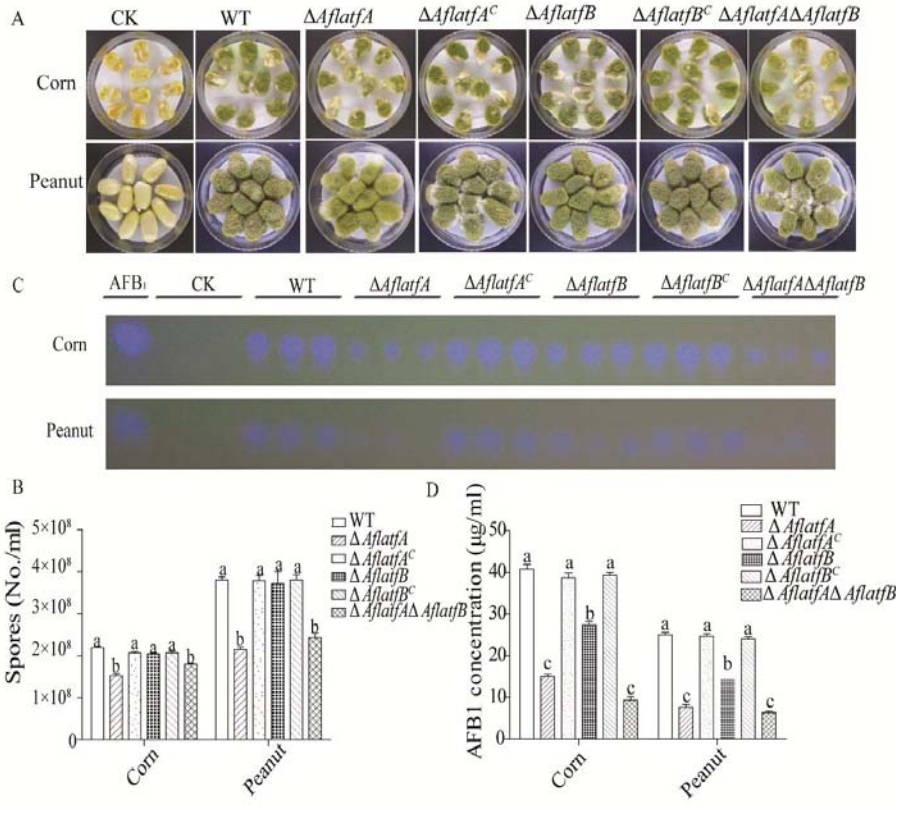

Figure 8. The pathogenicity of *Aspergillus flavus* on peanut and corn is regulated by AflatfA and AflatfB. (**A**) Growth of wild type, *AflatfA* and *AflatfB* mutants on corn and peanut after inoculation for 5 d. (**B**) Statistical analysis of conidia produced by wild type, *AflatfA* and *AflatfB* mutants on corn and peanut. (**C**) Thin layer chromatography analysis of aflatoxins extracted from corn and peanut. AFB1 = aflatoxin B1 standard. (**D**) Statistical analysis of aflatoxin B1 from corn and peanut infected by wild type, *AflatfA* and *AflatfB* mutant strains. Two independent biological experiments were performed with three replicates each time. Error bars represent the standard deviations. The different lowercase letter means that the difference is significant at $p < 0.05$.

The pattern of AFB1 production was not the same as that of sporulation. Relative to the WT and complementary strains, the yield of aflatoxin AFB1, produced by Δ*AflatfA*, Δ*AflatfB* and Δ*AflatfA*Δ*AflatfB* strains, significantly decreased (Figure 8C,D). When comparing AFB1 produced by the deletion strains, we found that the Δ*AflatfB* strain produced the most mycotoxin AFB1, followed by Δ*AflatfA* and Δ*AflatfA*Δ*AflatfB* (Figure 8C). Statistical analysis of AFB1 production showed that there was significant difference between Δ*AflatfA* and Δ*AflatfB* but no significant difference between Δ*AflatfA* and Δ*AflatfA*Δ*AflatfB* (Figure 8D). Thus, *AflatfA* and *AflatfB* are both important for AFB1 production, but *AflatfA* plays a more important role than *AflatfB*.

3. Discussion

Our interest in exploring the function of the CRE/ATF family AflatfA (ortholog Atf1/AtfA) and AflatfB on AFs biosynthesis in *A. flavus* arose from the known functions of Atf1/AtfA in the plant pathogenic fungus *F. graminearum* and AtfB in aflatoxin producer *A. parasiticus* [21,22,45]. In *F. graminearum*, *Fgatf1* deletion leads to the production of

higher amounts of mycotoxins DON and aurofusarin culturing in vitro, whereas Δ*Fgatf1* produced lower amounts of DON during the infection of the head of host wheat [21]. However, using another Δ*Fgatf1* mutant, Jiang et al. (2015) found that DON production was significantly reduced in the wheat head but no change was observed when using autoclaved rice grains cultures [22]. Conversely, in *F. verticillioides*, the regulation of *FvatfA* on the secondary metabolism is complex. *FvatfA* positively regulates the production of antioxidants carotenoids and mycotoxins fumonisin B1 and B2, whereas *FvatfA* deletion results in the yield of the red pigment bikaverin with anticancer and antimicrobial activities and increases without a change to *bik1* expression [19]. Temme et al. (2012) found that *Bcatf1* negatively regulates biosynthesis of secondary metabolites, including botrydial, botryendial and botcinin [17]. Similar to the known AtfA/Atf1 in other plant pathogenic fungi, *AflatfA* in *A. flavus* mediates AFB1 production. In contrast to the regulation of DON by *Fgatf1* in *F. graminearum* related with the host type and artificial medium [21,22], regulation of AflatfA on AFB1 production is independent on culture substrates, and the Δ*AflatfA* strain produced decreased AFB1 not only on the YES medium but also on host plants such as peanut and maize. Similar to the lesser amounts of the antioxidants carotenoids and mycotoxins fumonisin B1 and B2 produced by the *FvatfA* deletion strain [19], *AflatfA* deletion led to a decline in the AFB1 yield from the artificial medium and the host peanut and maize in this study. Zhao et al. (2022) found Δ*AtfA* produces reduced AFB1 on an artificial medium in *A. flavus* NRRL3357 [58]. Based on the above result, we speculate that AflatfA might bring about AFB1 production change by positively regulating AFB1 biosynthesis genes. The various functions of AftA/Atf1 orthologs from different fungi suggest that the role of AtfA/Atf1 in regulating fungal secondary metabolism is conserved but the regulation mechanism is divergent. However, there are fewer reports on the effect of AtfB, another member of the CRE/ATF family on secondary metabolism. In *A. flavus*, AtfB could down-regulate AFs biosynthesis at the transcription level analysis under inhibition condition of AFs biosynthesis [54,56,57]. Consistent with transcription level analysis, deletion of AtfB encoded by *A. flavus* genome results in a decline of AFB1 from an artificial medium [58]. In this study, we found the *AflatfB* deletion results in a decline in AFB1 yield in both the artificial medium and the host peanut and maize. Interestingly, the AtfB ortholog positively regulates AFB1 biosynthetic genes by binding the promoters that carry a CRE motif, and the five nucleotides immediately upstream from CRE1, AGCC(G/C) in *A. parasiticus* [44]. The AtfB protein sequence from *A. parasiticus* shares 96% of its identity with the amino acid sequence of *A. flavus* AtfB, suggesting that AtfB may directly bind the promoter of AFs biosynthesis [45]. In this study, AftA/Atf1 and AtfB orthologs from *A. flavus* both regulate AFB1 biosynthesis; however, AtfA develops a greater effect, when comparing the AFB1 yield of Δ*AflatfA*, Δ*AflatfB* and Δ*AflatfA*Δ*AflatfB* strains.

In various of fungi, AtfA/Atf1 and AtfB from the ATF/CREB family of bZIP transcription factors were found to couple biosynthesis of secondary metabolites with the stress response of fungi, such as *AtfA* in *A. nidulans* and AtfB in *A. parasiticus* [25,28,29,45]. The conidia of Δ*AflatfA*, Δ*AflatfB* and Δ*AflatfA*Δ*AflatfB* were more sensitive to H_2O_2, which is similar to AtfA in *S. pombe*, *A. oryzae*, *A. nidulans*, *A. fumigatus* and *M. oryzae* [11,18,26,27,43]. The abovementioned data indicated that *AtfA* and *AtfB* orthologs may have a conserved role in regulating the response of conidia to oxidative stress. Analysis of mycelium sensitivity to oxidative stress reveals that Δ*AflatfA* and Δ*AflatfB* strains are more sensitive to H_2O_2 than WT, and the sensitivity of Δ*AflatfB* strains to H_2O_2 is higher than Δ*AflatfA*. Therefore, AtfA and AtfB both positively regulate the oxidative stress response in fungal mycelium. Intriguingly, double deletion of *AflatfA* and *AflatfB* results in more tolerance to H_2O_2 in comparison with WT. We assume that the other regulators are activated after double deletion of *AflatfA* and *AflatfB*. When conidia were inoculated on a medium containing the oxidative agent H_2O_2, Δ*AflatfA* and Δ*AflatfB* strains are both more sensitive to oxidative stress than WT [58], as was reported in *M.* oryzae, *F. graminearum* and *F. verticillioide* [18,19,21,22], but contrary to what was reported in *A. oryzae* and *A. nidulans* [16,25,28,29]. In addition, Atf1/AtfA homologs in *P. marneffei*, *V. dahliae* and *B. cinerea* have no effect on oxidative

stress (H_2O_2) [17,23,31], but *atfA* in *P. marneffei* participates in oxidative stress (tBOOH) [31]. We deduce that the function of *atfA* in response to oxidative stress is related with not only species but also agent type. Thus, AflatfA and AflatfB have a positive oxidative stress response.

In the model filamentous fungus *A. nidulans*, the AtfA transcription factor interacts with the Sak/HogA MAPK and regulates various stress responses [28]. As the target gene of the Sak/HogA pathway, Atf1/AtfA orthoglogs mediate osmotic stress response in several fungi, including *S. pombe*, *A. nidulans*, *A. fumigatus* and *F. graminearum* [5,21,22,26,27]. However, Zhao et al. (2022) found that AtfA has no impact on the osmotic stress response in *A. flavus* strain NRRL 3357 [58]. Contrast to reported *AtfA* in *A. flavus*, we found that *AflatfA*, but not *AflatfB*, is involved in the response to osmotic stress in this study. Different recipient strain, osmotic reagents and selection marker RFP protein result in different effects of *AftA* on the osmotic stress response between this study and the previous study [58]. However, unlike the more sensitive to osmotic stress agents in above reported fungi, the *A. flavus* Δ*AflatfA* strain is more tolerant to NaCl, KCl and Sorbitol. It is noticeable that the osmotic stress response is not regulated by *Bcatf1* in *B. cinerea* [17]. Consequently, the osmotic stress sensing of Atf1/AtfA may demonstrate that AtfA/Atf1 may be not conserved in the osmotic stress response in fungi, and the regulatory mechanism is species-specific. The tolerance of *AflatfA* and *AflatfB* double mutant was increased to NaCl, KCl and Sorbitol, which is same to that of Δ*AflatfA* mutant, indicating that *AflatfA* and *AflatfB* may have no overlapping function in response to osmotic stress. Moreover, deletion of *AflatfA*, but not *AflatfB*, resulted in higher sensitivity to heat stress in *A. flavus*, which is similar to that in *S. pombe*, *C. neoformans*, *A. nidulans* and *A. fumigatus* [11,26,27,30,59]. Meanwhile, we found that the change trend of sensitivity to theΔ*AflatfA*Δ*AflatfB* strain to heat stress is the same as that of the Δ*AflatfA* mutant, suggesting that the response to heat stress is not regulated by *AflatfB*. Moreover, as the incubation time increases at 4 °C, the viability of conidia from the Δ*AflatfA* mutant dramatically decreased in *A. flavus* in comparison with WT, which is similar to *A. fumigatus* [27]. However, the phenomenon is not observed in the Δ*AflatfB* mutant. Interestingly, the germination rate of the Δ*AflatfA*Δ*AflatfB* mutant is higher than that of the Δ*AflatfA* mutant, but lower than that of WT. Thus, in fungi, the transcription factor *AtfA*, but not *AtfB*, might play a central role in temperature stress responses.

In fission yeast and filamentous fungi, *Atf1/AtfA* orthologs mediate vegetative growth and sexual and asexual development of fungi. Firstly, AflatfA contributes to the colony growth in *A. flavus*. Although Atf1/AtfA is conserved in the effects on radial growth, differences exist among fungi. In contrast to the moderate radial growth in *A. nidulans* [25,29], the lack of *Atf1/AtfA* led to a decreased colony diameter not only of *A. flavus* in this study on PDA and MM [58], but also of *S. pombe*, *F. verticillioides* and *M. oryzae* in previous studies [6,18,19]. Nevertheless, the lack of *AtfB* as an *AtfA* paralogous gene showed no obvious change of colony diameter on PDA compared to WT in this study; however, deletion of *AflatfB* brought about a decreased colony diameter in *A. flavus* NRRL3357 [58], suggesting that the effect of AtfB on vegetative growth is related with the medium type. Noticeably, we observed that the change trend in radial growth of the Δ*AflatfA*Δ*AflatfB* strain is the same as that of Δ*AflatfA* but not Δ*AflatfB*. Therefore, AflatfA and AflatfB both regulate colony growth, but the mechanism is complex. Moreover, similar to how the deletion of Atf1/AtfA homologous genes resulted in dramatically less conidia in fungi *A. nidulans*, *B. cinerea* and *V. dahliae* on an artificial medium [17,23,25,29], the Δ*AflatfA* mutant has a defect in conidia production not only on the artificial medium MM [58], but also on host plants such as corn and peanut in this study. A further study revealed that the germination ratio of the conidia of Δ*AflatfA* had declined. The deletion of the *AflatfB* gene showed no change to conidia production and the germination ratio of conidia, whereas the change trend of conidia production and its germination ratio of Δ*AflatfA*Δ*AflatfB* is similar to that of the Δ*AflatfA* mutant. The loss of *AflatfA* results in a strongly increased production of sclerotia in *A. flavus*. However, deletion of *AtfA* in *A. flavus* NRRL 3357 results in no sclerotia formation [58]. Conversely, the formation of sclerotia is both damaged in the

Δ*Cpatf1* mutant of *C. purpurea* and in the Δ*Bcatf1* mutant of *B. cinerea* [17,24]. Therefore, Atf1/AtfA orthologs of fungi play an important role in regulation of sclerotia formation, but the specific regulatory mechanism is dependent on the species and strain. Similar to the reported *AtfB* in a previous study [58], we reported that AtfB positively regulates the sclerotia formation in *A. flavus*. In contrast to the impact of *AflatfA* on sclerotia formation, the Δ*AflatfB* mutant showed defects in sclerotia formation. Interestingly, as with single deletion of *AflatfA*, the double deletion of *AflatfA*/*AflatfB* brought about an increased production of sclerotia. Thus, it can be seen that AflatfA plays an opposite role to *AflatfB* in the regulation of sclerotia formation, and the function of *AflatfA* is decisive, which is similar to Atf1/AtfA orthologs in *S. pombe*, *A. nidulans*, *F. verticillioides* and *M. oryzae* [6,18,19,25,29]. Thus, it can be seen that AflatfA involves mycelium growth, conidia germination and sclerotia formation, whereas AflatfB only the regulates sclerotia formation.

4. Materials and Methods

4.1. Fungal Strains and Culturing Conditions

A. flavus strains listed in Table 1 were used or generated in this study. The Czapek–Dox Medium supplemented with 10 mM uridine and 10 mM uracil as needed was used to construct the mutants. For spore collection or RNA and DNA extraction, strains were cultured on PDA at 37 °C for 5 d or 29 °C for 48 h. To assess the colony and growth characteristics, both WT strain and mutants were maintained on YES or GMM with or without different chemical agents for 5 d at 29 °C in dark. As for the oxidative stress conditions, mycelium sensitivity to oxidative agents was measured by YES media supplemented with 10 mM H_2O_2. To observe the vegetative growth under osmotic stress conditions, the strains were inoculated on GMM containing 1.5 M NaCl, 1.5 M KCl or 1.4 M Sorbitol, and then the colony diameters were measured after 5 d. The sensitivity to temperature stress was analyzed on GMM after spores were treated by different temperatures. All strains as glycerol stocks were maintained at −80 °C.

Table 1. Fungal strains used in this study.

Strain	Description	Reference
Recipient strain	PTSΔ*ku70*Δ*pyrG*	[60]
wild type (WT)	*PTS*Δ*ku70*Δ*pyrG::AfpyrG*	[60]
Δ*AflatfA*	Δ*ku70*Δ*pyrG*Δ*AflatfA::pyrG*	This study
Δ*AflatfB*	Δ*ku70*Δ*pyrG*Δ*AflatfB::pyrG*	This study
Δ*AflatfA*^{C}	Δ*ku70*Δ*pyrG*Δ*AflatfA::pyrG*, *AflatfA::pyrG*	This study
Δ*AflatfB*^{C}	Δ*ku70*Δ*pyrG*Δ*AflatfB::pyrG*, *AflatfB::pyrG*	This study
Δ*AflatfA*Δ*AflatfB*	Δ*ku70*Δ*pyrG*Δ*AflatfA::pyrG*Δ*AflatfB::ptrA*	This study

4.2. Identification, Gene Composition and Phylogentic Analysis of AflatfA and AflatfB

The protein sequence of AtfA (GeneID: 5991817, locus tag: AO0900003000685; Accession no.: XP_001824132) and AtfB (GeneID: 5996391, locus tag: AO090120000418, Accession no.: XP_001824132) from *A. oryzae* as the query were used to perform BLAST search to find the homologous genes in *A. flavus*. The AtfA and AtfB gene CDS region and upstream and downstream 2000 bp were loaded from the NCBI database. Then, the sequences were submitted to softberry web server, and the gene composition and protein sequence were re-predicted. We used the InterProScan 5 on EBI web server to predict the protein domain, including Atf1 from *S. pombe* (accession no. BAA09841.1), AoatfA from *A. oryzae* (accession no. XP_001819834.1), AfatfA from *A. fumigatus* (accession no. XP_754486.2), AtfA from *A. terreus* (accession no. EAU35111.1), AnAtfA from *A. nidulans* (accession no. ANN75015.1), PmAtfA from *T. marneffei* (accession no. KFX50645.1), ATF-1 from *N. crassa* (accession no. KFX50645.1), VdATF-1 from *V. dahliae* (accession no. XP_009621680.1), CPTF1 from *C. purpurea* (accession no. CCE33955.1), FgATF1 from *F. graminearum* (accession no. XP_011319081.1), MoATF1 from *M. oryzae* (accession no. ELQ67298.1) and Bcatf1 from *B. cinerea* (accession no. XP_024550682.1). The domains were visualized using IBS software.

The protein sequences of AtfA homologous from fungi functionally verified by experiments were aligned with AtfA from *A. flavus* with Clustal X 2.0. A maximum likelihood tree was generated using a JTT Matrix model with 1000 replicates for bootstrapping by MEGA X software [61].

4.3. RNA Isolation and Reverse-Transcription PCR of AflatfA and AflatfB

A. flavus WT, Δ*AflatfA* and Δ*AflatfB* strains were inoculated on cellophane sheets laid on the PDA plates and cultured on media at 29 °C, and then the mycelia were harvested after 36 h. Then, total RNA was extracted using TRIzol Reagent, and DNA was digested with RNase-free DNase I. Subsequently, RNA was reverse transcribed into first-strand cDNA using the RevertAid First Strand cDNA Synthesis Kit (ThermoFisher Scientific, Waltham, MA, USA). To explore the transcription levels between the *AflatfA* and *AflatfB* genes, the sequence of the gene coding region was amplified using pairs 031340RT and 94010RT. The house-keeping gene actin was used as the internal control. The sequence of primers are listed in Table S1.

4.4. Gene Deletion and Complementation of AflatfA and AflatfB

For constructing the *AflatfA* and *AflatfB* genes replacement, 1.1-kb upstream and 1.1-kb downstream fragments of a part of *AflatfA* and 1.1-kb upstream and 1.1-kb downstream fragments of a part of *AflatfB* were amplified from *A. flavus* genomic DNA, respectively. Meanwhile, the orotidine-5′-monophosphate decarboxylase (*pyrG*) gene was amplified from *A. fumigatus* gDNA. Then, the two flanking sequences of *AflatfA* and *pyrG* were joined together by overlap PCR with the primer pairs 31340 5F/F and 31340 3F/R, and the two flanking sequences of *AflAtfB* and *pyrG* were joined together by overlap PCR with the primer pairs 094010 5F/F and 094010 3F/R. Then, both approximately 3.8-kb segments were purified and transformed into the *A. flavus* recipient strain,. To construct the double deletion mutant, the gene knockout cassette comprising 2-kb of upstream and downstream fragments of *AflatfB* and a 1.8 kb of *ptrA* gene was generated by fusion PCR. Subsequently, the purified fragment was transformed into the *A. flavus* Δ*AflatfA* strain. To generate the complementation of the *AflatfA* and *AflatfB* mutants, the fragment of the ORF and its downstream and upstream flanking sequences of *AflAtfA* and *AflAtfB* were amplified and transformed into Δ*AflatfA* and Δ*AflatfB* strains, respectively. Then, the putative mutants were selected after being cultured on YGT containing 5-fluoroorotic acid (5-FOA) at 37 °C for 5 d. Subsequently, 1.0-kb fragment containing 500 bp terminator and its upstream 500 bp and 1.0-kb downstream fragments of the terminator were amplified from *A. flavus* genomic DNA. Then, two flanking sequences were fused with the *pyrG* gene amplified from *A. fumigatus* genomic DNA. At last, two purified segments were transformed into the Δ*ku70*Δ*pyrG*Δ*AflatfA*::*pyrG*, *AflatfA* strain and the Δ*ku70*Δ*pyrG*Δ*AflatfB*::*pyrG*, *AflatfB* strain to generate the complementation of the *AflatfA* and *AflatfB* deletion mutants. The preparation of *A. flavus* protoplasts and fungal transformation were both performed as the described method in the reference [62]. All mutants were firstly verified using diagnostic PCR with primers inside and outside the corresponding gene (Table S1). Then, Southern blot was used to further verify the disruption strains.

4.5. Observation of Developmental Phenotype

To observe the radial colony growth, wild type and mutants were inoculated on PDA for 5 d at 29 °C. Conidia were harvested from 5-day-old colonies grown on PDA in 5 mL of distilled water containing 0.1% Tween 80, and then conidia were counted using a hemocytometer. Then, two hundred freshly grown conidia suspended in 2 μL 0.1% Tween 80 were inoculated. After 5 d, the colony diameters were measured, and the pictures were taken at the same time. To investigate the sclerotia production, 10^4 fresh conidia (5 d) suspended in 2 μL 0.1% Tween 80 were spotted on modified Wickham medium plates. The plates were incubated in the dark at 37 °C for 12 d. To help the enumeration of sclerotia, 70% ethanol was used to kill and wash away conidia. Then, seven 7 mm-diameter agar plugs

were taken from each plate, and the number of sclerotia was counted. Three biological replicates were included in each treatment, and whole experiment was repeated two times.

4.6. Oxidative Stress Bioassay

For the oxidative stress response assay of *A. flavus* conidia, 2 M H_2O_2 was added to conidia suspensions (H_2O_2 final concentration 100 mM and 200 mM respectively). The suspensions were immediately diluted to 10^5 conidia/mL after 20 min of incubation at room temperature. In total, 200 spores suspended in 100 μL 0.01% Tween 80 were spread onto GMM agar plates, and were incubated at 29 °C for 48 h. Then, the number of colonies were counted, and the germinating rate was calculated. To test the H_2O_2-sensitivity of *A. flavus* mycelia, fresh conidia (5 d) were pipetted onto cellophane sheets (circle-shaped, 2-cm-diameter) laid on the YES agar plates and cultured for 24 h in the dark. Mycelial mates with sheets were transferred onto fresh YES or YES supplemented with 10 mM H_2O_2. Then, all plates were incubated at 29 °C, and the colony diameters were measured after being incubated for two to three days. All treatments included three replicates, and whole experiments were repeated two times.

4.7. Osmotic Stress Bioassay

To investigate the osmotic stress sensitivity of all mutants, the osmotic reagents NaCl, KCl and Sorbitol were chosen and added into the GMM medium. The concentration of osmotic reagents was as follows: 1.5 M NaCl, 1.5 M KCl or 1.4 M Sorbitol. Two hundred conidia were suspended in 2 μL 0.01% Tween 80 and spotted onto GMM plates with or without the abovementioned concentration reagents. All plates were incubated at 29 °C in dark for 5 d. From the second day to the fifth day, the colony diameters were measured. All treatments included three replicates, and whole experiments were repeated two times.

4.8. Temperature Treatment Assay

Conidia suspension of each strain was diluted to 10^5 conidia/mL for the heat stress assay and the survival rate of the conidia upon incubation at the 4 °C assay. To analyze the heat stress response, 200 μL diluted conidia suspensions from each strain in 1.5 mL tube were incubated on block heaters at 50 °C for 1 h. Then, the tubes were immediately transferred and cooled on ice. The conidia were diluted to 2×10^3 conidia/mL, and 100 μL conidia suspension was transferred and spread onto the GMM medium. After incubation at 29 °C in the dark for 48 h, the number of colonies was counted. Conidia without heat stress treatment were used as control. The germinating rate of conidia were calculated. To test the viability during preservation at 4 °C, the diluted suspensions (200 μL) from each strain were kept at 4 °C for 7 d and 14 d. As per the above description, the survival rates were calculated. All treatments included three replicates, and whole experiments were repeated two times.

4.9. Aflatoxin B1 Production Analysis

To measure the aflatoxin B1 production in vitro, 200 spores of WT, *AflatfA* and *AflatfB* mutant strains were spotted on a plate (Φ = 60 mm) containing 10 mL artificial YES medium (15% sucrose, 2% yeast extract, and 1% soytone), and cultured at 29 °C. After 5 d, six 7-mm-diameter agar plugs were taken from each plate, and transferred to an Eppendorf tube. Then, 3 mL dichloroethane was added into each plate, which were then sonicated for 1 h at room temperature. In total, 2 mL of extract was transferred to a new Eppendorf tube, and dried completely at room temperature. A total of 50 μL dichloroethane was used to suspend the dry extract, and 5 μL AFB1 standard (1 mg/mL) and extract were applied to TLC plates for analysis. A dichloroethane: acetone (90: 10, vol/vol) solvent system was used to develop TLC plates, and the bands were visualized under 254 nm light.

4.10. Virulence Assays on Corn and Peanut

The infection experiments of corn and peanut were mainly performed as per the method invented by Chang et al. [63]. The following steps were modified. The eight seeds as a group were placed onto a Petri dish plate (Φ = 60 mm). Subsequently, a suspension of 3000 freshly harvested conidia in 3 μL of WT and all mutants were inoculated onto the surface of each seed. The seeds were spotted with 3 μL 0.01% Tween 80 solution as the controls. All seeds from each plate were transferred to tubes, and 10 mL of the 0.02% Triton-X 100 water was added into each tube. After being vortexed vigorously for 2 min to dislodge conidia, 500 μL suspension from each tube was used to count conidia using a hemocytometer, and the rest of the suspension was extracted with 8 mL dichloroethane. Subsequently, the extracts were shaken at 180 rpm/min for 30 min, and 5 mL extracts from every tube were transferred to a new tube. After being dried completely at room temperature, the extracts were resuspended in 100 μL dichloroethane. In total, 5 μL AFB1 standard (1 mg/mL) and extracts from each tube were applied to the TLC plates, respectively. The dichloroethane: acetone (90: 10, vol/vol) solvent system was used to develop the TLC plates, and TLC plates were visualized under 254 nm light.

4.11. Statistical Analysis

For statistical analysis, data were analyzed using the GraphPad Instat software package, version 5.01 (GraphPad software Inc.), according to the Tukey–Kramer multiple comparison test at $p < 0.05$. The different letters indicate the significant difference between data.

Supplementary Materials: The following supporting information can be downloaded at: https://www.mdpi.com/article/10.3390/toxins14120857/s1, Table S1: PCR primers used in this study, Figure S1: Construction stratgy of AflatfA and AflatfB double knock mutant.

Author Contributions: Conceptualization, S.W. and X.W.; methodology, X.W. and W.Z.; validation, X.W., W.Z. and B.Y.; formal analysis, X.W. and W.Z.; investigation, W.Z., B.Y. and L.Y.; resources, X.W., W.Z., B.Y. and L.Y.; data curation, W.Z., B.Y. and L.Y.; writing—original draft preparation, X.W.; writing—review and editing, X.W. and S.W.; visualization, X.W. and W.Z.; supervision, S.W.; project administration, X.W.; funding acquisition, X.W. All authors have read and agreed to the published version of the manuscript.

Funding: This research was funded by the National Natural Science Foundation of China, 31800040 and the Natural Science Foundation of Fujian Province, 2017J05044.

Institutional Review Board Statement: Not applicable.

Informed Consent Statement: Not applicable.

Conflicts of Interest: The authors declare no conflict of interest.

References

1. Brakhage, A.A. Regulation of fungal secondary metabolism. *Nat. Rev. Microbiol.* **2013**, *11*, 21–32. [CrossRef] [PubMed]
2. Leiter, É.; Emri, T.; Pákozdi, K.; Hornok, L.; Pócsi, I. The impact of bZIP Atf1 ortholog global regulators in fungi. *Appl. Microbiol. Biotechnol.* **2021**, *105*, 5769–5783. [CrossRef] [PubMed]
3. Amoutzias, G.D.; Veron, A.S.; Weiner, J.; Robinson-Rechavi, M.; Bornberg-Bauer, E.; Oliver, S.G.; Robertson, D.L. One billion years of bZIP transcription factor evolution: Conservation and change in dimerization and DNA-binding site specificity. *Mol. Biol. Evol.* **2007**, *24*, 827–835. [CrossRef] [PubMed]
4. Wilkinson, M.G.; Samuels, M.; Takeda, T.; Toone, W.M.; Shieh, J.C.; Toda, T.; Millar, J.B.; Jones, N. The Atf1 transcription factor is a target for the Sty1 stress-activated MAP kinase pathway in fission yeast. *Genes Dev.* **1996**, *10*, 2289–2301. [CrossRef] [PubMed]
5. Shiozaki, K.; Russell, P. Conjugation, meiosis, and the osmotic stress response are regulated by Spc1 kinase through Atf1 transcription factor in fission yeast. *Genes Dev.* **1996**, *10*, 2276–2288. [CrossRef]
6. Takeda, T.; Toda, T.; Kominami, K.; Kohnosu, A.; Yanagida, M.; Jones, N. *Schizosaccharomyces pombe* atf1+ encodes a transcription factor required for sexual development and entry into stationary phase. *EMBO J.* **1995**, *14*, 6193–6208. [CrossRef]
7. Watanabe, Y.; Yamamoto, M. *Schizosaccharomyces pombe* pcr1+ encodes a CREB/ATF protein involved in regulation of gene expression for sexual development. *Mol. Cell. Biol.* **1996**, *16*, 704–711. [CrossRef]

8. Kon, N.M.; Krawchuk, D.; Warren, B.G.; Smith, G.R.; Wahls, W.P. Transcription factor Mts1/Mts2 (Atf1/Pcr1, Gad7/Pcr1) activates the M26 meiotic recombination hotspot in *Schizosaccharomyces pombe*. *Proc. Natl. Acad. Sci. USA* **1997**, *94*, 13765–13770. [CrossRef]
9. Koda, W.; Senmatsu, S.; Abe, T.; Hoffman, C.S.; Hirota, K. Reciprocal stabilization of transcription factor binding integrates two signaling pathways to regulate fission yeast fbp1 transcription. *Nucleic Acids Res.* **2021**, *49*, 9809–9820. [CrossRef]
10. Nickels, J.F.; Della-Rosa, M.E.; Goyeneche, I.M.; Charlton, S.J.; Sneppen, K.; Thon, G. The transcription factor Atf1 lowers the transition barrier for nucleosome-mediated establishment of heterochromatin. *Cell Rep.* **2022**, *39*, 110828. [CrossRef]
11. Sansó, M.; Gogol, M.; Ayté, J.; Seidel, C.; Hidalgo, E. Transcription factors Pcr1 and Atf1 have distinct roles in stress- and Sty1-dependent gene regulation. *Eukaryot. Cell* **2008**, *7*, 826–835. [CrossRef]
12. Bandyopadhyay, S.; Ghosh, P.M.; Basu, S.; Paul, M.; Alam, S.B.; Das, E.; Sundaram, G. Antagonistic regulation of cyclin expression by the bZIP transcription factors Pcr1 and Atf1 during G2/M transition. *FEMS Microbiol. Lett.* **2017**, *364*, 14. [CrossRef] [PubMed]
13. Lawrence, C.L.; Jones, N.; Wilkinson, C.R. Stress-induced phosphorylation of *S. pombe* Atf1 abrogates its interaction with F box protein Fbh1. *Curr. Biol.* **2009**, *19*, 1907–1911. [PubMed]
14. García, P.; Paulo, E.; Gao, J.; Wahls, W.P.; Ayté, J.; Lowy, E.; Hidalog, E. Binding of the transcription factor Atf1 to promoters serves as a barrier to phase nucleosome arrays and avoid cryptic transcription. *Nucleic Acids Res.* **2014**, *42*, 10351–10359. [CrossRef] [PubMed]
15. Hagiwara, D.; Takahashi, H.; Kusuya, Y.; Kawamoto, S.; Kamei, K.; Gonoi, T. Comparative transcriptome analysis revealing dormant conidia and germination associated genes in *Aspergillus* species: An essential role for *AtfA* in conidial dormancy. *BMC Genom.* **2016**, *17*, 358. [CrossRef]
16. Sakamot, K.; Iwashita, K.; Yamada, O.; Kobayashi, K.; Mizuno, A.; Akita, O.; Mikami, S.; Shimoi, H.; Gomi, K. *Aspergillus oryzae* atfA controls conidial germination and stress tolerance. *Fungal Genet. Biol.* **2009**, *46*, 887–897. [CrossRef]
17. Temme, N.; Oeser, B.; Massaroli, M.; Heller, J.; Simon, A.; Collado, I.G.; Viaud, M.; Tudzynski, P. BcAtf1, a global regulator, controls various differentiation processes and phytotoxin production in *Botrytis cinerea*. *Mol. Plant Pathol.* **2012**, *13*, 704–718. [CrossRef]
18. Guo, M.; Guo, W.; Chen, Y.; Dong, S.; Zhang, X.; Zhang, X.; Zhang, H.; Song, W.; Wang, W.; Wang, Q.; et al. The basic leucine zipper transcription factor Moatf1 mediates oxidative stress responses and is necessary for full virulence of the rice blast fungus *Magnaporthe oryzae*. *Mol. Plant Microbe Interact.* **2010**, *23*, 1053–1068. [CrossRef]
19. Szabó, Z.; Pákozdi, K.; Murvai, K.; Pusztahelyi, T.; Kecskeméti, Á.; Gáspár, A.; Logrieco, A.F.; Emri, T.; Ádám, A.L.; Leiter, É.; et al. FvatfA regulates growth, stress tolerance as well as mycotoxin and pigment productions in *Fusarium verticillioides*. *Appl. Microbiol. Biotechnol.* **2020**, *104*, 7879–7899. [CrossRef]
20. Colot, H.V.; Park, G.; Turner, G.E.; Ringelberg, C.; Crew, C.M.; Litvnkova, L.; Weiss, R.L.; Borkovich, K.A.; Duanlap, J.C. A high-throughput gene knockout procedure for *Neurospora* reveals functions for multiple transcription factors. *Proc. Natl. Acad. Sci. USA* **2006**, *103*, 10352–10357. [CrossRef]
21. Nguyen, T.V.; Kröger, C.; Bönnighausen, J.; Schäfer, W.; Jörg, B. The ATF/CREB transcription factor Atf1 is essential for full virulence, deoxynivalenol production, and stress tolerance in the cereal pathogen *Fusarium graminearum*. *Mol. Plant Microbe Interact.* **2013**, *26*, 1378–1394. [CrossRef] [PubMed]
22. Jiang, C.; Zhang, S.; Zhang, Q.; Tao, Y.; Wang, C.; Xu, J. FgSKN7 and FgATF1 have overlapping functions in ascosporogenesis, pathogenesis and stress responses in *Fusarium graminearum*. *Environ. Microbiol.* **2015**, *17*, 1245–1260. [CrossRef]
23. Fang, Y.; Xiong, D.; Tian, L.; Tang, C.; Wang, Y.; Tian, C. Functional characterization of two bZIP transcription factors in *Verticillium dahliae*. *Gene* **2017**, *626*, 386–394. [CrossRef] [PubMed]
24. Nathues, E.; Joshi, S.; Tenberge, K.B.; von den Driesch, M.; Oeser, B.; Bäumer, N.; Mihlan, M.; Tudzynski, P. CPTF1, a CREB-like transcription factor, is involved in the oxidative stress response in the phytopathogen *Claviceps purpurea* and modulates ROS level in its host Secale cereale. *Mol. Plant Microbe Interact.* **2004**, *17*, 383–393. [CrossRef] [PubMed]
25. Balázs, A.; Pócsi, I.; Hamari, Z.; Leiter, É.; Emri, T.; Miskei, M.; Oláh, J.; Tóth, V.; Hegedus, N.; Prade, R.A.; et al. AtfA bZIP-type transcription factor regulates oxidative and osmotic stress responses in *Aspergillus nidulans*. *Mol. Genet Genom.* **2010**, *283*, 289–303. [CrossRef] [PubMed]
26. Hagiwara, D.; Asano, Y.; Yamashino, T.; Mizuno, T. Characterization of bZip-type transcription factor AtfA with reference to stress responses of conidia of *Aspergillus nidulans*. *Biosci. Biotechnol. Biochem.* **2008**, *72*, 2756–2760. [CrossRef]
27. Hagiwara, D.; Suzuki, S.; Kamei, K.; Gonoi, T.; Kawamoto, S. The role of AtfA and HOG MAPK pathway in stress tolerance in conidia of *Aspergillus fumigatus*. *Fungal Genet. Biol.* **2014**, *73*, 138–149. [CrossRef]
28. Lara-Rojas, F.; Sanchez, O.; Kawasaki, L.; Aguirre, J. *Aspergillus nidulans* transcription factor AtfA interacts with the MAPK SakA to regulate general stress responses, development and spore functions. *Mol. Microbiol.* **2011**, *80*, 436–454. [CrossRef]
29. Emri, T.; Szarvas, V.; Orosz, E.; Antal, K.; Park, H.; Han, K.H.; Yu, J.H.; Pócsi, I. Core oxidative stress response in *Aspergillus nidulans*. *BMC Genom.* **2015**, *16*, 478. [CrossRef]
30. Silva, L.P.; Horta, M.A.C.; Goldman, G.H. Genetic interactions between *Aspergillus fumigatus* basic leucine zipper (bZIP) transcription factors AtfA, AtfB, AtfC and AtfD. *Front. Fungal Biol.* **2021**, *2*, 632048. [CrossRef]
31. Nimmanee, P.; Woo, P.C.Y.; Vanittanakom, P.; Youngchim, S.; Vanittanakom, N. Functional analysis of *atfA* gene to stress response in pathogenic thermal dimorphic fungus *Penicillium marneffei*. *PLoS ONE* **2014**, *9*, e111200. [CrossRef] [PubMed]

32. Qi, X.; Guo, L.; Yang, L.; Huang, J. Foatf1, a bZIP transcription factor of *Fusarium oxysporum* f. sp. *cubense is involved in pathogenesis by regulating the oxidative stress responses of Cavendish banana (Musa spp.). Physiol. Mol. Plant Pathol.* **2013**, *84*, 76–85.
33. Hagiwara, D.; Asano, Y.; Marui, J.; Yoshimi, A.; Mizuno, T.; Abe, K. Transcriptional profiling for *Aspergillus nidulans* HogA MAPK signaling pathway in response to fludioxonil and osmotic stress. *Fungal Genet. Biol.* **2009**, *46*, 868–878. [CrossRef]
34. Yamashita, K.; Shiozawa, A.; Watanabe, S.; Fukumori, F.; Kimura, M.; Fujimura, M. ATF-1 transcription factor regulates the expression of *ccg-1* and *cat-1* genes in response to fludioxonil under OS-2 MAP kinase in *Neurospora crassa*. *Fungal Genet. Biol.* **2008**, *45*, 1562–1569. [CrossRef] [PubMed]
35. Valero, C.; Colabardini, A.C.; Chiaratto, J.; Pardeshi, L.; de Castro, P.A.; Filho, J.A.F.; Silva, L.P.; Rocha, M.C.; Malavazi, I.; Costa, J.H.; et al. *Aspergillus fumigatus* transcription factors involved in the caspofungin paradoxical effect. *mBio* **2020**, *11*, e00816-20. [CrossRef] [PubMed]
36. Silva, L.P.; Alves de Castro, P.; Dos Reis, T.F.; Paziani, M.H.; Von Zeska Kress, M.R.; Riaño-Pachón, D.M.; Hagiwara, D.; Ries, L.N.A.; Brown, N.A.; Goldman, G.H. Genome-wide transcriptome analysis of *Aspergillus fumigatus* exposed to osmotic stress reveals regulators of osmotic and cell wall stresses that are $SakA^{HOG1}$ and MpkC dependent. *Cell. Microbiol.* **2017**, *19*, e12681. [CrossRef] [PubMed]
37. Emri, T.; Gila, B.; Antal, K.; Fekete, F.; Moon, H.; Yu, J.-H.; Pócsi, I. AtfA-independent adaptation to the toxic heavy metal cadmium an *Aspergillus nidulans*. *Microorganisms* **2021**, *9*, 1433. [CrossRef]
38. Tang, C.; Li, T.; Klosterman, S.J.; Tian, C.; Wang, Y. The bZIP transcription factor VdAtf1 regulates virulence by mediating nitrogen metabolism in *Verticillium dahliae*. *New Phytol.* **2020**, *226*, 1461–1479. [CrossRef]
39. Jung, M.-G.; Kim, S.S.; Yu, J.-H.; Shin, K.S. Characterization of gprK encoding a putative hybrid G-protein-coupled receptor in *Aspergillus fumigatus*. *PLoS ONE* **2016**, *11*, e0161312. [CrossRef]
40. Gressler, M.; Meyer, F.; Heine, D.; Hortschansky, P.; Hertweck, C.; Brock, M. Phytotoxin production in *Aspergillus terreus* is regulated by independent environmental signals. *eLife* **2015**, *4*, e07861. [CrossRef]
41. Pérez-Arques, C.; Navarro-Mendoza, M.I.; Murcia, L.; Lax, C.; Martínez-García, P.; Heitman, J.; Nicolás, F.E.; Garre, V. *Mucor circinelloides* thrives inside the phagosome through an Atf-mediated germination pathway. *mBio* **2019**, *10*, e02765-18. [CrossRef]
42. Missall, T.A.; Lodge, J.K. Function of the thioredoxin proteins in during stress or virulence and regulation by putative transcriptional modulators. *Mol. Microbiol.* **2005**, *57*, 847–858. [CrossRef]
43. Sakamoto, K.; Arima, T.; Iwashita, K.; Yamada, O.; Gomi, K.; Akita, O. *Aspergillus oryzae atfB* encodes a transcription factor required for stress tolerance in conidia. *Fungal Genet. Biol.* **2008**, *45*, 922–932. [CrossRef] [PubMed]
44. Roze, L.V.; Miller, M.J.; Rarick, M.; Mahanti, N.; Linz, J.E. A novel cAMP-response element, CRE1, modulates expression of nor-1 in *Aspergillus parasiticus*. *J. Biol. Chem.* **2004**, *279*, 27428–27439. [CrossRef]
45. Roze, L.V.; Chanda, A.; Wee, J.; Awad, D.; Linz, J.E. Stress-related transcription factor AtfB integrates secondary metabolism with oxidative stress response in Aspergilli. *J. Biol. Chem.* **2011**, *286*, 35137–35148. [CrossRef]
46. Baidya, S.; Duran, R.M.; Lohmar, J.M.; Harris-Coward, P.Y.; Cary, J.W.; Hong, S.Y.; Roze, L.V.; Linz, J.E.; Calvo, A.M. VeA is associated with the response to oxidative stress in the aflatoxin producer *Aspergillus flavus*. *Eukaryot. Cell* **2014**, *13*, 1095–1103. [CrossRef]
47. Wee, J.; Hong, S.Y.; Roze, L.V.; Day, D.M.; Chanda, A.; Linz, J.E. The fungal bZIP transcription factor AtfB controls virulence-associated processes in *Aspergillus parasiticus*. *Toxins* **2017**, *9*, 287. [CrossRef] [PubMed]
48. Pleadin, J.; Frece, J.; Markov, K. Mycotoxins in food and feed. *Adv. Food Nutr. Res.* **2019**, *89*, 297–345. [PubMed]
49. Dey, D.K.; Kang, J.I.; Bajpai, V.K.; Kim, K.; Lee, H.; Sonwal, S.; Simal-Gandara, J.; Xiao, J.; Ali, S.; Huh, Y.S.; et al. Mycotoxins in food and feed: Toxicity, preventive challenges, and advanced detection techniques for associated diseases. *Crit. Rev. Food Sci.* **2022**, *21*, 1–22. [CrossRef] [PubMed]
50. Wen, Y.; Hatabayashi, H.; Arai, H.; Kitamoto, H.K.; Yabe, K. Function of the *cypX* and *moxY* genes in aflatoxin biosynthesis in *Aspergillus parasiticus*. *Appl. Environ. Microbiol.* **2005**, *71*, 3192–3198. [CrossRef] [PubMed]
51. Pickova, D.; Ostry, V.; Toman, J.; Malir, F. Aflatoxins: History, significant milestones, recent data on their toxicity and ways to mitigation. *Toxins* **2021**, *13*, 399. [CrossRef] [PubMed]
52. Amaike, S.; Keller, N.P. *Aspergillus flavus*. *Annu. Rev. Phytopathol.* **2011**, *49*, 107–133. [CrossRef] [PubMed]
53. Caceres, I.; Khoury, A.A.; Khoury, R.E.; Lorber, S.; Oswald, I.P.; Khoury, A.E.; Atoui, A.; Puel, O.; Bailly, J.D. Aflatoxin biosynthesis and genetic regulation: A review. *Toxins* **2019**, *12*, 150. [CrossRef] [PubMed]
54. Caceres, I.; Khoury, E.R.; Bailly, S.; Oswald, I.P.; Puel, O.; Bailly, J.-D. Piperine inhibits aflatoxin B1 production in *Aspergillus flavus* by modulating fungal oxidative stress response. *Fungal Genet. Biol.* **2017**, *107*, 77–85. [CrossRef]
55. Xu, D.; Peng, S.; Guo, R.; Yao, L.; Mo, H.; Li, H.; Song, H.; Hu, L. EGCG alleviates oxidative stress and inhibits aflatoxin B1 biosynthesis via MAPK signaling pathway. *Toxins* **2021**, *13*, 693. [CrossRef]
56. Ma, L.; Li, X.; Ma, X.; Yu, Q.; Yu, X.; Liu, Y.; Nie, C.; Zhang, Y.; Xing, F. The regulatory mechanism of water activities on aflatoxins biosynthesis and conidia development, and transcription factor AtfB is involved in this regulation. *Toxins* **2021**, *13*, 431. [CrossRef]
57. Li, X.; Ren, Y.; Jing, J.; Jiang, Y.; Yang, Q.; Luo, S.; Xing, F. The inhibitory mechanism of methyl jasmonate on *Aspergillus flavus* growth and aflatoxin biosynthesis and two novel transcription factors are involved in this action. *Foo. Res. Int.* **2021**, *140*, 110051. [CrossRef]

58. Zhao, Q.; Pei, H.; Zhao, X.; Zhao, K.; Yu, M.; Han, G.; Fan, J.; Tao, F. Systematic characterization of bZIP transcription factors required for development and aflatoxins generation by high-throughput gene knockout in *Aspergillus flavus*. *J. Fungi* **2022**, *8*, 356. [CrossRef]
59. Kim, M.S.; Ko, Y.-J.; Maeng, S.; Floyd, A.; Heitman, J.; Bahn, Y.-S. Comparative transcriptome analysis of the CO_2 sensing pathway via differential expression of carbonic anhydrase in *Cryptococcus neoformans*. *Genetics* **2010**, *185*, 1207–1219. [CrossRef]
60. Chang, P.K.; Scharfenstein, L.L.; Wei, Q.; Bhatnagar, D. Development and refinement of high-efficiency gene-targeting system for *Aspergillus flavus*. *J. Microbiol. Methods.* **2010**, *81*, 240–246. [CrossRef]
61. Kumar, S.; Stecher, G.; Li, M.; Knyaz, C.; Tamura, K. MEGA X: Molecular evolutionary genetics analysis across computing platforms. *Mol. Biol. Evol.* **2018**, *35*, 1547–1549. [CrossRef] [PubMed]
62. Szewczyk, E.; Nayak, T.; Oakley, C.E.; Edgerton, H.; Xiong, Y.; Taheri-Talesh, N.; Osmani, S.A.; Oakley, B.R. Fusion PCR and gene targeting in *Aspergillus nidulans*. *Nat. Protoc.* **2006**, *1*, 3111–3120. [CrossRef]
63. Chang, P.K.; Ehrlich, K.C.; Yu, J.J.; Bhatnagar, D.; Cleveland, T.E. Increased expression of *Aspergillus parasiticus* AflR, encoding a sequence-specific DNA-binding protein, relieves nitrate inhibition of aflatoxin biosynthesis. *Appl. Environ. Microbiol.* **1995**, *61*, 2372–2377. [CrossRef] [PubMed]

toxins

MDPI

Article

Histone 2-Hydroxyisobutyryltransferase Encoded by *Afngg1* Is Involved in Pathogenicity and Aflatoxin Biosynthesis in *Aspergillus flavus*

Jing Wang [1,2,†], Liuke Liang [1,2,†], Shan Wei [1,2], Shuaibing Zhang [1,2], Yuansen Hu [1,2] and Yangyong Lv [1,2,*]

[1] College of Biological Engineering, Henan University of Technology, Zhengzhou 450001, China
[2] Henan Provincial Key Laboratory of Biological Processing and Nutritional Function of Wheat, Zhengzhou 450001, China
* Correspondence: lvyangyong@haut.edu.cn
† These authors contributed equally to this work.

Abstract: Aflatoxin, a carcinogenic secondary metabolite produced by *Aspergillus flavus*, is a significant threat to human health and agricultural production. Histone 2-hydroxyisobutyrylation is a novel post-translational modification that regulates various biological processes, including secondary metabolism. In this study, we identified the novel histone 2-hydroxyisobutyryltransferase Afngg1 in *A. flavus*, and explored its role in cell growth, development and aflatoxin biosynthesis. *Afngg1* gene deletion markedly decreased lysine 2-hydroxyisobutyrylation modification of histones H4K5 and H4K8 compared with the control strain. Additionally, *Afngg1* deletion inhibited mycelial growth of *A. flavus*, and the number of conidia and hydrophobicity were significantly decreased. Notably, aflatoxin B_1 biosynthesis and sclerotia production were completely inhibited in the Δ*Afngg1* strain. Furthermore, the pathogenicity of the Δ*Afngg1* strain infecting peanut and corn grains was also diminished, including reduced spore production and aflatoxin biosynthesis compared with *A. flavus* control and *Afngg1* complementation strains. Transcriptome analysis showed that, compared with control strains, differentially expressed genes in Δ*Afngg1* were mainly involved in chromatin remodelling, cell development, secondary metabolism and oxidative stress. These results suggest that Afngg1 is involved in histone 2-hydroxyisobutyrylation and chromatin modification, and thus affects cell development and aflatoxin biosynthesis in *A. flavus*. Our results lay a foundation for in-depth research on the 2-hydroxyisobutyrylation modification in *A. flavus*, and may provide a novel target for aflatoxin contamination prevention.

Keywords: *Aspergillus flavus*; aflatoxin; pathogenicity; 2-hydroxyisobutyryltransferase; Afngg1

Key Contribution: The 2-hydroxyisobutyryltransferase Afngg1 affects 2-hydroxyisobutyrylation modification of histones H4K5 and H4K8 and blocks aflatoxin biosynthesis in *Aspergillus flavus*.

Citation: Wang, J.; Liang, L.; Wei, S.; Zhang, S.; Hu, Y.; Lv, Y. Histone 2-Hydroxyisobutyryltransferase Encoded by *Afngg1* Is Involved in Pathogenicity and Aflatoxin Biosynthesis in *Aspergillus flavus*. *Toxins* **2023**, *15*, 7. https://doi.org/10.3390/toxins15010007

Received: 23 November 2022
Revised: 7 December 2022
Accepted: 16 December 2022
Published: 21 December 2022

1. Introduction

Aspergillus flavus, one of the most abundant and widely distributed fungi on earth, is often found in pre- or post-harvest crops, and it causes serious economic losses [1,2]. It can produce teratogenic and carcinogenic aflatoxins that pose a serious safety hazard to both humans and animals [3]. It is estimated that aflatoxin contamination costs the US corn industry nearly USD 1.68 billion annually [4]. Aflatoxin causes 28% of hepatocellular carcinoma worldwide [5]. Therefore, an in-depth understanding of aflatoxin biosynthetic pathways and their regulatory mechanisms is urgently required to develop effective strategies to control aflatoxin contamination.

Histone post-translational modifications (HPTMs), including acetylation, phosphorylation, ubiquitination and 2-hydroxyisobutyrylation, play a crucial role in many cellular processes in eukaryotes, including secondary metabolite biosynthesis and chro-

matin regulation [6]. Among them, 2-hydroxyisobutyrylation is a recently discovered post-translational modification that plays an important regulatory role in gene transcription, metabolism and enzyme activity [7]. Previous studies have shown that lysine de-2-hydroxyisobutyrylase CobB can regulate the catalytic activity of enolase by decreasing modification at the K343 site, thereby regulating glycolysis and cell growth in bacteria [8]. In *Ustilaginoidea virens*, mutation of the 2-hydroxyisobutyrylation modification site of mitogen-activated protein kinase UvSlt2 decreased UvSlt2 enzyme activity and significantly reduced the development and virulence of plant pathogenic fungi [9]. Significantly, 2-hydroxyisobutyrylation modification is involved in the pathogenicity of *Botrytis cinerea*, *Candida albicans*, *Fusarium oxysporum* and *Toxoplasma gondii* [7,10–12]. Our previous studies have shown that 2-hydroxyisobutyrylation modification regulates mycelial growth and development of *A. flavus*, as well as aflatoxin biosynthesis [13]. These results indicate that lysine 2-hydroxyisobutyrylation modification plays a key role in *A. flavus*, but the enzymes involved in histone 2-hydroxyisobutyrylation modification have not been reported in *A. flavus*. Herein, we identified histone 2-hydroxyisobutyryltransferase Afngg1 in *A. flavus*, and explored its underlying gene regulatory mechanisms using RNA sequencing (RNA-seq)-based transcriptional analysis.

In this study, Afngg1, a homolog of *Candida albicans* histone acetyltransferase Ngg1, was found to be associated with histone 2-hydroxyisobutyrylation modification. Additionally, the functions of Afngg1 in cell development and aflatoxin B_1 (AFB_1) production were profiled, and the underlying regulatory mechanisms were investigated through transcriptome analysis. The findings suggest that Afngg1 is a potential target for the effective control of aflatoxin contamination.

2. Results

2.1. Characterisation of A. Flavus Histone 2-Hydroxyisobutyryltransferase Afngg1

In order to characterise homologs of Afngg1 in *A. flavus*, we obtained homologous sequences by BLAST searching the NCBI database, and constructed phylogenetic trees to analyse their evolutionary relationships. The results revealed that Afngg1 in *A. flavus* is closely related to homologs in other fungi, and most similar to homolog in *A. oryzae* RIB40 (Figure 1A). The analysis also indicated that it was homologous to *Candida albicans* histone acetyltransferase Ngg1. The domains in Afngg1 were further analysed via the NCBI database and visualised using DOG2.0. A conserved Ada3 (histone acetyltransferase subunit 3) domain was found in homologs of Afngg1 proteins in nine species (Figure 1B). Additionally, Afngg1 was localised in the nucleus of *A. flavus* (Figure 1C).

Given the similarity to Ngg1 in *C. albicans*, we speculated that Afngg1 might also be involved in histone modification. To test this hypothesis, the effects of Afngg1 on the level of acetylation of histone H3 and 2-hydroxyisobutyrylation modification of histone H4 were investigated by collecting mycelia of *A. flavus* control and Δ*Afngg1* strains, and proteins were extracted for Western blotting detection using corresponding antibodies. The results indicated that the acetylation modification level of H3K14 in strain Δ*Afngg1* was decreased compared with the *A. flavus* control strain, and notably, acetylation modification of H3K9 was completely absent (Figure S1). Unexpectedly, our results also showed that 2-hydroxyisobutyrylation modification levels of H4K8 and H4K5 were significantly lower than in the *A. flavus* control strain (Figure 1D). These results suggest that Afngg1 contributed to lysine acetylation and 2-hydroxyisobutyrylation as a histone acetyltransferase.

2.2. Afngg1 Is Involved in A. flavus Growth, Conidia Formation and Aflatoxin Biosynthesis

To further explore the potential role of *Afngg1* in *A. flavus*, we constructed Δ*Afngg1* and Δ*Afngg1*-Com strains (Figure S2), and the effects of *Afngg1* on *A. flavus* growth, conidia formation and biosynthesis of aflatoxin were evaluated. Unlike the *A. flavus* control strain, mycelia of the Δ*Afngg1* strain were white and fluffy (Figure 2Aa). Stereoscopic microscope observation showed that, compared with the *A. flavus* control strain, conidia heads of the Δ*Afngg1* strain were smaller and fewer in number (Figure 2Ab). Microscopy observation

revealed that deletion of *Afngg1* reduced the length of conidiophores and conidial number (Figure 2Ac). SEM results showed that conidial heads of the *A. flavus* control strain were fully formed, while conidial heads of the *Afngg1* strain were significantly smaller and deformed (Figure 2B). Additionally, compared with the *A. flavus* control strain, the mycelia growth rate was decreased after *Afngg1* deletion, and conidia production was decreased by 99.88%, consistent with microscopy observation (Figure 2C,D). Qualitative thin-layer chromatography (TLC) analysis showed that AFB_1 was no longer produced by the *A. flavus* strain lacking *Afngg1* (Figure 2E).

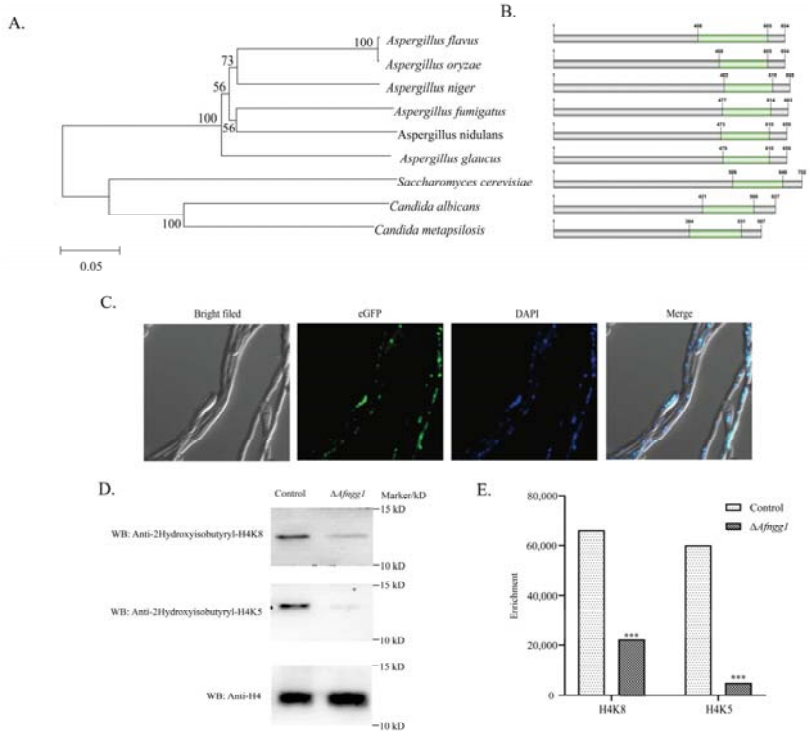

Figure 1. Bioinformatics analysis, subcellular localisation, and modification sites identification of Afngg1. (**A**) Phylogenetic tree based on sequence alignment. The numbers on the branches indicate bootstrap support value. (**B**) The domains of Afngg1 from the above nine species were further visualised by DOG2.0. The green area represented the Ada3 domain. (**C**) Subcellular localization of Afngg1. (**D**, **E**) Level of 2-hydroxyisobutyrylation modification of histones H4K5 and H4K8 in *A. flavus* control and Δ*Afngg1* strains. *** represents $p < 0.001$.

2.3. Effects of Afngg1 on Hydrophobicity and Sclerotia Formation of A. flavus Colonies

We studied the effects of *Afngg1* on the surface hydrophobicity of *A. flavus* cells. The results revealed spherical water droplets on *A. flavus* control strain colonies, but these were dispersed and absorbed on Δ*Afngg1* strain colonies (Figure 3(Aa,Ab)). In order to further probe the hydrophobicity differences, the droplet state of mycelia around droplets on colonies and Bromophenol Blue droplets were observed by stereoscopic microscope. The results showed that mycelia and spores around the *A. flavus* control strain were attached to the outer side of the droplet, while Bromophenol Blue solution of the Δ*Afngg1* strain was diffused throughout mycelia (Figure 3(Ac)). Additionally, the results showed that compared with the *A. flavus* control strain, the Δ*Afngg1* mutant did not produce sclerotia

at all on PDA medium (Figure 3B,C). These results indicate that *Afngg1* is essential for sclerotia formation in *A. flavus*.

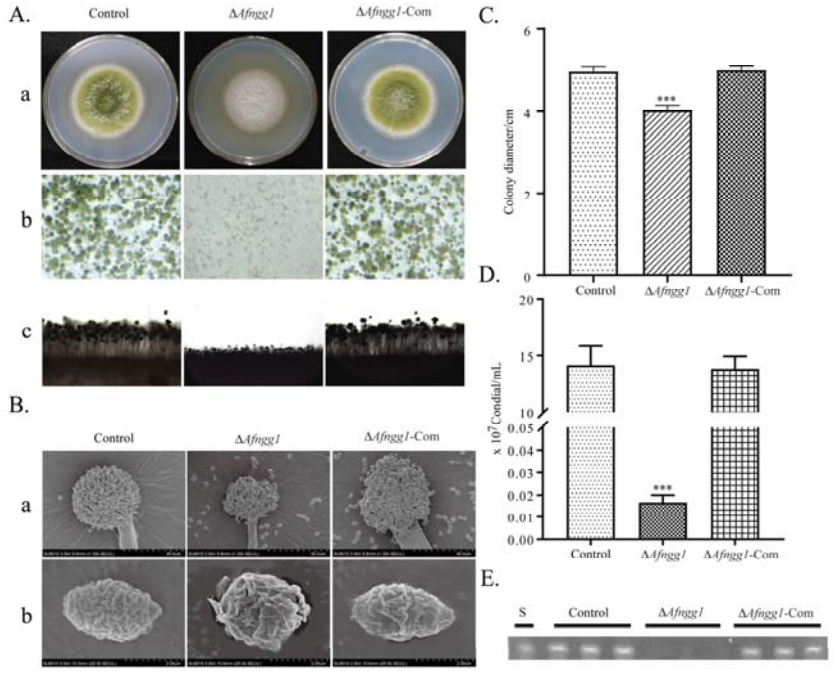

Figure 2. Effects of *Afngg1* on the growth, conidia and aflatoxin biosynthesis of *A. flavus*. (**A**) The colony (**a**), stereoscopic microscope (**b**) and conidiophores (**c**) analysis. *A. flavu*s control strain, Δ*Afngg1* and *Afngg1*-Com strains were cultivated on PDA medium at 37 °C for 5 days. (**B**) SEM analysis of conidia (**a**) and conidial heads (**b**). (**C**) Determination of colony diameter cultured on PDA medium. (**D**) Determination of the number of conidia from different strains. (**E**) TLC analysis of AFB_1 production. *** represents $p < 0.001$.

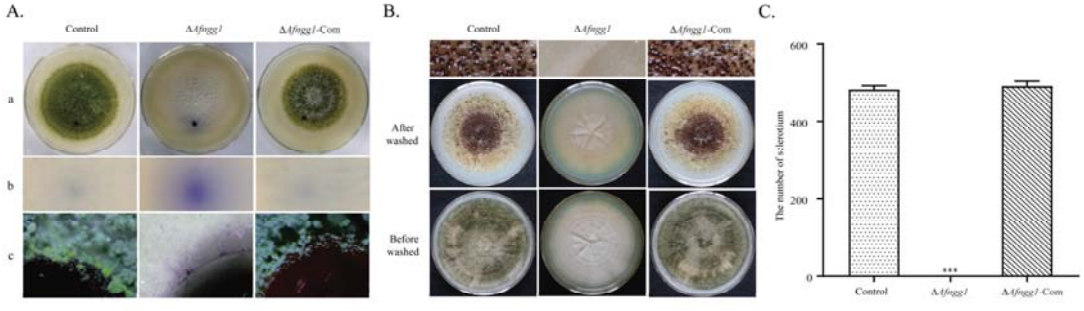

Figure 3. Analysis of hydrophobicity and sclerotium yield. (**A**) Determination of hydrophobicity of *A. flavus* control strain, Δ*Afngg1* and *Afngg1*-Com strains. Colony morphology (**a**), microscope (**b**) and stereoscopic microscopic (**c**) analysis after Bromophenol blue treatment. (**B**) Colony morphology of different strains after 7 days of culture on PDA medium. The plate was sprayed with 70% alcohol to expose the sclerotium. (**C**) Determination of the number of sclerotium in (**B**). *** represent $p < 0.001$.

2.4. Afngg1 Influences the Infection Ability of A. flavus on Peanut and Corn

In order to study the pathogenicity of *Afngg1* deletion in *A. flavus*, maize and corn grains were inoculated with spore suspensions. The results showed that the Δ*Afngg1* mutant had a decreased ability to colonise peanut and corn grains, and conidia production was decreased by 97.39% and 91.94%, respectively (Figure 4A,B). We also explored the yield of AFB_1 on peanut and corn, and AFB_1 was not detected on either peanut or corn grains infected with the Δ*Afngg1* mutant (Figure 4C). These results indicate that *Afngg1* plays a crucial role in conidia formation of *A. flavus*, and in the biosynthesis of aflatoxin during *A. flavus* colonisation on peanut and corn grains.

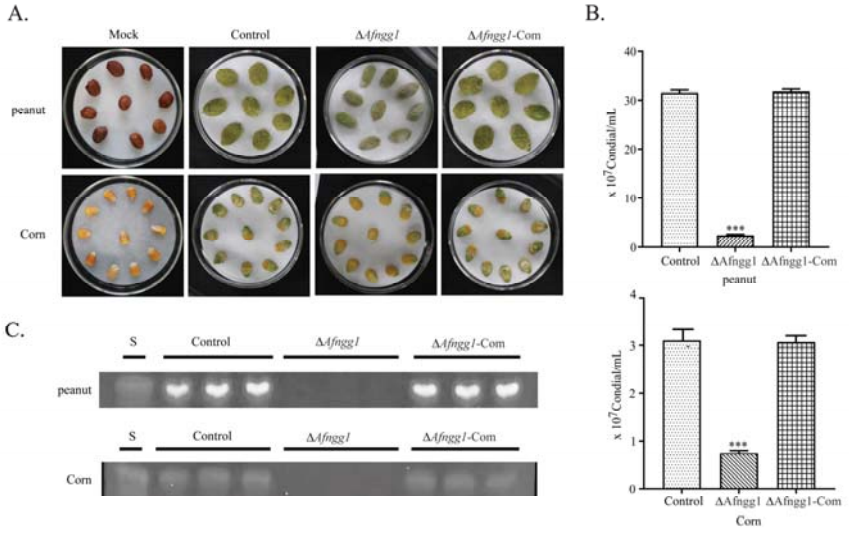

Figure 4. Effect of *Afngg1* on the ability of *A. flavus* to infect crops. (**A**) Colonisation of peanut and corn grains by *A. flavus* control, Δ*Afngg1* and Δ*Afngg1*-Com strains. (**B**) The number of conidia number was determined from the infected peanut and corn grains; (**C**) TLC analysis of AFB_1 production from infected peanut and corn grains. *** represents $p < 0.001$.

2.5. Transcriptome Overview

The Pearson correlation coefficient between all pairs of samples was >0.97, suggesting that samples were adequate for subsequent analysis (Figure 5A). Based on the FPKM (Fragments Per Kilobase per Million) value of each gene, gene expression levels were normalised and differentially expressed genes (DEGs) were compared (Figure 5B). The volcano map directly shows the expression ratio and significance of genes (Figure 5C). A total of 4008 significant DEGs were identified, among which 2186 (54.54%) were upregulated and 1822 (45.45%) were downregulated (Figure 5D).

The biological functions of DEGs were characterised by GO functional enrichment analysis. The results showed that most DEGs were linked to oxidation–reduction metabolic processes (Figure 6A). In terms of cellular components, DEGs were mainly associated with the plasma membrane, component of membrane and cell periphery subcategories (Figure 6B). The main molecular functions of DEGs were oxidoreductase activity, binding and catalytic activity (Figure 6C). KEGG pathway enrichment analysis results showed that DEGs were mainly involved in metabolic pathways, biosynthesis of secondary metabolites and aflatoxin biosynthesis (Figure 6D).

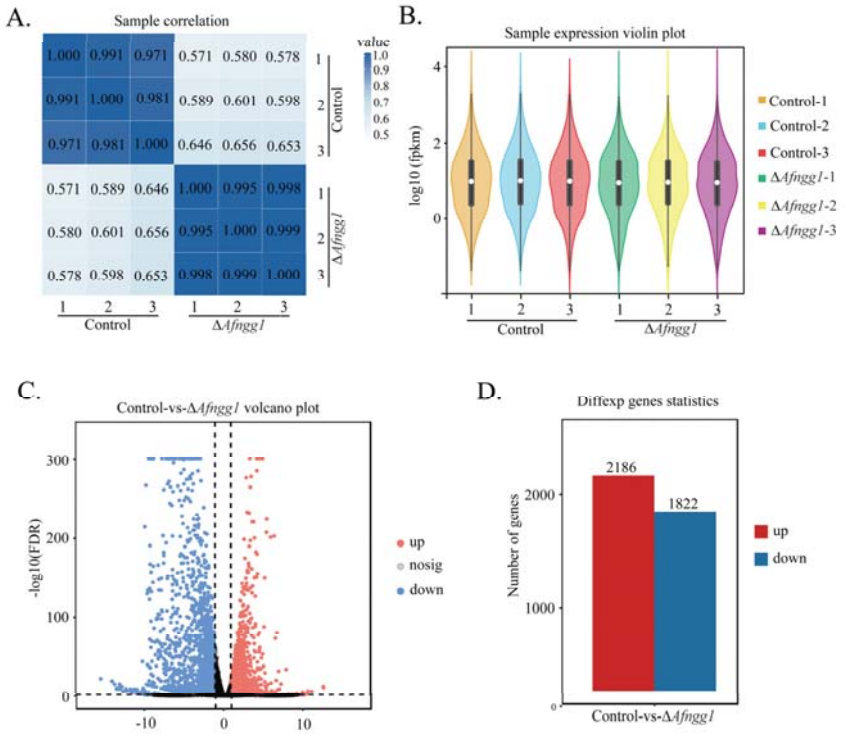

Figure 5. Sample correlation and gene expression analysis. (**A**) Person correlation coefficient. (**B**) Violin plot. (**C**) Volcano map of DEGs. (**D**) Total number of DEGs.

2.6. Categorisation of DEGs

To further elucidate the regulatory effects of Afngg1 on *A. flavus* cell development and aflatoxin biosynthesis, representative DEGs were divided into four groups: chromatin remodelling, cell development, secondary metabolism and oxidative stress (Table 1).

Table 1. Classification of representative DEGs in the Δ*Afngg1* strain vs. control strain.

Gene Category	Name	Log2(fc)	*p*-Value	Description
Chromatin remodelling				
AFLA_025120	clr3	1.089	2.82×10^{-21}	histone deacetylase
MSTRG.3596	RPD3	1.15	1.26×10^{-6}	histone deacetylase RPD3
AFLA_055490	epl1	1.51	5.53×10^{-44}	histone acetyltransferase complex component
AFLA_052300	mit1	1.49	7.93×10^{-28}	chromatin remodelling complex subunit (Chd3)
Cell development				
AFLA_052030	wetA	−2.32	1.96×10^{-120}	developmental regulatory protein WetA
AFLA_029620	abaA	−3.17	1.99×10^{-171}	transcription factor abaA
AFLA_082850	brlA	−5.27	0	C2H2 type conidiation transcription factor
AFLA_046990	stuA	−1.03	5.33×10^{-46}	APSES transcription factor StuA
AFLA_026900	vosA	−2.28	1.98×10^{-75}	developmental regulator VosA
AFLA_039530	fluG	−3.17	1.28×10^{-13}	FluG family protein
AFLA_044800	con-6	−8.10	7.93×10^{-60}	conidiation protein Con-6
AFLA_098380	rodA	−7.58	2.79×10^{-67}	RodA/RolA7
AFLA_060780	dewA	−6.81	8.80×10^{-9}	hydrophobin family protein

Table 1. *Cont.*

Gene Category	Name	Log2(fc)	*p*-Value	Description
AFLA_023460	ags1	−2.80	6.03×10^{-201}	alpha-1,3-glucan synthase Ags1
AFLA_134100	ags2	−2.28	4.34×10^{-119}	alpha-1,3-glucan synthase Ags2
AFLA_052780	MP65	−3.87	1.26×10^{-141}	cell wall glucanase (Scw4)
AFLA_104680	chiB1	−1.64	1.57×10^{-22}	class V chitinase ChiB1
AFLA_024280	dcw1	−5.49	0	cell wall glycosyl hydrolase Dfg5
AFLA_113120	ecm33	−1.02	6.90×10^{-76}	GPI-anchored cell wall organization protein
AFLA_138060	erg4	−2.95	1.32×10^{-108}	c-24(28) sterol reductase
AFLA_001030	erg7	−9.21	1.07×10^{-73}	lanosterol synthase
AFLA_028640	erg5	−5.79	2.08×10^{-143}	cytochrome P450 sterol C-22 desaturase
Secondary metabolism				
AFLA_139410	aflC	−1.00	3.76×10^{-32}	aflC/pksA/pksL1/polyketide synthase
AFLA_139330	aflH	−1.46	2.3×10^{-3}	aflH/short chain alcohol dehydrogenase
AFLA_139160	aflX	−2.37	1.05×10^{-2}	aflX/ordB/monooxygenase/oxidase
AFLA_139320	aflJ	−2.82	1.28×10^{-2}	aflJ/estA/esterase
AFLA_139170	aflW	−3.82	6.16×10^{-6}	aflW/moxY/monooxygenase
AFLA_002920	aflQ	−4.82	2.29×10^{-46}	flavonoid 3-hydroxylase
AFLA_024090	aflT	1.57	8.06×10^{-24}	efflux pump antibiotic resistance protein
AFLA_139310	norA	−8.34	7×10^{-4}	aflE/norA/aad/adh-2/ NOR reductase
AFLA_094990	ustYa	−7.92	2.80×10^{-21}	Ustiloxin B biosynthesis protein Ya
AFLA_094940	ustO	−2.98	2.18×10^{-108}	Ustiloxin B biosynthesis protein O
AFLA_094960	ustC	−4.14	1.27×10^{-48}	cytochrome P450
AFLA_095010	ustP	−4.59	1.18×10^{-84}	Ustiloxin B biosynthesis protein P
AFLA_095060	ustQ	−4.75	1.78×10^{-35}	tyrosinase
AFLA_095040	ustD	−6.18	9.10×10^{-2}	NRPS-like enzyme
AFLA_095050	ustF2	−7.29	5.02×10^{-20}	dimethylaniline monooxygenase
AFLA_064420	gliK	−3.26	3.49×10^{-12}	gliotoxin biosynthesis protein GliK
AFLA_118990	gliA	−4.91	1.47×10^{-127}	efflux pump antibiotic resistance protein
AFLA_064540	gliC	−6.69	1.62×10^{-55}	cytochrome P450 oxidoreductase
AFLA_114820	fluP	−1.44	1.78×10^{-50}	polyketide synthase
AFLA_006170	pksP	−6.54	0	polyketide synthetase PksP
AFLA_010000	aurA	−2.23	2.02×10^{-84}	polyketide synthase
AFLA_054090	pks1	−2.22	7.5×10^{-3}	polyketide synthase
Oxidative stress				
AFLA_034380	cta1	−7.68	0	catalase
AFLA_096210	ctl-2	−6.96	6.43×10^{-272}	catalase
AFLA_100250	cat	−1.57	6.97×10^{-16}	catalase

Means with *p*-value < 0.05 are considered to have significant difference.

Afngg1 deletion altered the expression of genes involved in chromatin remodelling, including histone deacetylases (*clr3*, *RPD3* and *epl1*) and chromatin remodelling complex subunits (*mit1*). Deletion of *Afngg1* inhibited the expression of conidia-related genes *wetA*, *abaA*, *brlA*, *stuA*, *vosA*, *fluG* and *con-6*, and conidia hydrophobicity-related genes *rodA* and *dewA*. Additionally, *ags1*, *ags2*, *MP65*, *chiB1*, *dcw1*, *ecm33*, *erg4*, *erg7* and *erg5* genes related to cell wall and membrane formation were downregulated.

Secondary metabolism was also affected. The results showed that AFB_1 biosynthetic pathway genes *aflC*, *aflH*, *aflX*, *aflJ*, *aflW*, *aflQ*, *aflT* and *norA* were downregulated after *afngg1* deletion. Genes associated with the synthesis of other secondary metabolites, including conidia pigments (*pksP* and *pks1*), polyketones (*fluP* and *aurA*), ustiloxin B (*ustYa*, *ustO*, *ustC*, *ustP*, *ustQ*, *ustD* and *ustF2*) and gliotoxin (*gliK*, *gliA* and *gliC*) were also downregulated. Furthermore, *afngg1* deletion inhibited the expression of catalase-related genes *cta1*, *ctl-2* and *cat*.

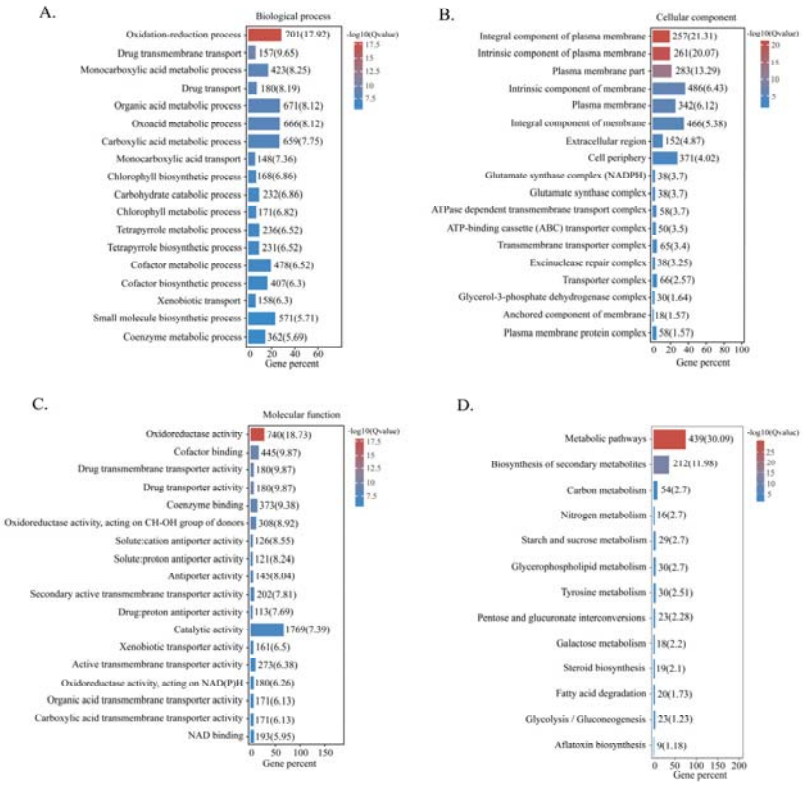

Figure 6. Biological process (**A**), cellular component (**B**), molecular function (**C**) and KEGG pathway (**D**) analysis of DEGs.

3. Discussion

As an important post-translational modification, 2-hydroxyisobutyrylation plays a vital role in protein synthesis, transcriptional regulation and metabolism [14]. In this study, we performed a functional analysis of histone 2-hydroxyisobutyryltransferase Afngg1 in *A. flavus*. Deletion of *Afngg1* reduced the level of histone 2-hydroxyisobutyrylation modification, indicating that Afngg1 functions as a histone 2-hydroxyisobutyrylyltransferase. Additionally, Afngg1 plays a crucial role in the growth and development of *A. flavus* and the biosynthesis of aflatoxin, and its potential regulatory mechanisms were explored through transcriptome analysis.

3.1. Afnng1 Correlates with the Level of Histone 2-Hydroxyisobutyrylation Modification

Previous reports have shown that Ngg1 is required for histone H3 acetylation of *Candida albicans* histone H3, and loss of *Ngg1* greatly reduced the level of acetylation modification of histone H3 in *Ngg1*-A and *Ngg1*-B strains compared with wild-type strains [15]. However, its specific lysine acetylation sites were not characterised. In the present study, we identified homologs of *C. albicans* acetyltransferase NGG1 in *A. flavus*, and identified K9ac and K14ac as the key sites for alteration of histone H3 acetylation. Notably, we also found that Afngg1 is associated with 2-hydroxyisobutyrylation of histone H4, and deletion of *Afngg1* significantly reduced lysine 2-hydroxyisobutyrylation levels at the K5 and K8 sites of histone H4.

3.2. Afnng1 Is Involved in Altering Chromatin Remodelling

Histone modification plays a crucial role in altering chromatin structure, among which histone acetylation and 2-hydroxyisobutyrylation modification are important contributors to chromatin remodelling [16,17]. RPD3 is a conserved histone deacetylase that regulates various cellular processes. In *Fusarium graminearum*, deletion of *FgRpd3* led to increased acetylation of histone H4 [18]. Additionally, the *crl3* gene encoding histone deacetylase affects the growth of *Penicillium brasilianum*, and the production of many secondary metabolites [16]. As a chromatin remodelling factor, Mit1 is mainly involved in regulating transcription of heterochromatin regions, and it promotes the deacetylation of histone H3 by clr3 [19]. We found that following deletion of *Afngg1*, expression levels of *clr3*, *RPD3*, *epl1* and *mit1* genes related to chromatin remodelling were altered. Additionally, previous studies have shown that cobB, de-2-hydroxyisobutyrylation enzyme, is involved in regulating the growth and metabolism of prokaryotes [8]. In human cells, deletion of the histone 2-hydroxyisobutyltransferase EP300 decreases the level of 2-hydroxyisobutyrylation modification at specific regulatory sites, and thus reduces the activity of cell metabolism-related enzymes [17]. Our current work showed that histone acetylation modification and 2-hydroxyisobutyrylation levels of the Δ*Afngg1* strain were reduced. These results suggest that Afngg1 may alter chromatin conformation, altering the accessibility of genes, thus affecting cell development and secondary metabolism of *A. flavus*.

3.3. Afngg1 Affects Conidial Development and Sclerotium Formation

Recent studies have shown that fungal growth, development and production of secondary metabolites are regulated by post-translational modifications such as 2-hydroxyisobutyrylation [13]. Expression of *A. flavus* conidiogenesis genes is regulated by a cascade involving *brlA*, *abaA* and *wetA* [20]. *BrlA* and *abaA* are key transcription factors, of which *brlA* initiates conidia formation, and *abaA* contributes to conidia development and also affects sclerotia formation and AFB_1 production [21,22]. *StuA* affects the expression of downstream genes by influencing *brlA* and *abaA*, and regulates sporulation [23]. *VosA*, a member of the velvet protein family, co-regulates spore-specific genes with *wetA*, and is critical for spore maturation and dormancy [24]. Loss of VosA resulted in increased sensitivity to oxidative stress and decreased trehalose content in *A. flavus* conidia [25]. *FluG* plays a balancing role in asexual and sexual development, and deletion of *fluG* can delay and reduce the formation of *A. flavus* conidia [26]; *fluG* can also interact with *velB* or *laeA* to control the production of conidia and sclerotia [27]. In the present study, the genes *wetA*, *abaA*, *brlA*, *stuA*, *vosA*, *fluG* and *con-6* related to conidia were downregulated following deletion of *Afngg1*, mutant strain colonies were white, conidia production was decreased significantly and the strain no longer produced sclerotia. These results suggest that Afngg1 may regulate developmental balance, oxidative stress and conidia trehalose synthesis, and thereby affect the formation of conidia. Additionally, our experiment found that the Δ*Afngg1* strain no longer produced sclerotia, consistent with the results of *fluG* deletion [27]. Transcriptomic analysis also showed downregulation of genes encoding hydrophobic proteins, namely *rodA* and *dewA*, which was confirmed by hydrophobic assay, and is reminiscent of the deletion of laeA in *A. flavus* [28].

3.4. Afngg1 Is Required in the Formation of the Cell Wall

The fungal cell wall is a complex structure composed of chitin, dextran and other polymers that play an important role in fungal growth and survival [29]. *Ags1* and *Ags2* are involved in glucan synthesis, and growth was inhibited after *Ags1* deletion [30]. *DCW1* is necessary for incorporation of cell wall glycoproteins into the cell wall, and deletion of the *dcw1* gene in yeast led to cell wall abnormalities [31]. *MP65* encodes β-glucan mannoprotein, which is associated with cell wall integrity and biofilm formation [32]. The GPI-anchored protein Ecm33 is required for cell wall composition, and is involved in fungal cell wall integrity and multiple stress tolerance [33]. One study found that the absence of *ecm33* and *MP65* increased sensitivity to cell wall degraders and altered morphology [32,33]. Herein,

transcriptomic results showed that expression levels of the cell wall-related genes *ags1*, *ags2*, *MP65*, *chiB1*, *dcw1* and *ecm33* in the Δ*Afngg1* strain were downregulated. Additionally, ergosterol is an important component of cell membranes, and we found that expression levels of genes associated with ergosterol biosynthesis such as *erg4*, *erg7* and *erg5* were significantly downregulated after deletion of *Afngg1*. These results suggest that Afngg1 may impede the synthesis of cell wall components such as glucan, reduce cell wall tolerance and cause cell wall defects.

3.5. Afngg1 Plays a Key Role in Secondary Metabolism

It has been reported that chromatin remodelling is closely related to the biosynthesis of aflatoxin [34]. Aflatoxin biosynthesis includes complex enzymatic reactions that require multiple enzymes, such as fatty acid synthases, polyketone synthases, oxidoreductases, cytochrome P450 monooxygenases, esterases, and others [35]. *AflC* (*pksA*) encodes a polyketone synthase that is involved in the conversion of acetate to norsolorinic acid, and AFB_1 production can be significantly increased by upregulating *aflC*, *aflR* and *aflK* [36,37]. Both *AflX* and *AflQ* encode oxidoreductases, and *AflQ* is involved in the formation of AFB_1 precursor hydroxyl-methylsterigmatocystin, and it plays a role in the later stages of the biosynthetic pathway [38,39]. Previous studies revealed a strong linear relationship between *aflQ* expression and aflatoxin biosynthesis [40]. *AflW* encodes a single monooxygenase that catalyses the conversion of hydroxyversicolorone to versiconal hemiacetal acetate [41]. Additionally, *aflS* encodes an esterase (*AflJ*) that interacts with nearby *aflR* genes to regulate the biosynthesis of aflatoxin [42]. Following *aflS* deletion, expression levels of aflatoxin biosynthetic pathway genes including *aflC*, *aflD*, *aflM* and *aflP* were reduced 5–20-fold, and biosynthesis of aflatoxin intermediates was blocked [43]. In the present study, deletion of *Afngg1* downregulated genes encoding enzymes related to the aflatoxin biosynthetic pathway, such as *aflC*, *aflX*, *aflJ*, *aflQ*, *aflT* and *norA*, indicating that Afngg1 can inhibit the biosynthesis of aflatoxin by regulating the expression of multiple genes in the gene cluster via chromatin modification. Our study also found that the Δ*Afngg1* strain no longer produced AFB_1, consistent with knockout of histone acetyltransferase AflGcnE [6].

Other secondary metabolic pathways are also affected. Ustiloxin B is a secondary metabolite of *Ustilaginoidea virens*, and 18 genes form a gene cluster for the synthesis of ustiloxin B. Deletion of a relevant gene led to a complete or substantial loss of ustiloxin B production in *A. flavus* [44]. Biosynthesis of gliotoxin is carried out by a synthetic gene cluster consisting of 12 genes in *A. fumigatus* [45]. Loss of *gliA* greatly reduced the biosynthesis of glioxin [46], and deletion of *gliK* significantly hindered efflux of glioxins, and increased sensitivity to exogenous glioxins [47]. Herein, we found that expression levels of *ustYa*, *ustO*, *ustC*, *ustP*, *ustQ*, *ustD*, *ustF2*, *gliK*, *gliA* and *gliC*, which are responsible for the biosynthesis of ustiloxin B and gliatoxin, were downregulated. In addition, *A. flavus* produces a variety of polyketone-derived secondary metabolites, which are the most abundant of fungal secondary metabolites [48]. *PksP* was found to be associated with the biosynthesis and virulence of *A. fumigatus* conidia pigments [49]. The *Pks1* gene encodes a polyketone synthase involved in melanin biosynthesis [50]. Deletion of polyketone synthase gene *Flup* resulted in decreased filament growth rate and conidial production in *A. parasitica* [51]. The present study found that expression levels of polyketone synthase-related genes *fluP*, *pksP*, *aurA* and *Pks1* were downregulated. These results suggest that Afngg1 may play an important regulatory role in mycotoxin efflux and self-protection.

3.6. Afngg1 Alters Oxidative Stress Homeostasis

Oxidative stress is often associated with the synthesis of fungal secondary metabolites. Biosynthesis of aflatoxin has been reported to be inhibited by increased reactive oxygen species (ROS) levels and decreased activity of antioxidant enzymes [52]. Cells produce a variety of antioxidant enzymes to remove excessive ROS to protect cells from oxidative stress [53]. Previous reports have shown that deletion of *cat1* significantly increased intracellular ROS levels, which in turn increased oxidative stress levels and reduced aflatoxin

biosynthesis and virulence [52]. In our current work, expression levels of catalase-related genes *cat1*, *ctl-2* and *cat* were downregulated, suggesting that deletion of *Afngg1* might prevent cells from clearing ROS in a timely manner, thereby diminishing their defences against oxidative stress, and inhibiting the biosynthesis of aflatoxin.

In conclusion, we identified histone 2-hydroxyisobutyryltransferase Afngg1 in *A. flavus*, and explored its potential roles in cell development and aflatoxin biosynthesis. The results indicated that deletion of *Afngg1* reduced the degree of lysine 2-hydroxyisobutyrylation modification of histone H4, inhibited cell growth, conidia formation, sclerotia production and AFB_1 production in *A. flavus*, and decreased hydrophobicity. RNA-seq was subsequently used to investigate the underlying regulatory mechanisms, and analysis of DEGs showed that genes associated with chromatin remodelling, cell development, oxygen stress and biosynthesis of aflatoxin, ustiloxin B and gliatoxin, were downregulated. Therefore, these results suggest that histone 2-hydroxyisobutyryltransferase Afngg1 affects chromosomal modification, alters gene expression and regulates the growth, development and aflatoxin biosynthesis of *A. flavus*. The findings enhance our understanding of the role of histone 2-hydroxyisobutyrylation in aflatoxin biosynthesis and fungal pathogenicity regulation, and provide potential targets for exploring new control strategies for *A. flavus*.

4. Materials and Methods

4.1. Strains and Culture Conditions

A. flavus CA14 (*kusA*$^-$, *pyrG*$^+$) served as a control strain, and the *Afngg1* knockout strain (Δ*Afngg1*), *Afngg1* complementation strain (Δ*Afngg1*-Com) and Afngg1-enhanced green fluorescence protein (eGFP) strain were derived in this study. Potato dextrose agar (PDA) was used to evaluate growth, conidia formation, cell hydrophobicity and aflatoxin B_1 production, with appropriate amounts of uridine (10 mmol/L) added to the medium as needed. For sclerotia production, spore suspensions were maintained on PDA medium at 37 °C for 7 days in the dark. Each experiment was repeated three times.

4.2. Sequence Resources and Phylogenetic Tree Analysis

We used the protein sequence of Afngg1 to perform a BLAST search to identify homologous sequences in the National Center for Biotechnology Information (NCBI) database. Afngg1 domains were predicted by DOG 1.0 software (Ren and Wen, Hefei, China). Afngg1 protein sequences were aligned by ClustalW using MEGA software (7.0 version, iGEM, Temple University, Philadelphia, PA, USA), and a neighbour-joining phylogenetic tree was constructed [54].

4.3. Construction of Δ*Afngg1,* Δ*Afngg1-Com and Afngg1-eGFP Strains*

The Δ*Afngg1* strains were constructed using homologous recombination with PCR primers listed in Table S1. PCR amplification was performed using P505 DNA polymerase (Vazyme, Nanjing, China). For construction of the Δ*Afngg1* strain, primers Δ*Afngg1*-1F, Δ*Afngg1*-1R, Δ*Afngg1*-2F and Δ*Afngg1*-2R were used to amplify the 1.1 kb upstream and 1.5 kb downstream regions of *Afngg1* fragments in the *A. flavus* genome, respectively. Meanwhile, primers pyrG-F and pyrG-R were used to amplify the pyrG selection marker. Fusion PCR was performed using primers Δ*Afngg1*-1F and Δ*Afngg1*-2R to generate a fragment containing the upstream and downstream segments, and the pyrG selection marker [55]. The fusion fragment was purified and transformed into the *A. flavus* control strain according to previous methods [34], and transformants were selected for verification.

Construction of the *Afngg1*-Com strain was performed according to previous methods [56]. Primers Δ*Afngg1*-Com-F and Δ*Afngg1*-Com-R were used to amplify a fragment including the promoter, coding sequence and terminator from *A. flavus* control strain genomic DNA, and this was ligated to the pPTRI plasmid following *Hind*III and *Sma*I restriction enzyme digestion. The resulting plasmid was transferred into *A. flavus* Δ*Afngg1* protoplasts, and the Δ*Afngg1*-Com strain was confirmed by PCR.

For construction of the Afngg1-eGFP strain, linker, eGFP and TglaA were sequentially connected next to the Afngg1 coding sequence without a stop codon, using primers Afngg1-eGFP-2F and Afngg1-eGFP-2R. The fragment was ligated to the pPTRI plasmid according to previous methods [52]. The confirmed plasmid was transferred into Δ*Afngg1* protoplasts, and transformants were selected for verification.

4.4. Subcellular Localisation

To detect subcellular localisation of Afngg1, *A. flavus* spore suspensions (10^6) were inoculated into Dextrose Peptone Yeast (DPY) liquid medium and cultured at 30 °C for 24 h. After collection, mycelia were washed with phosphate-buffered saline (PBS), stained with 4,6-diamidino-2-phenylindole for 10 min according to a previous method [57], and observed with an FV1000 laser confocal microscope (Olympus, Beijing, China).

4.5. Protein Extraction and Western Blotting Analysis

To explore the effect of *Afngg1* deletion on the acetylation level of histone H3 and the 2-hydroxyisobutyrylation level of histone H4 in *A. flavus*, *A. flavus* control and Δ*Afngg1* strains were cultured on PDA medium at 30 °C for 72 h. Mycelia were frozen with liquid nitrogen and ground to a powder. An appropriate amount of each protein sample was mixed with sample buffer and protein lysis solution to make a final concentration of 1–2 mg/mL, and heated at 95 °C for 10 min prior to sodium dodecyl sulphate polyacrylamide gel electrophoresis (SDS-PAGE). Proteins were transferred to a PVDF membrane, and this was blocked with 5% skimmed milk powder after transfer. For analysis of lysine acetylation of histone H3, anti-H3K9ac, anti-H3K14ac and anti-H3 were used as primary antibodies. For analysis of lysine 2-hydroxyisobutyrylation, anti-H4K5$_{hib}$ (PTM-854; 1:10,000 dilution; PTM-Bio, Hangzhoou, China) and anti-H4K8$_{hib}$ (PTM-805; 1:10,000 dilution; PTM-Bio, Hangzhoou, China) were used as primary antibodies. Goat anti-mouse IgGI (1:10,000 dilution; Thermo, Shanghai, China) was used as secondary antibody, and chemiluminescent horseradish peroxidase (HRP) substrate (Millipore) was added and incubated for 2 min for signal detection. Meanwhile, protein gray scale analysis was performed using Image-Pro Plus software (4.5 version, Media Cybernetics, Silver Spring, USA) according to a previous method [6].

4.6. Morphological and Physiological Analyses

To investigate the effect of *Afngg1* on the growth of *A. flavus*, 2 μL spore suspensions (10^6 spores/mL) of *A. flavus* control, Δ*Afngg1* and Δ*Afngg1*-Com strains were separately inoculated in the centre of PDA plates and cultured at 30 °C for 5 days; then, the colony diameter was measured and conidial heads were counted under a stereoscopic microscope (Nikon, Shanghai, China). Next, 6 mL sterile water was added to each Petri dish to harvest the mycelium, and the number of conidia was calculated using a hemocytometer. To assess the hydrophobicity of *A. flavus* mycelia, 20 μL sterile water and 20 μL 3% Bromophenol Blue solution were added to the edges of colonies of *A. flavus* control, Δ*Afngg1* and Δ*Afngg1*-Com strains, cells were cultured at 30 °C for 2 days, and analysed by a stereoscopic microscope. Quantitative analysis of sclerotia production was performed at 37 °C for 7 days. After 7 days, 75% ethanol was sprayed to wash the medium and expose the sclerotia, and five holes were made along the diameter to count the number of sclerotia. Additionally, scanning electron microscopy (SEM) was used to photograph the conidia microstructure of *A. flavus* control, Δ*Afngg1* and Δ*Afngg1*-Com strains as described previously [58].

4.7. Determination of AFB_1 Production

AFB_1 production analysis was carried out according to a previously described method [59]. Spore suspensions (10^6 spores/mL) of *A. flavus* control, Δ*Afngg1* and Δ*Afngg1*-Com strains were cultured in 50 mL Yeast Extract Sucrose (YES) liquid medium at 30 °C in the dark for 5 days. An equal volume of chloroform was added to extract aflatoxin from the 50 mL medium. After the chloroform was completely volatilised, the residue was

dissolved in 1 mL methanol and then analysed by TLC. The AFB_1 yield of *A. flavus* strains was evaluated using an AFB_1 standard sample (0.1 mg/mL).

4.8. Peanut and Corn Infection Assay

A peanut and corn infection experiment was performed as described previously [60]. Peanut and corn seeds were inoculated with 10^6/mL spore suspensions of *A. flavus* control, Δ*Afngg1* strain and Δ*Afngg1*-Com strain and cultured at 28 °C in the dark for 6 days, with water replenished each day. Sterile water was added to collect the spore suspension and the number of conidia was calculated using a hemocytometer according to a previous method [34]. Finally, chloroform was added to extract aflatoxin as described above.

4.9. Transcriptome Analysis

Total RNA was extracted using Trizol reagent (Thermo Fisher, Shanghai, China) following the manufacturer's instructions. RNA quality and integrity analyses, cDNA library construction, and RNA-Seq were performed by Guangzhou Gene Denovo Biotechnology (Guangzhou, China). The Pearson correlation coefficient was used to analyse the accuracy and reliability of the three biological duplicate samples. DESeq was used to analyse differences in FPKM value, and differences were considered statistically when log2(fold change) >1 and p-value < 0.05 criteria were met. Genome Ontology (GO) functional analysis and Kyoto Encyclopedia of Genes and Genomes (KEGG) pathway analysis were carried out using FungiFun (https://sbi.hki-jena.de/FungiFun/FungiFun.cgi) (accessed on 15 August 2022) and the KEGG Automatic Annotation Sever (http://www.kegg.jp/ or http://www.genome.jp/kegg/) (accessed on 15 August 2022).

Supplementary Materials: The following supporting information can be downloaded at: https://www.mdpi.com/article/10.3390/toxins15010007/s1, Figure S1: Determination of acetylation modification levels of histone H3K9ac and H3K14ac in *A. flavus* control and Δ*Afngg1* strains; Figure S2: Construction and verification of Δ*Afngg1* strain, complement and localisation strains; Table S1: PCR primers were used in this study.

Author Contributions: Methodology, L.L.; validation, J.W.; data curation, S.W.; writing—original draft preparation, L.L. and J.W.; writing—review and editing, S.Z. and Y.L.; project administration, Y.H. All authors have read and agreed to the published version of the manuscript.

Funding: This work was sponsored by grants from the Natural Science Foundation of China (31972176), Natural Science Foundation of Henan Province (222300420037) and the Innovative Funds Plan of Henan University of Technology (2020ZKCJ01).

Institutional Review Board Statement: Not applicable.

Informed Consent Statement: Not applicable.

Data Availability Statement: The raw transcriptome read data are available in the SRA database under accession number SUB12287216.

Conflicts of Interest: The authors declare no conflict of interest.

References

1. Mahmoud, M.A.; El-Samawaty, A.M.; Yassin, M.A.; Abd El-Aziz, A.R. Genetic diversity analysis of Aspergillus flavus isolates from plants and air by ISSR markers. *Genet. Mol. Res.* **2016**, *15*, 1–9. [CrossRef] [PubMed]
2. Taniwaki, M.H.; Pitt, J.I.; Magan, N. Aspergillus species and mycotoxins: Occurrence and importance in major food commodities. *Curr. Opin. Food Sci.* **2018**, *23*, 38–43. [CrossRef]
3. Tumukunde, E.; Ma, G.; Li, D.; Yuan, J.; Qin, L.; Wang, S. Current research and prevention of aflatoxins in China. *World Mycotoxin J.* **2020**, *13*, 121–138. [CrossRef]
4. Mitchell, N.J.; Bowers, E.; Hurburgh, C.; Wu, F. Potential economic losses to the US corn industry from aflatoxin contamination. *Food Addit. Contam. Part A Chem. Anal. Control. Expo. Risk Assess.* **2016**, *33*, 540–550. [CrossRef]
5. Wu, F. Perspective: Time to face the fungal threat. *Nature* **2014**, *516*, 7. [CrossRef]

6. Lan, H.; Sun, R.; Fan, K.; Yang, K.; Zhang, F.; Nie, X.Y.; Wang, X.; Zhuang, Z.; Wang, S. The Aspergillus flavus Histone Acetyltransferase AflGcnE Regulates Morphogenesis, Aflatoxin Biosynthesis, and Pathogenicity. *Front. Microbiol.* **2016**, *7*, 1324. [CrossRef]
7. Qian, H.; Wang, L.; Ma, X.; Yi, X.; Wang, B.; Liang, W. Proteome-Wide Analysis of Lysine 2-Hydroxyisobutyrylated Proteins in Fusarium oxysporum. *Front. Microbiol.* **2021**, *12*, 623735. [CrossRef]
8. Dong, H.; Zhao, Y.; Bi, C.; Han, Y.; Zhang, J.; Bai, X.; Zhai, G.; Zhang, H.; Tian, S.; Hu, D.; et al. TmcA functions as a lysine 2-hydroxyisobutyryltransferase to regulate transcription. *Nat. Chem. Biol.* **2022**, *18*, 142–151. [CrossRef]
9. Chen, X.; Li, P.; Liu, H.; Chen, X.; Huang, J.; Luo, C.; Li, G.; Hsiang, T.; Collinge, D.B.; Zheng, L. A novel transcription factor UvCGBP1 regulates development and virulence of rice false smut fungus *Ustilaginoidea virens*. *Virulence* **2021**, *12*, 1563–1579. [CrossRef]
10. Xu, Y.; Li, X.; Liang, W.; Liu, M. Proteome-Wide Analysis of Lysine 2-Hydroxyisobutyrylation in the Phytopathogenic Fungus Botrytis cinerea. *Front. Microbiol.* **2020**, *11*, 585614. [CrossRef]
11. Zheng, H.; Song, N.; Zhou, X.; Mei, H.; Li, D.; Li, X.; Liu, W. Proteome-Wide Analysis of Lysine 2-Hydroxyisobutyrylation in Candida albicans. *mSystems* **2021**, *6*, e01129-20. [CrossRef] [PubMed]
12. Yin, D.; Jiang, N.; Zhang, Y.; Wang, D.; Sang, X.; Feng, Y.; Chen, R.; Wang, X.; Yang, N.; Chen, Q. Global Lysine Crotonylation and 2-Hydroxyisobutyrylation in Phenotypically Different Toxoplasma gondii Parasites. *Mol. Cell Proteom.* **2019**, *18*, 2207–2224. [CrossRef] [PubMed]
13. Lv, Y.; Wang, J.; Yang, H.; Li, N.; Farzaneh, M.; Wei, S.; Zhai, H.; Zhang, S.; Hu, Y. Lysine 2-hydroxyisobutyrylation orchestrates cell development and aflatoxin biosynthesis in *Aspergillus flavus*. *Environ. Microbiol.* **2022**, *24*, 4356–4368. [CrossRef] [PubMed]
14. Zhang, K.; Cao, H.; Ma, Y.; Si, H.; Zang, J.; Bai, H.; Yu, L.; Pang, X.; Zhou, F.; Xing, J.; et al. Global analysis of lysine 2-hydroxyisobutyrylation during Fusarium graminearum infection in maize. *Front. Plant Sci.* **2022**, *13*, 1000039. [CrossRef] [PubMed]
15. Li, D.-D.; Fuchs, B.B.; Wang, Y.; Huang, X.-W.; Hu, D.-D.; Sun, Y.; Chai, D.; Jiang, Y.-Y.; Mylonakis, E. Histone acetyltransferase encoded by *NGG1* is required for morphological conversion and virulence of *Candida albicans*. *Future Microbiol.* **2017**, *12*, 1497–1510. [CrossRef]
16. Akiyama, D.Y.; Rocha, M.C.; Costa, J.H.; Teles, C.B.; da Silva Zuccoli, G.; Malavazi, I.; Fill, T.P. The *Penicillium brasilianum* Histone Deacetylase Clr3 Regulates Secondary Metabolite Production and Tolerance to Oxidative Stress. *J. Fungi* **2022**, *8*, 514. [CrossRef] [PubMed]
17. Huang, H.; Tang, S.; Ji, M.; Tang, Z.; Shimada, M.; Liu, X.; Qi, S.; Locasale, J.W.; Roeder, R.G.; Zhao, Y.; et al. p300-Mediated Lysine 2-Hydroxyisobutyrylation Regulates Glycolysis. *Mol. Cell* **2018**, *70*, 663–678.e6. [CrossRef]
18. Lin, C.; Cao, X.; Qu, Z.; Zhang, S.; Naqvi, N.I.; Deng, Y.Z. The Histone Deacetylases MoRpd3 and MoHst4 Regulate Growth, Conidiation, and Pathogenicity in the Rice Blast Fungus Magnaporthe oryzae. *mSphere* **2021**, *6*, e0011821. [CrossRef]
19. Creamer, K.M.; Job, G.; Shanker, S.; Neale, G.A.; Lin, Y.-C.; Bartholomew, B.; Partridge, J.F. The Mi-2 Homolog Mit1 Actively Positions Nucleosomes within Heterochromatin to Suppress Transcription. *Mol. Cell Biol.* **2014**, *34*, 2046–2061. [CrossRef]
20. Zhou, D.; Xie, M.; Bai, N.; Yang, L.; Zhang, K.-Q.; Yang, J. The Autophagy-Related Gene Aolatg4 Regulates Hyphal Growth, Sporulation, Autophagosome Formation, and Pathogenicity in Arthrobotrys oligospora. *Front. Microbiol.* **2020**, *11*, 592524. [CrossRef]
21. Cho, H.-J.; Son, S.-H.; Chen, W.; Son, Y.-E.; Lee, I.; Yu, J.-H.; Park, H.-S. Regulation of Conidiogenesis in *Aspergillus flavus*. *Cells* **2022**, *11*, 2796. [CrossRef] [PubMed]
22. Mead, M.E.; Borowsky, A.T.; Joehnk, B.; Steenwyk, J.L.; Shen, X.-X.; Sil, A.; Rokas, A. Recurrent Loss of abaA, a Master Regulator of Asexual Development in Filamentous Fungi, Correlates with Changes in Genomic and Morphological Traits. *Genome Biol. Evol.* **2020**, *12*, 1119–1130. [CrossRef] [PubMed]
23. Miller, K.Y.; Wu, J.; Miller, B.L. StuA is required for cell pattern formation in Aspergillus. *Genes Dev.* **1992**, *6*, 1770–1782. [CrossRef] [PubMed]
24. Wu, M.-Y.; Mead, M.E.; Lee, M.-K.; Neuhaus, G.F.; Adpressa, D.A.; Martien, J.I.; Son, Y.-E.; Moon, H.; Amador-Noguez, D.; Han, K.-H.; et al. Transcriptomic, Protein-DNA Interaction, and Metabolomic Studies of VosA, VelB, and WetA in Aspergillus nidulans Asexual Spores. *mBio* **2021**, *12*, e03128-20. [CrossRef] [PubMed]
25. Eom, T.-J.; Moon, H.; Yu, J.-H.; Park, H.-S. Characterization of the velvet regulators in Aspergillus flavus. *J. Microbiol.* **2018**, *56*, 893–901. [CrossRef] [PubMed]
26. Chang, P.-K.; Scharfenstein, L.L.; Mack, B.; Ehrlich, K.C. Deletion of the Aspergillus flavus Orthologue of *A. nidulans fluG* Reduces Conidiation and Promotes Production of Sclerotia but Does Not Abolish Aflatoxin Biosynthesis. *Appl. Environ. Microbiol.* **2021**, *78*, 7557–7563. [CrossRef] [PubMed]
27. Chang, P.-K.; Scharfenstein, L.L.; Li, P.; Ehrlich, K.C. Aspergillus flavus VelB acts distinctly from VeA in conidiation and may coordinate with FluG to modulate sclerotial production. *Fungal Genet. Biol.* **2013**, *58–59*, 71–79. [CrossRef] [PubMed]
28. Chang, P.-K.; Scharfenstein, L.L.; Ehrlich, K.C.; Wei, Q.; Bhatnagar, D.; Ingber, B.F. Effects of laeA deletion on Aspergillus flavus conidial development and hydrophobicity may contribute to loss of aflatoxin production. *Fungal Biol.* **2012**, *116*, 298–307. [CrossRef]
29. Adams, D.J. Fungal cell wall chitinases and glucanases. *Microbiology* **2004**, *150*, 2029–2035. [CrossRef]
30. Bernard, M.; Latgé, J.-P. Aspergillus fumigatus cell wall: Composition and biosynthesis. *Med. Mycol.* **2001**, *39*, 9–17. [CrossRef]

31. Pan, S.; Tang, L.; Pan, X.; Qi, L.; Yang, J. A member of the glycoside hydrolase family 76 is involved in growth, conidiation, and virulence in rice blast fungus. *Physiol. Mol. Plant Pathol.* **2021**, *113*, 101587. [CrossRef]
32. Sandini, S.; Stringaro, A.; Arancia, S.; Colone, M.; Mondello, F.; Murtas, S.; Girolamo, A.; Mastrangelo, N.; De Bernardis, F. The MP65 gene is required for cell wall integrity, adherence to epithelial cells and biofilm formation in Candida albicans. *BMC Microbiol.* **2011**, *11*, 106. [CrossRef] [PubMed]
33. Chen, Y.; Zhu, J.; Ying, S.-H.; Feng, M.-G. The GPI-anchored protein Ecm33 is vital for conidiation, cell wall integrity, and multi-stress tolerance of two filamentous entomopathogens but not for virulence. *Appl. Microbiol. Biotechnol.* **2014**, *98*, 5517–5529. [CrossRef] [PubMed]
34. Lv, Y.; Yang, H.; Wang, J.; Wei, S.; Zhai, H.; Zhang, S.; Hu, Y. Afper1 contributes to cell development and aflatoxin biosynthesis in Aspergillus flavus. *Int. J. Food Microbiol.* **2022**, *377*, 109828. [CrossRef]
35. Li, Q.Z.; He, Z.M. Advances in research of the structural gene characteristics of the aflatoxin biosynthetic gene cluster. *J. Plant Sci. Phytopathol.* **2015**, *2*, 068–082. [CrossRef]
36. Crawford, J.M.; Korman, T.P.; Labonte, J.W.; Vagstad, A.L.; Hill, E.A.; Kamari-Bidkorpeh, O.; Tsai, S.-C.; Townsend, C.A. Structural basis for biosynthetic programming of fungal aromatic polyketide cyclization. *Nature* **2009**, *461*, 1139–1143. [CrossRef]
37. Li, Y.; He, Y.; Li, X.; Fasoyin, O.E.; Hu, Y.; Liu, Y.; Yuan, J.; Zhuang, Z.; Wang, S. Histone Methyltransferase aflrmtA gene is involved in the morphogenesis, mycotoxin biosynthesis, and pathogenicity of Aspergillus flavus. *Toxicon* **2017**, *127*, 112–121. [CrossRef]
38. Cary, J.W.; Ehrlich, K.C.; Bland, J.M.; Montalbano, B.G. The Aflatoxin Biosynthesis Cluster Gene, *aflX*, Encodes an Oxidoreductase Involved in Conversion of Versicolorin A to Demethylsterigmatocystin. *Appl. Environ. Microbiol.* **2006**, *72*, 1096–1101. [CrossRef]
39. Ren, X.; Branà, M.T.; Haidukowski, M.; Gallo, A.; Zhang, Q.; Logrieco, A.F.; Li, P.; Zhao, S.; Altomare, C. Potential of *Trichoderma* spp. for Biocontrol of Aflatoxin-Producing *Aspergillus flavus*. *Toxins* **2022**, *14*, 86. [CrossRef]
40. Jamali, M.; Karimipour, M.; Shams-Ghahfarokhi, M.; Amani, A.; Razzaghi-Abyaneh, M. Expression of aflatoxin genes aflO (omtB) and aflQ (ordA) differentiates levels of aflatoxin production by Aspergillus flavus strains from soils of pistachio orchards. *Res. Microbiol.* **2013**, *164*, 293–299. [CrossRef]
41. Yabe, K.; Chihaya, N.; Hamamatsu, S.; Sakuno, E.; Hamasaki, T.; Nakajima, H.; Bennett, J.W. Enzymatic Conversion of Averufin to Hydroxyversicolorone and Elucidation of a Novel Metabolic Grid Involved in Aflatoxin Biosynthesis. *Appl. Environ. Microbiol.* **2003**, *69*, 66–73. [CrossRef] [PubMed]
42. Chang, P.-K. The Aspergillus parasiticus protein AFLJ interacts with the aflatoxin pathway-specific regulator AFLR. *Mol. Genet. Genom.* **2003**, *268*, 711–719. [CrossRef] [PubMed]
43. Yu, J.; Chang, P.K.; Ehrlich, K.C.; Cary, J.W.; Bhatnagar, D.; Cleveland, T.E.; Payne, G.A.; Linz, J.E.; Woloshuk, C.P.; Bennett, J.W. Clustered Pathway Genes in Aflatoxin Biosynthesis. *Appl. Environ. Microbiol.* **2004**, *70*, 1253–1262. [CrossRef]
44. Umemura, M.; Nagano, N.; Koike, H.; Kawano, J.; Ishii, T.; Miyamura, Y.; Kikuchi, M.; Tamano, K.; Yu, J.; Shin-Ya, K.; et al. Characterization of the biosynthetic gene cluster for the ribosomally synthesized cyclic peptide ustiloxin B in Aspergillus flavus. *Fungal Genet. Biol.* **2014**, *68*, 23–30. [CrossRef] [PubMed]
45. Kwon-Chung, K.J.; Sugui, J.A. What do we know about the role of gliotoxin in the pathobiology of *Aspergillus fumigatus*? *Med. Mycol.* **2009**, *47*, S97–S103. [CrossRef] [PubMed]
46. Wang, D.-N.; Toyotome, T.; Muraosa, Y.; Watanabe, A.; Wuren, T.; Bunsupa, S.; Aoyagi, K.; Yamazaki, M.; Takino, M.; Kamei, K. GliA in Aspergillus fumigatus is required for its tolerance to gliotoxin and affects the amount of extracellular and intracellular gliotoxin. *Med. Mycol.* **2014**, *52*, 506–518. [CrossRef]
47. Gallagher, L.; Owens, R.A.; Dolan, S.K.; O'Keeffe, G.; Schrettl, M.; Kavanagh, K.; Jones, G.W.; Doyle, S. The Aspergillus fumigatus Protein GliK Protects against Oxidative Stress and Is Essential for Gliotoxin Biosynthesis. *Eukaryot. Cell* **2012**, *11*, 1226–1238. [CrossRef]
48. Keller, N.P.; Turner, G.; Bennett, J.W. Fungal secondary metabolism—From biochemistry to genomics. Nature reviews. *Nat. Rev. Microbiol.* **2005**, *3*, 937–947. [CrossRef]
49. Langfelder, K.; Jahn, B.; Gehringer, H.; Schmidt, A.; Wanner, G.; Brakhage, A.A. Identification of a polyketide synthase gene (pksP) of Aspergillus fumigatus involved in conidial pigment biosynthesis and virulence. *Med. Microbiol. Immunol.* **1998**, *187*, 79–89. [CrossRef]
50. Takano, Y.; Kubo, Y.; Shimizu, K.; Mise, K.; Okuno, T.; Furusawa, I. Structural analysis of PKS1, a polyketide synthase gene involved in melanin biosynthesis in Colletotrichum lagenarium. *Mol. Gen. Genet.* **1995**, *249*, 162–167. [CrossRef]
51. Zhou, R.; Rasooly, R.; Linz, J.E. Isolation and analysis of fluP, a gene associated with hyphal growth and sporulation in Aspergillus parasiticus. *Mol. Gen. Genet.* **2000**, *264*, 514–520. [CrossRef] [PubMed]
52. Zhu, Z.; Yang, M.; Bai, Y.; Ge, F.; Wang, S. Antioxidant-related catalaseCTA1regulates development, aflatoxin biosynthesis, and virulence in pathogenic fungus *Aspergillus flavus*. *Environ. Microbiol.* **2020**, *22*, 2792–2810. [CrossRef] [PubMed]
53. Domènech, A.; Ayté, J.; Antunes, F.; Hidalgo, E. Using in vivo oxidation status of one- and two-component redox relays to determine H2O2 levels linked to signaling and toxicity. *BMC Biol.* **2018**, *16*, 61. [CrossRef] [PubMed]
54. Kumar, S.; Stecher, G.; Tamura, K. MEGA7: Molecular Evolutionary Genetics Analysis Version 7.0 for Bigger Datasets. *Mol. Biol. Evol.* **2016**, *33*, 1870–1874. [CrossRef]
55. Szewczyk, E.; Nayak, T.; Oakley, C.E.; Edgerton, H.; Xiong, Y.; Taheri-Talesh, N.; Osmani, S.A.; Oakley, B.R. Fusion PCR and gene targeting in Aspergillus nidulans. *Nat. Protoc.* **2006**, *1*, 3111–3120. [CrossRef] [PubMed]

56. Ren, S.; Yang, M.; Yue, Y.; Ge, F.; Li, Y.; Guo, X.; Zhang, J.; Zhang, F.; Nie, X.; Wang, S. Lysine Succinylation Contributes to Aflatoxin Production and Pathogenicity in Aspergillus flavus. *Mol. Cell Proteom.* **2018**, *17*, 457–471. [CrossRef]
57. Mengjuan, Z.; Guanglan, L.; Xiaohua, P.; Weitao, S.; Can, T.; Xuan, C.; Yanling, Y.; Zhenhong, Z. The PHD transcription factor Cti6 is involved in the fungal colonization and aflatoxin B1 biological synthesis of Aspergillus flavus. *IMA Fungus* **2021**, *12*, 12. [CrossRef]
58. Zhang, W.; Lv, Y.; Lv, A.; Wei, S.; Zhang, S.; Li, C.; Hu, Y. Sub3 inhibits *Aspergillus flavus* growth by disrupting mitochondrial energy metabolism, and has potential biocontrol during peanut storage. *J. Sci. Food Agric.* **2021**, *101*, 486–496. [CrossRef]
59. Hu, Y.; Yang, G.; Zhang, D.; Liu, Y.; Li, Y.; Lin, G.; Guo, Z.; Wang, S.; Zhuang, Z. The PHD Transcription Factor Rum1 Regulates Morphogenesis and Aflatoxin Biosynthesis in Aspergillus flavus. *Toxins* **2018**, *10*, 301. [CrossRef]
60. Chang, P.-K.; Zhang, Q.; Scharfenstein, L.; Mack, B.; Yoshimi, A.; Miyazawa, K.; Abe, K. Aspergillus flavus GPI-anchored protein-encoding ecm33 has a role in growth, development, aflatoxin biosynthesis, and maize infection. *Appl. Microbiol. Biotechnol.* **2018**, *102*, 5209–5220. [CrossRef]

toxins

MDPI

Article

Efficient Inhibition of *Aspergillus flavus* to Reduce Aflatoxin Contamination on Peanuts over Ag-Loaded Titanium Dioxide

Dandan Yang [1], Hailian Wei [1], Xianglong Yang [1], Ling Cheng [1], Qi Zhang [1,2], Peiwu Li [1,2] and Jin Mao [1,2,*]

[1] National Reference Laboratory for Agricultural Testing P.R. China, Key Laboratory of Detection for Mycotoxins, Laboratory of Quality & Safety Risk Assessment for Oilseed Products (Wuhan), Quality Inspection & Test Center for Oilseed Products, Key Laboratory of Biology and Genetic Improvement of Oil Crops, Ministry of Agriculture, Oil Crops Research Institute, Chinese Academy of Agricultural Sciences, Wuhan 430062, China

[2] Hubei Hongshan Laboratory, Wuhan 430062, China

* Correspondence: maojin106@whu.edu.cn

Abstract: Peanuts are susceptible to aflatoxins produced by *Aspergillus flavus*. Exploring green, efficient, and economical ways to inhibit *Aspergillus flavus* is conducive to controlling aflatoxin contamination from the source. In this study, Ag-loaded titanium dioxide composites showed more than 90% inhibition rate against *Aspergillus flavus* under visible light irradiation for 15 min. More importantly, this method could also reduce the contaminated level of *Aspergillus flavus* to prevent aflatoxins production in peanuts, and the concentrations of aflatoxin B_1, B_2, and G_2 were decreased by 96.02 ± 0.19%, 92.50 ± 0.45%, and 89.81 ± 0.52%, respectively. It was found that there are no obvious effects on peanut quality by evaluating the changes in acid value, peroxide value, and the content of fat, protein, polyphenols, and resveratrol after inhibition treatment. The inhibition mechanism was that these reactive species ($\bullet O_2^-$, $\bullet OH^-$, h^+, and e^-) generated from photoreaction destroyed cell structures, then led to the reduced viability of *Aspergillus flavus* spores. This study provides useful information for constructing a green and efficient inhibition method for *Aspergillus flavus* on peanuts to control aflatoxin contamination, which is potentially applied in the field of food and agri-food preservation.

Keywords: peanuts; *Aspergillus flavus*; inhibition; visible light; Ag-loaded titanium dioxide; quality

Key Contribution: This study provides a green and efficient way to inhibit *Aspergillus flavus* on peanuts, which can reduce the aflatoxin contamination from the source. Ag-loaded titanium dioxide composites showed excellent activity in inhibiting *Aspergillus flavus* to reduce aflatoxin contamination on peanuts under visible light irradiation.

Citation: Yang, D.; Wei, H.; Yang, X.; Cheng, L.; Zhang, Q.; Li, P.; Mao, J. Efficient Inhibition of *Aspergillus flavus* to Reduce Aflatoxin Contamination on Peanuts over Ag-Loaded Titanium Dioxide. *Toxins* **2023**, *15*, 216. https://doi.org/10.3390/toxins15030216

Received: 16 February 2023
Revised: 5 March 2023
Accepted: 8 March 2023
Published: 10 March 2023

1. Introduction

Industrial wastes, pesticides, heavy metals, mycotoxins, etc. are becoming more and more serious threats to food safety [1–4]. Peanuts, with rich nutrients and health value, are a type of important oil crop [5], but they are susceptible to aflatoxin contamination. Aflatoxins, with high toxicity, teratogenicity, and carcinogenicity, have been regarded as the most toxic mycotoxins found in food and agri-food [6–8], which not only threaten human health, but also can lead to huge economic losses [9–13]. Aflatoxins are secondary metabolites, mainly produced by *Aspergillus flavus (A. flavus)* in food and agri-food, especially peanuts and corn [14,15]. Therefore, controlling *A. flavus* is a meaningful approach to reducing the contamination of aflatoxins in food and agri-food from the source.

The most frequently used measures for controlling *A. flavus* include physical, chemical, and biological measures, etc. Physical measures, such as high voltage atmospheric cold plasma, and chemical measures, such as Validamycin A, could control *A. flavus* [16,17]. For biological methods, *Bacillus subtilis* QST 713 [18], *Pseudomonas stutzeri* YM6 [19], and lactic

acid bacteria [20], etc. showed inhibition effects on *A. flavus*. Recently, it had been reported that photocatalysis based on semiconductors can be used as an effective way to control fungi [21].

Photocatalysis is regarded as a green, mild, and low-energy method [22]. However, exploring an efficient, low-cost, and stable catalyst that can be used in food and agri-food is challenging and significant. Titanium dioxide (TiO_2) is a low-cost, low-toxicity, and high-stability photocatalyst, which can be also used as a food additive authorized by the Food and Drug Administration [23]. It could be used as a food additive in bakeries, chewing gums, candies, chocolates, etc. [24]. In addition, Hwang et al. evaluated the physicochemical properties, intestinal transport, and cytotoxicity of food additive TiO_2, which were conducive to the application of TiO_2 in the food industry [25]. It was found that TiO_2 could inactivate *Escherichia coli* (*E. coli*) [26], *Staphylococcus aureus* (*S. aureus*) [27], and *Bacillus subtilis* [28] under ultraviolet (UV) light irradiation. However, only 5% of sunlight is UV light, which limits the practical application of TiO_2 [29]. Ag nanoparticles (Ag NP_S) can present the surface plasmon resonance (SPR) effect to enhance the visible light absorption region of TiO_2 [30]. Besides, the intrinsic disinfection property of Ag NP_S had been proved in the field of food disinfection. Bandpey et al. made Ag-coated low-density polyethylene films, which presented promising disinfectant activity against microbes and prolonged the shelf life of milk [31]. Wu et al. reported that Ag/TiO_2 composites showed excellent photocatalytic activity in the disinfection of *E. coli* and *S. aureus* under visible light irradiation [32]. Based on the above introduction, this study intends to combine Ag and TiO_2 to utilize their synergistic effects for controlling *A. flavus* in food and agri-food.

Herein, Ag-loaded titanium dioxide (Ag/TiO_2) composites were synthesized by a facile photodeposition method, and the composition and microstructure of Ag/TiO_2 were analyzed. Then, the inhibition performance of Ag/TiO_2 on *A. flavus* was evaluated by a modified plate colony counting method. The inhibition activity of Ag/TiO_2 on contaminated peanuts was also estimated, and the reduction of aflatoxins concentrations was evaluated by high-performance liquid chromatography (HPLC). In addition, the effects of photocatalytic inhibition on the quality of peanuts were discussed. Finally, the reasons for photocatalytic activity enhancement were investigated by UV-visible diffuse reflectance spectrum (UV-vis DRS) analysis and photoelectrochemical tests. The photocatalytic inhibition mechanism of *A. flavus* over Ag/TiO_2 was explored by radical trapping tests, electron spin resonance (ESR) analysis, and fluorescent spore staining tests.

2. Results

2.1. Characterization of Photocatalysts

XRD was used to study the crystal structure of as-prepared catalysts. As demonstrated in Figure 1a, the characteristic diffraction peaks of anatase and rutile were observed in TiO_2, consistent with its mixed-crystal phases [33]. The peaks located at 25.28°, 37.80°, 48.05°, and 62.69° could be identified as the (101), (004), (200), and (204) crystal planes of anatase (JCPDS No. 21-1272), while peaks at 27.44°, 36.09°, 41.23°, 54.32°, 56.64°, and 69.01°corresponded to the (110), (101), (111), (211), (220), and (301) planes of rutile (JCPDS No. 21-1276), respectively. As for Ag/TiO_2, an additional peak at 38.10° appeared in the enlarged XRD pattern (Figure 1b), which was ascribed to the (111) crystal plane of Ag (JCPDS No. 01-1167) [34]. This result indicated the introduction of metallic Ag on TiO_2 to form Ag/TiO_2, which was successfully synthesized via the photodeposition method.

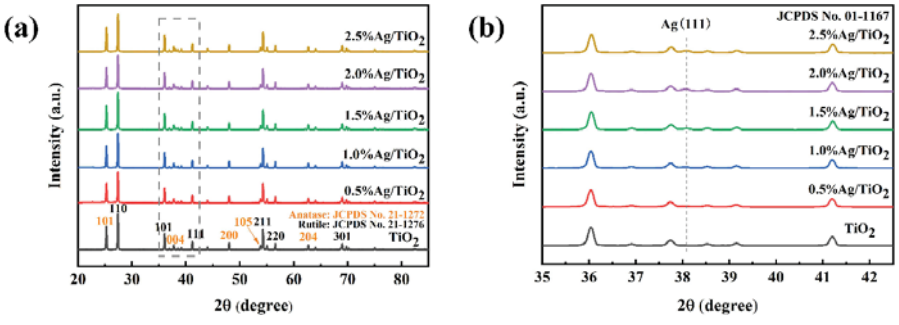

Figure 1. (**a**) XRD spectrum of TiO_2 and Ag/TiO_2 with different silver concentrations and (**b**) the enlarged pattern in 35–42.5° of Figure 1a.

The elemental compositions and chemical states of the Ag/TiO_2 were subsequently characterized by XPS. The spectra of Figure 2a implied that the catalyst was mainly composed of three elements, including Ti, O, and Ag, while the C 1s peak might be attributed to the adsorbed CO_2 or the contamination of hydrocarbons in the instrument [35]. In Ti 2p (Figure 2b) and O 1s (Figure 2c) spectra, peaks at 464.2 eV, 458.6 eV, 529.8 eV, and 531.8 eV were observed, which should be identified as the Ti $2p_{1/2}$ and Ti $2p_{3/2}$ spin orbitals of Ti^{4+} [36], lattice oxygen atoms, and oxygen atoms of surface hydroxyl [34], respectively. As for Ag 3d spectrum in Figure 2d, characteristic peaks of Ag $3d_{5/2}$ and Ag $3d_{3/2}$ appeared at 367.5 eV and 373.5 eV [37], which further confirmed the existence of metallic Ag in the catalysts.

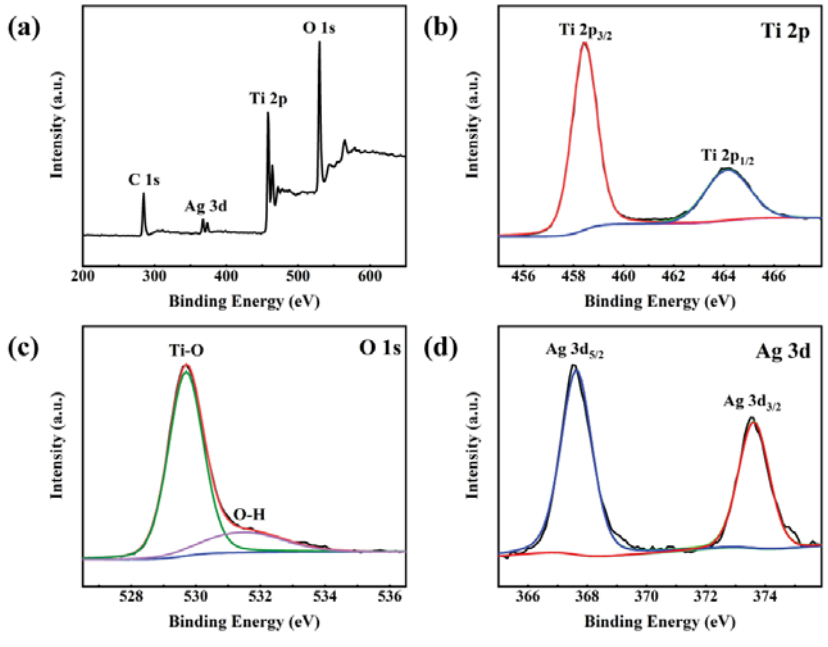

Figure 2. (**a**) XPS survey spectrum; high-resolution (**b**) Ti 2p spectrum; (**c**) O 1s spectrum; and (**d**) Ag 3d spectrum of 1.5% Ag/TiO_2.

SEM, TEM, and HRTEM were used to analyze the micromorphology of the as-prepared catalysts. As depicted in Figure 3a–c, Ag/TiO_2 was made up of TiO_2 irregular blocks with

deposited Ag NP_S. In accordance with the XRD results, typical lattice fringes with spacings of 0.170, 0.323, and 0.236 nm were observed, corresponding to the (105) plane of anatase, (110) plane of rutile, and (111) plane of Ag, respectively (Figure 3d). Moreover, the element mapping of Ag/TiO_2 visually displayed its elemental distribution, where Ag was observed on the surface of the TiO_2 block with uniformly distributed Ti and O. Based on the XRD, XPS, TEM, and mapping characterizations, it can be concluded that Ag/TiO_2 was successfully synthesized by depositing Ag NPs over the TiO_2.

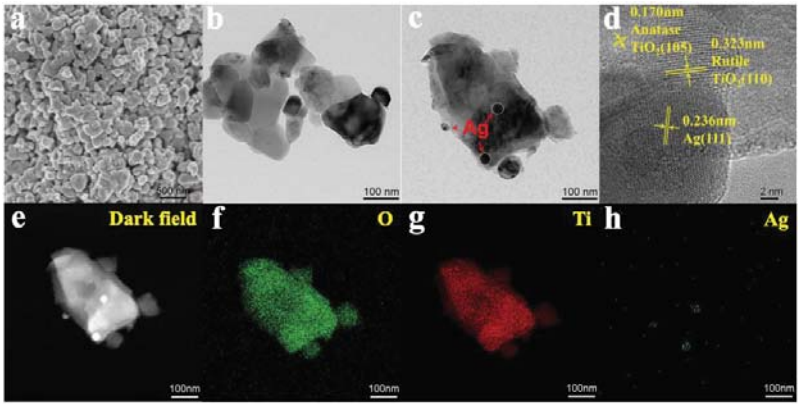

Figure 3. (**a**) SEM; (**b**,**c**) TEM; (**d**) HRTEM; the corresponding elemental mappings of (**e**) dark field; (**f**) O; (**g**) Ti; and (**h**) Ag of 1.5% Ag/TiO_2.

2.2. Photocatalytic Inhibition Tests

2.2.1. Inhibition Activities of Different Conditions

The photocatalytic inhibition activity of *A. flavus* over as-prepared Ag/TiO_2 was investigated by a modified plate colony counting method. As displayed in Figure 4a, there were no inhibition activities in either darkness or light without catalysts; the inhibition rate of Ag/TiO_2 under visible light irradiation was much higher than that in the dark, illustrating that the catalyst and visible light were necessary for photocatalytic inhibition activity. The inhibition rate of Ag/TiO_2 was 27.58 ± 1.86% in the dark, which was attributed to the intrinsic disinfection effect of Ag NPs. It was also found that the composites presented a higher inhibition rate than the single catalyst under visible light irradiation in Figure 4a. Figure 4b indicated that the inhibition rate of *A. flavus* in the presence of Ag/TiO_2 gradually increased with the increase in irradiation time. The inhibition rate of Ag/TiO_2 against *A. flavus* was > 90% after irradiation for 15 min.

2.2.2. Inhibition Activities of Ag/TiO_2 with Different Silver Concentrations

In addition, the inhibition activities of Ag/TiO_2 with different silver concentrations were explored. As demonstrated in Figure 4c, it was presented that the colony units in the presence of 1.5% Ag/TiO_2 were the least compared with the others. The result was in accordance with the content in Figure 4d and suggested that 1.5% Ag/TiO_2 has the highest inhibition rate of *A. flavus* under visible light. With the increase in silver concentrations, the photocatalytic inhibition rate of *A. flavus* firstly increased, followed by decreasing gradually when the silver concentrations were higher than 1.5% in Figure 4d. The reason for this phenomenon might be that too many Ag NPs generated a masking effect on the surface of TiO_2 [38]. Therefore, the light-harvesting ability of the photocatalyst was reduced, which led to a reduction in the inhibition rate.

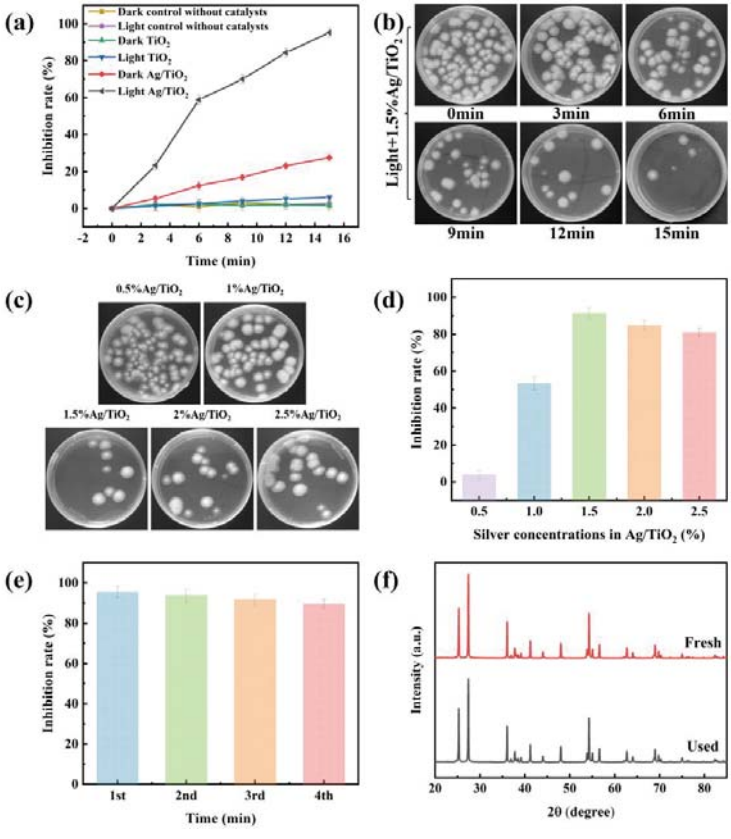

Figure 4. (**a**) The inhibition rates correspond to different treatment conditions; (**b**) the colony units under different irradiation times; (**c**) the colony units and (**d**) the corresponding inhibition rates over Ag/TiO_2 with different silver concentrations; (**e**) the inhibition rates of four-cycle tests; and (**f**) XRD spectra of 1.5% Ag/TiO_2 before and after four-cycle tests.

2.2.3. Stability and Reusability of Catalysts

The stability of the catalyst was a decisive factor in long-term and continuous utilization, which was evaluated via the cyclic tests of 1.5% Ag/TiO_2. As demonstrated in Figure 4e, 1.5% Ag/TiO_2 maintained efficient photocatalytic activity during the consecutive runs, suggesting that Ag/TiO_2 had good stability and reusability. The stability was further confirmed by the XRD pattern of the recycled 1.5% Ag/TiO_2 (Figure 4f), which displayed no significant change after the fourth cycle. The above discussions verified that 1.5% Ag/TiO_2 was potentially used in the photocatalytic inhibition of *A. flavus*.

2.3. Photocatalytic Inhibition in Peanuts

Peanuts were susceptible to *A. flavus* and aflatoxin contamination, which were regarded as some of the most serious problems for food safety [39]. Thus, the inhibition performance of *A. flavus* over the as-prepared 1.5% Ag/TiO_2 on peanuts was evaluated. As shown in Figure 5a, the number of mycelia and spores on the surface of peanuts began to decrease gradually with the prolongation of irradiation time. Additionally, the contamination of *A. flavus* on peanuts was greatly inhibited after irradiation for 15 min. In addition, the concentrations of AFB_1, AFB_2, AFG_2, and AFG_1 were determined by the HPLC to analyze the contaminated level of aflatoxins in the above peanuts. As displayed in Figure 5b, the concentrations of aflatoxins on peanuts treated by photocatalysts under

visible light were notably reduced. The corresponding inhibition rates of AFB_1, AFB_2, and AFG_2 were 96.02 ± 0.19%, 92.50 ± 0.45%, and 89.81 ± 0.52%, respectively. These results illustrated that the 1.5% Ag/TiO_2 can effectively inhibit *A. flavus* growth to control aflatoxin contamination in peanuts.

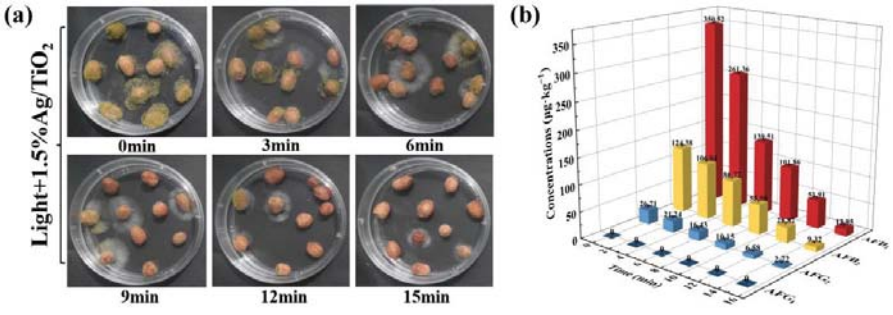

Figure 5. (**a**) The colonies of *A. flavus* on peanuts under different irradiation times and (**b**) the concentrations of aflatoxins in peanuts treated with 1.5% Ag/TiO_2.

2.4. Peanut Quality Analysis after Photocatalytic Inhibition

The acid value (AV), peroxide value (POV), and the contents of fat, protein, polyphenols, and resveratrol after the treatment were estimated to investigate the effects of photocatalytic inhibition treatment on the quality of peanuts. AV and POV were two important indicators for testing whether peanuts were oxidatively deteriorated. The AV and POV before and after photocatalytic treatment were unchanged (Table 1), and they were lower than 3 mg/g and 0.4 g/100 g, which were the recommended values of the China Agricultural Industry Recommended Standard, respectively. The results of the correlational analysis suggested that photocatalytic treatment did not cause oxidation or deterioration of peanuts. Peanuts were rich in fat and protein [40], which belonged to six basic nutrients. The results showed the contents of fat and protein in peanuts were 51.64 ± 0.54% and 28.44 ± 0.76 before inhibition treatment, respectively. It has become apparent that the changes in fat and protein content were negligible after photocatalytic treatment. Polyphenols and resveratrol were nutrients with antioxidative functions in peanuts. Furthermore, it was found that the contents of polyphenols and resveratrol hardly changed after photocatalytic treatment. The above results suggest that the photocatalytic inhibition treatment could be a promising and efficient method to prevent *A. flavus* and to control aflatoxin contamination in peanuts.

Table 1. The determination results of peanut samples before and after photocatalytic treatment.

Peanuts	Acid Value (mg/g)	Peroxide Value (g/100 g)	Fat (%)	Protein (%)	Polyphenols (mg/kg)	Resveratrol (mg/kg)
Control *	1.46 ± 1.80	0.06 ± 1.41	51.64 ± 0.54	28.44 ± 0.76	27.48 ± 0.58	5.44 ± 1.15
1d	1.40 ± 2.88	0.06 ± 1.00	51.32 ± 0.35	28.32 ± 0.70	27.41 ± 0.67	5.35 ± 1.54
7d	1.45 ± 2.35	0.06 ± 1.38	51.49 ± 0.33	28.40 ± 0.29	27.45 ± 0.78	5.29 ± 1.01
14d	1.51 ± 1.74	0.06 ± 1.23	51.53 ± 0.43	28.42 ± 0.50	27.39 ± 0.56	5.24 ± 1.09
21d	1.47 ± 1.40	0.06 ± 1.18	51.48 ± 0.29	28.32 ± 0.46	27.33 ± 0.88	5.23 ± 1.06

* Control represented the peanuts without photocatalytic treatment. The form of data: mean of three values ± relative standard deviation.

3. Discussion

The above results had shown that the method was feasible and efficient in inhibiting *A. flavus* to reduce aflatoxin contamination in peanuts. The discussion of the inhibition mechanism helped to have an in-depth understanding and provided a theoretical basis and reference for the subsequent optimization of the method.

3.1. Photocatalytic Activity Enhancement Mechanism

The light-harvesting ability was one of the most significant factors for photocatalytic performance. Enhanced light-harvesting ability was conducive to photocatalytic activity. Thus, the UV-vis DRS absorption spectra of 1.5% Ag/TiO_2 and TiO_2 were recorded in Figure 6a. It is worth noting that the absorption range of Ag/TiO_2 demonstrated an increase in the visible light region compared with pristine TiO_2, which should be attributed to the SPR effect of metallic Ag NPs [41].

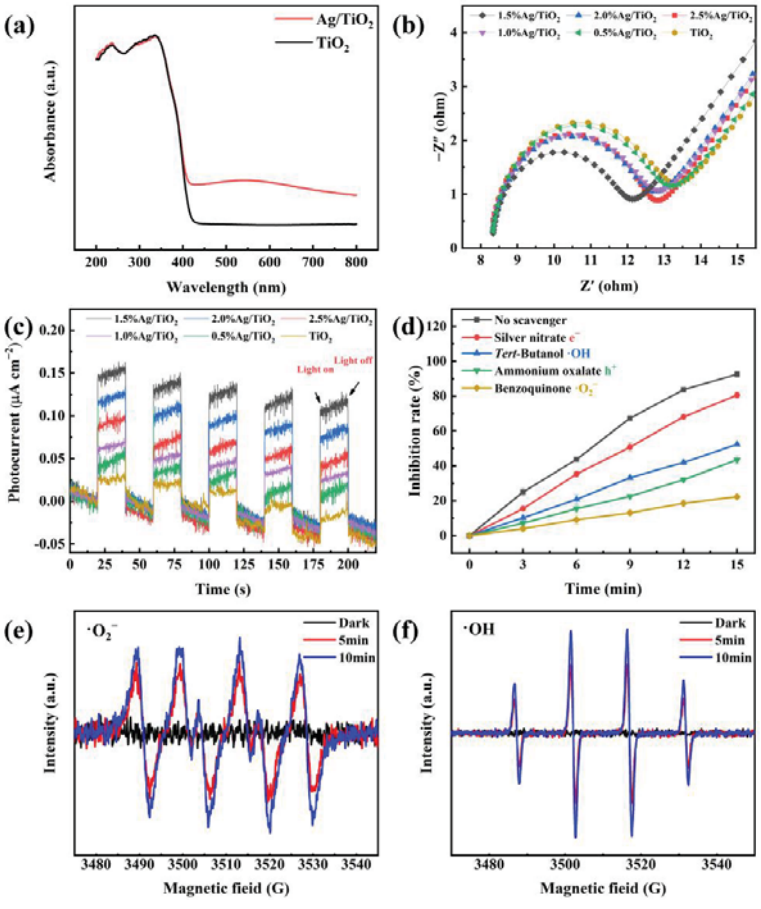

Figure 6. (**a**) UV-vis DRS spectra of 1.5% Ag/TiO_2 and TiO_2; (**b**) EIS and (**c**) transient photocurrent response spectra of TiO_2 and Ag/TiO_2; (**d**) the inhibition rates that correspond to different radical scavengers; ESR spectra of (**e**) $\bullet O_2^-$ and (**f**) •OH for 1.5% Ag/TiO_2.

Electrochemical impedance spectroscopy (EIS) and transient photocurrent responses were employed to investigate the separation and transfer ability of the photogenerated carriers (h^+ and e^-). Generally, the higher the separation and the transfer efficiency of carriers, the better the photocatalytic activity. The smaller arc radius represented the smaller charge transfer resistance of as-prepared samples in EIS. Obviously, 1.5% Ag/TiO_2 was the smallest one (Figure 6b), which indicated the most efficient charge-transfer property of the photocatalyst. Transient photocurrent responses were also measured to further observe the separation efficiency of carriers. As depicted in Figure 6c, the 1.5% Ag/TiO_2

photocatalyst shows the strongest transient photocurrent response, implying the highest charge separation ability of 1.5% Ag/TiO_2.

3.2. Photocatalytic Inhibition Mechanism

To explore the active species in photocatalytic inhibition of *A. flavus*, radical trapping tests were performed. As shown in Figure 6d, benzoquinone caused a prominent decrease in inhibition rate, which indicated that $\bullet O_2^-$ was the main active specie for inhibiting *A. flavus*. As for h^+ and •OH, the addition of ammonium oxalate and *tert*-Butanol generated a lower loss of inhibition rate. Taking into account that •OH mainly originated from the oxidation of H_2O driven by h^+, the inhibition of *A. flavus* should be ascribed to •OH, which suggested that •OH was a secondary active specie. $AgNO_3$ hardly had an effect on inhibition efficiency, indicating that e^- played the weakest role in this photoreaction system. The results of ESR tests were displayed in Figure 6e,f. Figure 6e showed that no $\bullet O_2^-$ was generated from the 1.5% Ag/TiO_2 in the dark, but it could be discovered that the $\bullet O_2^-$ had a 1:1:1:1 quartet pattern characteristic after irradiation for 5 and 10 min. Similarly, as demonstrated in Figure 6f, the obvious characteristic peak of •OH was observed, which suggested the production of •OH radicals from 1.5% Ag/TiO_2 under visible light irradiation.

To obtain a deeper understanding of the photocatalytic inhibition mechanism of *A. flavus*, morphological changes of *A. flavus* spores before and after the photocatalytic inhibition treatment were investigated through fluorescence-based live/dead fungal staining tests. In general, after staining by fluorescent dyes, SYTO 9 and PI, the living spores, which had intact cell membranes, would appear in green, while dead spores, which had damaged cell membranes, appeared in red [42]. As displayed in Figure 7a, almost all spore cells without visible light irradiation were alive. To the contrary, the number of dead spores increased considerably after irradiation for 15 min, indicating that photocatalytic treatment led to the damage of fungal cell structure.

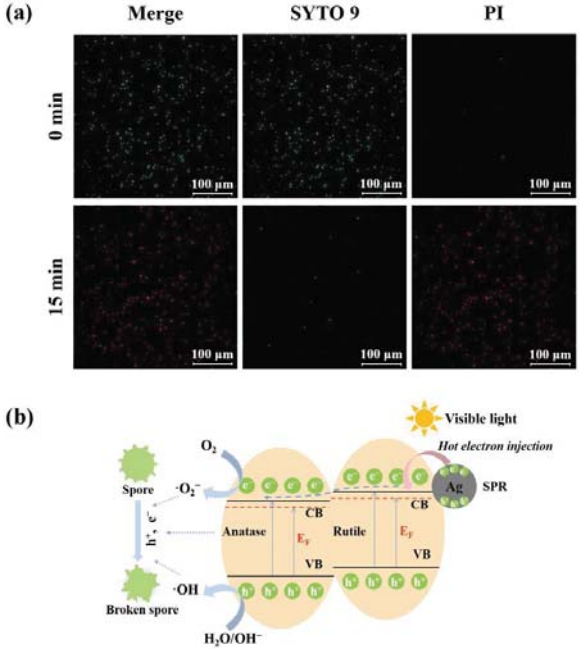

Figure 7. (**a**) Fluorescent images of live/dead spores of *A. flavus* and (**b**) the possible photocatalytic inhibition mechanism of Ag/TiO_2.

Based on the above analyses, a possible photocatalytic inhibition mechanism of *A. flavus* over Ag/TiO_2 was proposed and displayed in Figure 7b. When Ag/TiO_2 was irradiated by visible light, the deposited Ag NPs on TiO_2 improved the light-harvesting performance on account of the SPR effect, and they produced hot electrons. Hot electrons were transferred into the conduction band (CB) of TiO_2 to create additional Fermi levels, which reduce the band gap energy near the CB [43]. Meanwhile, because of the intense interfacial contact between anatase, rutile, and Ag NPs, the conduction band potential of anatase was more positive than that of rutile. Additionally, the hot electrons firstly tended to flow to the CB of the rutile, followed by flowing to the CB of anatase [44]. This type of flow prolonged the lifetime of carriers, enhanced the separation and transfer abilities of electron-hole pairs, and was conducive to photocatalytic activity [45]. O_2 was driven to reduction by e^- to $\bullet O_2^-$, and h^+ oxidized H_2O/OH^- to $\bullet OH$. These active species generated in the photocatalytic reaction attacked the spore cell membranes and caused damage to cell structures, which eventually led to reduced viability of *A. flavus* spores.

4. Conclusions

In conclusion, Ag/TiO_2 composites were synthesized by a facile photodeposition method, which could efficiently inhibit *A. flavus* growth under visible light irradiation. Ag/TiO_2 composites could also control *A. flavus* and then reduce the aflatoxin contamination in peanuts. Moreover, there were no obvious effects on the quality of peanuts after photocatalytic inhibition treatment. This efficient inhibition was due to the intrinsic disinfection and co-catalysis effects of Ag NP_S in composites. It was found that active species, such as $\bullet O_2^-$, $\bullet OH^-$, h^+, and e^-, generated in photocatalytic reactions, could destroy the integrity of spore cell membranes to cause the reduced viability of *A. flavus* spores. This study presented an efficient, economical, and sustainable inhibition method for inhibiting *A. flavus*, which provided a reference for the green control of other pathogenic fungi.

5. Materials and Methods

5.1. Materials

All reagents, of analytical grade, were used directly without any further purification. $AgNO_3$ was purchased from Guangdong Guanghua Sci-Tech Co., Ltd. (Guangdong, China). Tween 80, TiO_2, and ammonium oxalate were acquired from Sinopharm Chemical Reagents Co., Ltd. (Shanghai, China). Benzoquinone and *tert*-Butanol were obtained from Sigma-Aldrich. Deionized water was used in all experiments.

5.2. Synthesis and Characterization of Ag/TiO_2

5.2.1. Synthesis of Ag/TiO_2

Ag/TiO_2 was synthesized by a facile photodeposition method [30]. In detail, 625 mg TiO_2 powder was evenly dispersed in 200 mL methanol aqueous solution (10%) after sonication for 30 min, and then 868 μL $AgNO_3$ solution (0.1 mol/L) was added drop by drop. After vigorous stirring for 1 h, the suspension liquid was irradiated with an ultraviolet halogen lamp (365–405 nm) for 1 h. The precipitate was centrifuged, washed three times with ethanol and water, and dried at 80 °C for 18 h. In addition, in order to evaluate the effect of silver concentrations on the photocatalytic inhibition performance, a series of Ag/TiO_2 with different silver concentrations were prepared and labeled as 0.5%, 1%, 1.5%, 2%, and 2.5% Ag/TiO_2 (Figure S1).

5.2.2. Material Characterization

X-ray diffraction (XRD) analysis was recorded on a Bruker-AXS D8 X-ray diffractometer with a scan range of 20–80°. X-ray photoelectron spectroscopy (XPS, Thermo Escalab 250Xi, Waltham, MA, USA) was used to characterize the elemental compositions and chemical states of as-prepared Ag/TiO_2. The morphology and microstructure were observed by scanning electron microscopy (SEM, Hitachi Limited SU8020, Tokyo, Japan), transmission

electron microscopy (TEM, FEI Tecnai G2 F30, Hillsboro, TX, USA), and high-resolution transmission electron microscopy (HRTEM, FEI Tecnai G2 F30, Hillsboro, TX, USA).

5.3. Activation of Aspergillus flavus

All materials used in the process of the experiment were sterilized in advance [46]. The preserved spore suspension of *A. flavus* 3.4408 (China General Microbiological Culture Collection Center (Beijing, China)) was inoculated on AFPA Agar medium for activation, and it was cultured for three days (28 °C, 90% RH) until orange round colonies appeared. The activated mycelium of *A. flavus* was subsequently picked with sterile toothpicks and inoculated on Dichloran Glycerol (DG-18) Agar medium. After five to seven days of culture (28 °C, 90% RH), the spores were washed with Tween 80 (0.1%). Additionally, its concentration was estimated with blood counting plates under optical microscope. The obtained spores were stored in a refrigerator at 4 °C for later use.

5.4. Photocatalytic Inhibition Tests

5.4.1. The Method of Photocatalytic Inhibition Tests

The modified plate colony counting method was used to evaluate the inhibition activities of Ag/TiO_2. In detail, 25 mg of Ag/TiO_2 powder was firstly suspended in 50 mL of spore suspension (10^6 CFU/mL), followed by stirring for 30 min in the dark to reach sorption equilibrium. After that, the suspension was irradiated by a 300 W Xenon lamp (PLS SXE300, Beijing Perfectlight Inc., Beijing, China) with a visible light filter ($\lambda > 420$ nm). After given intervals (0, 3, 6, 9, 12, and 15 min), 1 mL of mixed liquid was taken as a sample, diluted with sterile water, and evenly coated on Malt Extract Agar medium. At last, the growing colony units were counted after culturing for 48 h at 28 °C. The inhibition rate (R) was calculated by comparing the colony number of *A. flavus* at the beginning (C_0) and treatment time t (C_t): $R\ (\%) = (C_0 - C_t)/C_0 \times 100\%$.

5.4.2. The Effect of Ag/TiO_2 with Different Silver Concentrations

According to the above method, photocatalytic inhibition tests were carried out with 0.5%, 1%, 1.5%, 2%, and 2.5% Ag/TiO_2, respectively. Then, the inhibition performances were compared and analyzed.

5.4.3. Cyclic Tests

The cyclic tests of photocatalytic inhibition of *A. flavus* were conducted to analyze the stability and reusability of the as-prepared Ag/TiO_2 [47]. To be specific, the Ag/TiO_2 composites were collected and reused by centrifuging, washing, and drying after each cycle.

5.5. Photocatalytic Inhibition of Aspergillus flavus on Peanuts

The peanuts with complete grains and uniform shapes were sterilized (121 °C, 30 min) and placed on Petri dishes (10 grains per plate). The spore suspension (1×10^4 CFU/mL, 20 μL per grain) was inoculated on the surface of the peanuts and dried naturally. Subsequently, 200 μL of Ag/TiO_2 dispersion (0.5 mg/mL) was evenly added to the surface of the contaminated peanuts, followed by irradiating with a Xenon lamp. After that, these peanuts were cultured for seven days at 28 °C. The growth situation of *A. flavus* on peanuts was observed. Whereafter, the treated peanuts were sterilized, dried at 105 °C, and ground for the determination of aflatoxins (AFB_1, AFB_2, AFG_1, and AFG_2) using HPLC (Agilent 1100, Palo Alto, CA, USA). Specific parameters were shown in Table 2.

Table 2. Specific parameters of the HPLC method.

Project	Parameters
Mobile phase	Methanol aqueous solution (45%)
Velocity of flow	0.80 mL/min
Chromatographic column	Sycronis C18, 4.6 mm × 150 mm, 5 μm
Column temperature	35 °C
Excitation wavelength	360 nm
Emission wavelength	440 nm
Injection volume	10 μL
Analysis time	14 min

5.6. Evaluation of the Peanut Quality before and after Inhibition Treatment

In brief, the effects of inhibition treatment on peanut quality were investigated by determining acid value, peroxide value, and the contents of fat, protein, polyphenols, and resveratrol in peanuts before and after photocatalytic treatment. These indicators of peanuts were determined at the given times (1, 7, 14, and 21 days) after the treatment. The detailed detection methods of each indicator are in the Supplementary Materials.

5.7. Study of the Photocatalytic Inhibition Mechanism of Aspergillus flavus

5.7.1. Photocatalytic activity enhancement mechanism

The light absorption characteristics were analyzed through the UV-vis DRS (Shimadzu UV-3600, Kyoto, Japan). Photoelectrochemical properties were detected on a CHI 660E electrochemical workstation.

5.7.2. Photocatalytic Inhibition Mechanism

Radical trapping tests were conducted to confirm the main active species in the process of photocatalytic inhibition, where benzoquinone (1 mM), *tert*-Butanol (1 mM), ammonium oxalate (1 mM), and $AgNO_3$ (0.5 mM) were added to each parallel photocatalytic system to assume the role of scavengers for $\bullet O_2^-$, $\bullet OH$, h^+, and e^-, respectively [48].

ESR tests were employed to further explore the formation of reactive oxygen species. The production of $\bullet O_2^-$ and $\bullet OH$ by the as-prepared Ag/TiO_2 was quantified by ESR analysis (Bruker A300-10/12, Karlsruhe, Germany).

In addition, the fluorescence-based live/dead fungal viability assay was carried out using LIVE/DEAD® FungaLight™ Yeast Viability Kit (Waltham, MA, USA) to explore the integrity of spore cell membranes and cell viability. The spore suspension was centrifuged, followed by washing before and after the inhibition treatment. Then, the resultant spores were stained for 30 min with SYTO 9 (6 μg/mL) and PI (6 μg/mL) in the confocal dish in the dark. Finally, the results were observed by a super-resolution confocal laser microscope (Zeiss LSM980, Oberkochen, Germany).

Supplementary Materials: The following supporting information can be downloaded at: https://www.mdpi.com/article/10.3390/toxins15030216/s1, Figure S1: Ag/TiO_2 composites with silver concentrations of 0.5%, 1%, 1.5%, 2%, and 2.5%. References [49–54] are cited in the Supplementary Materials.

Author Contributions: Conceptualization, D.Y. and J.M.; Methodology, D.Y.; Formal Analysis, D.Y., X.Y. and L.C.; Investigation, D.Y. and H.W.; Writing—Original Draft Preparation, D.Y.; Writing—Review and Editing, J.M. and X.Y.; Supervision, Q.Z.; Project administration, P.L.; Funding acquisition, J.M. and L.C. All authors have read and agreed to the published version of the manuscript.

Funding: This work is supported by the National Key Research and Development Program (2022YFF 1100700), National Natural Science Foundation of China (32272447, 32102113), and the Agricultural Science and Technology Innovation Program of the Chinese Academy of Agricultural Science (CAAS-ASTIP-2021- OCRI).

Institutional Review Board Statement: Not applicable.

Informed Consent Statement: Not applicable.

Data Availability Statement: The data presented in this study are available in the article.

Conflicts of Interest: The authors declare no conflict of interest.

References

1. Gavahian, M.; Sarangapani, C.; Misra, N.N. Cold plasma for mitigating agrochemical and pesticide residue in food and water: Similarities with ozone and ultraviolet technologies. *Food Res. Int.* **2021**, *141*, 110138. [CrossRef] [PubMed]
2. Shen, Y.Z.; Nie, C.; Wei, Y.L.; Zheng, Z.; Xu, Z.L.; Xiang, P. FRET-based innovative assays for precise detection of the residual heavy metals in food and agriculture-related matrices. *Coord. Chem. Rev.* **2022**, *469*, 214676. [CrossRef]
3. Murugesan, P.; Brunda, D.K.; Moses, J.A.; Anandharamakrishnan, C. Photolytic and photocatalytic detoxification of mycotoxins in foods. *Food Control* **2021**, *123*, 107748. [CrossRef]
4. Leite, M.; Freitas, A.; Barbosa, J.; Ramos, F. Mycotoxins in Raw Bovine Milk: UHPLC-QTrap-MS/MS Method as a Biosafety Control Tool. *Toxins* **2023**, *15*, 173. [CrossRef]
5. Sharma, S.; Choudhary, B.; Yadav, S.; Mishra, A.; Mishra, V.K.; Chand, R.; Chen, C.; Pandey, S.P. Metabolite profiling identified pipecolic acid as an important component of peanut seed resistance against Aspergillus flavus infection. *J. Hazard. Mater.* **2021**, *404*, 124155. [CrossRef]
6. Ferrari, L.; Rizzi, N.; Grandi, E.; Clerici, E.; Tirloni, E.; Stella, S.; Bernardi, C.E.M.; Pinotti, L. Compliance between Food and Feed Safety: Eight-Year Survey (2013–2021) of Aflatoxin M1 in Raw Milk and Aflatoxin B1 in Feed in Northern Italy. *Toxins* **2023**, *15*, 168. [CrossRef]
7. Song, R.X.; Yao, L.T.; Sun, C.P.; Yu, D.C.; Lin, H.; Li, G.S.; Lian, Z.C.; Zhuang, S.L.; Zhang, D.W. Electrospun Membranes Anchored with g-C_3N_4/MoS_2 for Highly Efficient Photocatalytic Degradation of Aflatoxin B_1 under Visible Light. *Toxins* **2023**, *15*, 133. [CrossRef]
8. Alshannaq, A.F.; Gibbons, J.G.; Lee, M.K.; Han, K.H.; Hong, S.B.; Yu, J.H. Controlling aflatoxin contamination and propagation of Aspergillus flavus by a soy-fermenting Aspergillus oryzae strain. *Sci. Rep.* **2018**, *8*, 16871. [CrossRef]
9. Endre, G.; Nagy, B.E.; Hercegfalvi, D.; Kasuba, C.; Vágvölgyi, C.; Szekeres, A. Scale-up of Aflatoxin Purification by Centrifugal Partition Chromatography. *Toxins* **2023**, *15*, 178. [CrossRef]
10. Liang, L.K.; Yang, H.J.; Wei, S.; Zhang, S.B.; Chen, L.; Hu, Y.S.; Lv, Y.Y. Putative C_2H_2 Transcription Factor AflZKS3 Regulates Aflatoxin and Pathogenicity in Aspergillus flavus. *Toxins* **2022**, *14*, 883. [CrossRef]
11. Xu, D.; Wei, M.Q.; Peng, S.R.; Mo, H.Z.; Huang, L.; Yao, L.S.; Hu, L.B. Cuminaldehyde in cumin essential oils prevents the growth and aflatoxin B_1 biosynthesis of Aspergillus flavus in peanuts. *Food Control* **2021**, *125*, 107985. [CrossRef]
12. Shen, M.H.; Singh, R.K. Effective UV wavelength range for increasing aflatoxins reduction and decreasing oil deterioration in contaminated peanuts. *Food Res. Int.* **2022**, *154*, 111016. [CrossRef]
13. Wang, J.; Liang, L.K.; Wei, S.; Zhang, S.B.; Hu, Y.S.; Lv, Y.Y. Histone 2-Hydroxyisobutyryltransferase Encoded by Afngg1 Is Involved in Pathogenicity and Aflatoxin Biosynthesis in Aspergillus flavus. *Toxins* **2023**, *15*, 7. [CrossRef]
14. Guo, Y.P.; Zhao, L.H.; Ma, Q.G.; Ji, C. Novel strategies for degradation of aflatoxins in food and feed: A review. *Food Res. Int.* **2021**, *140*, 109878. [CrossRef]
15. Wang, X.N.; Zha, W.J.; Yao, B.; Yang, L.; Wang, S.H. Genetic Interaction of Global Regulators AflatfA and AflatfB Mediating Development, Stress Response and Aflatoxins B1 Production in *Aspergillus flavus*. *Toxins* **2022**, *14*, 857. [CrossRef]
16. Ott, L.C.; Appleton, H.J.; Shi, H.; Keener, K.; Mellata, M. High voltage atmospheric cold plasma treatment inactivates Aspergillus flavus spores and deoxynivalenol toxin. *Food Microbiol.* **2021**, *95*, 103669. [CrossRef]
17. Plabutong, N.; Ekronarongchai, S.; Niwetbowornchai, N.; Edwards, S.W.; Virakul, S.; Chiewchengchol, D.; Thammahong, A. The Inhibitory Effect of Validamycin A on Aspergillus flavus. *Int. J. Microbiol.* **2020**, *2020*, 3972415. [CrossRef]
18. Bertuzzi, T.; Leni, G.; Bulla, G.; Giorni, P. Reduction of Mycotoxigenic Fungi Growth and Their Mycotoxin Production by Bacillus subtilis QST 713. *Toxins* **2022**, *14*, 797. [CrossRef]
19. Gong, A.D.; Lei, Y.Y.; He, W.J.; Liao, Y.C.; Ma, L.; Zhang, T.T.; Zhang, J.B. The Inhibitory Effect of *Pseudomonas stutzeri* YM6 on *Aspergillus flavus* Growth and Aflatoxins Production by the Production of Volatile Dimethyl Trisulfide. *Toxins* **2022**, *14*, 788. [CrossRef]
20. Simões, L.; Fernandes, N.; Teixeira, J.; Abrunhosa, L.; Dias, D.R. Brazilian Table Olives: A Source of Lactic Acid Bacteria with Antimycotoxigenic and Antifungal Activity. *Toxins* **2023**, *15*, 71. [CrossRef]
21. Sheng, Z.K.; Hou, F.M.; Zou, L.L.; Li, Y.H.; Li, J.X.; Li, J.; Ai, L.B.; Wei, W.; Wei, A. Highly efficient and photo-triggered elimination of Aspergillus fumigatus spores by Zn-Ti layered double hydroxide. *J. Photochem. Photobiol. A Chem.* **2022**, *432*, 114114. [CrossRef]
22. Xu, C.P.; Anusuyadevi, P.R.; Aymonier, C.; Luque, R.; Marre, S. Nanostructured materials for photocatalysis. *Chem. Soc. Rev.* **2019**, *48*, 3868. [CrossRef] [PubMed]
23. Fonseca, J.D.M.; Alves, M.J.D.S.; Soares, L.S.; Moreira, R.D.F.P.M.; Valencia, G.A.; Monteiro, A.R. A review on TiO_2-based photocatalytic systems applied in fruit postharvest: Set-ups and perspectives. *Food Res. Int.* **2021**, *144*, 110378. [CrossRef] [PubMed]
24. Boutillier, S.; Fourmentin, S.; Laperche, B. History of titanium dioxide regulation as a food additive: A review. *Environ. Chem. Lett.* **2021**, *20*, 1017–1033. [CrossRef]

25. Hwang, J.S.; Yu, J.; Kim, H.M.; Oh, J.M.; Choi, S.J. Food Additive Titanium Dioxide and Its Fate in Commercial Foods. *Nanomaterials* **2019**, *9*, 1175. [CrossRef]
26. Ahmed, F.; Awada, C.; Ansari, S.A.; Aljaafari, A.; Alshoaibi, A. Photocatalytic inactivation of *Escherichia coli* under UV light irradiation using large surface area anatase TiO_2 quantum dots. *R. Soc. Open Sci.* **2019**, *6*, 191444. [CrossRef]
27. Podporska-Carroll, J.; Panaitescu, E.; Quilty, B.; Wang, L.L.; Menon, L.; Pillai, S.C. Antimicrobial properties of highly efficient photocatalytic TiO_2 nanotubes. *Appl. Catal. B Environ.* **2015**, *176–177*, 70–75. [CrossRef]
28. Zhang, Y.Q.; Zhou, L.L.; Zhang, Y.J. Investigation of UV-TiO_2 photocatalysis and its mechanism in Bacillus subtilis spore inactivation. *J. Environ. Sci.* **2014**, *26*, 1943–1948. [CrossRef]
29. Liu, N.; Ming, J.; Sharma, A.; Sun, X.; Kawazoe, N.; Chen, G.P.; Yang, Y.N. Sustainable photocatalytic disinfection of four representative pathogenic bacteria isolated from real water environment by immobilized TiO_2-based composite and its mechanism. *Chem. Eng. J.* **2021**, *426*, 131217. [CrossRef]
30. Yu, H.G.; Liu, W.J.; Wang, X.F.; Wang, F.Z. Promoting the interfacial H_2-evolution reaction of metallic Ag by Ag_2S cocatalyst: A case study of TiO_2/Ag-Ag_2S photocatalyst. *Appl. Catal. B Environ.* **2018**, *225*, 415–423. [CrossRef]
31. Bandpey, N.B.; Aroujalian, A.; Raisi, A.; Fazel, S. Surface coating of silver nanoparticles on polyethylene for fabrication of antimicrobial milk packaging films. *Int. J. Dairy Technol.* **2017**, *70*, 204–211. [CrossRef]
32. Wu, M.C.; Lin, T.H.; Hsu, K.H.; Hsu, J.F. Photo-induced disinfection property and photocatalytic activity based on the synergistic catalytic technique of Ag doped TiO_2 nanofibers. *Appl. Surf. Sci.* **2019**, *484*, 326–334. [CrossRef]
33. Hwang, H.M.; Oh, S.; Shim, J.H.; Kim, Y.M.; Kim, A.; Kim, D.; Kim, J.; Bak, S.; Cho, Y.; Bui, V.Q.; et al. Phase-Selective Disordered Anatase/Ordered Rutile Interface System for Visible-Light-Driven, Metal-Free CO_2 Reduction. *ACS Appl. Mater. Interfaces* **2019**, *11*, 35693–35701. [CrossRef]
34. Yu, X.; Huang, J.L.; Zhao, J.J.; Liu, S.F.; Xiang, D.D.; Tang, Y.T.; Li, J.; Guo, Q.H.; Ma, X.Q.; Zhao, J.W. Efficient visible light photocatalytic antibiotic elimination performance induced by nanostructured Ag/AgCl@Ti^{3+}-TiO_2 mesocrystals. *Chem. Eng. J.* **2021**, *403*, 126359. [CrossRef]
35. Duan, Y.Y.; Zhang, M.; Wang, L.; Wang, F.; Yang, L.P.; Li, X.Y.; Wang, C.Y. Plasmonic Ag-TiO_{2_x} nanocomposites for the photocatalytic removal of NO under visible light with high selectivity: The role of oxygen vacancies. *Appl. Catal. B Environ.* **2017**, *204*, 67–77. [CrossRef]
36. Yang, X.H.; Liang, J.N.; Fu, H.T.; Ran, X.L.; An, X.Z. Fabrication of Au-Ag@TiO_2 ternary core-shell nanostructures with enhanced sunlight photocatalytic activity. *Powder Technol.* **2022**, *404*, 117463. [CrossRef]
37. Gao, D.D.; Liu, W.J.; Xu, Y.; Wang, P.; Fan, J.J.; Yu, H.G. Core-shell Ag@Ni cocatalyst on the TiO_2 photocatalyst: One-step photoinduced deposition and its improved H_2-evolution activity. *Appl. Catal. B Environ.* **2020**, *260*, 118190. [CrossRef]
38. Zhang, J.; Cha, J.K.; Fu, G.M.; Cho, E.J.; Kim, H.S.; Kim, S.H. Aerosol processing of Ag/TiO_2 composite nanoparticles for enhanced photocatalytic water treatment under UV and visible light irradiation. *Ceram. Int.* **2022**, *48*, 9434–9441. [CrossRef]
39. Liu, X.; Guan, X.L.; Xing, F.G.; Lv, C.; Dai, X.F.; Liu, Y. Effect of water activity and temperature on the growth of Aspergillus flavus, the expression of aflatoxin biosynthetic genes and aflatoxin production in shelled peanuts. *Food Control* **2017**, *82*, 325–332. [CrossRef]
40. Liu, K.L.; Liu, Y.; Chen, F.S. Effect of gamma irradiation on the physicochemical properties and nutrient contents of peanut. *LWT* **2018**, *96*, 535–542. [CrossRef]
41. Qi, J.F.; Dang, X.N.; Hammond, P.T.; Belcher, A.M. Highly Efficient Plasmon-Enhanced Dye-Sensitized Solar Cells through Metal@Oxide Core–Shell Nanostructure. *ACS Nano* **2011**, *5*, 7108–7116. [CrossRef]
42. Gui, L.S.; Lin, J.; Liu, J.J.; Zuo, J.L.; Wang, Q.Y.; Jiang, W.F.; Feng, T.Y.; Li, S.L.; Wang, S.T.; Liu, Z.L. Difference and association of antibacterial and bacterial anti-adhesive performances between smart Ag/AgCl/TiO_2 composite surfaces with switchable wettability. *Chem. Eng. J.* **2021**, *431*, 134103. [CrossRef]
43. Huerta-Aguilar, C.A.; Gutiérrez García, Y.S.; Thangarasu, P. Crystal plane directed interaction of TiO_2 [101] with AgNPs [111] silver nanoparticles enhancing solar light induced photo-catalytic oxidation of ciprofloxacin: Experimental and theoretical studies. *Chem. Eng. J.* **2020**, *394*, 124286. [CrossRef]
44. Li, J.R.; Jin, Z.Z.; Zhang, Y.M.; Liu, D.; Ma, A.J.; Sun, Y.M.; Li, X.Y.; Cai, Q.; Gui, J.Z. Ag-induced anatase-rutile TiO_{2_x} heterojunction facilitating the photogenerated carrier separation in visible-light irradiation. *J. Alloys Compd.* **2022**, *909*, 164815. [CrossRef]
45. Tian, B.Z.; Zhang, J.L.; Tong, T.Z.; Chen, F. Preparation of Au/TiO_2 catalysts from Au (I)–thiosulfate complex and study of their photocatalytic activity for the degradation of methyl orange. *Appl. Catal. B Environ.* **2008**, *79*, 394–401. [CrossRef]
46. Li, P.; Li, J.Z.; Feng, X.; Li, J.; Hao, Y.C.; Zhang, J.W.; Wang, H.; Yin, A.X.; Zhou, J.W.; Ma, X.J.; et al. Metal-organic frameworks with photocatalytic bactericidal activity for integrated air cleaning. *Nat. Commun.* **2019**, *10*, 2177. [CrossRef]
47. Li, G.H.; Sun, Y.Y.; Zhang, Q.M.; Gao, Z.; Sun, W.; Zhou, X.X. Ag quantum dots modified hierarchically porous and defective TiO_2 nanoparticles for improved photocatalytic CO_2 reduction. *Chem. Eng. J.* **2021**, *410*, 128397. [CrossRef]
48. Chen, Y.; Wang, Y.N.; Li, W.Z.; Yang, Q.; Hou, Q.D.; Wei, L.H.; Liu, L.; Huang, F.; Ju, M.T. Enhancement of photocatalytic performance with the use of noble-metal-decorated TiO_2 nanocrystals as highly active catalysts for aerobic oxidation under visible-light irradiation. *Appl. Catal. B Environ.* **2017**, *210*, 352–367. [CrossRef]
49. *GB 5009.229-2016*; National Standard for Food Safety: Determination of acid value in Food. National Health and Family Planning Commission of the People's Republic of China: Beijing, China, 2016; pp. 1–15.

50. *GB 5009.227-2016*; National Standard for Food Safety: Determination of peroxide value in Food. National Health and Family Planning Commission of the People's Republic of China: Beijing, China, 2016; pp. 1–8.
51. *GB 5009.6-2016*; National Standard for Food Safety: Determination of fat content in Food. National Health and Family Planning Commission of the People's Republic of China, National Food and Medical Products Administration: Beijing, China, 2016; pp. 1–8.
52. *GB 5009.5-2016*; National Standard for Food Safety: Determination of protein content in Food. National Health and Family Planning Commission of the People's Republic of China, National Food and Medical Products Administration: Beijing, China, 2016; pp. 1–9.
53. *ISO 14502-1: 2005*; Determination of substances characteristic of green and black tea. Part 1: Content of total polyphenols in tea. Colorimetric method using Folin-Ciocalteu reagent. International Organization for Standardization: Genève, Switzerland, 2005; pp. 1–10.
54. *GB/T 24903-2010*; Inspection of grain and oils—Determination of resveratrol in peanut by high performance liquid chromatography. General Administration of Quality Supervision, Inspection and Quarantine of the People's Republic of China, Standardization Administration of the People's Republic of China: Beijing, China, 2010; pp. 1–5.

MDPI
St. Alban-Anlage 66
4052 Basel
Switzerland
Tel. +41 61 683 77 34
Fax +41 61 302 89 18
www.mdpi.com

Toxins Editorial Office
E-mail: toxins@mdpi.com
www.mdpi.com/journal/toxins

MDPI
St. Alban-Anlage 66
4052 Basel
Switzerland

Tel: +41 61 683 77 34

www.mdpi.com

ISBN 978-3-0365-7385-4